## Economic Essays on Flexibility in Energy Systems

Inaugural dissertation

zur

Erlangung des Doktorgrades

der

Wirtschafts- und Sozialwissenschaftlichen Fakultät

 $\operatorname{der}$ 

Universität zu Köln

2025

vorgelegt

von

M. Sc. Nils Namockel

aus

Hagen

Referent: Prof. Dr. Marc Oliver Bettzüge

Korreferent: Jun.-Prof. Dr. Michael Bucksteeg

Tag der Promotion: 07.10.2025

### ACKNOWLEDGEMENTS

I would like to express my gratitude to Prof. Dr. Marc Oliver Bettzüge for his supervision, critical feedback, and continuous support throughout my doctoral project. His insightful comments and challenging questions consistently encouraged me to sharpen my thinking and significantly contributed to the academic quality of this dissertation. I also extend my thanks to Jun.-Prof. Dr. Michael Bucksteeg for co-reviewing my thesis.

It has been a privilege to conduct my research at the Institute of Energy Economics (EWI). I am especially grateful to Prof. Bettzüge and the EWI management team for offering me this unique opportunity for academic and personal development. I would also like to acknowledge the support of the administration, communication, and IT teams. Beyond the inspiring research and consulting projects, the collegial, supportive, and dynamic environment have made the EWI a great place to work. I am deeply grateful to my colleagues — many of whom became friends. My special thanks go to Arne Lilienkamp, Polina Emelianova, and Fabian Arnold, my co-authors with whom I shared both the highs and the challenges of this academic journey. This dissertation would not have been possible without their ideas, commitment, and fellowship.

I gratefully acknowledge financial support from the German Federal Ministery of Economy and Climate protection within the project 'GreenVEgaS - Gesamtsystemanalyse der Sektorenkopplung – Volkswirtschaftliche Bewertung der Energieinfrastruktur und –erzeugung für eine Kopplung der Sektoren Strom, Wärme und Verkehr' (grant number 03EI1009C), and by the Ministry of Economic Affairs, Industry, Climate Protection and Energy of the State of North Rhine-Westphalia within the project 'VISE - Smart Data: Mehrwertgenerierung durch Energiedaten' and '(grant number EFO 0151D).

Finally, I would like to thank my family for their continued patience and understanding — always believing in me without ever placing pressure on me. My deepest appreciation goes to Katharina, whose limitless support and empathy have been a constant source of motivation and optimism throughout this journey.

### Contents

Li	st of	Figure	es	ix
Li	st of	Table	s	xii
1.	Intr	oducti	ion	1
	1.1.	Motiva	ation	1
	1.2.	Outlin	ne	3
	1.3.	Metho	odological approaches	5
2.	Inte	gratin	g EVs into distribution grids – Examining the effects	
	of v	arious	DSO intervention strategies on optimized charging	9
	2.1.	Introd	luction	9
	2.2.	Electr	icity tariff designs and possibilities for DSO interventions .	13
		2.2.1.	Electricity tariff designs	13
		2.2.2.	DSO interventions	14
		2.2.3.	Combining tariff designs and DSO intervention strategies	15
	2.3.	Grid i	nterventions in the context of optimizing charging processes	16
		2.3.1.	General model approach and structure	16
		2.3.2.	Optimization of decentralized energy systems	18
		2.3.3.	Grid model	21
		2.3.4.	Coupling of the asset optimization model and grid model	22
	2.4.	Case s	study - Technical and economic effects of different interven-	
		tion co	oncepts	25
		2.4.1.	Analysis environment	25
		2.4.2.	Impact of different tariff structures on optimal charging	
			strategies and grid utilization	30
		2.4.3.	Impact of different intervention options of the grid opera-	
			tor on optimal charging strategies	33
	2.5.	Discus	ssion	36
	2.6	Concl	usion	40

3.	Diff	usion (	of electric vehicles and their flexibility potential for	
	smo	othing	g residual demand - A spatio-temporal analysis for	
	$\mathbf{Ger}$	many		43
	3.1.	Introd	uction	43
	3.2.	Spatio	-temporal expansion of private electric vehicles	48
		3.2.1.	Regional diffusion of electric vehicles	49
		3.2.2.	User-specific load and flexibility profiles	53
	3.3.	Region	nalization of demand and supply	58
		3.3.1.	Spatial distribution of annual electricity demand	59
		3.3.2.	Temporal distribution of regional electricity demand $$	60
		3.3.3.	Spatial distribution of annual renewable electricity capacities	60
		3.3.4.	Temporal distribution of regionally renewable electricity	
			generation	61
	3.4.	Model	ling electric vehicle charging flexibility	62
		3.4.1.	Flexibility on regional level	62
		3.4.2.	Flexibility on national level	64
	3.5.	Analys	sis and results	64
		3.5.1.	Residual load analysis	64
		3.5.2.	Flexibility of electric vehicles	68
	3.6.	Conclu	usion	77
		3.6.1.	Main results	77
		3.6.2.	Policy implications	78
		3.6.3.	Limitations and further research	79
1.	Wel	fare re	edistribution through flexibility - Who pays?	81
	4.1.		uction	81
	4.2.		aced modeling of decentralized flexibility	84
			Decentralized heating	84
			Road transport	87
	4.3.		tudy - Energy system dispatch under different flexibility use	
		cases		90
		4.3.1.	General model scope	90
		4.3.2.	Different use cases for end-use sectors	91
	4.4.	Result	SS	92
		4.4.1.	Results without decentralized flexibility	92
		4.4.2.		94
	4 5	Discus	Ů	103

	4.6.	Conclu	usion	106
		4.6.1.	Main results	106
		4.6.2.	Future research	107
<b>5.</b>	Und	lerstar	nding the fundamentals of hydrogen price formation	
	and	its re	elationship with electricity prices - Insights for the	
	futu	re ene	ergy system	109
	5.1.	Introd	luction	109
	5.2.	Metho	odology, input data and scenario design	113
		5.2.1.	Modeling the equilibrium for hydrogen	114
		5.2.2.	Scenario design and related assumptions	119
	5.3.	The re	elationship between electricity and hydrogen prices	121
		5.3.1.	System configuration	121
		5.3.2.	Price formation and price duration curves	121
		5.3.3.	Data separation	124
		5.3.4.	Analysis of co-integration	125
		5.3.5.	Analysis of statistical properties	126
		5.3.6.	Analysis of coupling and decoupling dynamics	129
	5.4.	Impac	t of the system configurations on the relationship between	
		electri	city and hydrogen prices	132
		5.4.1.	Changes in system configurations and derived price data . $$	132
		5.4.2.	Analysis of changes in statistical properties and price ratio	s 133
		5.4.3.	Analysis of changes in coupling and decoupling dynamics	136
	5.5.	Discus	ssion	138
	5.6.	Conclu	usion	141
		5.6.1.	Main results	141
		5.6.2.	Future research	142
Α.	Sup	pleme	ntary material for chapter 2	143
	A.1.	Sets, p	parameters and decision variables	143
	A.2.	Calcul	lation of maximum active power on each line and transforme	er 146
	A.3.	Prope	rties of the low voltage grids	147
в.	Sup	pleme	ntary material for chapter 3	149
	B.1.	The fu	ıll Bass model	149
	B.2.	Functi	ion transformation to $\Delta t$	151
	B.3.	Descri	ptive analysis of mobility data	152
	B.4.	Distril	bution of daily energy consumption per EV	152

	B.5.	Weekend flexibility clusters and in-depth analysis of the flexibility	
		clusters	153
	B.6.	Shares of charging scenarios	155
	B.7.	Distribution of demand to federal states	155
	B.8.	Demand profiles	156
	B.9.	Residual load duration curves	157
	B.10	Cluster properties	158
C.	Sup	plementary material for chapter 4	161
	C.1.	Sets, parameters and decision variables	161
	C.2.	DIMENSION model description	163
	C.3.	Data	167
	C.4.	Additional results	170
D.	Sup	plementary material for chapter 5	177
	D.1.	Sets, parameters and decision variables	177
	D.2.	$H_2$ supply curve	179
	D.3.	Trade capacities	179
	D.4.	Installed capacities	181
	D.5.	Electricity and hydrogen demand	182
	D.6.	Hydrogen balances	182
	D.7.	Storage level	184
	D.8.	$\mathrm{H}_2$ balance and residual load in each subset for the reference scenario	185
	D.9.	Check for co-integration	186
	D.10	.Hydrogen and electricity price duration curves	187
Bi	bliog	raphy	189
Cu	ırricı	ılum Vitae	206

# List of Figures

2.1.	Combinations of electricity tariff designs and possibilities for in-	
	terventions by the DSO	15
2.2.	Process diagram illustrating the various optimization and compu-	
	tation steps	17
2.3.	PQ-Diagram to determine the maximum, controllable active power	
	on grid elements $\dots$	24
2.4.	Configuration of the distribution grid based on Meinecke et al.	
	$(2020) \ldots \ldots$	26
2.5.	Electricity prices - Cumulated distribution of assumed electric-	
	ity wholesale prices for 2030 (left) and final composition of the	
	electricity prices for the Fix and ToU tariff for 2030 (right) $$	28
2.6.	Cumulated distribution of EVs' daily energy consumption (left)	
	and share of EVs with grid connection over time (right)	29
2.7.	Impact of tariff structures on optimal charging strategies and re-	
	lated charging costs without curtailment	31
2.8.	Flexibility provision by electric vehicles	33
2.9.	Comparison of cost deltas	35
3.1.	Methodological steps	44
3.2.	Development of regional diffusion curves	51
3.3.	Number of electric vehicles in each NUTS 3 region for the years	
	2030 and 2045	53
3.4.	Selected load profiles for a medium-sized city in 2045	55
3.5.	Concept for generating flexibility clusters (stylized example)	56
3.6.	Flexibility clusters for weekdays	57
3.7.	Selected flexibility profiles for a medium-sized city in 2045	58
3.8.	Clustering and mapping of the 401 NUTS 3 regions	65
3.9.	Comparison of regional residual load curves prior to the activation	
	of flexibility	66
3.10.	Optimal activation of flexibility in region DE111 (Stuttgart)	69

3.11.	Activation of flexibility of EVs in 2045 after national and regional	
	optimization	70
3.12.	Properties of the national residual load curve before and after the	
	use of flexibility	71
3.13.	Imbalance ratios before and after the use of flexibility in $2030$	73
3.14.	Imbalance ratios before and after the use of flexibility in $2045$	74
4.1.	Charging and flexibility profiles for different mobility cluster	89
4.2.	Definition of flexibility use cases	91
4.3.	Electricity price, average market values and producer surplus for	
	producer groups as well as average electricity costs for consumer	
	groups in the use case M0/H0	93
4.4.	Variation of electricity prices across different flexibility use cases	95
4.5.	Changes in average producer and consumer surplus under different	
	flexibility use cases, measured in EUR/MWh $\ \ldots \ \ldots \ \ldots$	97
4.6.	Changes in average electricity costs across mobility cluster under	
	different flexibility use cases, in EUR/MWh $\ldots$	101
4.7.	Changes in average electricity costs across buildings types under	
	different flexibility use cases, in EUR/MWh	102
5.1.	Overall model approach covering a reference scenario and three	
	system sensitivities	120
5.2.	Price data and duration curves for hydrogen and electricity $\ . \ . \ .$	122
5.3.	Daily pairs of electricity and hydrogen prices split in four subsets	125
5.4.	Electricity and hydrogen price pairs split in four subsets for the	
	three system sensitivities	133
5.5.	Distribution of the daily electricity-to-hydrogen price ratio for dif-	
	ferent system sensitivities and subsets	135
B.1.	Key parameters of the used MOP dataset (KIT - Institut für	
	Verkehrswesen, 2021)	152
B.2.	Distribution of daily energy consumption per EV based on average	
	specific fleet consumption by year	152
В.3.	Flexibility clusters for weekends	153
B.4.	Demand profiles per application. Heat profiles are exemplary:	
	shown are the profiles for the region DEA23 (Cologne) on 3 ex-	
	emplary days of the year	156

B.5.	Normalized residual load duration curves for all NUTS3 regions	
	and Germany for 2019, 2030 and 2045 $\hdots$	157
B.6.	Distribution of the population density within each cluster in $2045$	158
B.7.	Distribution of EVs per $km^2$ within each cluster in 2045	159
B.8.	Distribution of Wind Onshore capacities per $km^2$ within each clus-	
	ter in 2045	159
B.9.	Distribution of PV capacities (large-scale PV and rooftop PV) per	
	$km^2$ within each cluster in 2045	159
B.10	Distribution of large-scale PV capacities per $km^2$ within each clus-	
	ter in 2045	160
B.11	. Distribution of rooftop PV capacities per $km^2$ within each cluster	
	in 2045	160
	DIMENSION sector overview	163
C.2.	Changes in total producer and consumer surplus under different	
	use cases, measured in billion EUR	170
C.3.	Changes in total electricity costs across building types under dif-	
	ferent flexibility use cases, in million EUR $\dots \dots \dots$ .	171
C.4.	Changes in total electricity costs for different mobility clusters	
	under different flexibility use cases, in million EUR	171
C.5.	Flexibility decisions across different building types for the use case	
	$\rm M0/H1$ compared to $\rm M0/H0$	172
C.6.	Flexibility decisions across different mobility clusters for the use	
	case M1/H0 compared to M0/H0 $\hdots$	173
C.7.	Flexibility decisions in the road transport sector for the use case	
	M2/H0 compared to $M0/H0$	174
C.8.	Residual load duration curve in the reference use case $\mathrm{M}0/\mathrm{H}0$	
	(above) and its deviations in flexibility use cases (below)	175
D 1		150
	Supply curve for H <sub>2</sub> imports via ship	179
	Daily H <sub>2</sub> balance for the different system sensitivities	183
	H <sub>2</sub> storage level in Europe in each sensitivity	184
D.4.	Daily H <sub>2</sub> balance in each subset with the corresponding residual	105
<b>5</b> -	load in sorted order	185
D.5.	Price duration curves for hydrogen and electricity	187

### List of Tables

2.1. 2.2.	EV curtailment in use cases with basic curtailment	30 32
3.1.	Annual electricity demand by sector and application in TWh	59
3.2. 3.3.	Annual electricity demand by sector and application in TWh Correlation between residual load and electric vehicle load curves	60 67
4.1.	Number of heat pumps and share of total heat demand by building	0.0
4.0	type	86
4.2.	Annual average COP by heat pump technology and building type	86
4.3. 4.4.	Distribution of EVs across mobility clusters MC1 to MC10 Changes in national CO <sub>2</sub> emissions under different flexibility use	90
	cases, in million tons of CO <sub>2</sub> eq	96
4.5.	Absolute welfare changes for specific producer and consumer groups,	
	in million EUR	99
5.1.	Statistical summary of hydrogen and electricity prices for the full	
	year	122
5.2.	Statistical summary of hydrogen and electricity prices for each	
	subset	126
5.3.	Statistic on the distribution of daily electricity-to-hydrogen price	
	ratios	128
5.4.	Regression and correlation results	130
5.5.	Statistical summary of hydrogen and electricity prices for the sys-	
	tem sensitivities	134
5.6.	Regression results and correlation for the system sensitivities $$ . $$	137
A.1.	Sets	143
A.2.	Decision variables	144
A.3.	Parameters	145
A.4.	Properties of low voltage grids 1-6 depending on the penetration	
	rate of electric vehicles	147

A.5.	Properties of low voltage grids 7-12 depending on the penetration	
	rate of electric vehicles	148
В.1.	Characteristics of the weekday flexibility clusters	154
B.2.	Characteristics of the weekend flexibility clusters	154
В.3.	Shares of charging scenarios per settlement type	155
B.4.	Distribution keys of sectoral electricity demand to federal states . $$	155
B.5.	Properties of the regions within the three cluster in $2045$	158
C.1.	Sets	161
C.2.	Decision variables	161
C.3.	Parameters	162
C.4.	Overview of key input data sources	167
C.5.	Heating shares for decentralized heating in Germany in $2030$	167
C.6.	Commodity prices and EU Carbon Permits in 2030	167
C.7.	Installed capacities in Germany per generation group and corre-	1.00
$\alpha$	sponding efficiencies	168
	Electricity demand in TWh	169
C.9.	Heating shares for central heating (district heat)	169
D.1.	Sets	177
D.2.	Parameters	177
D.3.	Decision variables	178
D.4.	Trade capacities for hydrogen and electricity	179
D.5.	Installed electrical capacities in Germany per generation group	
	in $\mathrm{GW}_{el}$ and corresponding efficiencies for the different system	
	configuration scenarios	181
D.6.	Installed hydrogen storage capacities in Germany in $\mathrm{TWh}_{th}$ and	
	corresponding efficiencies for the different system configuration	
	scenarios	181
D.7.	Electricity and hydrogen demand in TWh for different sectors and	
	system configuration scenarios	182
D.8.	$H_2$ origin and export balance in $TWh_{th}$	182
D.9.	Results of the ADF-test for stationarity	186

### 1. Introduction

### 1.1. Motivation

The transition to climate neutrality fundamentally reshapes the structure of the energy system. In the power sector, a shift toward intermittent energy sources, most notably wind and photovoltaics (PV), introduces inherent volatility due to their weather dependence. This volatility leads to temporal mismatches between electricity supply and demand. On the demand side, decarbonization through the electrification of transport, heating, and industry results in a growing share of heterogeneous and partially flexible electrical loads, particularly electric vehicles (EVs), heat pumps, and electrolyzers. Their techno-economic flexibility potential is shaped by user behavior and process constraints (Gillingham et al., 2009, Palensky and Dietrich, 2011). Most of these loads are located in distribution grids.

In short-term electricity markets, where supply and demand must be balanced continually under fixed infrastructure and generation capacity, demand elasticity affects dispatch outcomes. It shapes the residual load curve and thus influences price formation, while being constrained by grid capacity. If activated and coordinated appropriately, flexibility can increase the static efficiency in terms of reducing total system costs, grid congestion, and curtailment of renewables (Hirth et al., 2016). However, the potential benefits of flexibility are not automatically realized. Without effective coordination, flexible demand may respond to static incentives, exogenous schedules, or behavioral routines. Such uncoordinated behavior can result in synchronized peaks, local congestion, and increased balancing requirements, ultimately leading to inefficient dispatch outcomes and welfare losses (Borenstein and Holland, 2005).

In theory, efficient coordination means that flexible resources are allocated dynamically and selectively, considering wholesale market balancing requirements and grid capacity. Coordination mechanisms can include price-based signals, such as dynamic tariffs reflecting marginal system costs, or volume-based signals, such as interventions from distribution system operators. Each of these mechanisms has several design options, which involve trade-offs between efficiency, granularity, transparency, and feasibility (Laffont and Tirole, 1993). Their interaction raises additional questions regarding overlapping incentives when multiple signals coexist.

Importantly, utilizing flexibility not only affects aggregate welfare, but also redistributes surplus among market participants, across technologies, user groups,

### 1. Introduction

and sectors. These effects are particularly important as they shape the incentives and outcomes of flexibility deployment. Moreover, the welfare effects of flexibility integration are highly context-specific. The value of allocating different sources of flexibility is influenced by timing, location, system conditions, and interactions with other flexible resources (Goutte and Vassilopoulos, 2019).

Notable interaction effects are introduced by electrolyzers, which link electricity consumption with hydrogen production and thereby introduce cross-market dependencies in price formation. These dependencies shape short-term equilibrium outcomes in both sectors. Understanding the dynamics of this coupling is critical for both policymakers and market participants to ensure efficient market operation and prevent new inefficiencies from emerging as sectors become more integrated.

Against this backdrop, this dissertation examines the economic implications of the described structural changes by analyzing and quantifying short-term equilibrium outcomes under varying system configurations and coordination schemes. It explores how flexible demand reshapes price formation, quantity allocation, and welfare distribution in electricity markets with fixed infrastructure and generation capacity. The dissertation spans multiple segments of the energy system, from distribution grids to national and European markets, and explores cross-sectoral interactions. Each chapter reflects an individual research paper to which all authors contributed equally:

- Integrating EVs into distribution grids Examining the effects of various DSO intervention strategies on optimized charging. Joint work with Arne Lilienkamp. Published in Applied Energy Vol. 378, 2025 (Lilienkamp and Namockel, 2025).
- Diffusion of electric vehicles and their flexibility potential for smoothing residual demand A spatio-temporal analysis for Germany. Joint work with Fabian Arnold and Arne Lilienkamp. Published in Energy Vol. 308, 2024 (Arnold et al., 2024).
- Welfare redistribution through flexibility Who pays?. Joint work with Polina Emelianova. Published in Energy Policy Vol. 205, 2025 (Emelianova and Namockel, 2025).
- Understanding the fundamentals of hydrogen price formation and its relationship with electricity prices Insights for the future energy system. EWI Working Paper 25/06 (Namockel, 2025).

The following provides an outline of the individual Chapters (Section 1.2), and discusses the methodological approaches as well as limitations (Section 1.3).

### 1.2. Outline

# Integrating EVs into distribution grids – Examining the effects of various DSO intervention strategies on optimized charging

Adopting EVs and implementing variable electricity tariffs increases the risk of congestion in distribution grids due to herding behavior. To avert critical grid situations and avoid expensive grid expansions, Distribution System Operators (DSOs) have intervention rights, allowing them to curtail charging processes. Chapter 2 investigates how various DSO intervention schemes, in combination with different electricity tariffs, affect the optimal charging strategy of EV users in terms of charging costs as well as the required flexibility to avoid grid congestion. Various curtailment strategies are possible, varying in spatio-temporal differentiation and possible discrimination. However, evaluating different strategies is complex due to the interplay of economic factors, technical requirements, and regulatory constraints — a complexity not fully addressed in the current literature. The chapter introduces a model to optimize electric vehicle charging strategies to address this gap. The model considers different tariff schemes (Fixed, Time-of-Use, and Real-Time) and incorporates DSO interventions (basic, variable, and smart) within its optimization framework. Based on the model, the chapter analyzes the flexibility demand needed to resolve grid congestion and total electricity costs from the users' perspective.

The results show that time-variable tariffs yield only modest cost savings for consumers — while potentially increasing peak loads due to synchronized charging. All curtailment strategies are effective in mitigating congestion, but their efficiency varies with granularity: more differentiated interventions approach the benchmark of system-optimal outcomes. Importantly, from the user perspective, curtailment has only a limited effect on charging costs, particularly under low penetration and Time-of-Use pricing. At higher EV uptake, curtailment becomes more relevant, but financial impacts remain moderate.

### Diffusion of electric vehicles and their flexibility potential for smoothing residual demand - A spatio-temporal analysis for Germany

Incentivizing EVs to reduce stress on distribution grids affects regional peaks in load and feed-in, but also alters the national residual load curve. To understand the potential of EV charging flexibility for reducing peaks on regional and national levels, **Chapter 3** first constructs regional residual load profiles for 2019, 2030, and 2045 using a scenario aligned with Germany's 2045 climate neutrality target. It models region-specific EV diffusion via sigmoid functions and derives user- and location-specific load and flexibility profiles from empirical mobility data. Based on these inputs, a spatio-temporal optimization model is developed to assess the impacts of EV charging flexibility under two contrasting deploy-

ment strategies: (1) all vehicles contribute to flattening the national residual load curve; (2) vehicles contribute to flattening regional residual load curves.

The results show that the national and regional residual load curves change structurally as positive and negative peaks in residual demand increase over the years. While the absolute potential of EV flexibility grows over time with increasing EV penetration, its marginal effectiveness in reducing system-wide peaks declines. In load-dominated regions, the national deployment of flexibility can result in higher regional demand peaks compared to a scenario without charging flexibility. The two approaches of flexibility activation can be contradictory in their effects: While regional incentivization is less efficient in reaching the smoothing in the national residual demand curve, national incentivization can even lead to increased strain on the local level.

### Welfare redistribution through flexibility - Who pays?

Flexible operation of EVs and heat pumps influence electricity price formation and trigger a redistribution of welfare from producers to consumers. The magnitude and direction of this redistribution are likely to vary across technologies and end-user groups, depending on their flexibility potential and usage behavior. To explore these dynamics, **Chapter 4** quantifies redistributional effects by integrating diverse flexibility options and user groups into a high-resolution European dispatch model, simulating multiple flexibility use cases across the transport and heating sectors in Germany. This approach allows to simulate the interaction between decentralized flexible assets - such as EVs and heat pumps - and the energy system. The analysis is based on a case study for Germany, reflecting the country's technology-specific targets for 2030.

The results show that while decentralized flexibility has a limited impact on average wholesale price levels, it significantly reduces price volatility by smoothing demand peaks and aligning load with renewable energy generation. While total system welfare increases slightly, flexibility leads to a redistribution of welfare from producers to consumers. On aggregate, consumers benefit regardless of whether they actively provide flexibility. However, the extent of these benefits varies considerably across user groups, shaped by their consumption profiles and the temporal availability of flexibility. Among the assessed flexibility options, electric vehicles - particularly through bidirectional charging - offer greater welfare gains compared to heat pumps. EVs flexibility leads to notable variations in electricity costs depending on charging behaviors. In the heating sector, commercial buildings with flatter load profiles benefit most from flexibility, while residential buildings see moderate cost changes. The competition introduced by decentralized flexibility impacts commercial users especially, raising off-peak prices and indicating cannibalization effects.

### Understanding the fundamentals of hydrogen price formation and its relationship with electricity prices - Insights for the future energy system

The increasing role of hydrogen in decarbonization strategies introduces new interactions between energy sectors that affect market outcomes. In particular, the coupling between electricity and hydrogen markets through electrolysis establishes interdependencies in short-term price formation. **Chapter 5** investigates fundamental price formation mechanisms for hydrogen and electricity, emphasizing their mutual dependencies, volatility, and the impact of short-term system conditions such as weather and demand variability. Additionally, it explores how these dynamics respond to variations in system configurations. Using the European energy system model DIMENSION, enhanced to incorporate detailed hydrogen supply and demand options including storage, cross-border trade, and import, this study derives shadow prices as the basis for the subsequent statistical analysis.

Results show that hydrogen and electricity prices are governed by short-term interactions. While electricity price formation can be well explained by renewable generation and demand, hydrogen prices emerge to be more structurally driven. Storage dynamics and cross-border trade significantly influence hydrogen price formation next to electrolysis. Strong price coupling between the hydrogen and electricity markets likely occurs under low residual load conditions dominated by electrolysis, whereas decoupling arises during high residual load situations dominated by storage discharge. The electricity-to-hydrogen price ratio averages 0.56, lower than previous estimates, primarily due to the consideration of inflexible hydrogen imports and infrastructure constraints. Furthermore, the analysis indicates that short-term price signals alone may be insufficient for investment recovery, highlighting the need for complementary market mechanisms to develop a liquid hydrogen market.

### 1.3. Methodological approaches

Each chapter of this thesis analyzes specific aspects of the economics of flexibility integration in energy systems using quantitative modeling. These models are formulated as partial-equilibrium representations of selected system segments. They are calibrated to scenario-specific assumptions and designed to capture key technical and economic dynamics relevant to their respective research questions.

Chapter 2 develops a modeling framework to evaluate the impact of electricity tariffs and grid operator interventions on optimized EV charging strategies in distribution grids. A synthetic SimBench grid for the German context, based on Meinecke et al. (2020), comprises twelve low-voltage networks that reflect varying topologies, transformer capacities, and settlement types ranging from rural to urban. Within this system, EV users optimize charging behavior under

### 1. Introduction

different time-variable electricity tariffs (Fixed, ToU, Real-Time). Three intervention strategies are considered: a uniform, basic intervention with no temporal and spatial differentiation; a variable intervention that adjusts control based on temporal and spatial grid load conditions; and an idealized benchmark with full system information and individual signals. The model simulates charging cost savings, grid utilization, and flexibility requirements across multiple EV penetration levels. By comparing intervention strategies under identical system conditions, the paper isolates the effectiveness of volume signals in mitigating herding behavior and preventing transformer overloads, while preserving user benefits from dynamic tariffs.

While the use of synthetic grids ensures controlled comparability across scenarios, the results are inherently shaped by the grid configurations and assumptions used. The behavior of EV users is modeled as fully responsive to tariffs and intervention signals, abstracting from potential behavioral heterogeneity and real-world frictions. Interactions with other flexible assets, such as heat pumps or batteries, are not captured in this analysis, nor is vehicle-to-grid functionality. Furthermore, the model adopts a price-taker assumption, focusing on system impacts without capturing potential feedback effects on wholesale electricity markets.

Chapter 3 develops a spatio-temporal modeling framework to quantify the potential of flexible electric vehicle (EV) charging to mitigate residual load peaks in Germany. The analysis contrasts two deployment strategies: one aiming to smooth the national residual load curve, and another targeting the reduction of regional peaks. A linear optimization model minimizes the squared deviation of residual load from its mean. EV diffusion is modeled regionally using sigmoid functions, while charging profiles are derived from user- and location-specific mobility data (KIT - Institut für Verkehrswesen, 2021). Based on a scenario consistent with Germany's national climate and technology targets (dena, 2021), regional residual load profiles are generated for 2019, 2030, and 2045 at the NUTS 3 level, covering all German districts.

As the analysis is based on a single scenario for demand and generation development, alternative weather years or policy pathways may yield different absolute results, while the qualitative trends and regional trade-offs are expected to hold. The analysis focuses solely on unidirectional home charging with perfect foresight and information, and does not consider interactions with other flexible assets (e.g., batteries or heat pumps). User behavior is modeled deterministically under the assumption of full participation, potentially overstating the flexibility achievable in practice. Consequently, the results serve as an upper bound, quantifying the effects of flexible charging under perfect execution. Furthermore, grid constraints are reflected using residual load peaks as a proxy, without modeling voltage or reactive power constraints. Thus, further research may be necessary.

Both Chapter 4 and Chapter 5 employ the large-scale energy system optimization model DIMENSION, which is designed to simulate the integrated operation of the European energy system. DIMENSION is partially equilibrium model that minimizes total system costs subject to technical and economic constraints. The model assumes competitive and efficient markets, and rational behavior of market participants with perfect foresight. Shadow prices of the equilibrium constraints for electricity (and hydrogen) are interpreted as market prices by abstracting from other components of prices, mark-ups or policy instruments. In both chapters, the model is extended to incorporate detailed representations of sector coupling technologies and decentralized flexibility options, including electric vehicles, heat pumps, electrolysers, and hydrogen storage. These enhancements enable a consistent analysis of short-term dispatch dynamics and system interactions — with **Chapter 4** focusing on welfare redistribution in the electricity market, and **Chapter 5** analyzing hydrogen price formation and its coupling with electricity prices.

In **Chapter 4** heterogeneous user groups and flexibility technologies in the road transport and building sectors are integrated in DIMENSION. Flexible assets are modeled with technology- and user-specific constraints and usage patterns. The simulation is performed for Germany in 2030, assuming the achievement of national technology targets. Different flexibility use cases are compared to assess their impacts on electricity price formation, CO<sub>2</sub> emissions, system welfare, and consumer and producer surplus.

While the modeling captures detailed interactions in the day-ahead electricity market, the analysis abstracts from balancing and intraday markets, where additional value from flexibility could emerge. Moreover, distribution grid constraints are not considered, which may overstate the realizable welfare gains. Finally, the cost of enabling flexibility — such as smart meters or bi-directional charging — is excluded, implying that user-level benefits reflect gross rather than net gains.

Chapter 5 expands DIMENSION to model the integrated dispatch of the electricity and hydrogen systems under a future climate-neutral scenario for 2050. The analysis incorporates hourly dispatch with daily resolution for hydrogen, modeling hydrogen production via electrolysis, hydrogen storage, long-term contracts (LTCs), and cross-border pipeline trade. The resulting shadow prices serve as the basis for co-integration tests, regression and correlation analysis, price ratio distributions, and statistical comparisons between electricity and hydrogen markets. This approach enables an in-depth examination of short-term price dynamics and their dependence on system configurations, such as hydrogen demand levels and trade capacity expansions.

The analysis focuses on Germany and assumes a liquid market for hydrogen in 2050 with daily resolution. Different system configurations help to evaluate the robustness of the results. Limitations arise from the separation of investment and dispatch stages in the model: shadow prices do not reflect full-cost recovery and may underestimate actual hydrogen prices. Additionally, the model assumes price-inelastic hydrogen demand, and excludes explicit risk premiums or market

### 1. Introduction

mark-ups. As such, price levels represent conservative estimates and do not capture long-term investment incentives or real-world market volatility.

In addition to this discussion, each of the following four chapters provides a comprehensive description of the methodology, its limitations, and emerging questions for future research.

# 2. Integrating EVs into distribution grids – Examining the effects of various DSO intervention strategies on optimized charging

### 2.1. Introduction

As part of the global energy transition, there is a concerted effort to expand renewable energies (RES) and electrify various end-use sectors. Contributing to the ongoing electrification of the transportation sector, the increasing adoption of electric vehicles (EVs) plays a pivotal role in this transition. 14% of all new cars sold globally were electric in 2022, up from around 9% in 2021 and less than 5% in 2020. An even stronger increase is projected throughout 2023 (IEA, 2023b). Simultaneously, integrating digital technologies such as Smart Meters is a crucial component of the energy transition. Whereas some countries already experience a high penetration of smart meters, such as Italy, Sweden, Finland, or Spain, other countries plan to force the roll-out in the next years (Schnaars et al., 2022).

The digitization and the electrification of transportation not only underpin the shift towards cleaner energy sources but also results in sector coupling. Electric vehicles, with their increasing demand and through their interaction with the electricity system, will thus become an important actor within the future electricity system (IEA, 2023c). In this context, the ongoing digitization offers the prospect of employing electric vehicles in a way that actively supports and enhances the overall functionality of the electricity system. But, also, EV users can potentially benefit from exploiting the inherent flexibility of EVs (Englberger et al., 2021). By offering variable electricity tariffs to EV users, electricity providers can forward price signals from the electricity market, mirroring the state of the energy system. This has two implications. First, EV users can optimize their charging to minimize electricity costs, and second, the shifting of load implicitly contributes to balancing supply and demand in the energy system. For example, Schittekatte et al. (2022) show how Time-of-Use (ToU) tariffs incentivize load-shifting while simultaneously addressing consumer preferences.

Dynamic tariffs, however, abstract from the grid, as neither the retailers nor the consumers consider the grid infrastructure in their calculus. Given the divergent objectives of retailers, consumers, and grid operators, this poses a challenge and may lead to conflicts. Electric vehicle users prioritize low charging costs and meeting their mobility or electricity demand, while retailers align their tariffs with wholesale prices. In contrast, grid operators strive for stable grid operation. The pursuit of cost savings, often driven by a desire to benefit from low prices, can result in a high simultaneity of charging processes among electric vehicle users, leading to load peaks that strain the grid infrastructure. This herding behavior poses a significant threat to distribution grids, where most electric vehicle demand is concentrated and becomes more pronounced with higher electric vehicle penetration rates. As highlighted by Birk Jones et al. (2022), ToU tariffs can increase peak demand by up to 20% when many users charge simultaneously after peak times, causing grid stress. This is further supported by Reibsch et al. (2024), who show that market-based charging strategies tied to wholesale power prices can exacerbate grid overloads, particularly in areas with high photovoltaic (PV) penetration.

To avoid grid congestion, three options exist in general. First, distribution system operators (DSOs) could restrict the access of EVs to the grid by limiting the installation of charging stations and wall boxes. This, however, is detrimental to the desired large-scale EV adoption and interferes with EV users' objectives. Second, DSOs could expand the grid so that even herding behavior does not cause congestion. However, designing a grid based on uncoordinated load peaks is considered a highly inefficient and overly expensive approach, especially as load peaks will increase in amplitude more than in frequency in the future (Arnold et al., 2024). Moreover, grid expansion faces delays in numerous countries and struggles to keep pace with the rising demand (IEA, 2023a). The third option involves granting DSOs the authority to intervene and limit EV charging during critical hours to prevent grid congestion, as proposed by von Bonin et al. (2022). This can be achieved through methods such as volume signals. Actively restricting charging processes allows the grid operator to ensure stable grid operation, whereas passive solutions like time-varying grid fees may encourage herding behavior. While volume signals still impact EV users' goals, they represent a more cost-effective approach than extensive grid expansion, as demonstrated by Spiliotis et al. (2016) and Heilmann and Wozabal (2021). The inconvenience of adjusting the charging strategy could be compensated, as proposed by Schittekatte et al. (2023). Consequently, the third option emerges as the most promising strategy for integrating more electric vehicles into distribution grids in the short and medium term, forming the central focus of this paper.

With an intervention, the actual charging strategy would need to be adjusted whenever bottlenecks in the distribution grid are imminent. The grid operator would thus have to influence the charging process by sending out signals. In electricity markets, where DSOs have to be unbundled, such as in Europe<sup>1</sup>, grid operation and the optimization of EVs charging strategies have to take place separately due to regulatory provisions. However, the current discussions revolve around granting the grid operator access to a certain extent, thereby

<sup>&</sup>lt;sup>1</sup>Exceptions exist for DSOs with more than 100,000 customers European Commission (2010)

considering constraints from grid operation in optimizing charging processes. Uncertainty surrounds how the grid operator gains influence over the charging process and how the characteristics of the grid can be taken into account in optimizing charging processes. In Germany, this discussion is taking place within the framework of the design of §14a EnWG (BNetzA, 2023). Here, the DSO could limit charging power with high grid utilization in certain hours. In general, intervention options vary in terms of the information involved, from details about grid utilization to individual load profiles and the potential for discrimination. These interventions can treat all households equally, or the grid operator could have the authority to exert individualized control.

Although various academic papers address optimized charging based on price signals and DSO interventions to avoid grid congestions, comparative studies on the effectiveness of different curtailment strategies under various tariff designs are limited. Research by Schittekatte et al. (2022) and Valogianni et al. (2020) has highlighted the importance of dynamic pricing and ToU tariffs in incentivizing load shifting and addressing consumer preferences. However, these studies often do not fully account for the grid infrastructure's constraints, potentially leading to increased peak loads and grid congestion as seen in Daneshzand et al. (2023). In contrast, research by Spiliotis et al. (2016) and Heilmann and Wozabal (2021) discusses the potential of volume signals and other intervention mechanisms to prevent grid overloads. Yet, comparative analyses of different curtailment strategies alongside diverse tariff designs remain sparse. For example, while von Bonin et al. (2022) explores the feasibility of curtailing EV charging during critical hours, the interactions between these interventions and various dynamic pricing models have not been thoroughly examined. Similarly, as Stute and Klobasa (2024) investigates the interaction between electricity tariffs and grid charges, further research is needed to explore the interplay between electricity tariffs and curtailment strategies. This includes understanding how different tariff designs impact the effectiveness and financial implications of curtailment measures, ensuring a balanced approach that considers both grid stability and user cost efficiency.

Our paper contributes to the ongoing discussion by examining the effects of different intervention designs on optimal charging strategies within a case study centered on a synthetic German grid. The synthetic grid consists of 12 different distribution grids, accounting for heterogeneous configurations. We aim to understand how various intervention options impact the optimal charging strategy. Initially, we identify optimal charging strategies based on different tariff designs, excluding considerations related to the grid. If grid congestion becomes a concern, we then introduce grid interventions through various curtailment strategies. We differentiate between generalized curtailment (treating all electric vehicle users equally behind the bottleneck) and differentiated curtailment (adjusting curtailment based on each user's impact on the bottleneck). Additionally, we explore fixed curtailment rates, independent of factors like current transformer overloads and variable curtailment rates, which depend on the real-time load.

We address the following research questions: How do different tariff designs influence the optimal charging strategy of EV users and the resulting grid utilization? How do various DSO intervention rights affect the optimal charging strategy of EV users in terms of charging costs and required flexibility under different tariffs? Besides answering these questions, our research contributes to the existing literature as follows:

- Analysis of mutual influences of charging strategies and interventions of grid operators.
- Development of a model framework to analyze the interdependencies of users, retailers, and grid operators in distribution grids.
- Application of the model framework to a case study for Germany based on a synthetic distribution grid.
- Sensitivity analyses on the effect of different EV penetration rates.

Consistent with prior research, such as von Bonin et al. (2022), our findings indicate that implementing time-variable tariffs brings financial advantages for consumers, but they are relatively minor. The weighted average cost savings reach 47.2 EUR per year in the case of Real-time tariffs and 16.9 EUR per year with ToU tariff, reflecting only 1 to 3% of total electricity costs. However, we find that time-variable tariffs, especially at high EV penetration rates, can lead to herding behavior and increase the peak load. To address this issue, DSOs need intervention rights to avoid grid congestion effectively. We show that all proposed intervention strategies are suitable to prevent congestion, although differences can be observed regarding their efficiency. The extent to which the DSO can convey differentiated signals, incorporating spatial and temporal differences, correlates closely with the optimal benchmark's accuracy, assuming perfect information and user discrimination. The choice of the curtailment strategy has a greater influence on the need for flexibility than the design of time-variable tariffs. From the end user's perspective, curtailment does not affect charging costs significantly, especially concerning ToU tariffs or low EV penetration rates. With RT tariffs and higher penetration rates, the choice of the curtailment strategy is more relevant. Then, basic curtailment increases charging costs by 4.7 EUR per year, while more sophisticated curtailment results in a slightly lower increase of 2.6 EUR per year. But still, from the end user's perspective, the financial benefits of smart tariffs outweigh the cost increase due to curtailment.

The paper is structured as follows. Section 2.2 introduces the electricity tariff designs and possibilities for DSO interventions. Section 2.3 details a method for modeling different grid intervention strategies in optimizing charging processes based on tariff designs. Section 2.4 applies this method to a synthetic distribution grid, while Section 2.5 discusses our findings. Section 2.6 concludes this paper.

# 2.2. Electricity tariff designs and possibilities for DSO interventions

The charging processes of electric vehicles can be controlled both passively and actively. With passive control, users are incentivized to shift their load, e.g., in response to price signals. Thus, users' charging decisions are influenced only indirectly. With active control, users' charging decisions can be overruled remotely, e.g., by volume signals to modulate the charging power of charging processes (IEA, 2022b). In this study, we analyze the interdependencies of time-varying electricity prices provided by retailers and volume signals from the DSO to curtail charging processes to avoid grid congestion. In this section, we introduce the different considered design options for these signals. Section 2.2.1 introduces the different retailer tariffs and Section 2.2.2 presents possibilities for interventions by the DSO. The combination of different retailer tariffs and intervention strategies is presented in Section 2.2.3.

### 2.2.1. Electricity tariff designs

In terms of (retail) price signals, there are various tariff models with different structures, ranging from flat rates to piece-wise flat rates to fully dynamic pricing. The latter two belong to the group of (time-)variable price signals, which can help address the growing price volatility in wholesale markets while consumers can benefit economically. By shifting charging processes to periods of lower prices, charging processes are implicitly shifted according to the availability of intermittent resources (Schittekatte et al., 2022). In this paper, we distinguish three specific tariff designs: a Fixed (Fix) tariff and two time-dependent tariffs known as Time-of-Use (ToU) and Real-Time (RT) tariffs.

### Fixed (Fix) tariff

Consumers pay the same electricity price regardless of when they consume electricity. Thus, Fixed tariffs do not incentivize a shift in charging processes. The retailer bears the price risk of the wholesale market but adds a risk premium to the tariff.

### Time-of-Use (ToU) tariff

Time-of-Use tariffs provide time-variable electricity prices in certain predefined time windows. The tariffs segment the day into sections with equal price levels corresponding to the overall load (i.e., low, mid, and high). The differentiated prices incentivize a shift of charging processes into lower price windows.

### Real-Time (RT) tariff

Real-Time tariffs are fully time-variable, with the retailer forwarding volatile wholesale prices and price risk to the customers. However, if all EVs in a distribution grid receive the same high-resolution variable electricity price signal, it can lead to herding behavior and a high simultaneity of charging processes.

### 2.2.2. DSO interventions

Responding to electricity price signals could result in herding behavior of charging processes, which may cause congestion issues in the distribution grid by concentrating charging power within specific time intervals. Consequently, the DSO may need to intervene actively and provide signals to electric vehicles, including curtailing their charging processes. To determine effective signals, the DSO requires access to information on grid utilization and user behavior, as well as the ability to interact with the charging stations of electric vehicles. In future energy systems, the level of digitization and the corresponding availability of information remains uncertain. Additionally, the treatment of charging stations, whether equal or individually controlled with possible discrimination, depends on the regulation of DSO. Consequently, various design options for DSO interventions are possible, differing regarding information availability and discrimination. We consider three different curtailment strategies to reflect different intervention options: basic curtailment, variable curtailment, and smart curtailment.

### Basic Curtailment

Basic curtailment involves limiting charging processes based on anticipated congestion. DSOs use standard load profiles and probabilistic methods in non-digitized distribution grids to predict grid congestion. Once a DSO anticipates congestion in the distribution grid for a specified time interval, it can reduce the charging power of all charging stations downstream of the bottleneck. In this approach, the DSO applies the same fixed curtailment factor for the entire distribution grid. Charging processes are implicitly shifted to less critical time intervals by curtailing peak loads. However, this approach can be overly restrictive and may result in inefficiencies.

### Variable Curtailment

Variable curtailment builds upon the Basic Curtailment approach but introduces time-dependent curtailment signals. Instead of applying a fixed curtailment factor for the entire distribution grid, the DSO selectively curtails only the electric vehicles behind the anticipated bottleneck as necessary. Consequently, all users behind the bottleneck are treated similarly but more efficiently than under Basic Curtailment.

### **Smart Curtailment**

Smart curtailment, as defined in this paper, represents the optimal intervention of the DSO assuming perfect information and individual treatment of each charging process. With perfect information, the DSO is aware of EV users' economically optimal charging schedules and can calculate each household's time-dependent impact on grid elements. Based on this information, the DSO can forward individual and time-dependent curtailment factors to each household, effectively managing and optimizing charging processes within the grid.

### 2.2.3. Combining tariff designs and DSO intervention strategies

By combining different tariff designs with various DSO intervention strategies, nine different use cases are formulated, as represented by the boxes in Figure 2.1. Additionally, a hypothetical case with no curtailment is considered a reference to illustrate potential bottlenecks that may occur before curtailment.

#### Tariff designs Real-Time tariff (RT) Fixed tariff (Fix) Time-of-Use tariff (ToU) Tariff with three price levels (low. Flexible tariff representing the Time independent flat price mid, high) in different time windows wholesale price fluctuations No curtailment Fix RT ToU Hypothetical case Basic curtailment (Basic) **DSO intervention** Basic-Fix Basic-ToU Basic-RT Charging power is limited across the board in critical situations Variable curtailment (Var) Var-Fix Var-ToU Var-RT Charging power is limited with variable factors in critical situation Smart curtailment (Smart) Smart-Fix Smart-ToU Smart-RT Charging power limited according to marginal contributions of assets

Figure 2.1.: Combinations of electricity tariff designs and possibilities for interventions by the DSO

The figure illustrates how we label our different use cases. Each combination of DSO intervention and tariff design is labeled with an individual name.

Combining a specific tariff design with one possible intervention strategy reflects one setting for optimizing households and the related charging processes. Our model approach will be described in the following section.

# 2.3. Grid interventions in the context of optimizing charging processes

This section introduces a new model to analyze the effects of different electricity tariff designs combined with DSO intervention concepts on grid utilization and electricity costs. The model comprises two key components: an asset optimization model and a grid model. The asset optimization model enables households to optimize their charging strategies based on price signals. It incorporates grid information through load and generation distribution factors, calculated by the grid model. These factors are integrated into the optimization model using new equations that account for physical constraints. The linkage between the two components is implemented in three distinct ways, each corresponding to different intervention strategies. By integrating grid signals into the central asset optimization, our comprehensive model captures the interplay between grid characteristics and the economic optimization of charging processes. This approach maintains the computational efficiency of both the market and grid models while providing a holistic perspective on their mutual dependencies. The modular nature of the model linkage, distinguishing controllable from non-controllable assets, ensures applicability to various distribution grid topologies and scenarios.

We assume rational behavior for households and do not consider individual utility functions. Additionally, all electric vehicles in the distribution grid are subject to the same tariff, without exploring tariff differentiation between users. The model is based on exogenous electricity prices, meaning that feedback from EV charging behavior on the electricity wholesale market is not considered. Furthermore, while the model focuses on congestion in distribution lines and transformers, it does not account for potential voltage band violations. Another important assumption is that only electric vehicles are controllable within the model to separate the impact, whereas other distributed energy resources, such as photovoltaic systems and heat pumps, are assumed to operate independently of the optimization process.

The structure of this section begins with Section 2.3.1 providing an overview of the general modeling process. Subsequently, the asset optimization model, aimed at minimizing household electricity costs, and the grid model are detailed in Sections 2.3.2 and 2.3.3, respectively. Finally, the three different approaches for linking the models are discussed in Section 2.3.4.

### 2.3.1. General model approach and structure

Figure 2.2 shows how the asset optimization model and grid model interact in an iterative process to quantify the effects of different tariff structures and intervention options of the DSO. The process slightly differs between basic, variable, and smart curtailment. The columns relate to different simulation or optimization steps.

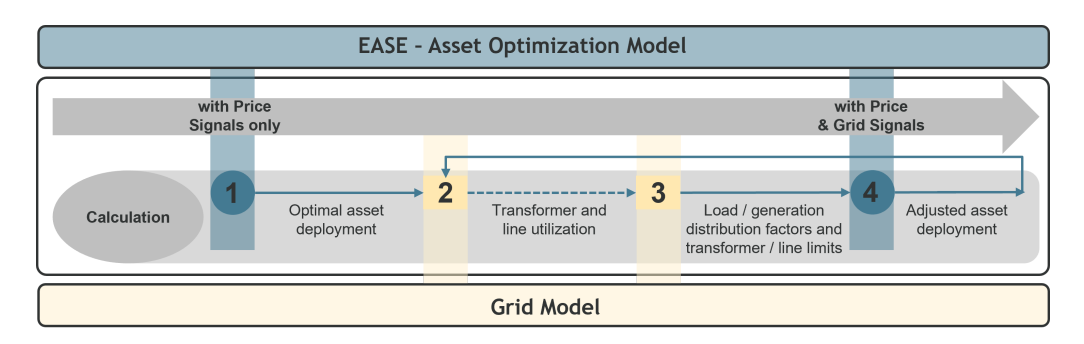


Figure 2.2.: Process diagram illustrating the various optimization and computation steps

In the first step, the simulation and optimization of all decentralized assets and households are done by running the optimization model without considering the grid. Fixed, ToU or Real-Time prices are used depending on the selected tariff design. One of the results is the optimal charging strategy for each household.

In the second step, an AC power flow is performed to check the validity of the optimization results. The analysis leverages the outputs from the asset optimization model EASE, including the generation and load time series for all assets within the distribution grid, along with their locations and the associated grid components. If there is no congestion, the model will stop here, which is indicated by a dotted line.

In the case of line or transformer overloading, the third step follows. Here, the necessary parameters are calculated to consider the grid situation within the optimization model. The method of calculation varies according to the curtailment strategy. Regarding basic and variable curtailment, the generation and load distribution factors are calculated only for the respective time intervals and congested elements. In the case of smart curtailment, the generation and load distribution factors are calculated for all time intervals and grid elements together with the line and transformer capacity limits, representing perfect information. Generation and load distribution factors as well as the capacity limits are passed to EASE. Depending on the curtailment strategy, the respective constraints are parameterized and used in the optimization model to reflect the signals from the grid, as described later in Section 2.3.4.

Then, the optimization model is rerun in the fourth step, considering the additional constraints depending on the curtailment strategy. These new constraints are constructed with the generation and load distribution factors as well as the line and transformer limits and reflect the signals from the grid.

The validity of the asset operations concerning potential grid constraints is rechecked by repeating the second step. If there is no congestion remaining, the process stops now. But, in the case of basic and variable curtailment, new congestion can occur by shifting the load to time intervals when charging power is not limited. Consequently, these additional time intervals must then be considered additionally. This is done by rerunning step 3 and updating the matrices

with generation and load distribution factors. In the case of variable curtailment, the curtailment factor  $e_{c,q}$  is increased marginally when necessary. In the case of smart curtailment, the process ends here, except that the nodal balance of individual nodes within the distribution system after step four changes the sign from the result after step one.<sup>2</sup>

The two main components of the model, the asset optimization model EASE and the grid model, are explained in greater detail in the following sections, before presenting the formulation of the new constraints for the asset optimization model to account for grid limitations.

### 2.3.2. Optimization of decentralized energy systems

In this study, we develop a model for the economic analysis of decentralized energy systems. It is designed as a linear optimization program that maximizes individual entities' profits following a price-taking assumption and the assumption of perfect foresight.<sup>3</sup> The operation of decentralized, controllable assets is optimized based on technical and economic parameters. The model also allows for analyzing the effects of fixed and variable retail tariffs.

The model can simultaneously optimize the electricity and heat turnover for multiple households in a distribution grid. The model comprises electricity-related consumption and production technologies with all relevant parameters, such as heat pumps, electric vehicles, storage units, and entities with heat and electricity demand. Although our primary focus is on EVs, we include all relevant technologies in our model to provide a more comprehensive and realistic representation of the grid. This holistic perspective allows us to understand the broader implications of EV charging strategies and DSO interventions within the distribution system. The model maximizes each household's profit while covering the heat and electricity demand. Depending on the setting, the required electricity for direct consumption or heat production is either produced by the households' technologies, such as PV systems, or obtained from an electricity supplier. Maximizing the profits, thus, is equivalent to minimizing the cost of energy supply. The objective function is expressed in Equation (2.1).

$$\max \sum_{q \in Q} \left[ \sum_{c \in G_{el}} P_{c,q}^{g_{el},f} * m_c^f - \sum_{c \in L_{el}} P_{c,q}^{l_{el},p} * (p_q^w + t) \right]$$
(2.1)

The model optimizes the asset deployment for each time interval q. The first term of the objective function, for each generation unit c, represents the generation

<sup>&</sup>lt;sup>2</sup>Nodal balance could switch from positive to negative or the other way round after one iteration. For example, a load node could become a generation node if PV generation remains high and the load is curtailed and shifted to other time intervals. Then, the generation and load distribution factors are calculated again in step three for all time intervals and nodes. The highest values from the first and second iterations determine the new matrices.

 $<sup>^3\</sup>mathrm{We}$  have formulated the model in GAMS version 45.0.

ated electricity in the interval q, which is fed into the grid and reimbursed by the feed-in tariff  $m_c^f$ . The second term represents electricity procurement for each electricity-consuming asset. The parameter  $p_q^w$  represents the provisioning component of the consumer price, while t comprises the taxes and levies. The optimization process is subject to several constraints.

The Equations (2.2) to (2.5) are demand and supply equations for electricity (2.2, 2.3) and heat (2.4, 2.5). The equations break down energy generation and consumption to their purposes. The electricity generation  $P_{c,q}^{gel}$  splits into electricity fed into the grid  $(P_{c,q}^{gel,f})$  and provided for electricity consumers  $c' \in C$  on-site  $(P_{c,c',q}^{gel})$ . The electricity consumption  $(P_{c,q}^{lel})$  in Equation (2.3) splits correspondingly into electricity procured  $(P_{c,q}^{lel,p})$  from an electricity provider, and the consumption covered by on-site generation units.

$$P_{c,q}^{g_{el}} = P_{c,q}^{g_{el},f} + \sum_{c' \in L_{el}} P_{c,c',q}^{g_{el}} \quad \forall q \in Q \land c \in G_{el}$$
 (2.2)

$$P_{c,q}^{l_{el}} = P_{c,q}^{l_{el},p} + \sum_{c' \in G_{el}} P_{c,c',q}^{l_{el}} \quad \forall q \in Q \land c \in L_{el}$$
 (2.3)

$$P_{c,q}^{g_{th}} = \sum_{c' \in L_{th}} P_{c,c',q}^{g_{th}} \quad \forall q \in Q \land c \in G_{th}$$
 (2.4)

$$P_{c,q}^{l_{th}} = \sum_{c' \in G_{th}} P_{c,c',q}^{l_{th}} \quad \forall q \in Q \land c \in L_{th}$$
 (2.5)

The Equations (2.6) to (2.16) set the technical constraints for the considered technologies. Equation (2.6) limits the variable quarter-hourly generation of electricity generators ( $P_{c,q}^{g_{el}}$ ) by their installed capacity  $i_c$  and the time-dependent availability profile  $s_q$ . For intermittent resources like PV systems,  $s_q$  varies during the day based on the considered weather year.

$$P_{c,q}^{g_{el}} \le \frac{1}{4} i_c * s_q \quad \forall q \in Q \land c \in G_{el}$$
 (2.6)

Power-to-heat technologies, such as heat pumps and heating rods, are defined by Equations (2.7) and (2.8) based on Frings and Helgeson (2022). The first equation determines the conversion of electricity into thermal energy  $(P_{c,q}^{gth})$ . The conversion is based on the time- and asset-dependent efficiency  $\eta_{c,q}^{el}$ , including the coefficient of performance (COP). The latter equation restricts the electricity consumption  $P_{c,q}^{lel}$  based on the installed electric power.

$$P_{c,q}^{l_{el}} * \eta_{c,q}^{el} = P_{c,q}^{g_{th}} \quad \forall q \in Q \land c \in (L_{el} \cup G_{th})$$

$$(2.7)$$

$$P_{c,q}^{l_{el}} \le \frac{1}{4} i_c^{el} \quad \forall q \in Q \land c \in (L_{el} \cup G_{th})$$
 (2.8)

Finally, electric and thermal storage equations are defined in constraints (2.9) to (2.12). Equations (2.9) and (2.10) restrict the maximum state of charge (SOC) for thermal and electric storage units, including electric vehicles. Equations (2.11) and (2.12) limit the charging and discharging of storage units alike. The factor  $d_{c,q}$  represents a storage's grid connection. For regular storage units, the grid connection is constantly given  $(d_{c,q} = 1)$ . Electric vehicles, however, are disconnected from the grid during their trips  $(d_{c,q} = 0)$ .

$$SOC_{c,q}^{el} \le i_c^{soc,el} \quad \forall q \in Q \land c \in (L_{el} \cup G_{el})$$
 (2.9)

$$SOC_{c,q}^{th} \le i_c^{soc,th} \quad \forall q \in Q \land c \in (L_{th} \cup G_{th})$$
 (2.10)

$$P_{c,q}^{g_{el}}, P_{c,q}^{l_{el}} \le \frac{1}{4}i_c^{el} * d_{c,q} \quad \forall q \in Q \land c \in (L_{el} \cup G_{el})$$
 (2.11)

$$P_{c,q}^{g_{th}}, P_{c,q}^{l_{th}} \le \frac{1}{4} i_c^{th} * d_{c,q} \quad \forall q \in Q \land c \in (L_{th} \cup G_{th})$$
 (2.12)

For storage units, the continuity and the balancing constraints are shown in Equations (2.13) to (2.16). In the first equation, the SOC is determined by the SOC of the previous interval, the charged and discharged energy. Electric vehicles' electricity consumed in trips is removed once at departure. It is included in addend  $r_{c,q}$ .  $\eta$  represents the charging and discharging efficiency. The balancing equation (2.15) ensures that, at large, demand and supply are balanced, including the consumption by trips for electric vehicles.

$$SOC_{c,q}^{el} = SOC_{c,q-1}^{el} + P_{c,q}^{l_{el}} * \eta_{c,q}^{el} - \frac{P_{c,q}^{g_{el}}}{\eta_{c,q}^{el}} - r_{c,q} \quad \forall q \in Q \land c \in (L_{el} \cup G_{el}) \quad (2.13)$$

$$SOC_{c,q}^{th} = SOC_{c,q-1}^{th} + P_{c,q}^{l_{th}} * \eta_{c,q}^{th} - \frac{P_{c,q}^{g_{th}}}{\eta_{c,q}^{th}} \quad \forall q \in Q \land c \in (L_{th} \cup G_{th}) \quad (2.14)$$

$$\sum_{q \in Q} \frac{P_{c,q}^{g_{el}}}{\eta_{c,q}^{el}} + r_{c,q} = \sum_{q \in Q} (P_{c,q}^{l_{el}} * \eta_{c,q}^{el}) \quad \forall c \in (L_{el} \cup G_{el}) \quad (2.15)$$

$$\sum_{q \in Q} \frac{P_{c,q}^{g_{th}}}{\eta_{c,q}^{th}} = \sum_{q \in Q} (P_{c,q}^{l_{th}} * \eta_{c,q}^{th}) \quad \forall c \in (L_{th} \cup G_{th}) \quad (2.16)$$

Given the explained model, various operating schemes are deployed and used to analyze the different combinations of tariffs and DSO interventions explained in Section 2.2. The different electricity tariffs are modeled by parameterizing  $p_q^w$ . For the fixed tariff, the parameter is constant for all time intervals, while for the ToU tariff, it is piece-wise constant in different time windows. For modeling the RT tariff, the parameter is fully flexible in each time interval.

### 2.3.3. Grid model

The optimization model initially determines the operational strategy for the assets without considering potential grid constraints. Therefore, we perform an AC power flow to check whether the computed solution is physically feasible.<sup>4</sup> If bottleneck situations occur, assets affecting congestion have to change their load or supply. Given the various DSO intervention strategies, ranging from simple curtailment to more sophisticated approaches, it is essential to determine the impact of individual assets on the power flow through specific lines and transformers. This involves curtailing all EVs behind a bottleneck or selectively controlling the charging processes. Generation and load distribution factors provide information about the contribution of single assets to the total flow on a line. With the help of those distribution factors and the information on maximum line utilization, new constraints in the optimization model prevent bottlenecks in the distribution grid during asset optimization. While the application of distribution factors varies depending on the curtailment strategy, the calculation of these factors remains consistent across strategies. This consistency eliminates the need for multiple models, enhancing the model's simplicity and efficiency.

To calculate the contribution of single assets on line and transformer loading, we follow the approach according to Schneider et al. (2018) and Kłos et al. (2015). The approach distinguishes between generation distribution factors (gdf) and load distribution factors (ldf), allowing for the capture of both load-driven and generation-driven congestions. The most important steps to obtain the distribution factors are described in the following paragraphs.

As a first step, the AC power flow is performed with each asset's active and reactive power time series input. Based on the optimization results, the AC power flow uses the time series of each asset located in the distribution grid as input. Market results only contain information on active power dispatch, so the reactive power is calculated afterward. Based on Dynge et al. (2021), we assume a fixed power factor of  $\cos(\varphi)$  equal to 0.98 for all loads. Reactive power is calculated as given in Equation (2.17). Batteries and generators do not provide or consume reactive power.

$$Q = \sqrt{\frac{P^2}{\cos(\varphi)^2} - P^2} = \sqrt{\frac{1}{\cos(\varphi)^2} - 1} * P = k * P$$
 (2.17)

The results of the AC power flow, such as line loading and line flows, are then used as necessary inputs for the following matrix operations.

In a next step, the total flow P(Nx1) is calculated using either an upstream or a downstream approach based on power flow results. The upstream approach

<sup>&</sup>lt;sup>4</sup>The grid model is implemented in Python 3.7. The optimal power flow is calculated using pandapower version 2.2.2.

considers all feeding flows, while the downstream approach accounts for all draining flows of a given node. Following the upstream approach, an element  $F_{nm}^{in}$  of  $F^{in}$  contains the power injected at the node m if a line between n and m exists. Otherwise, the entry is zero. Additionally, the nodal generation  $p_n^g$  is added. On the other hand, the downstream approach accumulates all flows draining node nand the nodal load  $p_m^l$ .

$$P = \begin{pmatrix} P_n \\ \vdots \\ P_N \end{pmatrix} \text{ with } P_n = \sum_{n \in N} F_{n,m}^{in} + P_n^g = \sum_{m \in N} F_{n,m}^{out} + P_m^l$$
 (2.18)

Virtual nodes with generation or supply equal to the line loss are added at the middle of each line. The line is then split into two parts. Both are then without losses.

Next, the matrices of flow contribution C(NxN) and flow distribution A(NxN) are computed as shown in Equations (2.19) to (2.22), I describing the identity matrix.

$$C_u = diag^{-1}(P) * F^{in} (2.19)$$

$$A_u = I - C_u^T (2.20)$$

$$A_u = I - C_u^T$$

$$C_d = F^{out} * diag^{-1}(P)$$

$$(2.20)$$

$$A_d = I - C_d \tag{2.22}$$

The matrices C and A can be used to obtain generation distribution factors GDF (MxN) and load distribution factors LDF (MxN).

$$GDF = diag(\Lambda(G_f C_u C_t^T))G_f A_u^{-1}$$
(2.23)

$$LDF = diag(\Lambda(G_f C_d C_t^T))G_f A_d^{-1}$$
(2.24)

The  $\Lambda$  operator returns the diagonal elements of a square matrix.  $G_f(NxM)$ represents the incidence matrix with 'from'-nodes and  $G_t$  (NxM) is the incidence matrix with 'to'-nodes. The element  $gdf_{k,m}$  indicates the share of injected power at node m flowing on line k. Likewise,  $ldf_{k,m}$  indicates the share of withdrawn power at node m flowing on line k. With the distribution factors, new equations in the market model are formulated, as described in the next section.

### 2.3.4. Coupling of the asset optimization model and grid model

The way distribution factors are used to formulate new constraints in the asset optimization model reflecting line and transformer capacity limits depends on the type of grid signal associated with the curtailment approach. As presented in Section 2.2, three types of grid signals are considered. In the case of basic curtailment, the maximum load of each electric vehicle behind a bottleneck is limited during a specific time interval. Variable curtailment reflects curtailing all electric vehicles behind a bottleneck with the same time-dependent curtailment factor. In the case of smart curtailment, single EVs are individually controlled optimally to resolve congestion, assuming perfect information.

#### **Basic Curtailment**

Equation (2.25) is used for the basic curtailment concept, where the DSO applies the same fixed and time-constant curtailment factor for the entire distribution grid. In situations with bottlenecks, all EVs behind that bottleneck are curtailed with the same factor. Here, only information about congested lines and transformers is considered in the LDF matrix. Consequently, values larger than 0 reflect a contribution of node n to the power flow on a congested line or transformer k. Transferred into reality, LDF is a model-based approximation of the information regarding congestions and affected nodes behind that bottleneck. If a node with an EV contributes to congestion, the maximum charging power  $i_c^{el}$  is multiplied by 0 < e < 1.  $\alpha_c$  is a set of nodes connected to a component c. The value of e depends on the penetration rate for EVs and represents a curtailment factor determined a priori. All EVs behind a bottleneck face the same curtailment.

$$\frac{4}{h} * P_{c,q}^{l_{el}} \le \begin{cases} i_c^{el} * e & \text{,if } \sum_{k \in K} \sum_{n \in \alpha_c} ldf_{k,n,q} > 0 \\ i_c^{el} * 1.0 & \text{,if } \sum_{k \in K} \sum_{n \in \alpha_c} ldf_{k,n,q} = 0 \end{cases} \quad \forall q \in Q \land c \in L_{el} \quad (2.25)$$

#### Variable Curtailment

Variable curtailment builds upon the principles of Basic Curtailment but incorporates additional information concerning the actual load and congestion levels. Instead of applying a fixed curtailment factor to all EVs located behind a bottleneck, time-dependent signals on a quarter-hourly basis are transmitted to them. Although all EVs behind the bottleneck experience the same level of curtailment, the intensity varies over time, aligning with the real-time utilization patterns. Equation (2.26) can be formulated based on these assumptions.

$$\frac{4}{h} * P_{c,q}^{l_{el}} \le \begin{cases} i_c^{el} * e_{c,q} & \text{,if } \sum_{k \in K} \sum_{n \in \alpha_c} ldf_{k,n,q} > 0\\ i_c^{el} * 1.0 & \text{,if } \sum_{k \in K} \sum_{n \in \alpha_c} ldf_{k,n,q} = 0 \end{cases} \forall q \in Q \land c \in L_{el} \quad (2.26)$$

#### **Smart Curtailment**

For modeling smart curtailment, two more advanced equations are used instead of Equation (2.25) or (2.26) to consider optimally determined grid signals within the optimization model to prevent grid congestions. With these equations, the

selective and time-variable control of single EVs in possible. To achieve this, we assume perfect information regarding grid utilization, the impact of single nodes on power flow, and the possibility of controlling each electric vehicle individually. Assuming that only a fraction of the assets in the distribution grid is controllable, GDF and LDF only include the contribution values of the respective nodes. Consequently, for all transformers and loads, we differentiate between the total maximum capacity limit  $P_{k,q}^{max}$  and the maximum capacity limit  $P_{k,q}^{max,controllable}$  related to the nodes with controllable assets. Figure 2.3 visualizes this relationship. For simplicity, S, P, and Q reflect power values with no temporal and spatial component.

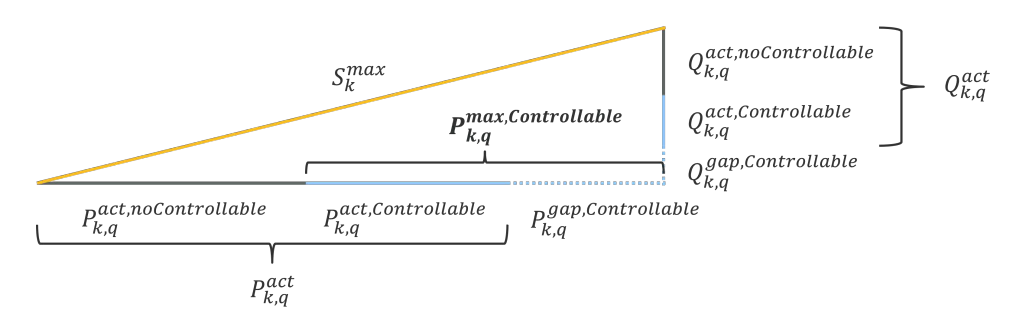


Figure 2.3.: PQ-Diagram to determine the maximum, controllable active power on grid elements

The capacity limit of each line or transformer k is defined by the maximum apparent power  $S_k^{max}$ . The apparent power consists of an active and reactive part. Each part can be further decomposed into three parts. The first part  $(P_{k,q}^{act,noControllable}$  and  $Q_{k,q}^{act,noControllable})$  respectively includes the contribution of all nodes in a specific time interval q on line and transformer flow that have no controllable assets. A second part  $(P_{k,q}^{act,Controllable})$  and  $Q_{k,q}^{act,Controllable}$  includes the actual contribution of all nodes on line and transformer flow which have controllable assets such as electric vehicles. The last part  $(Q_{k,q}^{gap,Controllable})$  and  $Q_{k,q}^{gap,Controllable})$  defines a gap that reflects the maximum additional active and reactive power on a line or transformer until the maximum apparent power is reached. In case the maximum apparent power is already reached by the actual active  $(P_{k,q}^{act})$  and reactive power  $(Q_{k,q}^{act})$ , this gap has to be negative. Dispatch of the different controllable assets has to be readjusted to stay within the maximum apparent power. In the market model, only  $P_{k,q}^{max,Controllable}$  is used, which corresponds to  $i_{k,q}^{max}$  there. Appendix A.2 describes its calculation in detail.

With the values for LDF and GDF, calculated in Section 2.3.3, and  $i_{k,q}^{max}$ , Equations (2.27) and (2.28) can be formulated in the optimization model. Equation (2.27) considers all controllable nodes with generation larger than load (genera-

tion nodes), and Equation (2.28) does the same for all controllable load nodes.

$$\frac{4}{h} * \sum_{n \in N} [max(0_{n,q}, \sum_{c \in \alpha_n} P_{c,q}^{g_{el}} - \sum_{c \in \alpha_n} P_{c,q}^{l_{el}}) * gdf_{k,n,q}] \le i_{k,q}^{max} \quad \forall k \in K \land q \in Q$$

$$(2.27)$$

$$\frac{4}{h} * \sum_{n \in N} [max(0_{n,q}, \sum_{c \in \alpha_n} P_{c,q}^{l_{el}} - \sum_{c \in \alpha_n} P_{c,q}^{g_{el}}) * ldf_{k,n,q}] \le i_{k,q}^{max} \quad \forall k \in K \land q \in Q$$
(2.28)

Components are mapped to the respective node with the matching set  $\alpha_n$ , and the balance is calculated. From the generation perspective, by multiplying the nodal generation  $(\sum_{c \in \alpha_n} P_{c,q}^{g_{el}} - \sum_{c \in \alpha_n} P_{c,q}^{l_{el}})$  with the GDF matrix, the power flow on each line caused by the respective node is computed. After summing over all nodes, the total power flow on each line or transformer k is the result. For all lines and transformers in the system, the total power flow has to be lower than the maximum capacity limit  $i_{k,q}^{max}$ . The same can be formulated for nodes treated as load nodes, as done in Equation (2.28).

# 2.4. Case study - Technical and economic effects of different intervention concepts

We employ the formulated model alongside the proposed combinations of tariff schemes and diverse intervention methods by the DSO to a synthetic distribution grid represented as a case study. Within this section, we focus on optimal EV charging strategies in combination with various electricity tariff schemes and examine the implications of distinct DSO intervention methods. The computed outcomes cater to a range of EV penetration rates. Section 2.4.1 details the case study's context and base data. Section 2.4.2 explores the first research question addressing the impact of disparate tariff structures on optimal EV charging strategies and, subsequently, grid utilization under various EV penetration rates. Section 2.4.3 is devoted to the second research question, focusing on the implications of the DSO's varied intervention concepts on optimal charging strategies, accounting for differing penetration rates. We analyze the impacts considering factors such as flexibility demand and charging costs.

#### 2.4.1. Analysis environment

We parameterize the optimization model and a synthetic distribution grid to analyze the interdependencies of various tariff designs and DSO interventions. In the following section, we provide details regarding the grid configuration, the profiles used (including renewables, electricity prices, and charging profiles), the factors for curtailment (see Section 2.3.3), and the considered period in the form of type days.

The analysis is based on the grid configuration "1-MVLV-semiurb-all-0-sw" made available by the SimBench project (Meinecke et al., 2020). The grid comprises 115 medium-voltage nodes with downstream low-voltage grids, as illustrated in Figure 2.4. However, only 12 connected low-voltage grids with six different topologies, consisting of 1015 low-voltage nodes in three different settlement types (rural, semi-urban, urban), are explicitly modeled. In contrast, the remaining 103 low-voltage grids are aggregated with a predefined load pattern at their respective medium-voltage node. The Simbench project provides a comprehensive open-source benchmark data set for the simulation of distribution grids to enable research in the field of grid analysis. The data is compared to real grid data to ensure applicability and relevance.<sup>5</sup>

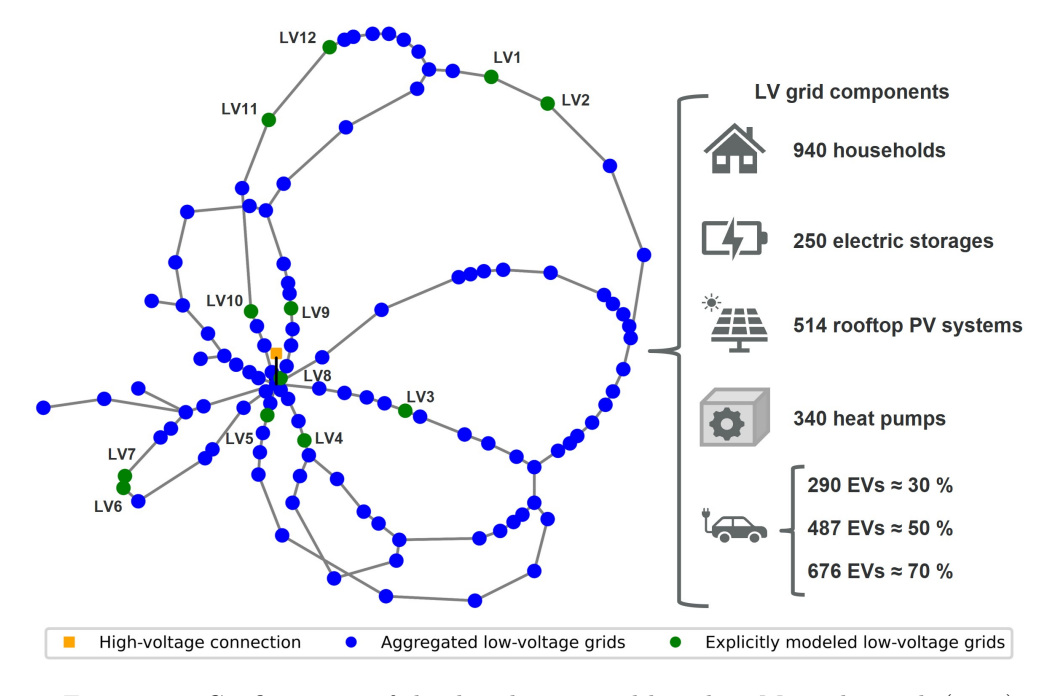


Figure 2.4.: Configuration of the distribution grid based on Meinecke et al. (2020)

Note: The distribution grid consists of 103 medium-voltage nodes with aggregated low-voltage grids and 12 medium-voltage nodes with explicitly modeled low-voltage grids. In total, 1015 downstream low-voltage nodes are considered.

The analysis encompasses various distributed energy resources, including power-to-heat, photovoltaic (PV) systems, energy storage systems, and electric vehicles (EVs). For the year 2030, the penetration rates of the individual technologies are derived from the energy system study dena (2018) for Germany and are allocated randomly. The installed capacity of the PV systems ranges from 1.7 kW to

<sup>&</sup>lt;sup>5</sup>The data is accessible via a Python API (simbench 1.5.3) and can be processed using pandapower.

around 10 kW, with a mean value of 6 kW. The batteries are 1C batteries, with capacities between 3.7 kWh and 8.8 kWh, averaging around 6 kWh. The heat pumps have an evenly distributed installed capacity of either 3 kW or 4 kW.

We model 940 households at individual nodes within the 12 low-voltage grids of different sizes. These low-voltage grids are assumed to represent relatively homogenous settlements with single-family houses. The base demand of households, excluding EVs and electric heating, is generated using a publicly available load profile generator (Pflugradt et al., 2022). In line with Birk et al. (2021), the profiles differ regarding the number of persons per household (two or four), efficiency levels, the number of gainfully employed persons, and vacation behavior, resulting in sixteen different types of households. Only households with an EV are considered controllable, as detailed in Section 2.3.

The baseline configuration assumes an EV penetration rate of 30%, representing the proportion of households within the grid area possessing both an EV and a charging station. Scaling this proportion would lead to approximately 14 million EVs in Germany (Kraftfahrt-Bundesamt, 2023), close to the target of 15 million EVs set by the German government (German Federal Government, 2022). In addition to the baseline rate, the analysis considers increased EV penetration rates of 50% and 70% to account for varying diffusion rates across individual neighborhoods and the anticipated higher overall EV penetration in the future. Within individual low-voltage grids, the EV penetration rates fluctuate between 23% and 68% for the baseline rate of 30%, reflecting variations in neighborhood affluence. Corresponding rates for EV penetration rates of 50% and 70% range from 41% to 79% and 65% to 100%, respectively. For the 12 lowvoltage grids included in this study, the total energy consumption, inclusive of EVs, equals 7.3 GWh/a for the baseline EV penetration rate of 30%, 8.7 GWh/a for 40%, and 10.7 GWh/a for 50%. Additional details regarding the properties of the modeled 12 low-voltage grids, including their topologies, can be found in Tables A.4 and A.5 in the Appendix.

Renewable generation profiles are determined based on the weather year 2015 and a representative weather station in North Rhine-Westphalia, Germany. For modeling the retail prices, we adjust the procurement component of the consumer prices for the different tariffs based on expected day-ahead wholesale prices. The prices are calculated using the energy system model DIMENSION<sup>6</sup> (Helgeson and Peter, 2020). Consistent with the penetration of individual technologies, the model is parameterized according to the future energy system scenario "EL80" from dena (2018). All components of the consumer price, such as the grid usage fees, levies, and electricity tax, are taken from the selected scenario and consistently applied across all tariffs. The value-added tax of 19% is subsequently calculated based on the consumer price components. We disregard the retailer's added margin and distribution components to streamline the model. The distribution component includes a risk premium depending on the respective tariff.

<sup>&</sup>lt;sup>6</sup>The energy system model is implemented in GAMS.

As the dynamics of the tariffs increase, the risk premium reduces due to price risks being transferred to consumers. The risk premium is virtually zero for fully dynamic tariffs. The distribution of the resulting wholesale prices and the derived average consumer prices for both the Fixed tariff and the ToU tariff can be seen in Figure 2.5. The 2030 quarter-hourly wholesale prices on the left fluctuate around 59.6 EUR/MWh with an average peak price of about 62.3 EUR/MWh.



Figure 2.5.: Electricity prices - Cumulated distribution of assumed electricity wholesale prices for 2030 (left) and final composition of the electricity prices for the Fix and ToU tariff for 2030 (right)

Note: The ToU tariff consists of three eight-hour time windows with distinct prices. The first ToU period (0-8) covers the first eight hours of the day. For the RT tariff, the grid usage fee, levies, and taxes are added to the wholesale price, resulting in different prices for each interval.

For each type day, consisting of three consecutive days, we define the Fixed and the ToU tariff based on the respective wholesale prices individually to ensure comparability of prices. On average, the procurement component for the Fixed tariff corresponds to the average wholesale price of 59.6 EUR/MWh, culminating in an average total fixed consumer price of 251.3 EUR/MWh. The ToU tariff features three price levels that apply regardless of the type of day (weekends or weekdays). The procurement components mirror the average annual prices within three time windows. On average, the tariff structure encourages charging in the first third of the day (246.3 EUR/MWh) over the last third (249.2 EUR/MWh), with charging in the second third of the day being the least favored (253.1 EUR/MWh). For the RT tariff, the procurement component of the consumer prices equals the quarter-hourly wholesale price. For the year under consideration, the prices vary between -33.2 and 475.7 EUR/MWh, with the average price aligning with the fixed consumer price. The characteristics of the EVs are summarized in Figure 2.6. The left side shows the cumulative distribution of daily energy consumption, with a mean value of about 11 kWh daily.

The EV users, thus, represent frequent commuters. The right side shows the share of EVs connected to the grid during three representative days. It shows a typical commuting pattern. At noon, EVs are not at home and, thus, not connected to the grid, while they are at night. The electric vehicles are charged up to a maximum capacity of 11 kW. EVs can be charged anything between sufficiently charged for the next trip and until the batteries are fully charged. EVs are connected to the charging station when they arrive home, even though the charging processes do not necessarily start immediately. Additionally, maximizing the self-consumption, i.e., if a PV system is available, is a fundamental consumption strategy that also affects the charging behavior. The EV data is derived from the German Mobility Panel (MOP) (KIT - Institut für Verkehrswesen, 2021), a survey-based longitudinal study of the mobility behavior in Germany, which has been published annually in several data sets since 1994. Besides household-specific information, it includes data on the households' trips, including timestamps, destinations, distances, and modes of travel. The relevant information are derived using Python.

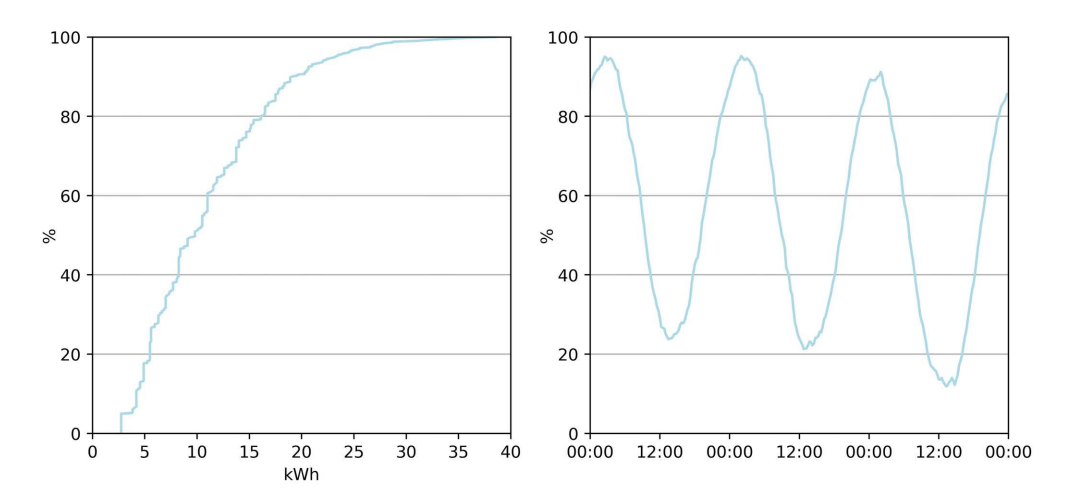


Figure 2.6.: Cumulated distribution of EVs' daily energy consumption (left) and share of EVs with grid connection over time (right)

Depending on the penetration rate and the tariff design, the curtailment factor for basic curtailment (e) (see Equation (2.25)) is varied according to Table 2.1. Each factor is used for the whole distribution grid. The variation is necessary because the need for curtailment increases with higher penetration rates and more dynamic electricity tariffs.

Table 2.1.: EV curtailment in use cases with basic curtailment

Concept	$rac{ ext{EV penetration}}{30~\%}$	EV penetration $50~\%$	EV penetration 70 %
	/ 0		.0 /0
Basic-Fix	0 %	0 %	20~%
Basic-ToU	35~%	60~%	75 %
Basic-RT	35~%	60~%	75~%

For performance reasons, the year under consideration is divided into 16 typical days to reduce the computation time. The 16 days correspond to eight winter and eight summer days, as well as eight working days and eight weekend days. The days are weighted individually and add up to 365 days. To analyze storage operation for more than one day, the preceding and following days for each typical day are included in the calculations. A detailed description is given in Birk et al. (2021) regarding the production and consumption profiles for the considered assets.

## 2.4.2. Impact of different tariff structures on optimal charging strategies and grid utilization

This section investigates how tariff structures alter EV charging strategies and consequently impact grid utilization. Initially, we scrutinize load pattern variations specific to an individual transformer and a three-day time interval across different tariff schemes. This analysis is conducted for the three EV penetration rates, denoted as 'dRates'. Additionally, we calculate changes in absolute electricity costs for each tariff design and penetration rate. We use the costs associated with the fixed-tariff scheme as a benchmark, enabling a standardized comparison of tariff cost-effectiveness and highlighting the economic implications of different tariff structures for EV charging. The results of this analysis are illustrated in Figure 2.7, divided into two parts. The left-hand side demonstrates the demand profile, visualizing how EV charging demands fluctuate under various tariff structures and penetration rates. Conversely, the right-hand side represents absolute electricity costs.

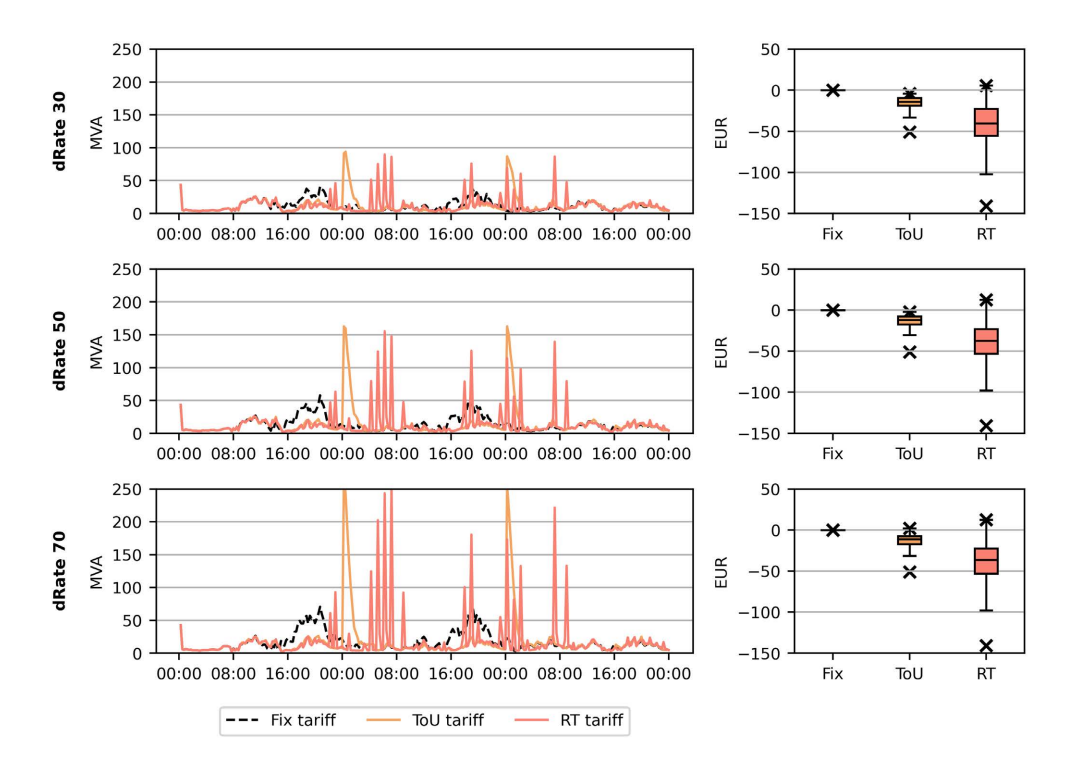


Figure 2.7.: Impact of tariff structures on optimal charging strategies and related charging costs without curtailment

Note: The left segment of the figure concretely portrays the demand patterns tied to a singular transformer for three days. The distribution of charging costs depicted on the right is calculated annually, encompassing all vehicles distributed across the twelve grids. Each row reflects the results for a given penetration rate.

Examining variations in total electricity costs for individual electric vehicles reveals interesting trends. Notably, the implementation of dynamic tariffs results in a reduction in total costs for almost all households when compared to the Fixed tariff. Among the dynamic tariff structures, Real-Time Pricing emerges as particularly influential, outweighing the impact of ToU tariffs. With the ToU tariff, households experience weighted average savings of 16.9 EUR across all penetration rates. At the same time, a stronger trend is observed with the RT tariff, where households save an average of 47.2 EUR across all penetration rates. Only a few households experience increasing electricity costs, driven by individual charging patterns correlated with high-price windows. However, when compared to the total electricity expenses of each household, the changes in costs are relatively small. Specifically, the ToU tariff decreases relative electricity costs by about 1%, whereas the RT tariff yields slightly higher savings of about 3%.

The observed fluctuations in charging costs can be attributed to the shifting demand in response to price signals. In the case of the ToU tariff, we observe demand being diverted primarily towards the early hours of the day, between 00:00 and 09:00. This shift is driven by the lower electricity prices prevalent

during this time window. Conversely, under the RT tariff scheme, the charging mechanisms are more reactive to granular, 15-minute price signals, with the demand being lowest during the night.

When considering all tariff schemes, it's important to understand that adjusting optimal charging strategies and increasing the penetration rate of EVs could potentially lead to congestion in the distribution feeders. The provided Table 2.2 analyses potential transformer overloads in the twelve Low Voltage grids, given different EV penetration rates and under various electricity tariff schemes.

Table 2.2.: Number of events of potential transformer overloadings

-	(	dRate 30 dRate 5			0 dRate 70				
$\operatorname{Grid}$	Fix	$\mathbf{ToU}$	RT	Fix	$\mathbf{ToU}$	RT	Fix	$\mathbf{ToU}$	RT
LV1	0	0	0	0	0	0	0	0	0
LV2	0	378	220	0	1014	982	41	1272	1387
LV3	0	303	180	0	920	1000	59	1218	1437
LV4	0	0	0	0	933	859	0	1077	1098
LV5	0	278	106	0	664	618	0	957	951
LV6	0	319	185	0	603	625	0	898	960
LV7	0	79	48	0	647	632	0	937	1005
LV8	0	0	0	0	23	0	0	27	19
LV9	0	0	0	0	0	0	0	0	0
LV10	0	0	0	0	0	0	0	47	17
LV11	0	0	0	0	26	20	0	497	383
LV12	0	0	6	0	0	0	0	96	43
Total	0	1357	739	0	4830	4736	100	7026	7300

Note: The number of events in each distribution grid refers to a whole year with a maximum of 35040 time steps. The total value is the sum over all events in one column.

The absence of overload events in grids LV1 and LV9, across all scenarios, indicates the resilience of these grids to increased EV penetration and tariff variations. On the other hand, for grids like LV2, LV4, LV6, and LV7, the number of overload events tends to increase with the EV penetration rate and varies significantly between tariff schemes. The RT tariff scheme shows increased susceptibility to overloads as the EV penetration rate rises. This suggests that while RT tariff schemes may offer real-time pricing benefits, they could lead to potential grid congestion when not adequately managed, particularly in scenarios of high EV penetration. The ToU tariff scheme exhibits a moderate number of overload events in the scenario with a low penetration rate, suggesting a balanced approach, but records a significant rise in potential overloads as EV penetration rates increase. The results stress the vital role that DSOs must play in ensuring the stability of the power grid. Interventions by DSOs become crucial to prevent potential transformer overloads and maintain the grid's reliability and resilience in the case penetration rates increase and dynamic electricity tariffs are introduced. The effects of different DSO intervention strategies are evaluated in the following section.

## 2.4.3. Impact of different intervention options of the grid operator on optimal charging strategies

In this section, we address the second research question of quantifying the impact of different intervention options of the grid operator on optimal charging strategies. We do so by focusing on flexibility demand to avoid grid congestion and the change of charging costs.

#### Flexibility provision in the whole grid area

The congestion on transformers and lines in the distribution grid is mitigated by flexible EV charging, as charging is shifted to other time intervals. The amount of shifted energy can be interpreted as a flexibility provision. Its value is calculated as the positive delta between the charging power of each electric vehicle before and after the grid signals as described in Equation (2.29).

$$Flex = \sum_{EV} \sum_{t} \left[ \max(i_{EV,t}^{before} - i_{EV,t}^{after}, 0) \right]$$
 (2.29)

The amount of provided flexibility by electric vehicles to avoid congestion is visualized in Figure 2.8.

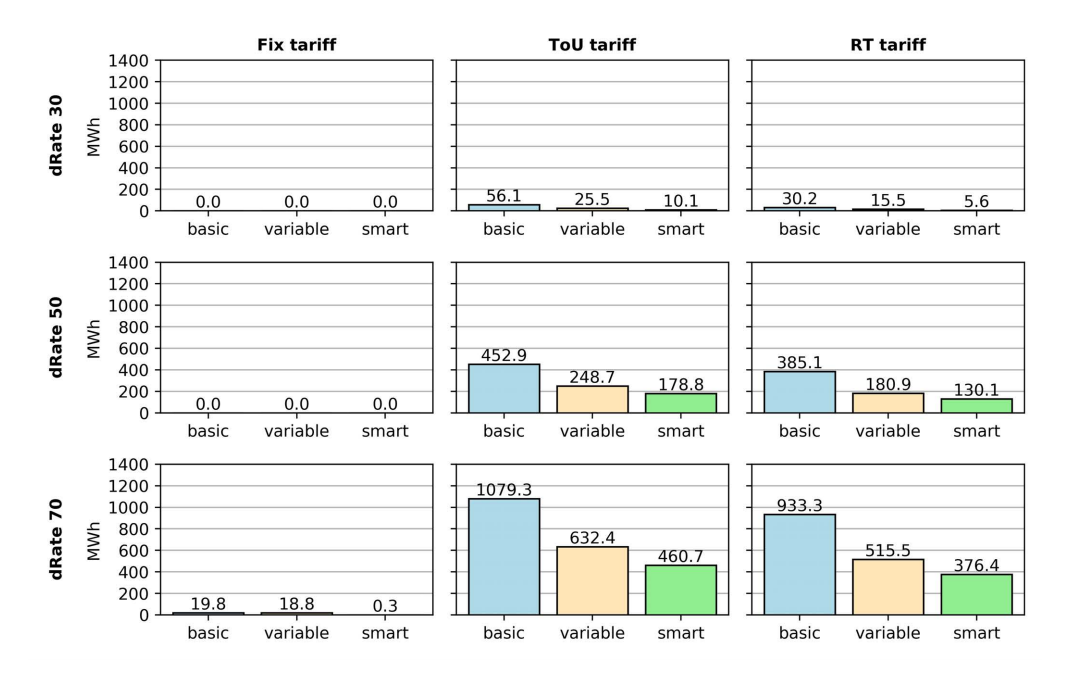


Figure 2.8.: Flexibility provision by electric vehicles

The figure above shows a significant trend: introducing time-varying tariffs, such as ToU and RT tariffs, directly correlates with increased flexibility demand

to avoid congestion. When considering a 30% or even a 50% EV penetration rate, curtailment is not required under Fixed tariffs but becomes necessary as dynamic tariffs are introduced. The magnitude of the increase in flexibility demand due to the implementation of dynamic tariffs is not constant but depends on the electric vehicle penetration rate. Specifically, it is observed that with increasing EV penetration rates, the necessity for flexibility increases across all electricity pricing schemes and both curtailment strategies. For example, in the case of the ToU tariff combined with basic curtailment, the flexibility demand increases eightfold when comparing the results for a penetration rate of 30% with those for a rate of 50%. The demand reaches even more than 1000 MWh with basic curtailment if a penetration rate of 70% is assumed. Upon reaching the maximum analyzed penetration rate of 70%, the demand for flexibility experiences a substantial surge across all electricity pricing schemes and curtailment strategies. With increasing EV penetration rates, curtailment becomes indispensable even for Fixed tariffs. Regarding the effectiveness of curtailment strategies, smart curtailment, the optimal benchmark, requires uniformly less flexibility than basic and variable curtailment across all pricing schemes, regardless of the EV penetration rate. Furthermore, variable curtailment always outweighs basic curtailment. This steady advantage highlights how a spatial and temporal differentiation of curtailment reduces the amount of flexibility and thus can help integrate more EVs into the electricity grid more easily. However, even in challenging scenarios, smart curtailment maintains its superiority over basic and variable curtailment, exemplifying its robustness and efficiency.

#### **Electricity Costs**

Figure 2.9 illustrates a comparative analysis of the annual variations in electricity costs, considering the ToU and RT tariffs, EV penetration, and the three different curtailment strategies. The comparison is made to the scenario featuring a fixed tariff without curtailment. Notably, the cost differentials for the fixed tariff are not visualized, as this tariff structure entails consistent costs irrespective of the employed curtailment approach.

The boxplots depict that both ToU and RT tariffs exhibit reduced overall electricity costs for most households with flexible charging, both before and after the application of curtailment. However, a minor increase in costs is observed for some households under variable tariffs. This is attributed to the limited flexibility of charging demand coincidentally aligning with higher electricity prices. Furthermore, on average, the RT tariff demonstrates an approximately threefold higher cost reduction than the ToU tariff. However, it is essential to note that the weighted average cost reductions compared to the fixed tariff are modest—around 1% for the ToU tariff and approximately 3% for the RT tariff. This is due to the variable component constituting only a minor fraction of the retail price. The cost delta for the ToU tariff appears almost independent of the curtailment strategy, as the deltas remain unchanged compared to the scenario before cur-

tailment. This can be attributed to the length of the chosen ToU tariff intervals, which allows for sufficient load shifting to meet the grid limitations at the same price level.

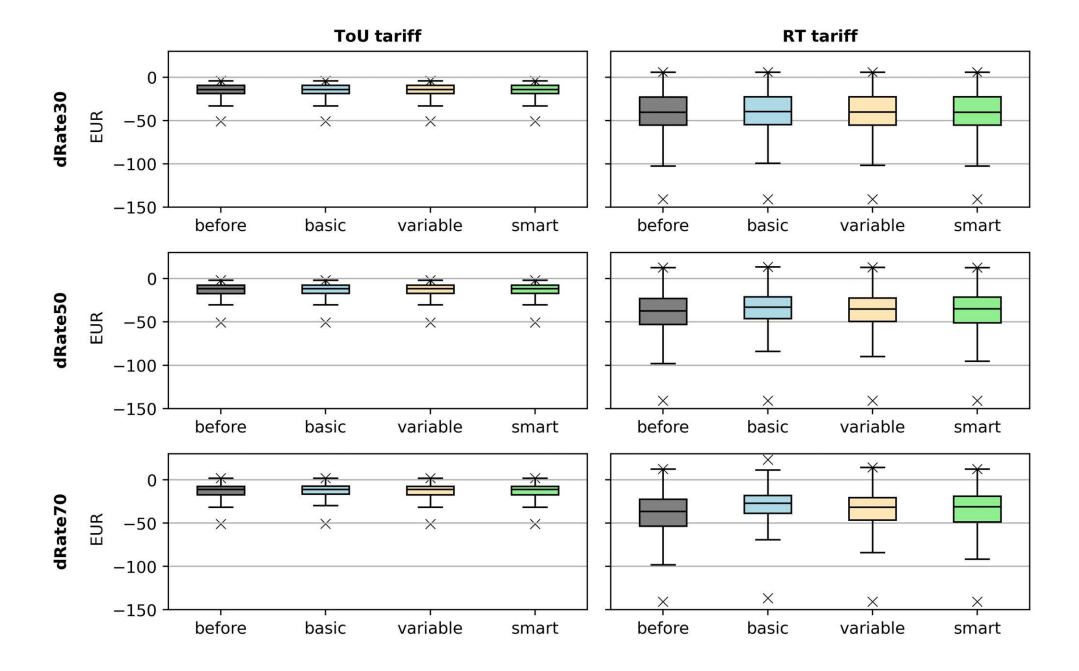


Figure 2.9.: Comparison of cost deltas

Note: 'before' refers to the hypothetical case of charging exclusively based on price signals before curtailment strategies are deployed.

In contrast, for the RT tariff, the curtailment strategy impacts the cost delta, which depends on the EV penetration rate. While curtailment has a marginal impact on cost deltas at an EV penetration rate of 30%, its effects become more pronounced at rates of 50% and 70%. Comparing these scenarios to cases without curtailment, basic curtailment, the least efficient concept, diminishes cost savings more significantly than variable and smart curtailment. This effect intensifies with an increasing EV penetration rate, necessitating more substantial load shifting to comply with grid constraints.

At an EV penetration rate of 50%, the weighted average cost delta under basic curtailment decreases by approximately 4.7 EUR compared to the scenario without curtailment. Variable and smart curtailment exhibit a milder reduction by 2.2 EUR and 1.4 EUR, respectively. Consequently, the cost savings under variable curtailment closely align with those achieved through smart curtailment. For an EV penetration of 70%, the weighted average cost delta under basic curtailment further decreases by 6.4 EUR. In contrast, variable and smart curtailment experience a more modest reduction of 2.6 EUR and 2.5 EUR, respectively. Despite this, the cost savings remain above those realized by the ToU tariff.

All in all, the shift from the Fixed tariff to a time-variable tariff has a stronger economic impact than the choice of the curtailment strategy, even at higher EV penetration rates. This implies that introducing the RT tariff, even under basic curtailment, is more efficient than a Fixed tariff or a ToU tariff. With an increasing EV penetration, however, a change from basic curtailment to smarter curtailment strategies becomes beneficial.

#### 2.5. Discussion

This study uses a synthetically constructed distribution grid consisting of several low-voltage grids to represent a future scenario concerning household generation and consumption patterns. Nevertheless, we consider our results to be generalizable for several reasons. Firstly, the synthetic grids are based on real distribution grids (see Meinecke et al. (2020)) and cover three different settlement types (rural, semi-urban, urban). Second, we distinguish a total of twelve distribution grids with six different grid topologies, which differ, among other things, in the capacity of the transformers and the number of buses. Thirdly, we distinguish ten different system combinations for households and finally, we model three different penetration levels of EVs, resulting in an EV penetration of 23% to 100% depending on the various distribution grids. In this way, we cover a wide range of load cases and different ratios of inflexible and flexible load (EVs only), implicitly considering various EV adoption rates. We cover a wide range of the inherent heterogeneity of distribution grids in terms of load, size and topology, but not completely. In this sense, the transferability of the findings from this study to other contexts may be limited. However, certain trends and findings have emerged regardless of the specific grid infrastructure.

The findings indicate that significant electric vehicle penetration does not necessarily cause grid congestion under the current market conditions, characterized by an absence of market and grid signals. For the analyzed use case, grid congestion occurs at EV penetration rates beyond 50% with a fixed tariff. This, however, is highly dependent on the respective grid topology and the current state of the expansion. IEA (2022a) find that, in German distribution grids, an EV penetration rate beyond 20% can cause significant grid adaption needs, affecting rural grids considerably stronger than urban grids. Transformers are by far the most affected grid element in this regard. An EV impact assessment study for Australia shows that depending on the grid, critical penetration rates vary significantly between 20% in rural and 80% in large urban distribution grids (Nacmanson et al., 2021). A similar study for California indicates that even EV penetration rates of 7% can cause significant overloading (Jenn and Highleyman, 2022). Rather than the EV penetration, the balance of regional demand and supply and the degree of correlation between EV load and the power generated by wind or PV systems determine how prone a distribution grid is to congestion. However, the probability of grid congestion rises due to the simultaneity of charging processes as the number of EVs increases (compare with Arnold et al. (2024))

Situations of abundant renewable feed-in are correlated with lower electricity prices. Flexible tariffs, which are driven by the electricity market prices, can thus help to integrate electricity from renewable resources, as they provide consumers with economic incentives to shift their demand to cheaper charging times with a high share of feed-in by renewables (compare with Powell et al. (2022)). This is called market-oriented charging. The results of this passive coordination in the form of a price signal depend on the consumers' willingness to participate and pay.

Like Daneshzand et al. (2023), we find that depending on the tariff design, purely market-oriented charging with a fully flexible electricity market retail price component could trigger herding behavior. It occurs when multiple users exploit the same low prices, resulting in a higher simultaneity of charging processes and, thus, higher peak loads in the respective time intervals. This would be exacerbated by additional flexible consumers, such as heat pumps. ToU tariffs represent a trade-off between non-existing (Fixed tariff) and fully dynamic market signals (RT tariff). They alleviate herding effects by incentivizing a shift of charging processes to certain time windows rather than specific points in time, as is the case with RT tariffs. This finding is consistent with Schittekatte et al. (2022), who see in ToU tariffs a reasonable intermediate step toward fully flexible time-dependent tariffs. Nevertheless, our study shows that, at high EV penetration rates, also ToU tariffs, and even Fixed tariffs, can lead to grid congestion. Price-signals, which do not take grid information into account, are not sufficient to manage grid congestion fully on their own when there is a high share of flexible demand. To enable this, prices either need a grid component (e.g., in the form of varying grid usage fees) to indirectly manage congestion based on the variable willingness-to-pay of consumers. Or they need to be complemented by volume signals which directly manage congestion as analyzed in this study.

We find that while variable tariffs cause significant load shifting, the consumers' resulting economic benefits are limited. For the chosen ToU tariff, households' cost savings are at about 1% compared to a flat tariff, while those for the RT tariff are at about 3%. This is due to the structure of retail prices, in which the electricity market component only has a small share, as electricity is taxed on a per-unit basis, and due to limited price fluctuations in the chosen use case. This is similar to Blaschke (2022), who makes the same observation for the current German electricity market. He finds that the average savings of flexible EV charging based on dynamic prices are about 22 EUR per year. In the presented future scenario, with a higher share of RES and resulting price volatility, the weighted average cost savings of EV charging with a fully dynamic tariff are 47.2 EUR per year.

Herding effects highlight the limitations of variable market signals, as they can potentially exacerbate critical load situations. But, when market signals are

paired with grid signals, grid constraints can be accounted for. However, curtailment dimensioning and planning become more complex due to the potential of passive control mechanisms to stimulate herding behavior. This complexity makes it challenging to curtail efficiently and system-oriented.

The proposed smart curtailment approach yields an optimal asset deployment considering both the electricity market and the grid. It intervenes only marginally with the purely market-oriented load duration curve and maximizes the load while complying with grid limitations. It, thus, predominantly affects higher load levels nearing full load. It marks an optimal system-oriented benchmark that indicates the minimum flexibility requirements to fulfill the charging demand under consideration of the grid, regardless of the underlying tariff. It corresponds to volume signals with the highest possible degree of spatial and temporal differentiation on a node level. However, it remains a theoretical optimum, which is challenging to implement due to the lack of transparency in distribution grids.

In distribution grids with low digitization and a lack of real-time load information, grid-oriented charging based on uniform volume signals to prevent congestion, e.g., ripple control signals is a common active control approach (basic curtailment). Fixed volume signals, with neither a spatial nor a temporal differentiation, are prone to inefficiencies since the curtailment rate might not be optimal, potentially leading to curtailment that exceeds peak load requirements. Furthermore, excessive curtailment could cause load loss if the grid signals are coordinated poorly with the market signals (Basic-RT). Although we do not observe a loss of load in the presented use case, we do see that, dependent on the EV penetration rate, close to three times more load is shifted than ultimately necessary to comply with the grid limits under consideration of an RT tariff. With a more targeted curtailment approach (variable curtailment) with a high-level spatio-temporal differentiation on a subgrid level, we observe that the flexibility demand can be reduced considerably to an offset of about 37-38% above the minimum requirements.

At the same time, we observe that the interventions of DSO only marginally affect the potential cost savings of time-variable tariffs. For the ToU tariff, we see hardly any difference in the cost savings, as the defined intervals of the ToU tariff are long enough to shift the load in a grid-oriented fashion. We observe more nuanced differences between the curtailment strategies regarding cost savings for the RT tariff, which become more pronounced with increasing EV penetration. At a 70% EV penetration, the weighted average cost savings with basic curtailment compared to purely market-oriented charging reduce by 24%, while, with a reduction of about 11%, variable curtailment is considerably closer to smart curtailment (-9%). Given the limited potential of demand flexibility to achieve electricity cost savings but a considerable potential to avoid grid expansion (Resch et al., 2021, Spiliotis et al., 2016), the real value of flexibility for households lies in avoiding grid expansion and, thus, higher grid usage fees.

Our results show that active control with volume signals can achieve feasible system states while complying with grid restrictions and avoiding loss of load, even if these are not necessarily optimal, depending on the curtailment strategy. However, without financial incentives, the acceptance of active control mechanisms is limited, as they restrict end use, impair consumer convenience, and potentially lead to, even if limited, a loss of profits, and as the necessary smart metering comes at a cost. A remuneration in case of curtailment, e.g., reduced grid usage fees, could overcome this. Nevertheless, effective coordination mechanisms between the market (electricity prices) and the grid (potential bottlenecks) cannot be overstated in ensuring the successful integration of EVs and other flexible assets. By integrating market incentives with grid constraints and capacity, we can foster user behaviors that uphold grid stability, contribute to integrating feed-in by renewable electricity resources, and provide economic benefits. It, thus, facilitates charging in a system-oriented manner. In this study, we explicitly analyze the combination of market-based price signals and grid-based volume signals. Another option would be to consider price-signals from the grid, i.e., via tariffs with varying grid usage fees. This would be equivalent to an indirect or incentive-based congestion management dependent on the consumers willingness-to-pay and their individual utility functions. While this study adds to the design of such tariffs by deriving the opportunity costs of grid congestion by determining an optimal benchmark through the smart curtailment approach, the study of EV users' utility functions is subject to further research.

In the context of implementing curtailment strategies with spatio-temporal discrimination, it is imperative that, firstly, the state of the grid is measured, that, secondly, this information is disseminated to all relevant stakeholders, and that, thirdly, it is metered at the lowest possible cost. In this regard, digitizing distribution grids by implementing smart meters and digital control devices to deliver real-time data on load, grid capacity, and constraints is inevitable. To achieve this, questions about data sovereignty and access must be answered. Additionally, the costs of smart metering are an important factor in the business case of demand response. The calculated weighted average yearly cost savings of 47.2 EUR or lower, if the grid is considered, mark an upper acceptable bound for households with a flexible EV only.

Our study reveals the opportunity costs of grid curtailment by comparing different curtailment strategies with an optimal benchmark (smart curtailment). Our research can support policymakers and DSOs in implementing curtailment strategies, which will be indispensable with the large-scale adoption of flexible technologies. Our findings indicate that even simplified methods can approach optimal performance at lower penetration levels of flexible consumers. Moreover, our results can aid in the development of incentive-based curtailment mechanisms, such as variable grid usage fees, which manage grid congestion indirectly based on consumers' willingness to pay. Additionally, it supports EV users in understanding the implications of potential tariff choices.

Policymakers should foster an environment conducive to this transformation. First and foremost, policymakers need to speed up the digitization of German distribution grids and the smart meter roll-out, as smart meters are imperative for sophisticated charging concepts. Additionally, policymakers must work towards open regulation where grid and market information can be used jointly in future energy systems. This would involve rethinking the unbundling principle, which currently limits the potential for fully integrated systems.

#### 2.6. Conclusion

As electrification of the transport sector progresses in the context of the global energy transition, fast and optimal integration of EVs into the existing energy system becomes crucial. While ensuring a market-oriented integration, the avoidance of grid congestion is imperative. For market-oriented EV charging, retailers use dynamic tariffs, incentivizing consumers to lower electricity costs by optimizing charging strategies based on those tariffs. However, due to herding behavior, this approach puts extra pressure on distribution grids, requiring DSOs to step in and curtail to prevent congestion. Design options for the intervention rights differ in the required information and the degree of spatio-temporal differentiation of the curtailment signals. The concrete design of DSO intervention rights is subject to political debate. We contribute to this by analyzing the implications of various active control approaches.

We have developed a model capable of assessing optimal charging strategies based on different tariff schemes, including fixed, Time-of-Use, and Real-Time tariffs. In the event of grid congestion concerns, we further explore various curtailment options by the DSO in optimizing charging strategies. The smart curtailment approach establishes an efficiency benchmark under the assumption of full information. Basic curtailment involves predefined curtailment factors in anticipation of congestion, while variable curtailment employs individual curtailment rates based on regional and temporal variations. By applying the model to a synthetic distribution grid configured with a future inventory of distributed assets, we show how different charging designs result in different grid loads, flexibility demands, and electricity costs.

Our research reveals that adopting time-variable tariffs yields marginal financial benefits for consumers. The weighted average cost savings amount to 47.2 EUR for the RT tariff and 16.9 EUR for the ToU tariff, representing only 1 to 3% of total electricity costs. However, we observe that time-variable tariffs, particularly at higher EV penetration rates, can induce herding behavior and increase peak load if they do not include information from the grid. To mitigate this issue, DSOs require intervention rights to prevent grid congestion effectively. Our findings indicate that all proposed intervention strategies effectively prevent congestion, although notable differences exist in efficiency. The DSO's ability to convey differentiated signals, incorporating spatial and tem-

poral nuances, closely correlates with the accuracy of the optimal benchmark. We show, that in the case of time-variable tariffs, the choice of the curtailment strategy is a stronger driver for flexibility requirements than the design of time-variable tariffs. From the end user's standpoint, curtailment has a negligible impact on charging costs, particularly with ToU tariffs. In the case of RT tariffs, cost savings diminish marginally after curtailment. Basic curtailment increases charging costs by 4.7 EUR per year, while variable curtailment only leads to a slightly lower increase by 2.6 EUR per year. While RT tariffs reduce charging costs the most, they require less flexibility to avoid grid congestion compared to ToU tariffs, although the differences are minimal. The choice of the curtailment strategy becomes relevant at higher EV penetration rates, while time-variable tariffs benefit consumers regardless of the EV penetration rate.

Based on our research, we identify several relevant areas for further investigation. While this work focuses on the flexibility of EV charging within a distribution grid, future research should explore the interactions with other flexible consumers, such as heat pumps and batteries or could even include Vehicleto-Grid. Understanding these interdependencies is crucial for a comprehensive assessment of grid flexibility. Additionally, the current approach is not limited to electrical loads. It can also be applied to generation units by utilizing both load distribution factors (LDF) and generation distribution factors (GDF). By extending the analysis to other distribution grids, potential grid bottlenecks caused by PV feed-in can also be addressed. Also, future research should analyze the impact of curtailed flexible demand on spot market outcomes, moving beyond the price-taker assumption. Additionally, examining the imbalances in power procurement by retailers and how these influence market dynamics is important for a holistic understanding of the market effects. Further investigation is needed into combining market- and grid-based price signals to evaluate the potential of incentive-based congestion management. In this context, understanding consumers' willingness-to-pay and individual utility functions, supported by empirical data, is essential to design effective incentives and policies. More sophisticated modeling techniques could be used to better model households' behavior. Finally, the economic value of using flexibility to avoid grid expansion should be a focus of future research. This analysis should be conducted from a system perspective to derive generalizable results, complementing the ongoing discussion on the value of flexibility in grid expansion.

# 3. Diffusion of electric vehicles and their flexibility potential for smoothing residual demand - A spatio-temporal analysis for Germany

#### 3.1. Introduction

The energy transition towards a decarbonized future brings about fundamental changes in the established power system, including increasing strain on distribution grid components. First, the widespread implementation of decentralized renewable energy systems, such as wind and photovoltaic (PV) systems, which are mostly connected to the low and medium-voltage grid, increases the feed-in of electricity into the distribution grid. Second, new demand applications emerge in the distribution grid, e.g., charging electric vehicles (EV), increasing the load. Both developments increase load and feed-in peaks on the national level as well as place an additional burden on the technical components of local grids, such as low and medium-voltage transformers, which were designed under different conditions and may need to be replaced or expanded to accommodate the changes. The charging of EVs can increase peak load and put a strain on existing distribution grid equipment. However, the flexibility in EV charging offers a solution to mitigate this impact. By charging during periods of high renewable energy generation, load and feed-in peaks can be reduced, thus reducing the strain on the grid.

The availability and necessity of EV charging flexibility depend on various regionally distinct factors, such as the share of the EV load in the total load, the level and structure of the residual load<sup>7</sup>, the correlation between flexibility potential and regional load or generation peaks, and the distribution of charging to the different locations (at home, at work, or other places). Thus, to fully comprehend the potential of EV charging flexibility in reducing peaks, a comprehensive regional analysis and quantification of the flexibility potential and its effects are crucial.

Two basic deployment strategies for deploying local EV charging flexibility can be distinguished. On the one hand, flexibility can be used to flatten the national residual load by reducing positive and negative peaks. That is, EV charging flexibility is used to reduce load during peak load situations and to absorb excess

<sup>&</sup>lt;sup>7</sup>The residual load is the difference between total load and generation by intermittent resources.

renewable generation during times of high generation. Such a deployment strategy aims to reduce system costs by not employing (or even investing in) expensive generation technologies and fully utilizing generated renewable electricity. An incentive scheme for such a deployment strategy would be the incentivization of flexibility deployment based on the uniform pricing signals of the national electricity market. Alternatively, flexibility can be dispatched to smooth the regional residual demand. Such a deployment strategy aims to reduce the load on regional distribution grid components. This approach would reduce costs for the expansion of these grids. Incentive schemes for such a deployment strategy would be, for example, quantity or price signals from distribution system operators according to the expected grid status. The goals of the deployment strategies may be partially opposed, and the question arises of how the two strategies affect the respective objectives.

This research paper therefore first examines the regional development of residual load, load peaks and feed-in peaks in Germany up to 2045. The analysis focuses on the spatial and temporal diffusion of EV charging, considering regional sigmoid transition pathways of EV adoption and regional and user-specific driving and load profiles. The analysis is based on NUTS 3 regional resolution level data (see Figure 3.1).

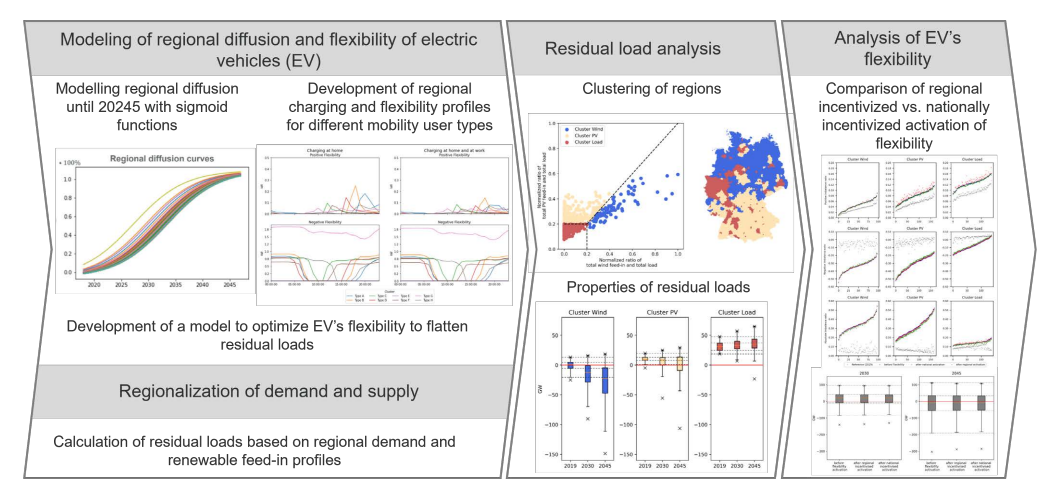


Figure 3.1.: Methodological steps

Germany is considered a suitable subject for this research as it is in an exposed position driven by its climate targets, i.e., emission reduction targets, and its geographical characteristics. Germany has pledged to reach net-zero emis-

<sup>&</sup>lt;sup>8</sup>Agora Verkehrswende et al. (2019) quantifies the investment costs in the low and medium voltage grid under the assumption of uncontrolled charging of EVs depending on the charging capacity and the number of electric cars for Germany to be 23 to 72 billion € between 2020-2030.

<sup>&</sup>lt;sup>9</sup>The Nomenclature of Territorial Units for Statistics (NUTS) is a hierarchical system for dividing European territory into territorial units. While, for example, NUTS 0 stands for states, NUTS 3 corresponds to smaller units within states, such as districts.

sions by 2045, while most other major economies are aiming for 2050 or later (United Nations, 2023). Since Germany, unlike other major economies, phased out nuclear energy and lacks significant additional hydro-power potentials, the target implies an earlier increase in decentralized renewable energy capacity than in other economies. The potential for decentralized renewable energy generation as well as (future) load is unevenly distributed within Germany. This initial situation and expected development put a strain on the grid infrastructure. The challenges that Germany faces apply to countries striving for climate neutrality in general, albeit potentially at a later stage and to a milder extent. Therefore, the findings from the study of Germany are generalizable, depending on country-specific situations and transformation paths.

Based on the analysis, a spatio-temporal optimization model for EV load flexibility is developed and implemented. The model aims to quantify the potential of EV load flexibility of home charging in smoothing residual load time series and reducing load and feed-in peaks. The focus is on the use of flexibility through the shifting of charging processes by EVs in isolation. The application of bidirectional charging or the interaction with other sources of flexibility, e.g. stationary storage, is not considered. This study compares two different deployment scenarios: (1) using flexibility to flatten the national residual load time series, which corresponds to the use of flexibility based on price signals from the national electricity market, and (2) using flexibility on regional residual load and, thus, reduce the strain on regional distribution grid components.

EV charging is considered a major source of demand flexibility, as shifting charging operations can reduce peak loads and thus reduce the need for grid expansion. Some sources note this at the transmission grid level, like Gunkel et al. (2020), who compare flexible charging and transmission grid expansion and find synergies between both, or Amann et al. (2022), who evaluate flexible charging from both, the transmission system and distributions system perspective. However, the impact of smart charging is predominantly analyzed at the level of the local distribution grid, as in Flataker et al. (2022). Powell et al. (2022) demonstrate that the flexibility of EV charging possesses not just a significant temporal component but also a geographical one, reflecting the propensity of EVs to move between locations over the course of a day. They underscore the necessity for a comprehensive area-wide charging infrastructure to facilitate daytime charging, which could utilize surplus PV generation and avert the late afternoon peak load, as exemplified by workplace charging. Such conditions have direct implications for power system requirements in terms of storage and ramping needs or emissions. Meiers and Frey (2024) find a limited peak reduction potential of EV flexibility when only unidirectional charging technologies are considered, analyzing a local microgrid. However, they find the added value of vehicle-togrid charging to be significantly higher. Analyzing the differences in national and regional impacts of EV flexibility on peak load as an important technical indicator for grid planning as well as analyzing heterogeneous regions are major contributions of this study. Given the residual load-smoothing potential of flexible end-uses, such as electric vehicle charging, there seems to be a general recognition in the European Union that local flexibility mechanisms are of significant interest for the operation of future distribution networks (CEER, Council of European Energy Regulators, 2020). Regulators have begun to put in place the regulatory framework to incentivize the provision of flexibility and its call-off by distribution system operators, which they are required to do by Article 32 of Directive (2019/944) as part of the clean energy package (Council of European Union and European Parliament, 2019).

There is an elaborated stream of research analyzing the provision of regional flexibility from a market design perspective. Radecke et al. (2019) analyze various proposed local flexibility market designs pointing out that there is no silver bullet as each design comes with deficiencies, especially regarding inc-dec gaming. Rebenaque et al. (2023) discuss flexibility market design regarding governing models, coordination problems, inc-dec gaming, and competition. However, to the best of current knowledge, there is no research addressing the concrete added value of local flexibility use in contrast to centralized electricity markets, neither for demand-side flexibility in general nor for EV charging in particular. This study attempts to fill this gap with a focus on the German power system at the national and regional levels.

From a system perspective, there are several studies that shed light on the transformation of the German energy and consumption sector until 2045 and beyond. Notably, the "Big 5 Energy System Studies", compared by dena (2022), develop various scenarios to reduce greenhouse gas emissions and implement technologies such as wind turbines, PV systems, and EVs on both the demand and supply sides. While the specific numbers on installed capacity and electric vehicles differ, the emerging trends, a significant increase compared to today, are the same. However, the studies only marginally touch on the regional perspective of the transition and the regional balance of supply and demand.

The regional matching of supply and demand for the German energy system is addressed by Kockel et al. (2022) and Kühnbach et al. (2021). Kockel et al. (2022) analyze the development of regional residual loads in Germany on a spatio-temporal basis, related to an emission reduction of 95% by 2050 based on dena (2018). They note significant potential for demand-side flexibility, but do not specifically model or quantify it. Because the study only considers 2019, with very low EV penetration, and 2050, with penetration near 100%, the EV load is determined by a uniform distribution of regional demand based on regional vehicle counts. However, this approach is not appropriate for modeling EV penetration for the years in between, as it neglects regionally varying penetration rates. For EV charging, the same profiles are used for each region, abstracting from regional characteristics such as longer driving distances in rural areas compared to urban areas.

Kühnbach et al. (2021) focuses primarily on regionalized demand and the potential of demand response. In addition to analyzing regional supply and de-

mand balancing, they examine the residual load-smoothing potential of flexible demand on a regional basis. They compare 2015 and 2030 and define indicators to measure supply-demand balance. They conclude that demand management is most effective in regions that frequently alternate between demand and supply deficits. However, the study lacks a comparison of regional results with a centralized energy system, and as in Kockel et al. (2022), the chosen scenario does not fit with Germany's recent climate protection goals of climate neutrality by 2045 (Deutscher Bundestag, 2021).

To be compatible with current German climate targets, a scenario based on KN100 from dena (2021) is developed. The analysis focuses on the years 2019, 2030 and 2045, with 2019 serving as the reference year due to a negligible penetration of electric vehicles. The year 2030 is a significant milestone in Germany's energy transition toward achieving net-zero emissions by 2045, as it is marked by numerous technology-specific and emission targets. In contrast to existing literature, this study focuses on the consistent regional and temporal modeling of EV charging demand and flexibility potentials. To this end, the EV diffusion for 2019, 2030, and 2045 is modelled by utilizing the Bass model (Bass, 1969), which has been applied to EV diffusion in various countries, such as the US (Becker et al., 2009), Korea (Won et al., 2009), China (Song, 2013), and Japan (Zhu et al., 2017). The load and flexibility profiles of EVs are derived from the mobility patterns of the German Mobility Panel (MOP) (KIT - Institut für Verkehrswesen, 2021).

This study addresses two key questions: To what extent can electric vehicle home charging flexibility reduce load and feed-in peaks at the national and regional levels? What are the impacts of the two different deployment strategies on national and regional residual demand curves, as well as load and feed-in peaks? Besides answering these questions, this paper adds to the existing literature in multiple ways:

- Analysis of the spatio-temporal evolution of residual demand under a current scenario for Germany's energy transition pathway until 2045 with a focus on EV diffusion and load.
- Introduction and application of a method for modeling target-consistent regional and temporal diffusion of electric vehicles using sigmoid functions.
- Derivation of user- and region-specific driving, load and flexibility profiles for electric vehicles in Germany until 2045.
- Development and implementation of a model for spatio-temporal deployment of electric vehicle load flexibility under different objectives.
- A comprehensive analysis of the regional and national effects of charging flexibility deployment on residual load for the case of Germany.

Concerning the development of future residual load, the analysis shows that positive and negative peaks in residual load increase over the years on the regional level and aggregated over Germany. The correlation between residual load and EV charging profiles is high in 2019 but decreases until 2045. This implies that the marginal utility of charging flexibility to reduce load peaks decreases over time, although the flexibility potential in absolute terms is increasing with growing EV adoption.

Especially in load- and PV-dominated regions, the nationally incentivized activation of flexibility can result in drastically higher regional demand peaks compared to a scenario without the use of charging flexibility. This study shows that the two scenarios of flexibility activation can be contradictory in their effects: While the regional incentivization is less efficient in reducing peaks on the national level, the national incentivization leads to increased strain on local level. The findings provide valuable insights into the challenges faced by regional grids and the development of strategies to harness EV flexibility to address these challenges.

The paper is structured as follows: In a first step (Section 3.2), regionalized diffusion curves for EV expansion from 2019 to 2045 and regionalized charging profiles for different user types are developed. Then a scenario of electricity demand development and renewable capacity expansion until 2045 is regionalized, and corresponding demand and renewable generation time series are presented (Section 3.3). In Section 3.4, a model for the regionalized optimization of EV charging flexibility is developed. The results (Section 3.5) address the estimation of residual demand time series for the years 2019, 2030, and 2045 on a regional and national level as well as the potential and effects of EV charging flexibility under two different deployment strategies. The paper concludes with a summary of the findings and their implications for the transformation of the power system and usage of EV charging flexibility.

## 3.2. Spatio-temporal expansion of private electric vehicles

This section focuses on the projection of regional expansion paths of electric vehicles and the development of a method to derive individual load and flexibility profiles for each region. Section 3.2.1 describes the applied method to derive regionalized transition pathways for electric vehicles. Each region reflects a NUTS 3 district of Germany. In Section 3.2.2, load profiles for each region are developed, distinguishing between different user types based on their charging locations and times.

#### 3.2.1. Regional diffusion of electric vehicles

Recently, several studies, summarized and compared in (dena, 2022), presented development pathways for the future energy system and the transition to e-mobility in Germany. The "dena study - towards climate neutrality" projects 14 mil. electric vehicles in 2030 and 36 mil. in 2045 in its climate neutrality scenario "KN100" (dena, 2021). Also, in the summer of 2022, the German Federal Ministry for Economic Affairs and Climate Action announced that 15 mil. electric vehicles should be achieved by 2030 (German Government, 2022). Despite these national projections and targets, there is a lack of scenarios at the regional level. Regions in Germany are very heterogeneous, and it can be assumed that the penetration rates of electric cars vary. Therefore, this study aims at decomposing the national transition scenarios to the local level based on a NUTS 3 resolution, which is, for Germany, equivalent to individual districts.

Forecasting methods for the regional diffusion of technologies can be primarily categorized into agent-based, consumer choice, and diffusion rate and timeseries methods (Ayyadi and Maaroufi, 2018). While methods of the first kind are simulation-based, simulating the interactions of agents and how these affect the market, consumer choice models depend on assumptions of consumer decisions about new technology according to certain characteristics (Kumar et al., 2022). Methods of the third kind rely on time series and diffusion rates to study technology diffusion. Existing research utilizing the latter methods primarily focuses on four diffusion models: Gompertz, as described in Gompertz (1825) and applied to hybrid vehicles in the UK by Muraleedharakurup et al. (2010), Logistic, as discussed by Kumar et al. (2022) for electric vehicles and applied to plant disease progress by Berger (1981), Bass, and Generalized Bass (Bass, 1969). The Bass diffusion model fits the described problem well because it can account for different speeds in the early and late stages of the diffusion, which is not the case for other models (Pavlidou, 2010). The choice of the Bass diffusion model is based on its ability to capture the inherent dynamics of technology adoption, particularly the distinction between early adopters and the majority who follow later. This distinction is crucial for accurately modeling the diffusion of electric vehicles, as the initial phase of adoption often involves different factors compared to the later stages. The sigmoid function form of the Bass model allows us to model these varying rates of adoption over time, providing a realistic projection of EV uptake. It has also been widely applied in the analysis of EV diffusion in other countries and for earlier years. For example, Becker et al. (2009) uses the Bass model to forecast the number of electric vehicles in the US until 2030 and Won et al. (2009) propose electricity demand by electric vehicles future prediction for Korea by using Bass' diffusion. Song (2013) and (Zhu et al., 2017) conduct similar forecasts for China and Japan respectively. The Bass diffusion model and its transformation are written in Equations (3.1) and (3.2) as a sigmoid function (Bass, 1969).

$$\frac{f(t)}{1 - F(t)} = p + q\frac{A(t)}{m} = p + qF(t)$$
(3.1)

$$F(t) = \frac{A(t)}{m} = \int_0^T f(t)dt \quad with F(0) = 0$$
 (3.2)

The function f(t) describes the likelihood of a purchase at time t with p being the probability of initial purchases at the start of the innovation (t = 0). p is referred to as the coefficient for innovators, while q is the coefficient for imitators. The two coefficients define the slope of the sigmoid function at the beginning and at the end. The cumulative diffusion level at time t F(t) equals the cumulative number of adopters A(t), which in this case reflects the number of EV owners divided by the total market size m, the total number of cars.

The diffusion level F(t) in this study's approach is described as shown in Equation (3.3).<sup>10</sup> The parameter  $t_0$  is included in the function to take the beginning of the diffusion into account and to move the diffusion curve in time. Further, the scaling factor s is introduced, which ensures that the diffusion curve reaches the maximum penetration rate in 2045. While improving the fit of the sigmoid function to the data points between 2019 and 2045, the scaling factor increases the maximum relative market potential in 2050 above 100%. Since this analysis focuses on the years until 2045, this is not an issue.

$$F(t) = s * \frac{1 - e^{-(p+q)(t-t_0)}}{1 + \frac{q}{p}e^{-(p+q)(t-t_0)}}$$
(3.3)

#### Fitting the curve

The regional scenarios of electric vehicle diffusion are derived by regional decomposition of the national scenario "KN100" of dena (2021), adjusted by the target of 15 million electric vehicles until 2030 defined by the German government (German Government, 2022). The development of regional scenarios using the Bass model is done in a two-step process, visualized in Figure 3.2.

<sup>&</sup>lt;sup>10</sup>The transformation steps are depicted in Appendix B.1.

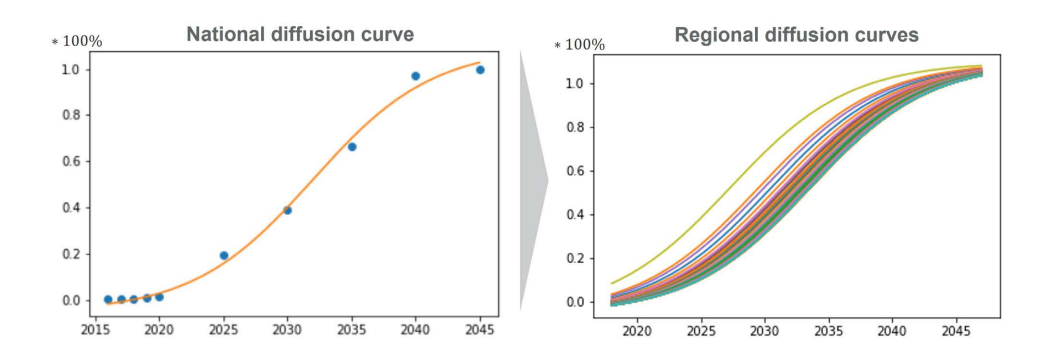


Figure 3.2.: Development of regional diffusion curves

In the first step, the Bass function is fitted to the national scenario using the non-linear least squares (NLLS) method according to Newville et al. (2016). The left part of Figure 3.2 shows the rate of electric vehicles over time. The blue dots represent the penetration rate in the different years based on historic developments (until 2020) and the national scenario. The penetration rate of 42% in 2030 matches the number of 15 mil. electric vehicles, and a penetration rate of 100% corresponds to 36 mil. electric vehicles. The parameter s, the maximum relative market potential of electric vehicles, is also computed by the fitting method. The computed values for the estimates are:  $\hat{s} = 1.096$ ,  $\hat{p} = 0.203$ and  $\hat{q} = 0.010$ .

While the derived national diffusion curve is fitted to the historic national electric vehicle penetration, historic developments in the specific German regions can drastically differ. In the start year  $t_0=2020$  (the last year regional data is available), every region has its individual position on the curve. Some regions are above the national average and some are below. Therefore, in a second step, the national diffusion curve is shifted individually along the time axis for each NUTS 3 region to achieve the specific penetration level, as it is visualized in the right part of Figure 3.2. The regional EV diffusion levels in 2020 is calculated based on historical data of the EV fleet from 2017 to 2020 on postcode level, provided by the Kraftfahrt-Bundesamt (KBA) in two data sets on car registration district (Kraftfahrt-Bundesamt, 2024b) and municipality basis (Kraftfahrt-Bundesamt, 2024a). The EV diffusion levels reached in  $t_0$ =2020 for each NUTS 3 region  $F^{nuts3}(t=t_0)$  are calculated by dividing a region's total EV fleet  $EV_{t_0}^{nuts3}$  by the ratio of the total region fleet  $Cars_{t_0}^{nuts3}$  to the total national fleet  $Cars_{t_0}^{DE}$  times the total German market size for EVs  $EV_{2045}^{DE}$ .

$$F^{nuts3}(t=t_0) = \frac{EV_{t_0}^{nuts3}}{EV_{2045}^{nuts3}}$$
(3.4)

$$F^{nuts3}(t = t_0) = \frac{EV_{t_0}^{nuts3}}{EV_{2045}^{nuts3}}$$

$$with \quad EV_{2045}^{nuts3} = \frac{Cars_{t_0}^{nuts3}}{Cars_{t_0}^{DE}} * EV_{2045}^{DE}$$

$$(3.4)$$

To create diffusion curves for each NUTS 3 region, the derived national diffusion curve is moved along the time axis according to the time difference  $\Delta t$  between  $t_0$  and the time t when the EV diffusion level for  $t_0$  of the respective NUTS 3 region is reached on the national diffusion curves. Equation (3.6) describes the approach. Here, the parameters  $\hat{s}$ ,  $\hat{p}$  and  $\hat{q}$  reflect the estimates of the national diffusion curve. The derivation of the formula, including  $\Delta t$ , can be found in Appendix B.2.

$$F^{nuts3}(t) = \hat{s} * \frac{1 - e^{-(\hat{p} + \hat{q})(t - t_0 + \Delta t)}}{1 + \frac{\hat{q}}{\hat{p}}e^{-(\hat{p} + \hat{q})(t - t_0 + \Delta t)}}$$
(3.6)

To get the total number of electric vehicles in each NUTS 3 region, the diffusion rates are multiplied by the total estimated market size of EVs for each NUTS 3 region. The latter is derived by multiplying the maximum estimated scenario value for EVs  $(EV_{2045}^{DE})$  with the ratio of the total vehicle fleet of each NUTS 3 region in  $t_0$  to the total national fleet according to Equation (3.7). To ensure that the national target of EVs in a specific year is equal to the sum of all regional numbers of EVs, a correction factor  $\sigma_t$  is used for scaling. The scaling factor adjusts the diffusion curves in a single point.

$$EV_t^{nuts3} = F^{nuts3}(t) * \frac{Cars_t^{nuts3}}{Cars_t^{DE}} * EV_{2045}^{DE} * \sigma_t$$

$$(3.7)$$

The result of the modeled diffusion of EVs is presented in Figure 3.3 for the years 2030 and 2045. In terms of consistency with the following sections, the historic distribution is visualized for the year 2019 instead of 2020. In the figure, the total number of EVs in every NUTS 3 region is normalized by the size of each region.

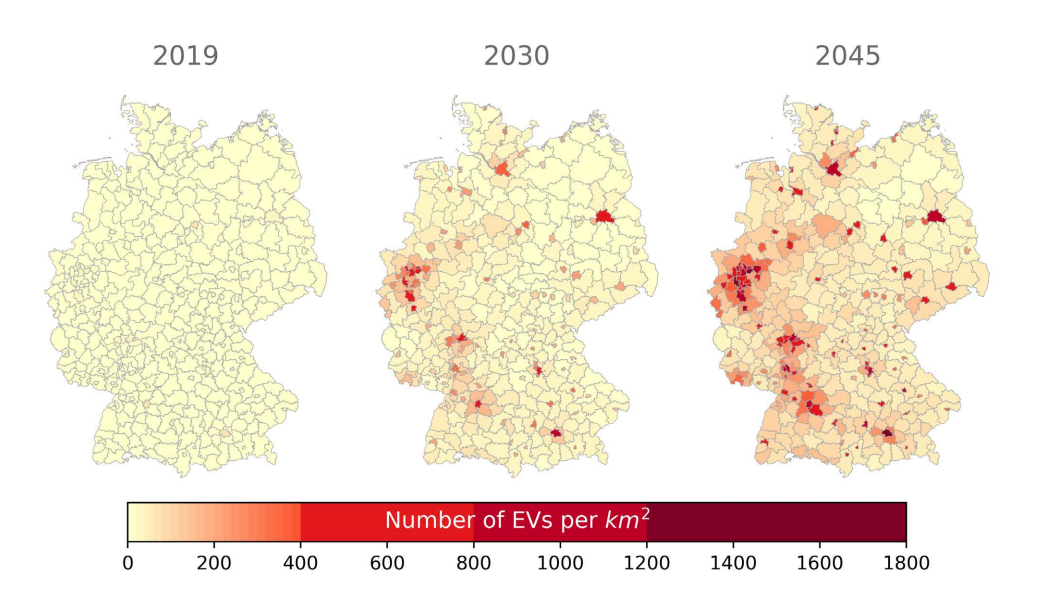


Figure 3.3.: Number of electric vehicles in each NUTS 3 region for the years 2030 and 2045

In 2019, around 239 thous. electric vehicles do not lead to high penetration rates per square kilometer. In 2030 mainly bigger cities such as Hamburg, Berlin and Munich, as well as some areas in North-Rhine Westphalia, such as Dusseldorf, do have a significant amount of electric vehicles per square kilometer. Later in 2045, the western part of Germany and the Rhine-Main region are highlighted in red. Also, smaller regions, in terms of area but with a high population per square kilometer, have a high relative amount of electric vehicles.<sup>11</sup>

#### 3.2.2. User-specific load and flexibility profiles

The electricity demand of electric passenger vehicles is determined by their underlying driving patterns. For Germany, there are two major panels surveying the mobility behavior of households, Mobility in Germany (MiD) (infas et al., 2018) and the German Mobility Panel (MOP) (KIT - Institut für Verkehrswesen, 2021). While the MiD is updated every six years, the MOP has been updated annually since 1994. It is a survey-based longitudinal study of the mobility behavior of the German population published yearly in several datasets. Besides household-specific information (datasets "HH<year>.csv"), it holds data on the households' individual trips (datasets "W<year>.csv"), including timestamps, destinations, distances, and modes of travel. The panel categorizes about 14 thousand surveyed households according to ten settlement types, from small villages to metropolises. The dataset and information on the regional settlement structure enable the assignment of households and their respective mobility pat-

<sup>11</sup> The regional diffusion curves are available in the supplementary material.

terns to different regions. The mobility behavior of EVs is assumed to not substantially differ from that of conventional passenger cars. The mobility patterns of vehicles considered constant until 2045. The detailed analysis of 500 thousand individual trips and car-based mobility patterns allows for deriving electric vehicles' energy demand and load profiles and the resulting inherent flexibility of their charging processes by user type, region, charging scenario, and day type for the years 2019, 2030, and 2045. 12

#### Computation of regional differentiated load profiles

By projecting the historical mobility data on the years 2019, 2030, and 2045, average load profiles per vehicle are calculated, which are later scaled by the individual region's total counts of EVs. <sup>13</sup> The load profiles are calculated for different settlement types, charging scenarios, and day types (weekend and weekday) for each year considered. A total of six settlement types are distinguished, ranging from rural communities to large cities. The charging scenarios represent combinations of three potential charging locations (at home, at work, at other locations). The combinatorial approach results in seven scenarios, e.g., charging at home and at work, but not at other locations. In this way, a total of 252 profiles are distinguished.

Starting from single trips, consecutive trips within a day are stacked into trip chains to derive the mobility patterns of individual cars in the form of binary time series indicating the standing and driving intervals of the vehicles, including their location. For the trips, the electricity demand is determined based on the distance traveled and the assumed EV fleet's average specific consumption of 0.21 kWh/km in 2019, 0.18 kWh/km in 2030, and 0.15 kWh/km in 2045 (dena, 2021). Assuming a charging power of 11 kW and an immediate start of charging upon arrival at a charging location, the energy demand is translated into profiles. Vehicles charge until the energy consumed during previous trips is recharged or a new trip begins. The approach therefore abstracts from modeling individual vehicle batteries and implicitly assumes that the vehicles only make trips that are covered by their batteries. <sup>14</sup> The average load profiles per vehicle are generated by aggregating all profiles and dividing them by the number of vehicles in the respective settlement type, charging scenario, and day type. As an example, the resulting profiles for medium-sized cities for the charging scenarios "charging at home" and "charging at home and work" for the year 2030 are shown in Figure 3.4. When vehicles can only be charged at home, a load peak is observed in the afternoon, while the load is more evenly distributed throughout the day when charging at home and work is possible.

<sup>&</sup>lt;sup>12</sup>A brief descriptive analysis of the mobility data is given in Appendix B.3.

<sup>&</sup>lt;sup>13</sup>All data processing, including profile computation and scaling, was conducted using Python version 3.8. In subsequent sections, region clustering is performed with the scikit-learn package, while the preparation of results predominantly utilizes pandas and numpy.

<sup>&</sup>lt;sup>14</sup>The distribution of the daily energy consumption per EV is shown in Appendix B.4 based on the EV fleet's average specific consumption in 2019, 2030, and 2045.

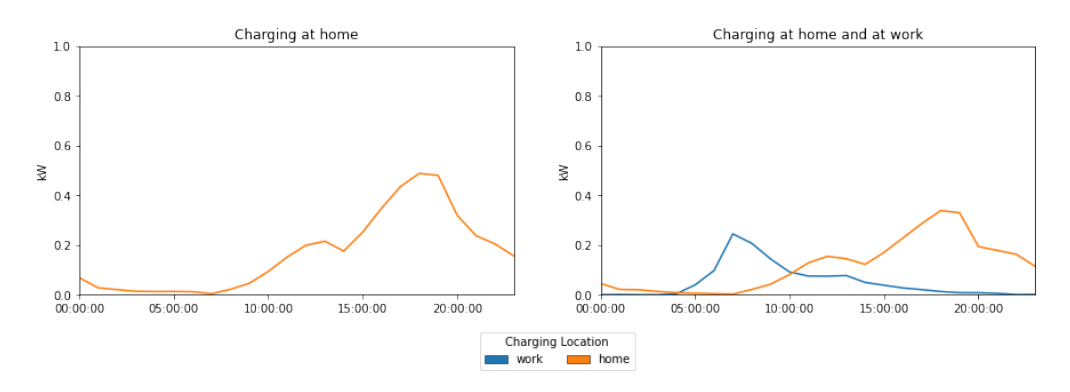


Figure 3.4.: Selected load profiles for a medium-sized city in 2045

The final hourly load time series are composed of the standardized profiles and scaled by the respective vehicle counts determined in Section 3.2.1 for each NUTS 3 region. To this end, the regional settlement types are given by BBSR (2022). The proportions of the seven charging scenarios are derived from data on vehicle parking situations at home, distinguished by settlement type based on dena and Prognos (2020).<sup>15</sup> The scaled load profiles are then used in combination with the results from Section 3.3 to calculate the regional residual load curves in Section 3.5.

#### Computation of regional differentiated flexibility profiles

To model the home charging flexibility, the flexibility potentials of the charging processes are derived from the mobility patterns and the generated load profiles. The time series of flexibility potential become an input for the flexibility model (Section 3.4), which optimizes the load shifts for charging processes relative to the determined load profiles. Generally, positive and negative charging flexibility is distinguished, with a focus on uni-directional home charging only. Positive flexibility can reduce the load of charging compared to the load profile generated in the previous section. Thus, the positive flexibility potential in each hour is equivalent to the determined load profile. Negative flexibility, in turn, means load can potentially be increased in certain intervals. Therefore, the negative flexibility potential is limited upwards by the maximum available capacity. It is calculated as the difference between the generated load profile and the maximum available capacity in each hour if the vehicle is home. Regarding the actual flexibility deployment, the use of negative flexibility is limited by the provision of positive flexibility. At any time, the cumulated negative flexibility deployment has to be smaller than or equal to the cumulated provision of positive flexibility. For computational reasons, the flexibility model does not model EVs individually (bottom-up), although this would ensure consistency in terms of EV flexibility provision: Car A reduces the load in hour X and increases the load in hour

<sup>&</sup>lt;sup>15</sup>The shares of the different charging scenarios are depicted in Appendix B.6. Within the two subgroups of charging scenarios, which include either at least partial charging at home or no charging at home, equal proportions are assumed.

Y. Aggregating all flexibility profiles (top-down) and centrally optimizing the deployment without restrictions would again lead to inconsistencies and, thus, overestimate the potential for smoothing the residual load: Car A reduces the load in hour X and car B increases the load in hour Y. To address this, this study suggests a trade-off between an aggregated centralized, top-down approach and a fully decentralized bottom-up approach using clusters. The mobility patterns are divided into multiple clusters by clustering the profiles' binary mobility patterns (at home, not at home) using k-medoids. <sup>16</sup> Bundling profiles with similar "at home" time windows ensures consistency within smaller segments of the observed trip chains. EVs are assumed to be connected to the grid while parked at home. Then, only the part of each trip chain's flexibility profile, both negative and positive, that is determined by each cluster centroid's mobility pattern, is considered, as conceptually shown in Figure 3.5 for a stylized flexibility profile.

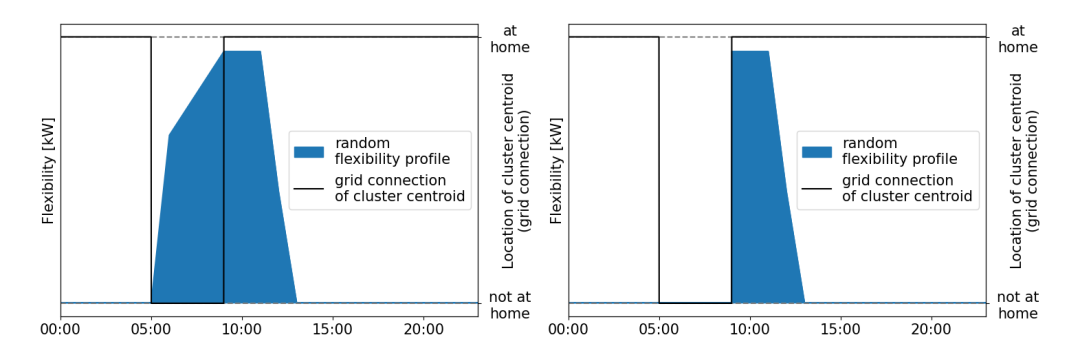


Figure 3.5.: Concept for generating flexibility clusters (stylized example)

Note: For each trip chain, the positive and negative flexibility profile is determined. However, only the part of the flexibility defined by the grid connection (at home) of the centroid of the associated cluster is considered. This ensures consistency regarding the flexibility deployment. In the left figure, the blue area illustrates the full flexibility potential of a trip chain. The right figure shows the same trip chain's flexibility potential curtailed by its cluster centroids grid connection profile.

The analysis finds eight clusters as a suitable segmentation for the observed mobility patterns for weekdays and weekends. Figure 3.6 shows the resulting eight clusters for weekdays. The respective figure for weekends and a cluster analysis is given in Appendix B.5.

<sup>&</sup>lt;sup>16</sup>In the clustering, the grid connection profiles (at home, not at home) are compared for similarity using the Python library scikit-learn.

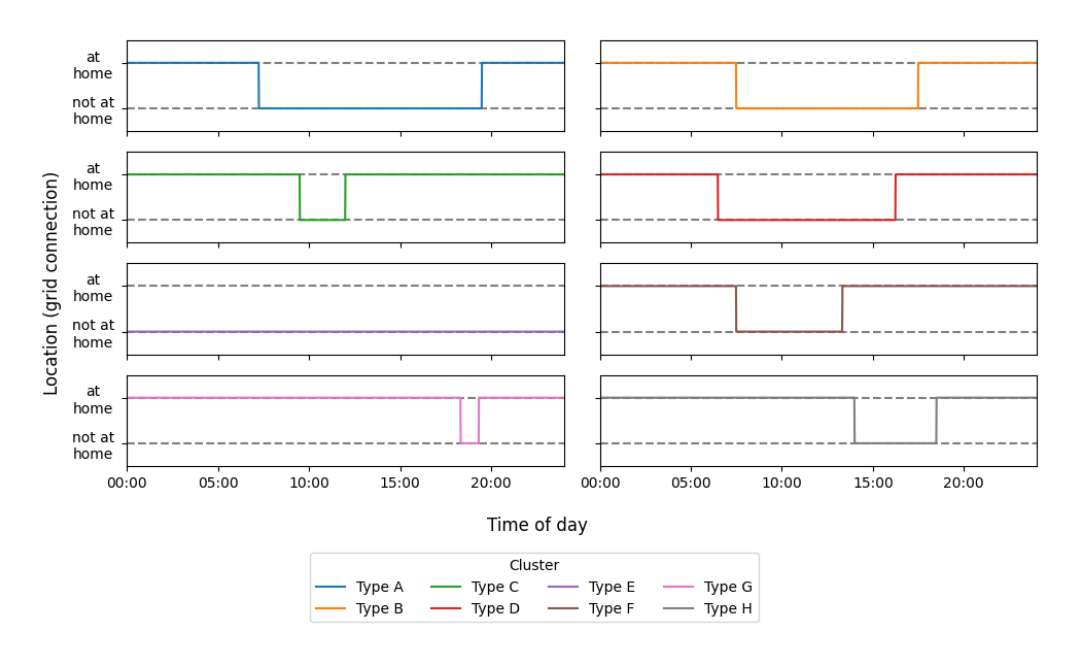


Figure 3.6.: Flexibility clusters for weekdays

Note: The figure shows the cluster centroids' binary grid connection time series (at home, not at home) for weekdays. Cars are assumed to be connected to the grid and provide flexibility while at home. The cluster centroids determine the time window for potential flexibility provision for all profiles assigned to a respective cluster.

The resulting flexibility profiles for a medium-sized city and the year 2030 are shown in Figure 3.7. Since this study only considers flexible charging at home, the positive flexibility is higher when vehicles can only charge at home. In general, the negative flexibility potential is much higher than the positive flexibility potential, as charging is generally only carried out over short periods in relation to the idle times of the vehicles.

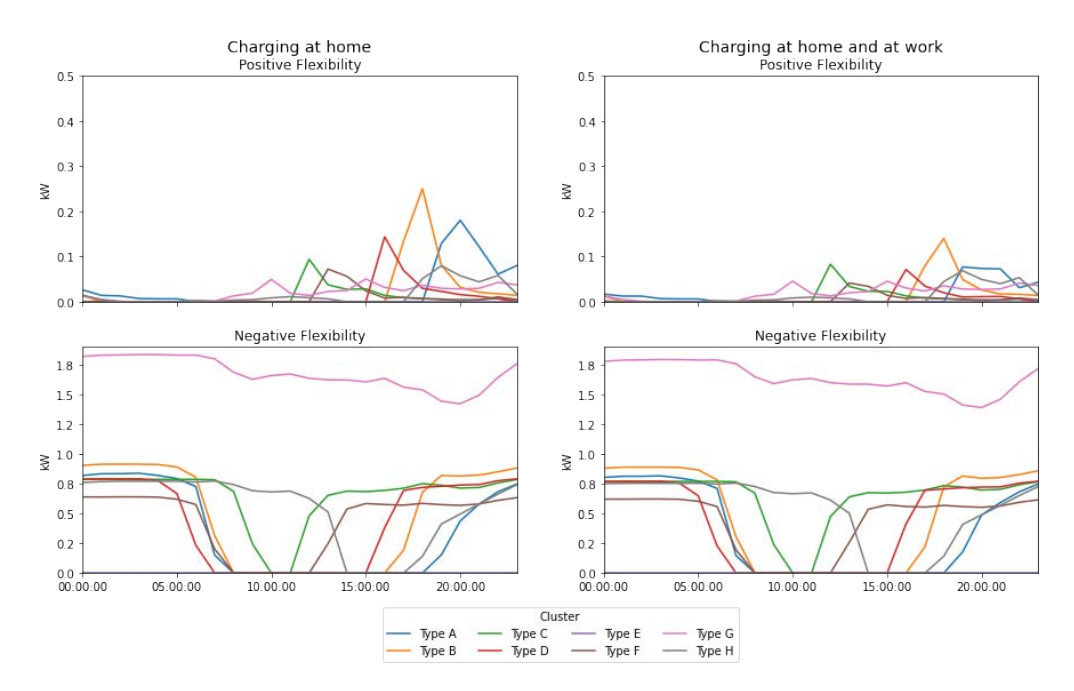


Figure 3.7.: Selected flexibility profiles for a medium-sized city in 2045

Note: Positive flexibility corresponds to a reduction, while negative flexibility corresponds to an increase of charging power. The positive flexibility potentials are determined by the charging demand at home. It is generally smaller if vehicles are partially charged at other locations as this study only considers charging flexibility at home. Also, the positive flexibility potential is smaller than the negative flexibility potential which is limited by the maximum charging power.

The final flexibility time series for each NUTS 3 region are composed the same way as the load profiles. First the average positive and negative flexibility profiles per settlement type, charging scenario, and day are determined and then scaled according to vehicle counts determined in Section 3.2.1 for each NUTS 3 region. All households charging at home are assumed to be willing to provide flexibility.

#### 3.3. Regionalization of demand and supply

In order to examine the potential of using EV home charging flexibility for smoothing national and regional residual demand, regional time series for electricity demand from other consumption sectors and electricity generation from renewable energy sources are derived. Regarding electricity demand, first the spatial distribution is calculated in Section 3.3.1 before regional profiles are derived in Section 3.3.2. Similarly, for electricity generation, Section 3.3.3 first describes the distribution of capacities, and Section 3.3.4 provides information on the associated profiles.

### 3.3.1. Spatial distribution of annual electricity demand

Consistent with the EV market development, the electricity demand development of the remaining consumption sectors until 2045 is adopted from the "KN100" scenario from dena (2021). Table 3.1 shows the assumed annual evolution of demand by consumption sector and application.

Table 3.1.: Annual electricity demand by sector and application in TWh

Sector	Application	2019	2030	2045
Households	SLP <sup>1</sup> residential	121	119	116
	Heat residential	6	20	29
	Light trucks	0	0	2
Small-scale Industries,	SLP commercial	133	129	118
Trade and Services	Heat commercial	9	21	28
	Base load	4	5	6
	Heavy trucks	0	1	2
	Light trucks	0	2	11
Industry	Heat commercial	4	9	12
	SLP commercial	17	16	19
	Base load	206	241	285
	Heavy trucks	0	5	10
	Light trucks	0	1	3
Rail transport		12	20	24
Conversion sector	8	8	8	
Passenger cars <sup>2</sup>		1	34	58
Total		522	625	732

<sup>&</sup>lt;sup>1</sup>standard load profile; <sup>2</sup>The allocation of the demand from EVs is discussed in Section 3.2. Values deviate from dena (2021) due to updated government targets (15 mil. EVs in 2030).

The spatial allocation of the demand is done in two steps. In the first step, distribution keys, matching the sector-specific electricity demand to the federal states, are derived based on data from Länderarbeitskreis Energiebilanzen (2022).<sup>17</sup> In the second step, sector-specific demand distribution keys to the regions within the federal states are derived. These are based on regional characteristics, such as residents, employees in the tertiary industry, income, and gross value added, taken from VWG (2022b) and VWG (2022a). Table 3.2 shows the weighting factors of these characteristics to allocate the demand of the individual sectors from the federal states to regions. The weighting factors are chosen similarly to BNetzA (2020).

<sup>&</sup>lt;sup>17</sup>A detailed discussion of the approach and the derived distribution keys are presented in Appendix B.7.

Table 3.2.: Annual electricity demand by sector and application in TWh

Sector	Allocated by	Weighting factor
Households, rail transport	Residents	90%
	Income	10%
Small-scale Industries,	Employed in sector	20%
Trade and Services	Gross value added in sector	80%
Industry, conversion	Gross value added in sector	100%

### 3.3.2. Temporal distribution of regional electricity demand

To derive the temporal distribution of demand, time series are determined for the individual applications, which are used to distribute the spatially distributed annual demand over the year. Four categories can be distinguished when creating the regional demand time series: Standard load profiles, time series for mobility applications, time series for heat generation, and applications for which a constant power consumption is assumed. The standard load profiles (SLP) for household consumption ("H0") and commercial consumption ("G0") are taken from VDEW (1999). The daily profiles are available separately by day of the week (Monday-Friday, Saturday, Sunday/holidays) and by season (Summer, Winter, Transition) and are matched to the calendar year 2015. The profiles for light and heavy electric trucks are taken from ENTSO-E (2022c). The daily profiles are available, separated by Monday-Friday and Saturday-Sunday, and are matched based on this distinction to the calendar year 2015. Due to the temperature dependency of the heat generation profiles, they are calculated for each region separately. To calculate the profiles for households, the standardized profiles for heat pump electricity consumption as a function of time of day and outdoor temperature from SWM (2022) are used as well as regional temperature data for 2015 from Copernicus Climate Change Service (2020). For electricity demand from commercial consumers for heat generation, the profile data from Ruhnau and Muessel (2022) is used and matched with temperature data for 2015. Last, a uniform consumption over the year for the base load, rail transport and conversion applications is assumed. Figure B.4 in Appendix B.8 illustrates the different profiles.

## 3.3.3. Spatial distribution of annual renewable electricity capacities

As a starting point, existing capacities in 2022 of onshore wind, rooftop PV, large-scale PV and hydropower are spatially distributed according to the Mark-tstammdatenregister (BNetzA, 2022). Offshore wind capacities are located in a separate offshore region and are not spatially distributed. For the future development of each technology, the methods described in the network development plan 2023 (German TSOs, 2022) are reproduced using regional capacity poten-

tials from Ebner et al. (2019). <sup>18</sup> For 2045, the announced capacity targets within the so-called "Easter package" (Bundesrat, 2022) were assumed: 160 GW on-shore wind, 200 GW large-scale and rooftop PV each.

For onshore wind, the distribution to regions is done according to the relative capacity potentials in the federal states compared to the total potential of Germany. As soon as the 2% target for each federal state is reached, the relative distribution factor in this federal state is devalued by 50%. The 2% area target thus represents a threshold value above which less area may be available for wind energy use in a federal state, thus slowing down the expansion. The remaining net expansion is then further distributed to the federal states in an iterative procedure based on the relative distribution of the respective potential. Based on the capacity assigned to each state, the capacity is further distributed to the NUTS 3 regions according to the relative potentials.

For the regional expansion of large-scale PV capacities until 2045, the regional potential areas for each federal state and the NUTS 3 regions are used as well. The target capacities for each federal state according to German TSOs (2022) are distributed by the weighted regional potentials. This is done by using a modification of the potentials. The potential area in the federal state with the highest average yield (Baden-Württemberg) is valued twice as high as the potential area in the federal state with the lowest average yield (Lower Saxony). For rooftop PV installations, the approach is postcode-specific. A constrained growth function is derived for each postcode using the change in existing installations to date and the maximum potential. This function is linear until 50% of potential is reached, and then approaches the potential limit asymptotically. This approach follows the observation that past additions have been largely linear. However, after a certain point, it decreases due to adding less suitable areas and slowly approaching the potential limit.

For hydropower, only existing capacities are regional distributed. No additional expansion is assumed.

## 3.3.4. Temporal distribution of regionally renewable electricity generation

Generation profiles for the spatially distributed renewable capacities are based on the COSMO-REA6 weather data of the year 2015 provided by HErZ, Hans-Ertel Centre for Weather Research (University of Bonn - Germany) and DWD, Deutscher Wetterdienst (2022). This dataset includes hourly measurements of wind speed, temperature, and solar irradiation across a geo-referenced weather grid spaced at 0.1-degree intervals. The weather time series nearest to the center of each region are selected to calculate feed-in profiles. For rooftop and large-scale photovoltaic systems, feed-in profiles are computed using the model for energy

<sup>&</sup>lt;sup>18</sup>The method and results are described in this publication and the corresponding data are published at: opendata.ffe.de/eem2019.

performance of PV modules described in Huld et al. (2010), incorporating the recommended coefficients. For onshore and offshore wind, power curves for standard wind turbines are utilized in combination with wind speed data. Feed-in time series for hydropower equal the historic time series from ENTSO-E (2022a).

### 3.4. Modelling electric vehicle charging flexibility

By aggregating the results of the previous sections, regionalized residual load time-series are computed and visualized in Figure B.5 in the Appendix. On the national level, positive peaks imply the utilization and steep ramping of (and the necessity of investment in) expensive dispatchable generation units. In contrast, negative peaks imply an excess of renewable energy generation. On the regional level, both positive and negative peaks put strain on distribution grid components such as transformers. Consequently, residual load curves should be smooth and close to zero. Electric vehicle charging represents one source of flexibility potential. An optimization model<sup>19</sup> for the deployment of regional flexibility of electric vehicles is developed. In the model, two deployment strategies are distinguished. Under the first strategy, the regional flexibility potential is used to flatten the corresponding regional residual load curves by reducing positive and negative peaks. This is the basic model, described in Section 3.4.1. Under the second strategy, the model is adjusted according to Section 3.4.2. Here, the flexibility potential of home charging processes is aggregated to flatten the national residual load curve instead.

### 3.4.1. Flexibility on regional level

The smoothing of the residual load has two objectives. First, to minimize the absolute distance to zero in every time step, and second, to minimize peaks. The objective functions in Equation (3.8) combines these by minimizing the square absolute value of the residual load. On a regional level, this optimization logic represents the minimization of grid expansion costs, which becomes necessary, especially when large positive or negative peaks occur. On the national level, the generation costs are to be minimized, which become disproportionately more expensive during positive peaks, which serves as a justification for the quadratic optimization approach. The objective function contains the adjusted residual load RL as a variable, which has two dimensions. One temporal  $t \in T$  and spatial  $n \in N$ . The set T contains the 8760 hours of a year, and the set N

<sup>&</sup>lt;sup>19</sup>Based on GAMS Version 42.

contains all NUTS 3 regions of Germany.

$$\min z = \sum_{t=0}^{T} \sum_{n=0}^{N} |RL_{t,n}|^2$$
(3.8)

The adjusted residual load curve  $RL_{t,n}$  equals the residual load curve before load shift  $rl_{t,n}$  plus the usage of load shift (LS), as it is shown in Equations (3.9) and (3.10).

$$RL_{t,n} = rl_{t,n} + \sum_{t_1}^{T} \sum_{u}^{User} (LS_{t,t_1,n,u} * ts_{t,t_1,u}^{max}) \quad \forall t \in T \land n \in N$$
 (3.9)

with 
$$LS_{t,t_1,n,u} = LS_{t,t_1,n,u}^{neg} - LS_{t,t_1,n,u}^{pos}$$
 (3.10)

The variable LS has two time-dimensions and is defined for every region nand every user type  $u \in User$ . Furthermore, the variable can be decomposed into a positive part  $LS^{pos}$  and a negative part  $LS^{neg}$ . Negative flexibility here means that the load increases so that the residual load moves upwards. Positive flexibility reflects load reduction. For every user type u, the binary parameter  $ts_{t,t_1,u}^{max}$  defines whether load shifting is possible from time step  $t_1$  to time step t.

With the following two Equations (3.11) and (3.12), it is ensured that the maximum LS potential is not exceeded in every time step t, in every region nand for every user type u. Two equations are necessary to distinguish between a positive and a negative flexibility potential (see Section 3.2.2).

$$\sum_{t}^{T} (LS_{t,t_{1},n,u}^{pos} * ts_{t,t_{1},u}^{max}) \le P_{t_{1},n,u}^{max,pos} \quad \forall t_{1} \in T \land n \in N \land u \in User$$
 (3.11)

$$\sum_{t}^{T} (LS_{t,t_{1},n,u}^{pos} * ts_{t,t_{1},u}^{max}) \leq P_{t_{1},n,u}^{max,pos} \quad \forall t_{1} \in T \land n \in N \land u \in User$$

$$\sum_{t}^{T} (LS_{t,t_{1},n,u}^{neg} * ts_{t,t_{1},u}^{max}) \leq P_{t_{1},n,u}^{max,neg} \quad \forall t_{1} \in T \land n \in N \land u \in User$$
(3.11)

The last Equation (3.13) ensures that shifted energy is balanced for every user type and region within a fixed period of 24 hours. For every from-to relationship (amount of energy shifted from  $t_1$  to t), the sum has to equal zero.

$$\sum_{t_1}^{T} (LS_{t,t_1,n,u} * ts_{t,t_1,u}^{max}) = 0 \quad \forall t \in T \land n \in N \land u \in User$$
 (3.13)

After the optimization of the use of flexibility, new residual loads are computed.

### 3.4.2. Flexibility on national level

To use the flexibility potential of home charging processes to flatten the national residual load curve, two equations of the basic model are adjusted. First, the residual load curve in the objective function (Equation (3.8)) has no regional dimension anymore (Equation 3.14).

$$\min z = \sum_{t=1}^{T} |RL_t|^2 \tag{3.14}$$

Second, flexibility from all NUTS 3 regions and all user types is aggregated to smooth the national residual load curve. Instead of Equation (3.9), the following equation is formulated to compute the new national residual load curve.

$$RL_{t} = rl_{t} + \sum_{t_{1}}^{T} \sum_{u}^{User} \sum_{n}^{N} (LS_{t,t_{1},n,u} * ts_{t,t_{1},u}^{max}) \quad \forall t \in T$$
 (3.15)

All other model equations stay the same as described in the previous section.

### 3.5. Analysis and results

Based on the methodologies and data presented in previous sections, a thorough analysis of the characteristics of regional and national residual load curves is conducted, and the impact of two deployment strategies for home charging flexibility is evaluated. This section is divided into two parts. The first part, Section 3.5.1, focuses on analyzing residual load curves, aiming to answer two primary questions. How do regional residual loads develop over time? And what is the relationship between the load profiles of electric vehicles and regional residual load curves?

In Section 3.5.2, the two deployment strategies for the flexibility provided by electric vehicles are analyzed. The analysis differentiates between national-oriented and regional-oriented activation of flexibility. The presented optimization approach is used to answer the following question: What is the effect of different strategies for activating the flexibility offered by electric vehicles on regional and national residual load curves?

### 3.5.1. Residual load analysis

The regions are categorized into three distinct clusters: Photovoltaic (PV)-dominated, wind-dominated, and load-dominated regions. The clustering is based on two dimensions: the normalized ratios of total PV feed-in to total load, and total wind feed-in to total load, calculated annually. The total values

equal the yearly sum. The ratios of feed-in and load are normalized by the highest ratio observed across all regions in 2045. The clustering results are presented in Figure 3.8. A region is deemed load-dominated if both dimensions have a normalized value smaller than 0.20. A region is considered wind-dominated if it has a normalized wind-to-load ratio greater than 0.20 and greater than the PV-to-load ratio. The definition for PV-dominated regions follows the same logic.

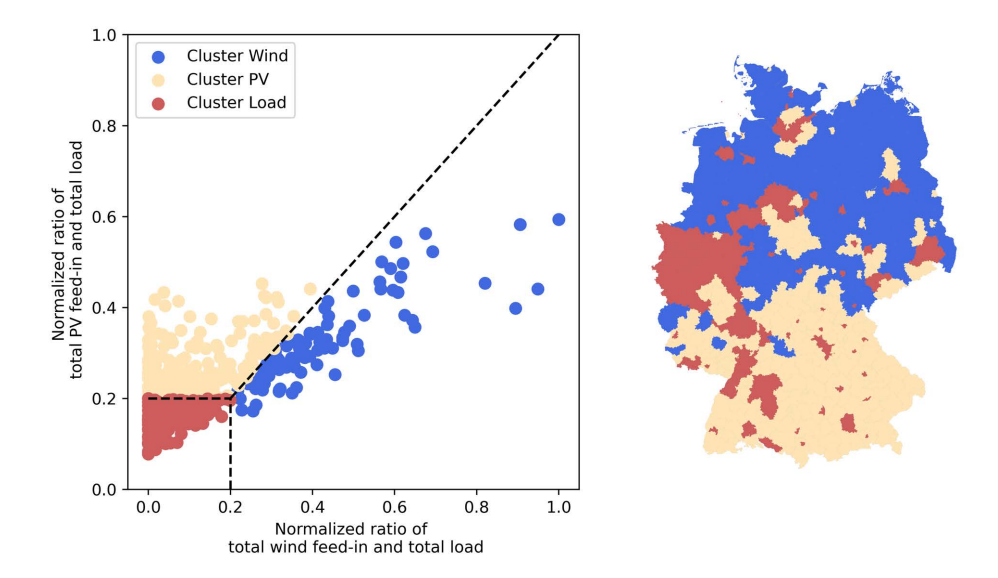


Figure 3.8.: Clustering and mapping of the 401 NUTS 3 regions

Note: The NUTS3 regions are clustered based on the normalized ratios of PV and wind feed-in compared to the total load. The clustering results in three different clusters, which are wind-, PV, or load-dominated.

The wind-dominated regions are primarily situated in the northern part of Germany and consist of 98 NUTS 3 regions, covering an area of 157,753 square kilometers, equivalent to 44% of the total land area of Germany (357,588 square kilometers). The PV-dominated regions are located predominantly in the southern region of Germany, particularly in Bavaria. These 166 NUTS 3 regions have a total area of 140,332 square kilometers, accounting for 39% of Germany's land area. Load-dominated regions are primarily located in Germany's western and southwestern regions and include major urban areas such as Berlin, Hamburg, and Munich. This cluster consists of 137 NUTS 3 regions and has a total area of 59,666 square kilometers, accounting for 17% of Germany's land area. The clusters differ not only in terms of load, wind and PV generation ratios but also, for example, in terms of population density and number of EVs. Both are high in load regions and low in wind regions. A detailed account of the distribution of regional properties for and within each cluster is provided in Appendix B.10.

Boxplots are computed for the three clusters and Germany to compare the properties of the residual load curves for the years 2019, 2030, and 2045 without considering flexibility. The results are presented in Figure 3.9.

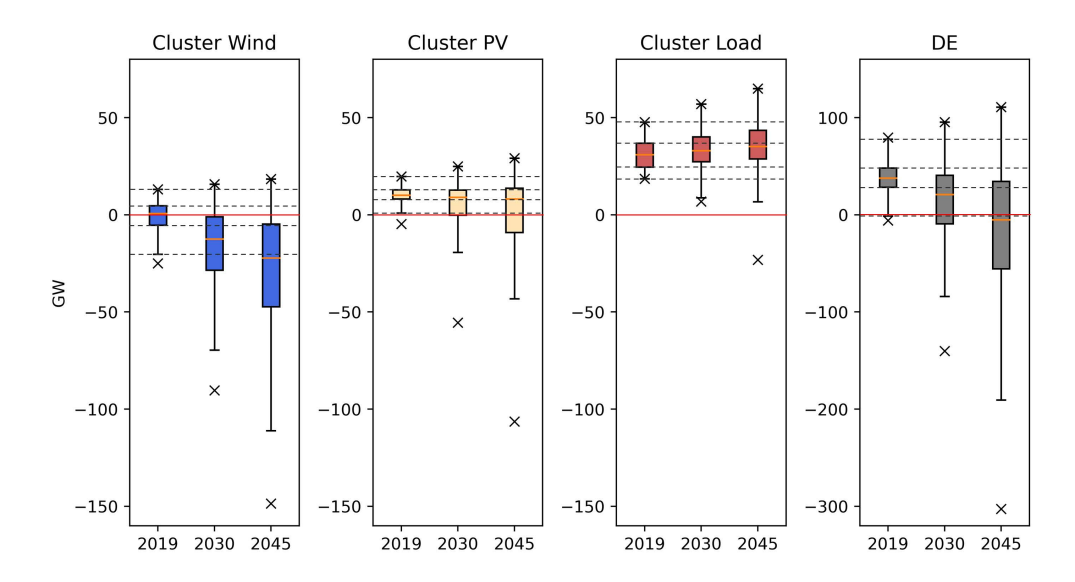


Figure 3.9.: Comparison of regional residual load curves prior to the activation of flexibility

Note: The minimum and maximum values are represented by crosses. The median is depicted by the orange line, while the colored box between the lower and upper quantiles represents 50% of all values. The maximum whiskers are equal or lower to 1.5 times the Inter-Quartile Range (range of the colored box)

Regarding the Cluster Wind, the majority of residual load curve values show a decrease from 2019 to 2045. The median of the residual load curve decreases from 0.7 GW in 2019 to -12.4 GW in 2030 and further to -22.2 GW in 2045. The increased dependence on the weather for electricity generation leads to an increase in the variance of the residual load curve. The distance between the minimum and maximum values of the boxplot, a measure of dispersion, increases by 178% from 2019 to 2030 and by 338% from 2019 to 2045. This increase is attributed to the significant expansion of wind capacities relative to electrical load growth. The minimum values of the residual load curve increase from -25.0 GW in 2019 to -148.6 GW in 2045, while the maximum value increases by 41% from 13.1 GW in 2019 to 18.5 GW in 2045. The Cluster PV displays relatively stable properties for the residual load curve, with a slight decrease in the median from 10.1 GW in 2019 to 8.2 GW in 2045. Similar to the wind-dominated cluster, the variance of the residual load curve increases, albeit to a lesser extent, due to the weather-dependent electricity generation and the limited impact of load. The properties of the residual load curve in **Cluster** Load display a different trend. The median increases from 30.9 GW in 2019 to a value of 35.2 GW in 2045, an increase of 14%. The maximum value of the residual load increases by around 36%, and the minimum value reduces from 18.5 GW in 2019 to -23.2 GW in 2045. The addition of new electric loads from electric vehicles and heat pumps in these regions is offset by the effect of rooftop PV expansion. As the peak demand occurs in the evening while the maximum feed-in from rooftop PV occurs at noon, the minimum and maximum values of the residual load curve diverge.

The residual load curve in Germany (**DE**) displays characteristics similar to those of the renewable-dominated clusters, as they represent a larger share of residual load. Additionally, the German residual load curve includes Offshore Wind feed-in, which is roughly correlated with the wind-dominated cluster.

### Correlation between residual load and electric vehicle load curves

Besides the ratios of renewable feed-in and load, the three clusters differ regarding the correlation between residual load and the electric vehicle load curves. Table 3.3 shows the coefficients of correlation for the three clusters and the years 2019, 2030 and 2045.

Table 3.3.: Correlation between residual load and electric vehicle load curves

Cluster	2019	2030	2045
Cluster Wind	0.08	-0.19	-0.25
Cluster PV	0.29	-0.21	-0.27
Cluster Load	0.74	0.46	0.11

The coefficients of correlation highlight that the residual load in the load-dominated cluster correlates most with the electric vehicles load profile. However, the correlation almost vanishes until 2045, caused by the penetration of rooftop PV applications and the electrification of further applications like heating or industrial processes. The residual load becomes less dominated by residential applications in the evening. The increasing weather dependency of electricity generation and a low share of load compared to renewable feed-in is the reason for the lower correlation in 2019 and even negative correlation in 2045 in the other two clusters.

This development is relevant for the use of EV charging flexibility to reduce the residual demand. Today, especially in Cluster PV and Cluster Load, there would be a strong incentive to shift the load of EV charging to counter the high correlation with the residual load peaks. In 2045, however, especially in Cluster Wind and Cluster PV, EVs tend to be charged when the residual load is low (or negative). This development implies that the marginal utility of charging flexibility to reduce load peaks is decreasing over time, although the flexibility potential is increasing in absolute terms with growing EV adoption.

### 3.5.2. Flexibility of electric vehicles

This section provides a detailed analysis of two deployment strategies for utilizing the flexibility provided by electric vehicles. The objective of the analysis is to understand the impact of these strategies on the residual load curves at both national and regional levels. Two deployment strategies are distinguished: First, flexibility is used to flatten the regional and, second, the national residual load curve. In the following, the formulations of "nationally incentivized" and "regionally incentivized" flexibility deployment for the use of the two deployment strategies are used. The optimization model outlined in Section 3.4 is used for the analysis. The properties of the resulting regional and national residual load curves for the years 2030 and 2045 are evaluated and compared.

### Characteristics of the activation of flexibility

Figure 3.10 illustrates the model results for a single region over a 48-hour period with hourly resolution. The figure highlights the differences in the shape of the residual load and load shifting between the two optimization schemes. For example, the charging process for user type C is shifted to hour 27 in the regional scheme but to hour 10 in the national scheme. The use of flexibility is mainly limited by the positive flexibility potential, as depicted by the dotted lines.

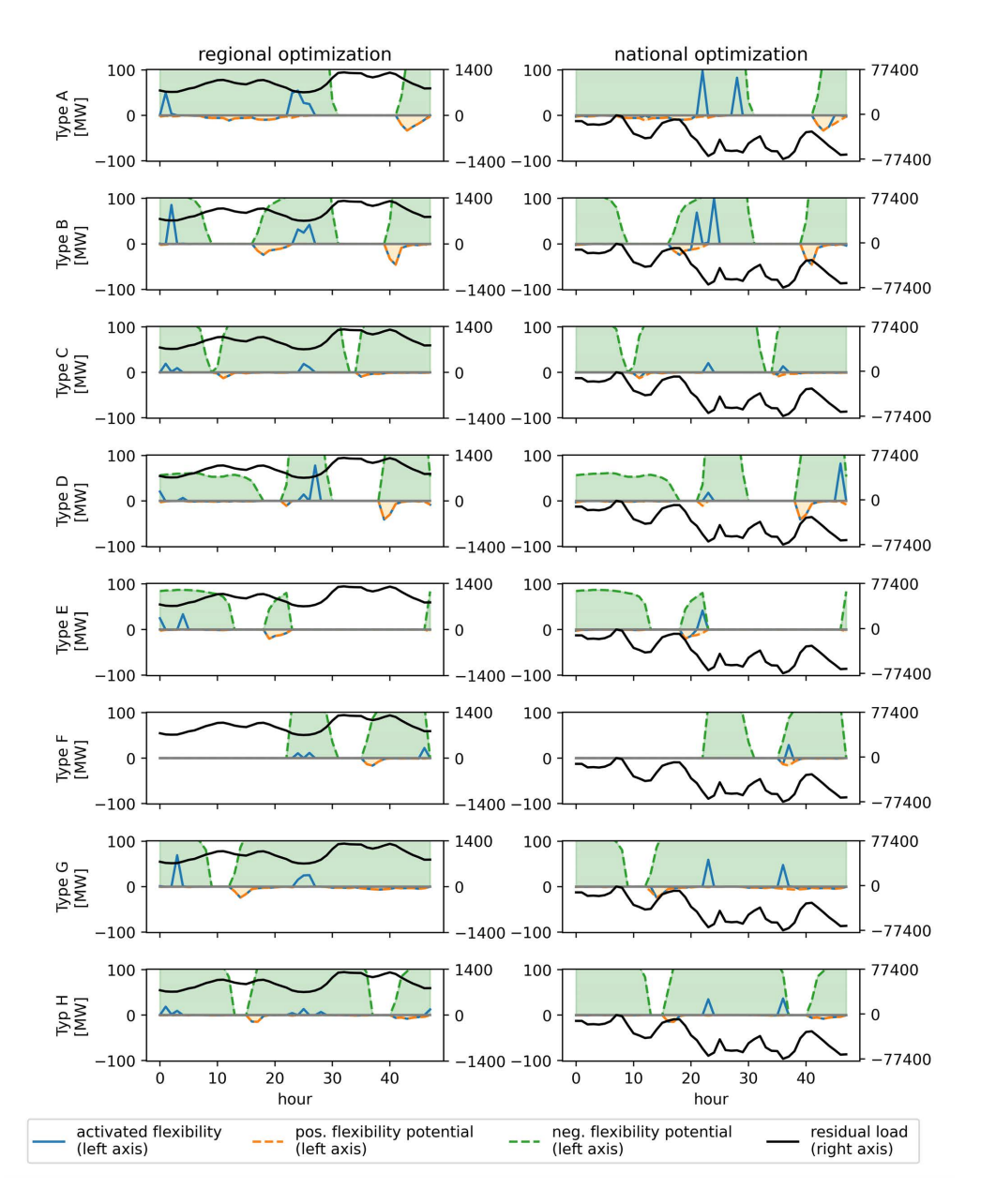


Figure 3.10.: Optimal activation of flexibility in region DE111 (Stuttgart)

Note: The left column of the figure shows the results of the regional optimization and the right column shows the results of the national optimization. The residual load before the activation of flexibility (regional on the left and national on the right) is depicted using a black line, and the change of charging processes for user types A to H are shown in blue.

Additionally, Figure 3.11 depicts the temporal patterns of flexibility activation. It compares the outcomes of regional and national optimization approaches.

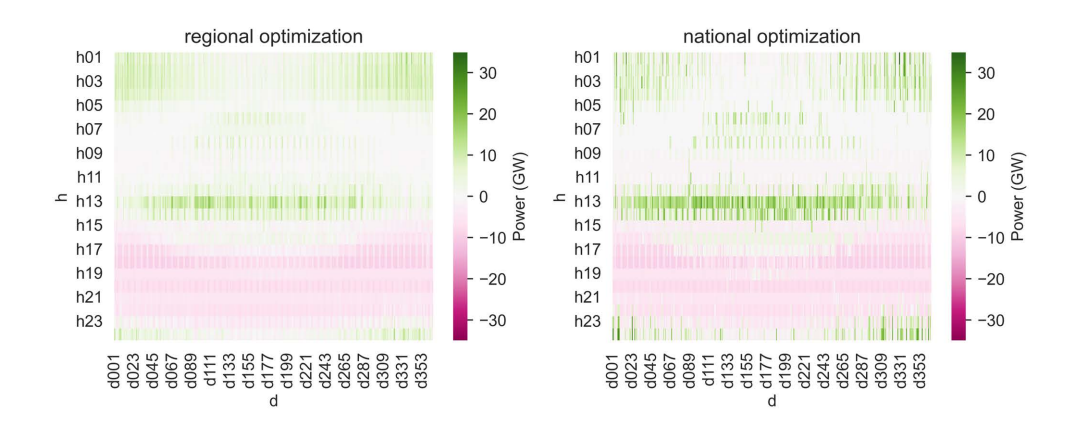


Figure 3.11.: Activation of flexibility of EVs in 2045 after national and regional optimization

Note: The x-axis represents the days of 2045, while the y-axis shows the hours of each day. The flexibility activation is shown in GW per hour. Green areas show positive flexibility activation (load reduction), purple areas show negative flexibility activation (load increase).

Generally, the power deltas are more significant under the national optimization approach. Conversely, the regional optimization approach results in less pronounced total power fluctuations due to the heterogeneity across regions.

### Model results on national level

The mechanisms for activating flexible charging processes impact the properties of the national residual load curve. In Figure 3.12, the residual load curves after regional and national incentivized activation of flexibility are compared to the residual load curve before the use of flexibility. This is done for the years 2030 and 2045.

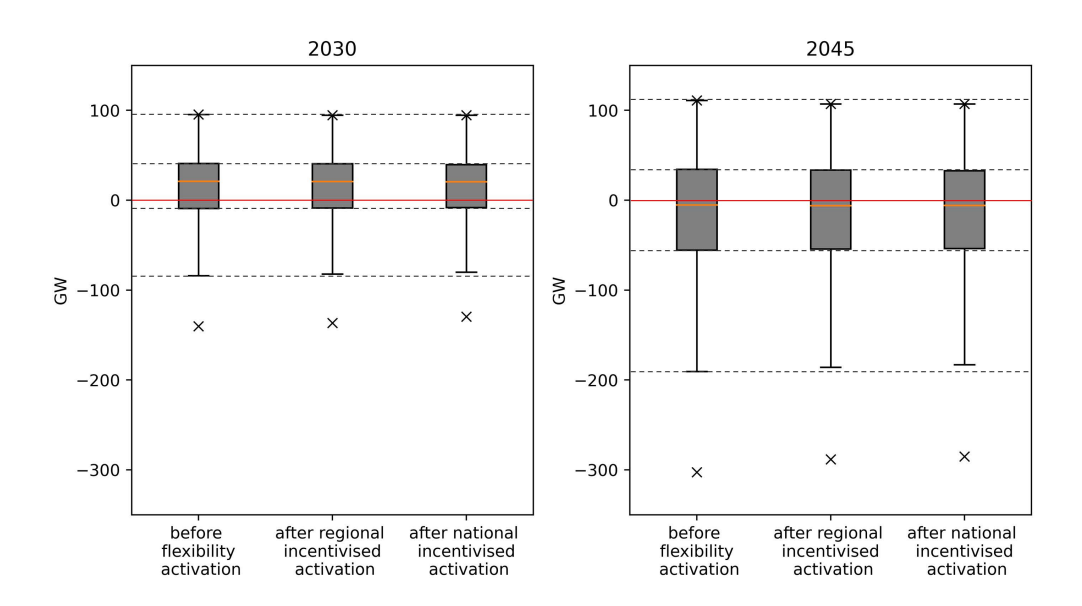


Figure 3.12.: Properties of the national residual load curve before and after the use of flexibility

Note: The minimum and maximum values are represented by crosses. The median is depicted by the orange line, while the colored box between the lower and upper quantiles represents 50% of all values. The maximum whiskers are equal or lower to 1.5 times the Inter-Quartile Range (range of the gray box).

For both years, the range between the minimum and maximum values, as well as the absolute value of the peak change to a small extent through both national and regional incentivization of flexibility. However, national incentivization has a greater impact compared to the regional approach. In 2030, regional incentivization decreases the range between the minimum and maximum values by 1.9%, while national incentivization decreases this range by 4.8%. Before the use of flexibility, the negative peak surpasses the positive one in absolute terms. Regional incentivization reduces the peak by 2.6%, and national incentivization reduces it by 7.5%. These characteristics observed in 2030 can also be seen in 2045, but with higher values and a greater variance of the residual load. The use of flexibility reduces the absolute value of negative peak demand. The minimum changes from -303 GW to -288 GW (-5.0%) with the regional approach and to -285 GW (-5.9%) with the national approach, while the maximum is only reduced by 4 GW (-3.6%) in both cases.

### Model results on regional level

Imbalance ratios are calculated to analyze the effects of the two flexibility deployment strategies on the regional feed-in and load peaks. These are defined as the positive or negative peaks in each region's residual demand divided by the respective regional total load and generation over a year.<sup>20</sup> The imbalance ratio can be formulated in a positive  $(PIR_r)$ , negative  $(NIR_r)$  and an absolute  $(AIR_r)$  way (see Equations (3.16) to (3.18)). Dividing the maximum amount of power needed in both the positive (RE deficit) and negative (RE surplus) direction in each region by total load and generation allows us to analyze and compare the development of peaks for the heterogeneous regions. Comparing the imbalance ratios before and after flexibility activation allows us to quantify how flexibility changes the magnitude of the maximum load and feed-in peaks.

$$PIR_{r} = \frac{\max_{h \in H}(residual load_{h,r})}{\sum_{h=1}^{8760}(total load_{h,r} + generation_{h,r})} * 1000 \quad \forall r \in R$$
 (3.16)

$$NIR_r = \frac{\min_{h \in H} (residual load_{h,r})}{\sum_{h=1}^{8760} (total load_{h,r} + generation_{h,r})} * 1000 \quad \forall r \in R$$
 (3.17)

$$AIR_r = \max(|PIR_r|, |NIR_r|) * 1000 \quad \forall r \in R$$
 (3.18)

Figure 3.13 visualizes the change of the imbalance ratios after the national and regional incentivized activation of flexibility in each region for the year 2030. Figure 3.14 shows the results for the year 2045. As reference values in both figures, highlighted in gray, the peaks in 2019 are normalized to the load and generation of 2030 and 2045, respectively.

 $<sup>^{20}\</sup>mathrm{The}$  use of this evaluation variable follows Kühnbach et al. (2021).

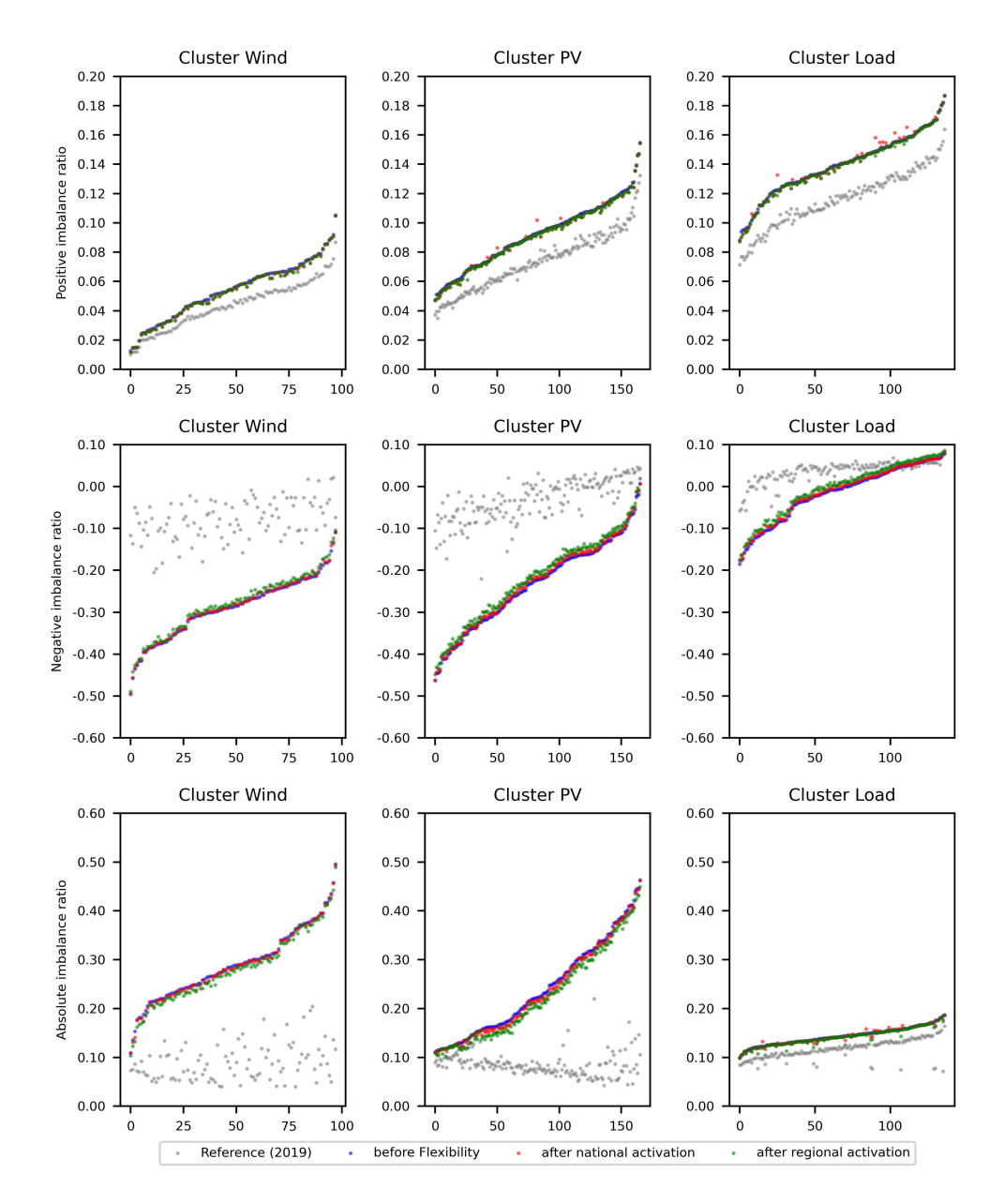


Figure 3.13.: Imbalance ratios before and after the use of flexibility in 2030

Note: The x-axis represents the regions in each cluster. In each of the nine sub-figures, the imbalances before flexibility are sorted in ascending order. The imbalance ratios after the activation of flexibility are then matched to the corresponding region.

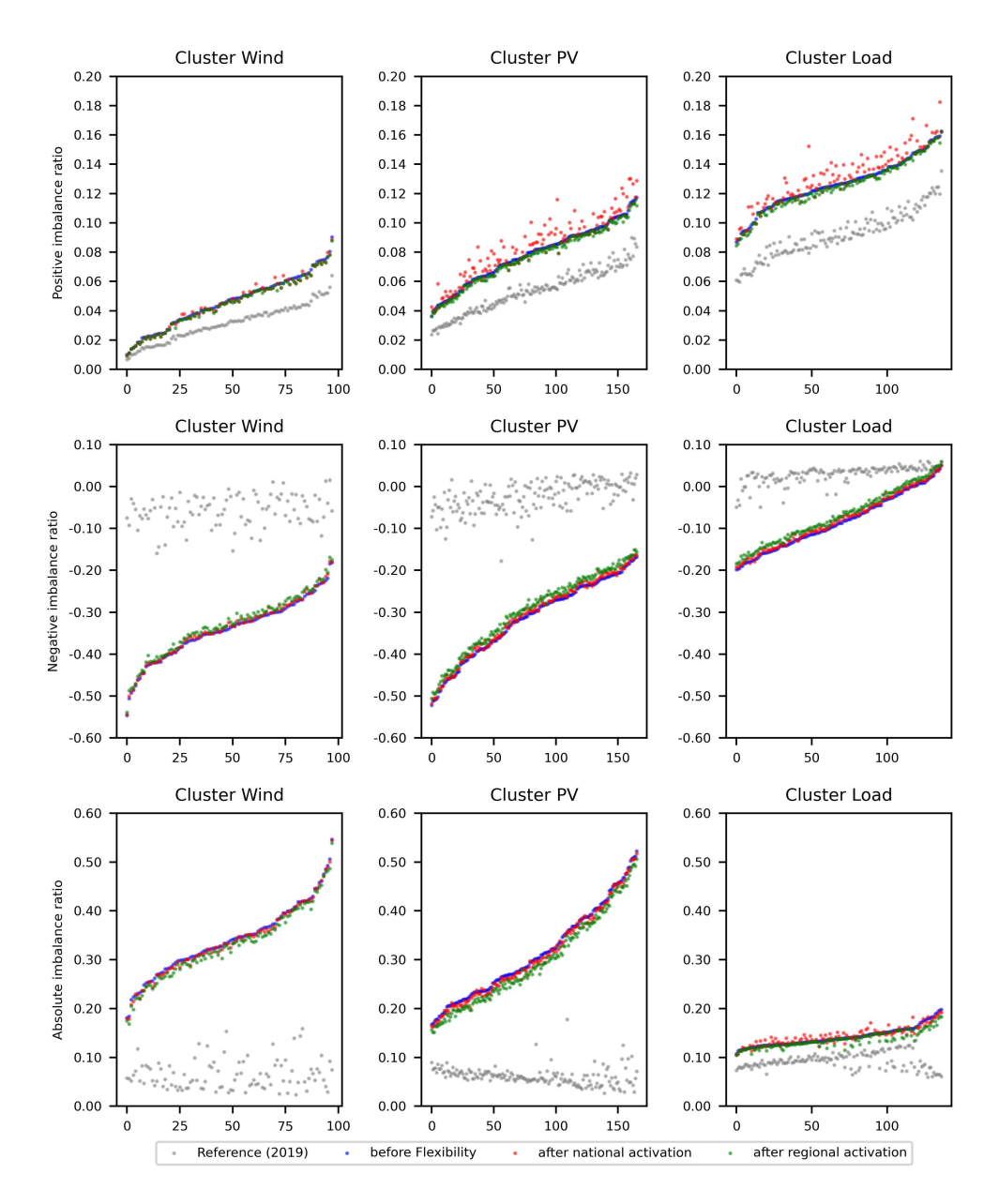


Figure 3.14.: Imbalance ratios before and after the use of flexibility in 2045

Note: The x-axis represents the regions in each cluster. In each of the nine sub-figures, the imbalances before flexibility are sorted in ascending order. The imbalance ratios after the activation of flexibility are then matched to the corresponding region.

In renewable-dominated regions in 2045, before the activation of flexibility, the negative imbalance ratio is always greater, in absolute terms, than the positive imbalance ratio. It thus defines the absolute imbalance ratio and the maximum strain on local grid components. In the load-dominated cluster, it is the other way around in about 66% of the regions.

In the Cluster Wind, the positive imbalance ratio decreases only slightly when applying both activation mechanisms for flexibility. On average, positive imbalance declines by 1.2% with national incentives and by 2.7% with regional ones. The positive peaks of the residual loads decrease by 0.002 MW/km<sup>2</sup> on average with national incentives and by 0.004 MW/km<sup>2</sup> with the regional approach. The decreasing effect is limited by low positive flexibility potentials and the fact that the charging processes and the situation of the highest residual load do not fall into the same periods, as discussed in Section 3.5.1. The correlation between residual load and charging profile decreases over time, which limits the potential for flexibility in peak load situations. This limitation applies to all three clusters. The negative imbalance ratio in the wind-dominated cluster remains largely unchanged under the national deployment strategy (-1.2% on average in absolute terms<sup>21</sup>, corresponding to -0.013 MW/km<sup>2</sup>). However, it decreases more when applying the regional strategy (-3.5\% in absolute terms, corresponding to -0.037 MW/km<sup>2</sup>). As the negative imbalance ratio is greater than the positive one for the regions in this cluster, the absolute imbalance ratio reproduces the negative one in absolute terms.

In the Cluster PV, the positive imbalance ratios display a different pattern than the ones in the wind-dominated cluster, with an increase in response to national incentives. The national deployment strategy results in an increase of 5.1% of the positive imbalance ratio on average, which corresponds to an increase of the positive residual peak demand of 0.008 MW/km<sup>2</sup> across all regions within this cluster. But, there are also regions which face distinct greater effects with up to 0.071 MW/km<sup>2</sup>. In these cases, peaks can increase by up to 35% following national incentives. This outcome is attributed to more electric vehicles in PV-dominated regions compared to wind-dominated regions, resulting in a greater potential for positive flexibility.<sup>22</sup> In contrast, positive imbalance ratios are lowered by 2.1% with regional incentives on average, corresponding to a reduction of 0.008 MW/km<sup>2</sup>. The negative imbalance ratio is consistently reduced by regional incentives in absolute terms (-6.3\% on average, corresponding to -0.068 MW/km<sup>2</sup>). National incentives reduce the absolute value of the negative imbalance ratio, too, but to a less extent (-1.2%; -0.023 MW/km<sup>2</sup>). Just as in the wind-dominated cluster, as the negative imbalance ratio is greater than the positive one, the absolute imbalance ratio reproduces the negative one in absolute terms.

Last, in the **load-dominated cluster**, it can be observed that following national incentivized activation of flexibility, positive imbalance ratios are the highest compared to their occurrence in renewable-dominated clusters. On average,

<sup>&</sup>lt;sup>21</sup>For the positive and absolute imbalance ratio, a reduction corresponds to an improvement: the (positive or negative) residual load peak becomes smaller. For the negative imbalance ratio, a reduction corresponds to a worsening: the negative residual load peaks (the absolute value) become larger. In order to be consistent in terms of the positive/negative impact, all described changes in the negative imbalance ratio refer to the absolute change.

<sup>&</sup>lt;sup>22</sup>Appendix B.10 gives details on cluster properties and the distribution of electric vehicles within each cluster.

the positive imbalance increases by 3.1% (0.043 MW/km<sup>2</sup>) with national incentives. But, just like in the PV-dominated cluster, there are also regions with high penetration rates of electric vehicles, which face a distinct greater effect with up to 0.349 MW/km<sup>2</sup>. In this case, the peak increases by around 27% following national incentives. Regional incentives instead lower the positive imbalance ratio by 1.4% (-0.018 MW/km<sup>2</sup>) on average. The negative imbalance ratio is consistently reduced both by regional and national incentives, but regional incentives have a greater effect (-2.1\% compared to -6.3\%, corresponding to -0.079 MW/km<sup>2</sup> and -0.208 MW/km<sup>2</sup>). In contrast to the separated effects on positive and negative imbalances, the effect of national incentives on the absolute imbalance ratio is region-specific, indicating the regions' heterogeneity in the load-dominated cluster. In some regions, the positive imbalance ratio exceeds the negative imbalance ratio (regions 0 to 90), while the opposite is true in others (regions 91 to 137). In regions with a greater positive imbalance than a negative, the absolute imbalance ratio increases by 3.2% on average with national incentives, corresponding to an increase of absolute residual peak demand by 0.056 MW/km<sup>2</sup> on average. Instead, local incentives lower the absolute imbalance ratio by 1.1% on average, corresponding to a decrease of the absolute peak by 0.019 MW/km<sup>2</sup> on average. In regions with a smaller positive imbalance than a negative, national incentives reduce the absolute imbalance ration by 1.9% on average (-0.036 MW/km<sup>2</sup>), whereas local incentives would lower the absolute imbalance ratio even more by 5.9% (-0.104 MW/km<sup>2</sup>) on average. Consequently, there are regions in the load-dominated cluster where national incentives are slightly beneficial in lowering the absolute imbalance ratio or do not significantly change it. However, there are also regions where national incentives result in an increase in the absolute imbalance ratio, stemming from the increase in positive peaks. Or, formulated differently, national incentives can significantly increase or slightly reduce the absolute peaks. Regional incentives may either lower the imbalance ratio or have an insignificant impact on the absolute value, depending on the flexibility potential and the correlation between charging profiles and residual load peaks.

Summarizing, national incentives tend to increase the positive imbalance ratio in PV- and load-dominated regions, whereas regional incentives decrease it, albeit to a small extent. However, regional incentives can significantly reduce the negative imbalance ratio.

In the context of the three clusters under consideration, it can be inferred that in regions dominated by wind energy, the national deployment strategy does not exert additional pressure on the distribution grid, but regional incentives can reduce imbalances. In PV-dominated regions, both the national and the regional incentives do lower the absolute imbalance ratio. However, regional incentives have a greater effect. For the regions of both clusters, it can be observed that the flexibility potential is used in particular to absorb excess renewable electricity and has less effect in smoothing load peaks. This is also manifested in the temporal shift patterns in the two clusters: For both the national and the regional

incentivization, load shifting takes place primarily from the evening to the times of surplus generation at noon.

In contrast, load-dominated regions are characterized by heterogeneity in terms of positive or negative peak dominance, so the impact of national incentives on imbalances can be either positive (worsen the situation) or negligible. That is because the national incentivization corresponds to the temporal scheme of the renewable-dominated regions: Load is shifted from the evening into the times of national renewable surplus, only that there is no renewable energy surplus in many load-dominated regions, leaving them worse off. Regional incentives, on the other hand, can reduce absolute imbalances in these regions, as the load is shifted into the night, to address load peaks during the day.

### 3.6. Conclusion

The expansion of decentralized renewable energy systems and electric vehicles is putting stress on the distribution grids. However, flexible EV charging can help alleviate this impact by reducing peak loads and feed-in by better matching load and supply. The paper conducted a comprehensive regional analysis of Germany to estimate the regional potential of EV charging flexibility for reducing peaks on regional and national levels. This was achieved by modeling regional EV diffusion with sigmoid functions and deriving individual charging and flexibility profiles for each NUTS 3 region in Germany. For both, a detailed method is presented. Further, a model to optimize the use of EV charging flexibility to either flatten the regional residual loads or the national one is developed.

### 3.6.1. Main results

In the first part of the analysis, this study examines the future development of residual load curves and their correlation with EV charging profiles. Three different clusters were formed: load-dominated, wind-dominated and PV-dominated. The analysis shows that the increased dependency on weather-based electricity generation leads to a significant increase in the variance of the residual load curve until 2045. The results reveal that the regional structure of electricity demand and supply is highly heterogeneous. Moreover, the correlation between residual load and EV charging profiles decreases over time, implying that the marginal utility of charging flexibility to reduce load peaks declines, even if the positive flexibility potential increases in absolute terms.

In the second part, the impact of two incentive mechanisms for activating the flexibility of electric vehicles is evaluated. One aims to flatten the regional residual load curves with local flexibility. The other uses the aggregated flexibility potentials to flatten the national residual load. Results show that both strategies reduce the variance of the residual load and peak demand and feed-in from a na-

tional perspective. In 2045, both strategies reduce the positive residual peak load by about 4 GW (3.6%), correspondingly less reserve capacity, storage or imports need to be kept available. The negative residual peak load, i.e. the maximum surplus of renewable capacity, is reduced by 15 GW (5.0%) in case of regional incentivization and even by 18 GW (5.9%) in case of national incentivization. I.e., the use of EV charging flexibility has a significantly greater potential in absorbing excess renewable generation than in lowering positive peak load. Regional incentivization generally leads to a decline in absolute values of peaks on regional level. Here, as well, the flexibility is particularly useful in absorbing excess renewable generation and thus reducing negative residual load peaks. The local impact of the national incentivized activation varies depending on the region's characteristics. In load- and some PV-dominated regions, national incentivization can result in drastically higher regional demand peaks compared to a scenario without charging flexibility (up to 35%). In wind-dominated regions, this effect is less pronounced. Furthermore, regions with higher shares of EV load than total load and regions with a higher correlation of EV charging profiles with the residual load have higher potential to flatten the residual load and reduce the peak demand.

The results contribute to existing literature by demonstrating the potential of EVs in smoothing residual loads. The developed model serves as a robust framework for potential transferability to other regions and countries, particularly where similar studies are scarce. For example, Schill and Gerbaulet (2015) examined the impact of various EV charging strategies on the load curve in Germany, reporting a reduction in peak load of 2.1 GW. However, this study involved fewer EVs and lacked regional differentiation, potentially overestimating the flexibility potential. The findings are consistent with Kühnbach et al. (2021), who emphasized the effectiveness of demand management in regions experiencing frequent fluctuations between demand and supply deficits. This analysis validates that load-dominated regions derive greater benefits from regional incentivization, cautioning that national approaches may inadvertently increase peak demand.

### 3.6.2. Policy implications

The developed method can support grid operators in their grid planning, both, on regional and national levels. It provides an extensive collection of data sources as well as insights into the development of regional and national residual load peaks. The two application scenarios of charging flexibility discussed aim at two very different targets: while national incentivization aims at reducing demand in times of low national renewable generation feed-in and thus times of high prices, the regional incentivization aims at reducing the regional strain on grid components. This study shows that these two targets can be contradictory in their effects: While the regional incentivization is less effective in reaching the smoothing in the national residual demand curve, the national incentivization

can even lead to increased strain on local level, especially in load-dominated regions. As the results of this study do not identify a dominant incentive scheme, but rather show the different effects, policymakers must be aware of their objectives when deciding on one incentive scheme or the other. Policymakers must be aware of the shown dynamics when designing incentive schemes for flexible EV charging. Uniform pricing at the national level may result in undesirable effects at the regional level, suggesting a need for regionally differentiated price signals (e.g., zonal or nodal pricing). Policymakers should consider the regional effects shown when implementing incentives to achieve maximum effectiveness in reducing peaks on regional and/or national levels and avoid unwanted additional strain on grid components. Overall, the effectiveness of EV charging flexibility is heavily influenced by the regulatory and market context. Policymakers should tailor their strategies to the specific regulatory and market conditions to maximize the benefits of EV flexibility for grid stability and efficiency.

### 3.6.3. Limitations and further research

The results of this study must be interpreted within the context of several limitations and assumptions. Firstly, by design, this analysis assumes one specific scenario concerning the numbers of EVs, their charging behavior, the development of the load, the renewable generation capacities, and the analyzed weather year. For example, other weather years would yield other results. However, this would only change the absolute numbers, rather than the identified trends and broader interrelations, especially as this study finds the flexibility potential to be the limiting factor in the results, not the renewable electricity feed-in. On a more fundamental level, the assumption of a specific scenario means, naturally, that the exact quantitative results only apply to this exact scenario. A lower expansion of EVs reduces the flexibility potential, and a different development in the expansion of other electrical loads and renewable electricity sources changes the charging behavior. Nevertheless, the structural relationships that arise in the defined scenario offer overarching insights, and the methods developed can be used for other scenario assumptions and expectations in the future. Secondly, the analysis abstracts from other flexibility options and their interdependencies with the flexible home charging of EVs. Particularly in view of the increasing expansion of home and large-scale battery storage systems, the question arises as to how the value of EV flexibility will change as a result. In general, additional flexibility from other sources is expected to reduce the value of EV flexibility. The deployment of bidirectional charging would increase the EV flexibility potential, as the battery capacity and the maximum charging power would limit the flexibility rather than the energy demand for driving. Extending the provision of EV flexibility from home charging to other charging locations, such as workplaces, would also increase the flexibility potential, as it enables charging during the day. Especially for regions with strong PV feed-in, this would be of high value. Furthermore, this study is based on the assumption that access to a home charger varies depending on the settlement type, while EVs parked at a home charger are always connected to the grid and provide flexibility. This neglects a potentially limited willingness or option to provide flexibility. Considering this, the flexibility potential would decrease. Finally, it is implicitly assumed that the residual peak load is the only factor that affects power grids. However, there are further aspects, such as voltage stability, which have to be considered in grid operation. It can be expected that the value of EV flexibility increases with the complexity of a grid operator's supply task.

While the developed method can be used to estimate regional effects of flexibility deployment at the level of NUTS 3 regions, there is a need for further research on its impact on actual distribution grids and grid components. In the course of this, the concrete grid expansion costs and electricity generation costs under different deployment strategies could be quantified and compared. One could also compare potential environmental benefits and drawbacks under different deployment strategies. Under national incentivization, renewable electricity capacities can be better utilized, so it is conceivable that fewer plants will needed to be installed and resources will be conserved. At the same time, there is less conventional power generation, which can potentially reduce emissions depending on the market design. Regional incentivization, on the other hand, may reduce the amount of resources required and, thus, the environmental impact of expanding distribution grids. Additionally, there remains a need for further research, including into the interdependencies with other flexibility technologies and the flexibility of workplace charging or charging in public spaces. This becomes particularly relevant in view of the current trends in the expansion of flexibility, e.g. increasing investment in home storage and stand-alone battery systems. It may be worth extending the present model to include these additional sources of flexibility and analyzing the change in the value of the flexibility provided by the various sources. The same applies to the question of how technological developments in EV influence the results. This includes the effects of the implementation of bidirectional charging. Finally, further research could investigate on the effects of different policy schemes aiming at the implementation of the discussed deployment strategies.

# 4. Welfare redistribution through flexibility- Who pays?

### 4.1. Introduction

Achieving climate neutrality necessitates a deep transformation of energy systems, particularly through the decarbonization of end-use sectors like transportation, heating, and industry. Electrification has emerged as the primary strategy for this transition, with Germany setting ambitious goals to deploy 15 million electric vehicles (EVs) and 6 million heat pumps by 2030 (BMWK, 2022a,b). While these targets demonstrate ambition towards a low-carbon economy, they also introduce significant challenges due to the increasing integration of decentralized, flexible actors into the electricity market. Their flexible consumption patterns - such as the ability to shift EV charging or heat pump operation to times of lower electricity prices - can alter demand profiles, influencing electricity price formation. Flexibility can potentially reduce the need for costly backup power plants and increase the integration of renewable energy sources (RES) by aligning consumption with periods of high RES generation (Kiviluoma and Meibom, 2010). However, shifting demand can also lead to increased electricity prices due to heightened consumption during periods of negative or low electricity prices.

The deployment of flexibility not only affects the electricity price formation but also leads to significant redistributional consequences in the electricity market. For example, Liski and Vehviläinen (2023) illustrate how increased demand-side flexibility, while reducing overall price volatility, leads to a redistribution of economic surplus from producers to consumers. Producers, especially those relying on price peaks, may see their profits diminish as flexible demand flattens price peaks, reducing their revenues. Furthermore, the interaction of decentralized flexible technologies can create cross-sectoral imbalances. For instance, while EV owners may benefit from lower electricity costs by charging during off-peak hours, this increased demand could raise prices for other groups, such as heat pump owners, who may be operating their systems at the same time. These dynamics complicate the electricity market by creating interactions where one group's flexibility influences the costs borne by others. As such, the introduction of flexibility could exacerbate inequalities, where certain user groups benefit disproportionately while others, including producers or less flexible consumers, face reduced revenues or higher costs.

This paper addresses these redistributional consequences by providing a detailed analysis of the economic implications of deploying flexibility from end-use sectors in the wholesale electricity market.

Extensive research has been conducted on the effects of flexibility provision, primarily focusing on two main objectives: analyzing system-wide impacts, such as market clearing and electricity price formation, and evaluating welfare effects, including technology-specific market values and the redistribution of economic gains among market participants.

The first body of literature focusing on system-wide effects of flexibility tends to adopt a top-down perspective, often analyzing the impact of flexibility on total system costs. For example, the Big-5 Energy System Studies (dena, 2022) explore the system-wide implications of decentralized flexibility deployment in costefficient pathways to achieve climate goals. Other works, such as those by Härtel and Korpås (2021) and Böttger and Härtel (2022), emphasize the importance of capturing cross-sectoral interactions in energy system models to better understand market dynamics. They show that technologies like EVs and heat pumps, which act as flexible, price-setting actors, can significantly influence electricity price formation and market clearing in low-carbon energy systems. Similarly, Nagel et al. (2022) examine the competition between different flexibility options in systems with high RES shares, focusing on how these technologies interact under varying climate targets. Felling and Fortenbacher (2022) further highlight the importance of sector coupling - integrating electricity, heating, and transport sectors - when analyzing price formation. Their research stresses the need for flexibility to be studied in an integrated way, considering multiple energy sectors simultaneously. Despite these advancements, the current literature on market clearing and price formation tends to focus on the overall system, neglecting the heterogeneous impacts of flexibility on different end-user groups, which is crucial for understanding the redistributional effects of flexibility deployment.

The second body of literature shifts the focus towards the welfare effects of flexibility deployment and the impact of specific technologies on market values. Studies like Hirth (2013) have analyzed how the variability of solar and wind power affects the market values of renewables, while others, such as Bernath et al. (2021), have examined sector coupling's impact on these market values. Ruhnau (2022) expands this discussion by exploring the role of electrolyzers in influencing wind and solar market values. Böttger and Härtel (2022) and Nagel et al. (2022) have studied the welfare effects of flexibility deployment, specifically focusing on the economic benefits for flexibility providers. While the existing studies provide valuable insights into the broader economic impact of flexibility deployment, they tend to aggregate flexibility providers, thus overlooking the impacts on various end-user groups. Neglecting heterogeneous flexibility potentials creates a critical gap in understanding how decentralized flexibility affects not only total system welfare but also the redistribution of economic gains and losses across different actors in the energy market. This study aims to fill this gap by providing

a granular analysis of decentralized flexibility deployment and exploring how flexibility affects the economic outcomes at the system, sector, and user levels.

Motivated by the growing relevance of end-user flexibility, this study explores to what extent the deployment of decentralized flexibility leads to a redistribution of welfare from electricity producers to consumers. Such redistribution effects are likely to depend on the characteristics of the flexibility provided, including the technologies used and the behavioral patterns of different user groups. To investigate these dynamics and quantify the effects, we enhance the existing European energy system model DIMENSION by incorporating a high-resolution dispatch for a range of end-consumer groups and flexibility technologies. This approach allows us to simulate the interaction between decentralized flexible assets - such as EVs and heat pumps - and the energy system. Our analysis is based on a case study for Germany, reflecting the country's technology-specific targets for 2030. By assuming the achievement of these targets, we model varying degrees of flexibility in the road transport and decentralized heating sectors through a range of use cases. This enables us to assess the economic consequences of decentralized flexibility provision across different market actors. Besides this, the paper adds to the existing literature by providing an in-depth analysis of the impacts of various decentralized flexibility use cases across three distinct levels:

- System level: We assess the system-wide impacts of flexibility deployment, including effects on electricity price formation and CO<sub>2</sub> emissions.
- Sector and technology level: We quantify the redistribution of consumer and producer surplus across different sectors and technology groups and estimate the changes in total system welfare.
- User level: We examine the economic impact of flexibility provision for decentralized user groups, accounting for their diverse characteristics and behaviors.

By focusing specifically on the wholesale electricity market, we isolate and quantify the effects of market-oriented provision of decentralized flexibility, while excluding potential gains from balancing and intraday markets and abstracting from distribution grid constraints. Moreover, we limit our analysis to the changes in marginal electricity generation costs, interpreted as wholesale electricity prices, without considering other components of the end-user electricity price such as taxes, levies, and network charges.

The paper is structured as follows: Section 4.2 describes the modeling approach. Section 4.3 presents the case study. Section 4.4 analyzes the impacts of decentralized flexibility on electricity prices, CO<sub>2</sub> emissions, and the redistribution of welfare between producers and consumers, with particular attention to differences across technology groups and user types. Section 4.5 discusses the results. Finally, Section 4.6 summarizes the main findings and suggests directions for future research.

### 4.2. Enhanced modeling of decentralized flexibility

To address the research questions posed in this study, we extend the existing DIMENSION modeling framework (Helgeson, 2024, Helgeson and Peter, 2020, Richter, 2011) to incorporate a more detailed representation of flexibility in the decentralized heating and road transport sectors. These enhancements focus specifically on Germany. By capturing the behavior of heterogeneous end-user groups in these sectors, the enhanced model allows us to study how varying degrees of flexibility influence electricity price formation and the redistribution of economic gains between producers and consumers. The model approach for the heating sector is described in Section 4.2.1 and for the transport sector in Section 4.2.2. The visualization of the model structure as well as the mathematical formulation of end-user flexibility is provided in Appendix C.2.

### 4.2.1. Decentralized heating

This section outlines our approach to modeling decentralized heating technologies, specifically focusing on heat pumps in both residential and commercial buildings.<sup>23</sup> The development of the building stock is modeled using the EWI building stock simulation tool (EWI, 2023a), which generates development pathways based on key indicators such as historical building stock data, renovation rates, demolition rates, and technological advancements. The tool categorizes buildings by type, renovation level, and installed heating systems. Simulations are carried out based on annual assumptions for heating system installations, replacements, and construction as well as demolition rates. The output includes metrics such as the projected number of heating systems and final energy demand for each building type.

In this model, five building types are defined, each reflecting different levels of passive building mass storage - a key factor influencing flexibility potential. In the residential sector, buildings are categorized into three groups: unrefurbished, refurbished, and new buildings, based on energy efficiency standards defined by KfW (2024). "Unrefurbished" refers to buildings without any energy efficiency classification, while "new" buildings comply with KfW efficiency classes 40 and 40+. Refurbished buildings represent those with intermediate energy efficiency levels. By 2030, the simulation estimates that approximately 20.5 million residential buildings will exist in Germany, with 33% unrefurbished, 62% refurbished, and 5% newly constructed.<sup>24</sup> For the commercial sector, buildings are categorized by insulation levels into two groups: non-insulated and insulated. By 2030,

<sup>&</sup>lt;sup>23</sup>Note that our enhancements in this study are limited to space heating and hot water. For a detailed description of the modeling approach for cooling and cooking, please refer to Helgeson (2024).

<sup>&</sup>lt;sup>24</sup>The simulation of the residential building stock is based on data from Heitkoetter et al. (2020) and aligned with the WP+|WN scenario from EWI (2023c).

71% of the 2.1 million commercial buildings are projected to be non-insulated, while 29% are expected to be insulated.  $^{25}$ 

We further differentiate between two types of heat pumps: air-source heat pumps (ASHPs) and ground-source heat pumps (GSHPs). These distinctions are based on differences in their coefficients of performance (COPs), which affect the relationship between electricity input and heat output and thus their flexibility potential (Rinaldi et al., 2021). By combining the five building stock categories with the two heat pump types, we define ten building types. Based on the simulation outcomes, the total demand for space heating and hot water is projected to reach 471 TWh for residential buildings and 124 TWh for commercial buildings by 2030.<sup>26</sup> The annual heat demand for each building type is distributed hourly using weather- and country-specific demand profiles from the when 2 heat dataset (Ruhnau and Muessel, 2022). The share of heat demand, including space heating and warm water, to be met by heat pumps in each building type is calculated based on the number of installed units, as shown in Table 4.1. In line with the German government's target, we assume approximately 6 million heat pumps to be installed in Germany by 2030 (BMWK, 2022b). Across all building types, ASHPs make up 80% of the total installed capacity, while GSHPs account for the remaining 20%. These assumptions are based on a linear interpolation of the observed technology distribution trends in Germany between 2012 and 2022 (BWP, 2023).

<sup>&</sup>lt;sup>25</sup>The commercial building stock simulation is based on the ENOB database and covers only heated or cooled buildings. More details can be found at https://www.datanwg.de/home/aktuelles/.

<sup>&</sup>lt;sup>26</sup>Building sector simulation is conducted in line with the current refurbishment targets (EWI, 2023a) and follows the current literature (Holm et al., 2021, Prognos et al., 2021, Repenning et al., 2023).

Table 4.1.: Number of heat pumps and share of total heat demand by building type

Building type	Building group	Heat pump type	Building condition	Number of heat pumps	Share of heat de- mand
Res1 ASHP	Residential	ASHP	Unrefurbished	1364062	4%
Res2 ASHP	Residential	ASHP	Refurbished	2740057	8%
Res3 ASHP	Residential	ASHP	New	550977	2%
Res1 GSHP	Residential	GSHP	Unrefurbished	341016	1%
Res2 GSHP	Residential	GSHP	Refurbished	685014	2%
Res3 GSHP	Residential	GSHP	New	137744	0%
Total				5818870	16%
Com1 ASHP	Commercial	ASHP	Non-insulated	470434	5%
Com2 ASHP	Commercial	ASHP	Insulated	188530	14%
Com1 GSHP	Commercial	GSHP	Non-insulated	117609	1%
Com2 GSHP	Commercial	GSHP	Insulated	47133	4%
Total		·		823706	24%

Note: The shares of heat demand shown in this table include the total demand for both space heating and warm water across all building types.

In addition to the passive storage potential, insulation levels affect the COPs of installed heat pumps. Heat pumps serve both space and water heating needs, with water heating accounting for around 20% of the total heat output in older buildings and 40% in newer buildings due to better insulation. Depending on the refurbishment status, heat pumps are paired with either floor/surface heating or radiators. As a result, the COPs vary across building types, as shown in Table 4.2, which outlines the annual average COPs for each heat pump and building type combination.

Table 4.2.: Annual average COP by heat pump technology and building type

Building	Space heating		Warm water	Annual average COP		
$\mathbf{type}$	Floor/surface	Radiator	-	ASHP	$\mathbf{GSHP}$	
Res1	0%	80%	20%	3.3	4.5	
Res2	40%	40%	20%	3.4	4.7	
Res3	45%	5%	50%	3.5	4.9	
Com1	15%	70%	15%	3.4	4.7	
Com2	15%	70%	15%	3.4	4.7	

Note: The hourly, weather-dependent COPs of the heat pumps are based on the when 2 heat dataset (Ruhnau and Muessel, 2022). The average annual COPs are derived for the weather year 2015, based on the assumptions regarding the heat sinks.

### 4.2.2. Road transport

This section outlines our modeling approach to account for the charging behavior of EVs within the dispatch model. We focus exclusively on passenger EVs, while light-duty and heavy-duty EVs are modeled using simplified, aggregated demand profiles. The central objective of this modeling approach is to account for heterogeneous charging patterns. Rather than applying average charging costs to all vehicles, we propose that unique cost structures should be applied exclusively to vehicles capable of responding to price signals, enabled by smart meters and user participation in demand-side flexibility. Flexibility in this context refers to the ability of vehicles to adjust their charging in response to wholesale electricity price fluctuations, offering potential cost-saving opportunities. A critical factor influencing this flexibility potential is the variation in driving and parking patterns among EV users. These patterns create varying opportunities for vehicles to shift their charging times, directly affecting their capacity to provide systemoriented flexibility. For instance, EVs with longer parking durations can offer more flexibility than those with shorter or more sporadic parking periods. Thus, our model enhancement aims at incorporating this heterogeneity to accurately capture the diverse flexibility contributions of different EVs. A fundamental challenge arises between the bottom-up approach, which models each vehicle individually, and the top-down approach, which uses aggregated demand profiles. To bridge this gap, we introduce ten distinct mobility clusters that capture different charging behaviors and flexibility patterns. These clusters vary based on the proportion of home, public, and workplace charging, as well as the flexibility to shift demand according to parking durations. This clustering approach enables us to capture diverse mobility behaviors while maintaining computational efficiency.

Electricity demand and potential flexibility of electric vehicles are driven by their driving patterns. For Germany, two primary surveys capture mobility behavior of households: *Mobility in Germany (MiD)* (infas et al., 2018) and the *German Mobility Panel (MOP)* (KIT - Institut für Verkehrswesen, 2021). Leveraging this data, we build upon the methodologies presented by Arnold et al. (2024) and Kröger et al. (2023).

First, we employ data from around 300,000 daily trip chains, incorporating information about the arrival time, duration of stays, specific parking locations, settlement type, and electricity consumption during the driving time. Based on this data, individual charging profiles are computed for different combinations of workplace, home or public charging of each daily trip chain. We assume that the charging process begins upon parking and ends either when a new trip begins or the battery is fully charged. Depending on seven different settlement types (urban, rural, semi-urban etc.), different possible charging profiles are weighted

and combined to one single profile.<sup>27</sup> As a result, each trip chain is transformed into charging profiles considering the different possibilities to start a charging process at different locations.

To capture the heterogeneity of home charging, we perform a k-medoids clustering based on home parking profiles. Thus, each charging profile is assigned to one mobility cluster. A total of ten mobility clusters are defined, with all individual charging profiles aggregated for each cluster. The charging profiles are then scaled to match the electricity demand of the number of EVs in the use cases presented in Section 4.3.2.

We further compute both positive and negative flexibility potentials for each cluster. Positive flexibility refers to the ability to reduce charging power (i.e., shifting or delaying charging). This potential is defined as the portion of home charging within the scaled charging profile of each cluster. In contrast, negative flexibility refers to the possibility of shifting charging to another time compared to the initial charging profile, allowing an increase in charging power at specific times. The potential is computed by aggregating the potential charging power of all cars parked at home and subtracting the initial charging profile. Both positive and negative flexibility profiles are intersected with the home parking time series of the cluster center following Arnold et al. (2024).

The results, illustrated in Figure 4.1, show that the ten distinct mobility clusters exhibit significant heterogeneity in their charging times, charging intensity, and flexibility potentials.<sup>28</sup>

<sup>&</sup>lt;sup>27</sup>Based on infas et al. (2018), we assume that profiles containing home charging are weighted with 90% and 42% in urban cities and rural areas respectively. Other settlement types are assigned intermediate weighting factors.

<sup>&</sup>lt;sup>28</sup>The source code and the profiles are published alongside this study: https://data.mendeley.com/datasets/bpwmxzhjx2/1.

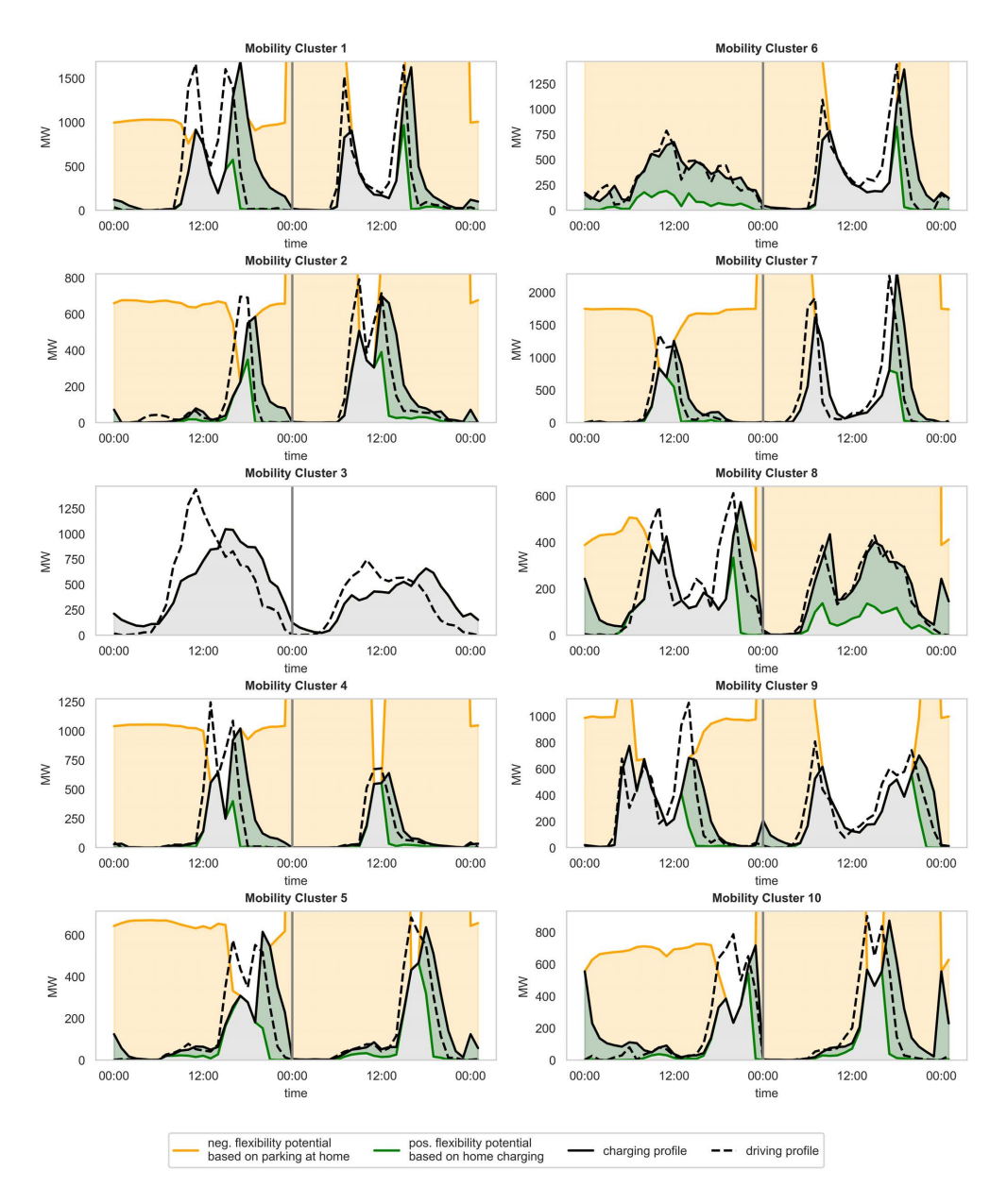


Figure 4.1.: Charging and flexibility profiles for different mobility cluster

Note: Each mobility cluster is characterized by distinct driving and charging patterns, as well as flexibility potentials. One weekend day and one weekday are shown at an hourly resolution, separated by a gray line, with the y-axis representing the total electricity demand.

For instance, mobility cluster 6 shows a dispersed charging pattern throughout the weekend, while mobility cluster 4 has concentrated midday charging. Conversely, mobility clusters 5 and 10 predominantly charge during the evening hours. Table 4.3 shows the distribution of the total number of EVs across the defined mobility clusters.

For 2030, we assume that the total number of passenger EVs reaches 15 million according to BMWK (2022b), with a total annual electricity demand of approximately 34 TWh.<sup>29</sup> This electricity demand remains constant across all use cases. EVs are assigned to the different clusters in proportion to their annual charging demand.

Table 4.3.: Distr	ibution of EVs	across mobility	clusters	MC1	to MC10

			v		
	MC1	MC2	MC3	MC4	MC5
Absolute [million]	1.97	0.87	2.31	0.86	0.83
Relative [%]	13.2	5.8	15.4	5.7	5.5
	MC6	MC7	MC8	MC9	MC10
Absolute [million]	1.93	2.24	1.14	1.71	1.10
Relative [%]	12.9	15.0	7.6	11 4	7.4

When addressing the future flexibility potential, Muessel et al. (2022) emphasizes the risk of overestimating the flexibility potential of EVs if one relies solely on overall charging profiles and aggregated flexibility potentials. We also recognize that only a fraction of home chargers may be equipped with smart meter technology, and only a limited number of users may be willing to provide flexibility. Considering these factors, we apply a conservative reduction to both the positive and negative flexibility potentials, using the same factor of 0.56 as in Agora and FfE (2023). Furthermore, we assume that only 25% of all EVs in 2030 will be equipped for bidirectional charging, consistent with the assumptions in Agora and FfE (2023).

## 4.3. Case study - Energy system dispatch under different flexibility use cases

This section describes the general model scope (Section 4.3.1) as well as the use cases defined to assess the impact of varying degrees of decentralized flexibility on electricity prices, producer and consumer rents and total system welfare (Section 4.3.2).

### 4.3.1. General model scope

Our analysis focuses on the year 2030 and is based on a comprehensive model of the European energy system that captures cross-sectoral interdependencies. The analysis relies on a broad range of data sources to accurately model the European energy system. Appendix C.3 provides information regarding capacity

 $<sup>^{29}</sup>$ Based on Helgeson and Peter (2020), we assume an annual driving distance of 11,200 km per EV and an average energy consumption of 0.2 kWh/km.

and profile assumptions and also includes input parameters, such as fuel prices, installed capacities and electricity demand. While the model covers the entire European electricity system, our primary focus is on Germany, where we introduce a high level of granularity in end-use sectors such as heating and transport as described in Section 4.2.

### 4.3.2. Different use cases for end-use sectors

We introduce different flexibility use cases for the heating and transport sectors. These use cases cover a range of potential flexibility degrees for EVs and heat pumps. We define three levels of flexibility for transport and two for the heating sector, resulting in six distinct flexibility use cases, as illustrated in Figure 4.2. By examining these combinations, we aim to gain insights into the impacts of flexibility on the overall energy system, various sectors, technologies, and the end-user groups involved.

#### **Heating sector** passive (H0) flexible (H1) only with buildings' inertia with additional heat storage passive (M0) M0/H0 M0/H1 Charging processes follow Transport sector (Reference) (Heating) exogenous profiles flexible (M1) M1/H0 M1/H1 charging processes can be shifted (Transport) (Interaction) according to flexibility potentials flexible + V2G (M2) M2/H0 M2/H1 Like M1, but additionally (Transport) (Interaction) considering bidirectional charging

### Figure 4.2.: Definition of flexibility use cases

Note: The figure illustrates the defined flexibility use cases for both transport and heating sectors. The rows represent flexibility levels for EVs, while the columns represent different flexibility assumptions for decentralized heating. The names for the use cases are displayed in the gray cells.

The following sections describe the flexibility use cases for the heating and transport sectors in more detail.

### Heating sector

In the passive use case (H0), the only flexibility considered is the thermal storage capacity of the building mass. A simplified approach is applied, in which the duration that buildings can passively maintain indoor temperatures within comfort limits - without active heating - is estimated based on the specific transmission heat loss of each building type.<sup>30</sup> The resulting volume factors indicate

<sup>&</sup>lt;sup>30</sup>A detailed description of the applied method is provided in Appendix C.2.

the number of hours the building can passively meet its heating demand from stored thermal energy. These are set to one hour for unrefurbished buildings, two hours for retrofitted buildings, and three hours for new constructions. In the flexible use case (H1), an additional thermal storage is introduced to enable more flexible heat pump operation. This is represented by increasing the respective volume factors by one hour, reflecting the availability of both passive and active (tank-based) storage. For example, in newly constructed buildings, the volume factor increases from three to four hours, representing the combined flexibility of building mass and dedicated heat storage.

### Transport sector

In the transport sector, we define three distinct use cases based on varying degrees of flexibility in charging behavior: passive charging, flexible charging, and bidirectional charging. In the passive use case (M0), EVs follow a predetermined charging profile with no flexibility in the timing of charging. In the flexible use case (M1), EVs are allowed to shift their charging within the limits of their positive and negative flexibility potentials, as described in Section 4.2.2. The final use case (M2) incorporates bidirectional charging, allowing vehicles not only to draw electricity from the grid but also to supply it back, thereby providing additional flexibility to the system. Across all flexible use cases, the energy balance must be maintained within each day.

### 4.4. Results

To evaluate the impact of varying degrees of flexibility provided by EVs and heat pumps on consumer and producer surplus, we apply the enhanced model to the defined use cases. By analyzing the changes in both surpluses, we aim to assess the overall impact on total system welfare, reflecting the economic benefits of market-driven flexibility provision at the wholesale level. This section is structured as follows: first, in Section 4.4.1, we present the results for the reference use case, which assumes no flexibility from heat pumps and EVs. In Section 4.4.2, we explore the changes in market outcomes resulting from different levels of flexibility provision.

### 4.4.1. Results without decentralized flexibility

In the absence of flexibility from EVs and heat pumps, the average electricity price, defined as the marginal cost of electricity, equals 51.39 EUR/MWh, as depicted in the cyan-colored box plot in Figure 4.3.<sup>31</sup> The electricity price for each

<sup>&</sup>lt;sup>31</sup>Refer to Appendix C.3 for the assumptions regarding fuel prices and EU carbon permits. The model's results remain structurally robust against variations in fuel and emission allowance prices.

hour serves as a key metric for determining the market values and surpluses for different producer groups, as well as the average electricity costs for consumers, all visualized in Figure 4.3. The distribution of market values, producer surpluses, and electricity costs is illustrated using box plots for each respective producer and consumer group. Market values for electricity producers - visualized by the blue dots in Figure 4.3 (top) - are calculated as the average revenue per unit of electricity sold, following the approach of Brown and Reichenberg (2021). Within the dispatch modeling framework, which assumes perfect competition, perfect foresight, and perfect information, short-term producer surplus can be achieved due to sunk investment costs. We define short-term producer surplus as the difference between the total market value (i.e., total revenue from electricity sold) and the sum of variable electricity generation costs over the analyzed period. The average producer surplus - represented by red dots - is calculated by dividing the absolute surplus (in EUR) by the respective production volumes. On the consumer side, we estimate average electricity costs, represented by the blue dots in Figure 4.3 (bottom).

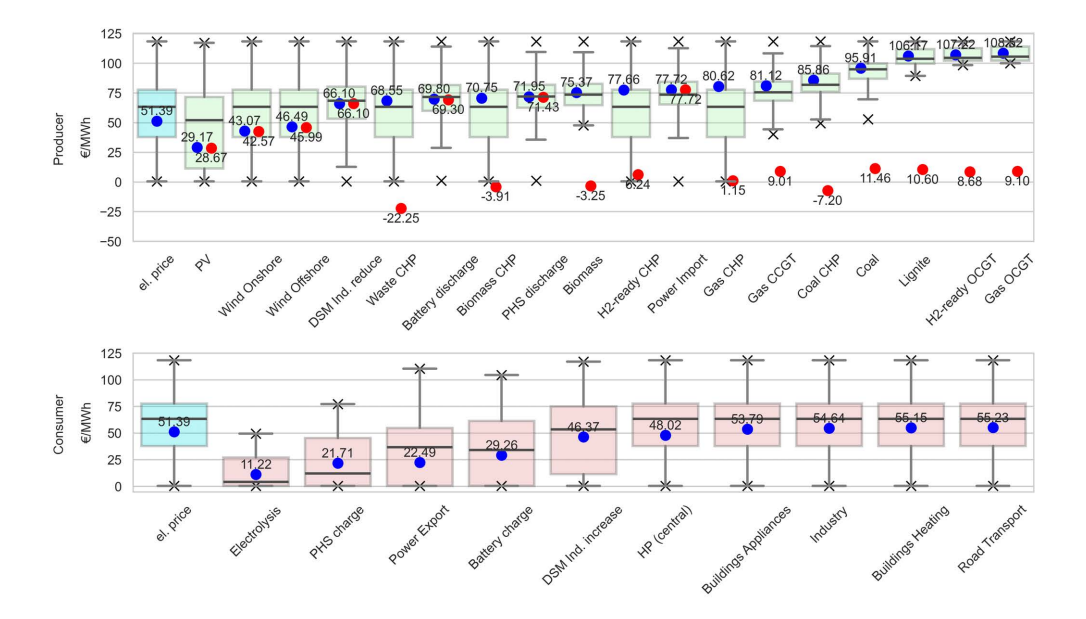


Figure 4.3.: Electricity price, average market values and producer surplus for producer groups as well as average electricity costs for consumer groups in the use case  $\rm M0/H0$ 

Note: Blue dots reflect the volume weighted market values for producer (top) and average electricity costs for consumer (bottom). Red dots denote the volume weighted short-term producer surplus (top). The box plots visualize the distribution of data points without volume weights. The minimum and maximum values are represented by crosses. The median is depicted by the gray line, while the colored box between the lower and upper quantiles represents 50% of all values. The maximum whiskers are equal or lower to 1.5 times the Inter-Quartile Range.

On the producer side, average market values (blue dots) indicate the merit order function. We observe that PV technologies exhibit the lowest market values, followed by onshore and offshore wind. This is primarily due to the influence of high renewable energy supply or low demand, which can push electricity prices downward. PV technologies tend to have lower market values as peak electricity demand often occurs in the afternoon or after sundown, especially in winter, when solar energy is unavailable. During periods of scarce renewable energy generation, NTCs and energy storage are used to meet electricity demand. In contrast, when renewable generation is low and demand is high, conventional power plants are deployed. Due to high fuel costs and comparably low efficiency, open-cycle gas turbines (OCGTs) have the highest average market values. We observe a wide range of producer surpluses (red dots) across the different technologies used for electricity production. Negative producer surplus values are particularly evident for CHP technologies, which are constrained by heat provision requirements. Biomass facilities also experience negative surplus values due to their assumed baseload generation, although in reality, subsidies prevent negative rents for these plants. Conventional power producers, such as coal, lignite, and gas plants, show comparatively low surplus values, reflecting their marginal position in the merit order and the impact of variable electricity generation costs.

On the consumer side, the order of average electricity prices paid by end-consumers reflects their load flexibility. Consumers with greater flexibility, such as electrolysis plants and batteries, tend to face lower electricity costs. Electrolysis plants can adjust their operations to take advantage of hours with high renewable energy supply or low demand, thereby reducing their costs. Compared to electrolysis plants, batteries exhibit higher average electricity costs due to technical constraints. In contrast, inflexible consumers, such as industrial users and households, face higher electricity costs. In the reference use case without decentralized flexibility, their electricity consumption remains relatively rigid, meaning less ability to avoid periods of high prices.<sup>32</sup> As a result, similar electricity costs are observed across various electricity-based applications for these end-consumers.

### 4.4.2. Results with decentralized flexibility

The introduction of decentralized flexibility affects electricity prices, leading to cascading effects on the economic outcomes of various producer and consumer groups. In this section, we first examine the effects of the defined flexibility use cases on electricity prices and CO<sub>2</sub> emissions. Next, we present welfare analysis results, focusing on the changes in producer and consumer surplus. Lastly, we assess welfare shifts within the heating and road transport sectors. This section, therefore, provides a comprehensive view of decentralized flexibility's impact on system-wide performance, sector- and technology group-specific dynamics, and user group-specific outcomes in the heating and road transport sectors.

 $<sup>^{32} \</sup>rm{For}$  certain industrial processes, demand-side management (DSM Ind.) is enabled, following Virtuelles Institut (2022).

### Impact of decentralized flexibility on electricity prices and CO<sub>2</sub> emissions

Decentralized flexibility has only a limited impact on wholesale electricity price levels, as shown by the blue dots representing the average level and by the box plots illustrating the distribution in Figure 4.4. However, while price levels remain relatively stable, decentralized flexibility helps reduce electricity price volatility. The mean 1-hour electricity price volatility, represented by the red dots in Figure 4.4, is defined as the average absolute price change from one hour to the next (Martinez-Anido et al., 2016).

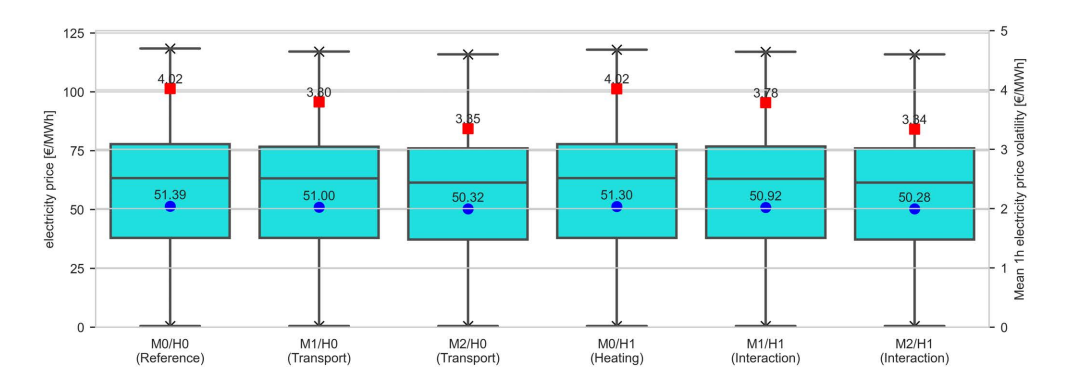


Figure 4.4.: Variation of electricity prices across different flexibility use cases

Note: The blue dots reflect the volume weighted marginal electricity generation costs, while the box plots visualize the distribution of data points without volume weights. The minimum and maximum values are represented by crosses. The median is depicted by the gray line, while the colored box between the lower and upper quantiles represents 50% of all values. The maximum whiskers are equal or lower to 1.5 times the Inter-Quartile Range (range of the colored box).

The system-oriented deployment of decentralized flexibility helps smooth demand fluctuations, flattening the hourly price curve and reducing price volatility. One way flexibility achieves this is through peak load reduction, which decreases the reliance on dispatchable generation. As a result, peak prices are lower across flexibility use cases compared to M0/H0. Although the number and magnitude of peak load hours decline with increased flexibility<sup>33</sup>, the maximum prices shown in Figure 4.4 exhibit only slight changes between the use cases. Another mechanism for reducing price volatility is demand shifting, where increased electricity consumption during hours with zero or negative prices helps smooth price curves further by reducing the frequency of such low-price hours. The overall small decline in average electricity prices suggests that the effects of peak shaving and demand shifting are nearly balanced. Together, these two effects contribute to a smoother residual load function, as illustrated in Figure C.8 in the Appendix. When comparing flexible assets, the results show that EVs, with their higher

<sup>&</sup>lt;sup>33</sup>This can be observed in Figure C.8 in the Appendix, which shows deviation in the residual load curve for each analyzed use case.

flexibility potential and longer flexibility windows, have a more substantial effect on price formation than heat pumps. The additional positive flexibility provided by EVs significantly reduces electricity price volatility and lowers the need for dispatchable generation.

Beyond mitigating electricity price volatility, decentralized flexibility also contributes to reducing CO<sub>2</sub> emissions in the energy sector, as shown in Table 4.4.

Table 4.4.: Changes in national  $\rm CO_2$  emissions under different flexibility use cases, in million tons of  $\rm CO_2eq$ 

Sector	M1/H0	M2/H0	M0/H1	M1/H1	M2/H1
Sector	(Transport)	(Transport)	(Heating)	(Interact.)	(Interact.)
Energy	-0.22	-0.37	-0.06	-0.27	-0.40

Note: Only changes in the CO<sub>2</sub> emission in the energy sector are included, while CO<sub>2</sub> emissions in sectors other than the energy sector remain constant across the flexibility use cases.

By lowering peak load hours and shifting demand, flexibility reduces the need for backup power plants and decreases RES curtailment, leading to lower overall  $\mathrm{CO}_2$  emissions. As evident from the deviations in the residual load curve from the reference use case (Figure C.8), the most significant impact on  $\mathrm{CO}_2$  emissions comes from flexible, and particularly bidirectional charging of EVs. EVs help reduce reliance on fossil-fuel-based backup generation and enable better utilization of renewable energy. In contrast, heat pumps - due to their lower flexibility potential and their tendency to operate during cold afternoon hours where RES availability is lower - show comparatively smaller potential to reduce RES curtailment. Consequently, their impact on  $\mathrm{CO}_2$  emission reductions is less pronounced than that of EVs. However, both technologies contribute to improving RES integration.

#### Welfare analysis for different sectors and technology groups

The introduction of decentralized flexibility through EVs and heat pumps results in a significant redistribution of economic welfare across various producer and consumer groups. The impact of the analyzed flexibility use cases varies greatly depending on the technology and end-use sector. While increased flexibility smooths the electricity price curve, it also leads to substantial reductions in producer surplus for dispatchable power plants, along with corresponding increases in consumer surplus, especially for EV owners. This consumer surplus is defined as the reduction in average electricity costs compared to the reference use case without decentralized flexibility (M0/H0). Figure 4.5 highlights these shifts across producer and consumer groups for the defined flexibility use cases compared to the reference use case (M0/H0), visually demonstrating how welfare redistribution varies with different levels of flexibility using a detailed heat map.

		M1/H0 (Transport)	M2/H0 (Transport)	M0/H1 (Heating)	M1/H1 (Interaction)	M2/H1 (Interaction)	-1070
	Road Transport	3.14	13.68	0.04	3.16	13.61	- <70%
	Buildings Heating	0.18	0.38	0.76	0.90	1.01	
	Non Roadtransport	0.20	0.82	0.04	0.23	0.84	- 80%
ပိ	Industry	0.20	0.79	0.04	0.23	0.81	- 80%
Consumer	Buildings Appliances	0.25	0.59	0.03	0.29	0.59	
Ĕ	HP (central)	-0.02	-0.71	-0.02	-0.08	-0.77	- 85%
er	DSM Ind. increase	-0.04	-1.16	-0.05	-0.27	-1.33	050/
	Battery charge	0.40	0.61	0.03	0.38	0.56	
	Power Export	-0.38	-2.43	-0.11	-0.50	-2.55	- 90%
	PHS charge	0.13	-0.28	0.01	0.12	-0.25	000/
	Electrolysis	-0.21	-1.45	-0.01	-0.28	-1.47	
	Power Import	-0.40	-1.54	-0.09	-0.50	-1.64	- 95%
	PHS discharge	-0.84	-3.60	-0.19	-1.00	-3.73	
	Battery discharge	-1.10	-4.28	-0.16	-1.26	-4.38	
	DSM Ind. reduce	-0.65	-1.99	-0.13	-0.53	-1.90	- 100%
	Hydro	-0.28	-1.30	-0.06	-0.33	-1.33	
	Wind Offshore	-0.25	-1.02	-0.06	-0.28	-1.04	
	Wind Onshore	-0.24	-0.69	-0.04	-0.24	-0.68	- 105%
ш	PV	0.14	1.32	0.04	0.16	1.38	
Producer	Coal	-0.13	-0.21	-0.03	-0.16	-0.25	
quc	Lignite	0.02	-0.90	0.05	-0.04	-0.91	- 110%
er	Gas OCGT	-0.42	-0.68	-0.03	-0.58	-0.56	
	Gas CCGT	-0.52	-2.72	-0.10	-0.65	-2.80	
	H2-ready OCGT	-0.29	-0.54	0.01	-0.39	-0.56	- 115%
	H2-ready CHP	-0.50	-2.88	-0.10	-0.58	-2.96	
	Gas CHP	-0.46	-2.35	-0.12	-0.55	-2.44	
	Biomass	-0.35	-1.60	-0.05	-0.42	-1.65	- 120%
	Biomass CHP	-0.24	-1.00	-0.04	-0.27	-1.04	1000/
	Coal CHP	-0.50	-2.43	-0.07	-0.55	-2.58	
	Waste CHP	-0.35	-1.70	-0.08	-0.41	-1.76	- >130%

Figure 4.5.: Changes in average producer and consumer surplus under different flexibility use cases, measured in EUR/MWh

Note: The columns represent the absolute changes in average producer and consumer surplus across different technology and end-user groups for the defined flexibility use cases compared to the reference use case (M0/H0). The estimated deviations in relative terms are visualized via heatmap.

The road transport sector, with the introduction of flexible (M1/H0) and bidirectional (M2/H0) charging, has the most significant impact on short-term producer surplus. Gas-fired power plants are particularly affected, with producer surplus changes reaching -2.72 EUR/MWh for gas CCGT (Combined Cycle Gas Turbine) plants and -2.35 EUR/MWh for gas CHP plants. In some cases, this represents a 70% reduction, highlighting the detrimental effect of EV flexibility on dispatchable assets. As EVs shift demand away from high-priced peak hours, gas power plants lose out on their ability to generate revenue during these times. This is visually illustrated in Figure 4.5, where the darkest shades correspond to the largest declines in producer surplus. Increasing flexibility further leads to cannibalization effects on other flexible assets, such as batteries, NTCs, and DSM, which face decreasing surplus. The flattening of the residual load curve due to flexible charging reduces price volatility, thereby limiting the profitability of technologies that store and/or shift electricity. Specifically, battery discharge experiences a significant decrease in producer surplus, declin-

ing by 4.28 EUR/MWh with increasing EV flexibility (M2/H1). The reduction in price peaks limits arbitrage opportunities for batteries. Similarly, power imports decrease by 1.54 EUR/MWh as domestic flexibility reduces the need for external electricity during peak demand hours. DSM in industrial processes also suffers a reduction in producer surplus, with decreases of 1.99 EUR/MWh in the M1/H0 use case. This is primarily due to the flattening of electricity prices, which reduces the effectiveness of DSM strategies. On the consumer side, the flexibility provided by EVs results in notable increases in consumer surplus. EV users see surplus gains of up to 13.68 EUR/MWh, reflecting a 30% increase in surplus when bidirectional charging is introduced. In contrast, other (nonflexible) end-use sectors such as non-road transport, industry, and buildings, show more modest increases in consumer surplus, ranging from 0.82 EUR/MWh and 0.59 EUR/MWh. These increases are driven by slightly lower electricity prices due to the additional system-oriented flexibility.

In comparison, the impact of heating sector flexibility (M0/H1) on welfare redistribution is less pronounced. For instance, gas CCGT plants experience a reduction in producer surplus of solely 0.10 EUR/MWh, which is significantly smaller than the impact of transport sector flexibility. Similarly, gas CHP plants see smaller but still notable reductions, with a 0.12 EUR/MWh decline in producer surplus, as shown in Figure 4.5. Decentralized flexibility from heat pumps also affects other flexible assets. However, due to the seasonal nature of heating demand, the overall impact is less severe compared to the transport sector. For example, PHS and battery discharge reduction only reaches -0.19 EUR/MWh and -0.16 EUR/MWh, respectively. Imports decrease by 0.09 EUR/MWh as domestic flexibility slightly reduces reliance on imported electricity during colder periods. DSM in industrial processes experiences a producer surplus reduction of 0.13 EUR/MWh compared to 1.99 EUR/MWh observed in the bidirectional charging use case (M2/H0). Heat pumps, which mainly provide flexibility during colder periods, have a limited ability to shift demand away from peak hours, resulting in smaller overall welfare gains for consumers. However, the highest gains, reaching 0.76 EUR/MWh, are observed in the heating sector with more flexible heating demand. Gains in other end-user sectors amount to 0.04 EUR/MWh, underscoring the limited potential of heating sector flexibility to substantially reduce electricity price volatility.

When flexibility from both sectors is combined (M1/H1 and M2/H1), the effects on welfare redistribution become more significant. Producer surplus for gas power plants continues to decrease, reaching up to 2.80 EUR/MWh for gas CCGT plants, further reducing profitability as both flexible EVs and heat pumps contribute to a stronger flattening of the residual load curve. Combined flexibility also affects batteries, imports, and DSM. Battery discharge experiences a reduction of 4.38 EUR/MWh, indicating that opportunities for batteries to capitalize on price fluctuations are further diminished in a highly flexible system. Gains from imports decrease by 1.64 EUR/MWh, reflecting the reduced need for external power as domestic flexibility improves the balancing of demand and

supply. DSM in industrial processes sees a drop of 1.90 EUR/MWh in producer surplus, underscoring the diminishing returns from DSM strategies in a market with decreasing price volatility. In contrast, consumer surplus increases significantly. The heating sector sees its largest welfare gains when flexibility from both heating and transport is combined, with consumer surplus increasing by up to 1.01 EUR/MWh for buildings heating. However, these gains remain modest compared to the road transport sector, which faces up to 13.64 EUR/MWh in consumer surplus.

#### Redistribution of total system welfare

Decentralized flexibility significantly reshapes total system welfare, redistributing economic benefits between producers and consumers. Table 4.5 summarizes the changes in total producer surplus and consumer surplus, categorized by three different technology groups. The last row shows the changes in the total system welfare.

Table 4.5.: Absolute welfare changes for specific producer and consumer groups, in million  $\overline{\mathrm{EUR}}$ 

Welfare changes	M1/H0 (Transport)	M2/H0 (Transport)	M0/H1 (Heating)	M1/H1 (Interact.)	M2/H1 (Interact.)
Total producer surplus	-259.5	-968.5	-43.3	-298.2	-993.9
- Renewable generation	-22.9	159.8	2.7	-13.9	180.0
- Conventional generation	-46.3	-226.9	-10.8	-55.3	-234.3
- Flexible assets	-190.3	-901.4	-35.4	-229.0	-939.6
Total consumer surplus	304.4	1031.0	57.4	353.9	1062.6
- End-use sectors	289.9	1057.0	56.7	340.5	1088.3
- Flexible assets	14.5	-26.0	0.7	13.3	-25.8
Total system welfare	44.9	62.5	14.0	55.7	68.7

Note: The estimated changes in total producer and consumer surplus are derived as the sum of technology and user-specific changes in total producer and consumer surplus for each analyzed flexibility use case compared to the reference use case without decentralized flexibility (M0/H0). Biomass and biomass CHP, hydro, PV, wind onshore, and wind offshore are included in the category renewable generation. Flexible assets encompass technologies used to shift, store, and/or provide electricity, such as DSM through industrial processes, batteries, PHS, and electricity imports/exports via NTCs from neighboring countries. Positive flexibility of these technologies (such as electricity provision or demand reduction) is denoted within the producer group, while negative flexibility (such as electricity infeed, export, or demand increase) is accounted for within the consumer group.

On the producer side, renewable generators benefit from increased flexibility with the introduction of V2G technology, which raises their surplus by up to 180 million EUR. In contrast, conventional power plants face substantial losses, with reductions in producer surplus reaching up to 234 million EUR. These losses are primarily due to fewer price peaks and the reduced need for dispatchable generation during high-demand periods. Flexible assets, such as batteries and DSM, experience mixed results. While these assets provide crucial flexibility, they suffer significant cannibalization as decentralized technologies like V2G erode their profitability. As a result, producer surplus for flexible assets decreases by up to

939.6 million EUR, reflecting the competition between centralized and decentralized flexible technologies for price arbitrage opportunities. On the consumer side, the introduction of decentralized flexibility leads to notable welfare gains, particularly in the transport and heating sectors. The most significant increases occur when both flexible EV charging and heating flexibility are combined, with consumer surplus rising by up to 1,088.3 million EUR. These gains are driven by consumers' ability to shift their electricity consumption to lower-cost hours, benefiting from reduced price volatility. However, as more flexibility is added to the system, it becomes increasingly difficult for flexible assets to capture value, as their ability to profit from price arbitrage diminishes.

When comparing the impacts across different use cases, decentralized flexibility in the transport sector - through flexible charging and V2G - has a far greater influence on system welfare than decentralized heating. While flexible charging (M2/H0) increases total system welfare by up to 62.5 million EUR, the impact of decentralized heating alone (M0/H1) is modest, with a welfare increase of just 14 million EUR. Even in combined use case (M2/H1), transport flexibility remains the dominant factor, contributing significantly to consumer surplus and system-wide efficiency improvements, while decentralized heating shows a much smaller incremental effect. This highlights the greater potential of transport sector flexibility to drive welfare gains compared to heating, which has a limited ability to shift demand.

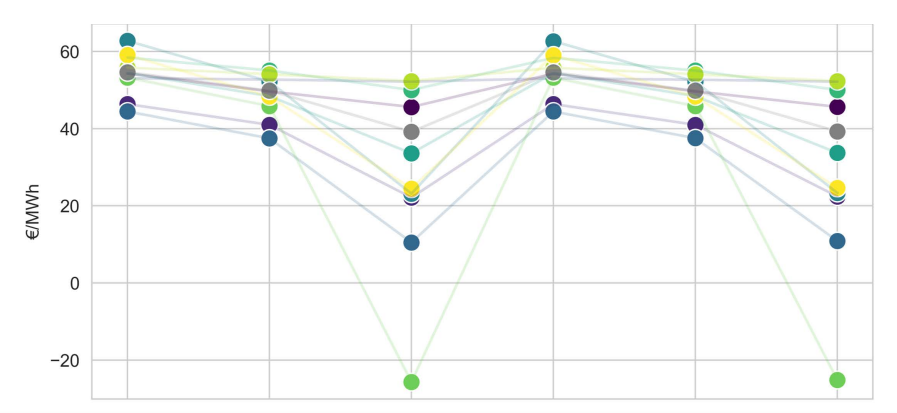
#### Impact of decentralized flexibility on electricity costs for distinct end-user groups

We further analyze the effects of the flexibility use cases on average electricity costs for decentralized heating in various building types, as well as on the average electricity costs for different mobility clusters.

#### Road transport

Average electricity costs differ significantly across mobility clusters, as shown in Figure  $4.6.^{34}$ 

<sup>&</sup>lt;sup>34</sup>Refer to Figure C.4 for supplementary data on the total electricity costs, and Figures C.6 and C.7 for calculated hourly deviations in EV charging compared to the reference use case (M0/H0) for each mobility cluster.



Mobility Cluster	M0/H0 (Reference)	M1/H0 (Transport)	M2/H0 (Transport)	M0/H1 (Heating)	M1/H1 (Interaction)	M2/H1 (Interaction)
MC1	54.31	49.65	45.61	54.28	49.66	45.64
MC2	46.35	40.99	22.15	46.35	41.0	22.42
MC3	53.07	52.71	52.18	53.04	52.67	52.19
MC4	44.45	37.49	10.5	44.44	37.53	10.87
MC5	62.75	52.2	23.14	62.66	52.16	23.32
MC6	54.44	48.43	33.59	54.4	48.42	33.7
MC7	58.43	55.07	50.0	58.36	55.04	50.03
MC8	53.23	45.85	-25.64	53.21	45.85	-25.17
O MC9	55.81	54.11	52.33	55.77	54.09	52.33
MC10	59.1	48.34	24.44	59.05	48.33	24.62
All	54.64	49.85	39.19	54.6	49.83	39.28

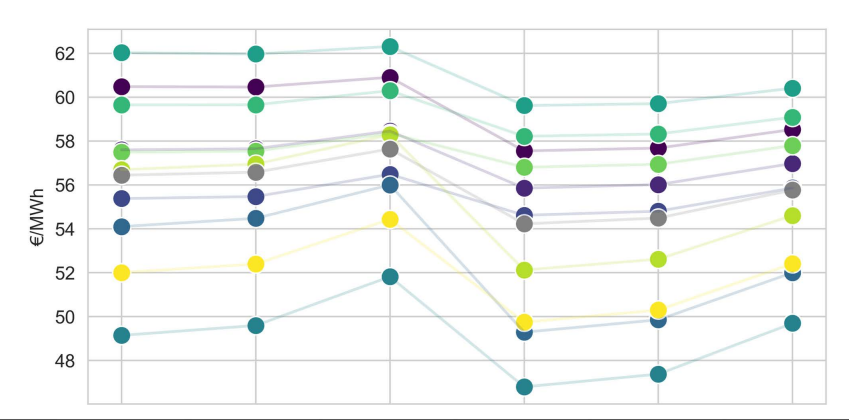
Figure 4.6.: Changes in average electricity costs across mobility cluster under different flexibility use cases, in EUR/MWh

Note: 'All' denotes the weighted average electricity costs across analyzed mobility clusters.

In the reference use case without decentralized flexibility (M0/H0), average electricity costs range from 44.45 EUR/MWh in MC4 to 62.75 EUR/MWh in MC5, reflecting variations in consumption and charging behavior patterns. When flexible charging is introduced (M1/H0), average electricity costs decrease across all clusters. On average, costs fall to 49.85 EUR/MWh, with the largest reduction seen in MC10, where costs drop from 59.1 EUR/MWh to 48.34 EUR/MWh. By contrast, MC4 shows a smaller reduction, declining from 44.45 EUR/MWh to 37.49 EUR/MWh. The introduction of demand flexibility leads to significant cost reductions, with an average decrease of around 8.7%. When bidirectional charging is employed (M2/H0), the impact on costs varies significantly among clusters. On average, electricity costs drop further to 39.19 EUR/MWh. MC8 shows a substantial deviation, with negative electricity costs of -25.64 EUR/MWh due to the cluster's ability to shift nearly all charging demand across the day. Conversely, MC4, with less flexibility, experiences a much smaller reduction, with costs declining only to 10.5 EUR/MWh. The addition of heat pump flexibility in the M0/H1 use case leads to a slight increase in electricity costs, with average costs increasing to 54.6 EUR/MWh. Similarly, in the M1/H1 and M2/H1 use cases - where both electric vehicle and heat pump flexibility are incorporated - results are mixed. Average costs stabilize around 49.83 EUR/MWh in M1/H1 and 39.28 EUR/MWh in M2/H1. These findings underscore the substantial savings associated with charging flexibility, particularly when V2G is implemented, although the benefits vary greatly across different mobility clusters.

#### Decentralized heating

In the heating sector, average electricity costs for heat pump operation vary significantly across building types, as shown in Figure 4.7.<sup>35</sup>



Buildings			M2/H0 (Transport)	M0/H1 (Heating)	M1/H1 (Interaction)	M2/H1 (Interaction)
Res1 ASHP	60.48	60.46	60.9	57.55	57.68	58.53
Res2 ASHP	57.6	57.65	58.46	55.85	56.01	56.98
Res3 ASHP	55.38	55.47	56.48	54.62	54.8	55.86
Com1 ASHP	54.1	54.48	56.0	49.28	49.85	52.0
Com2 ASHP	49.14	49.59	51.82	46.79	47.37	49.69
Res1 GSHP	62.03	61.97	62.31	59.62	59.7	60.41
Res2 GSHP	59.65	59.65	60.3	58.22	58.32	59.09
Res3 GSHP	57.49	57.54	58.35	56.8	56.94	57.8
Com1 GSHP	56.69	56.95	58.29	52.12	52.62	54.6
Com2 GSHP	52.0	52.39	54.43	49.74	50.29	52.41
All	56.44	56.58	57.64	54.22	54.49	55.77

Figure 4.7.: Changes in average electricity costs across buildings types under different flexibility use cases, in EUR/MWh

Note: 'All' denotes the weighted average electricity costs across analyzed building types.

While the direction of the effects of additional flexibility from both heat pumps and electric vehicles is consistent across building types, the magnitude of these effects differs. The introduction of thermal storage (M0/H1) results in a general reduction in electricity costs across all building types, with the average cost decreasing from 56.44 EUR/MWh to 54.22 EUR/MWh. Commercial buildings experience a sharper decline, reflecting their high degree of flexibility with additional thermal storage, whereas residential buildings see a more moderate impact.

<sup>&</sup>lt;sup>35</sup>Refer to Figure C.3 for supplementary data on the total electricity costs, and Figure C.5 for hourly deviations in heat pump operation compared to the reference use case (M0/H0) for each building type.

Notably, unrefurbished buildings benefit the most from thermal storage, while more efficient buildings see smaller reductions in costs. When road transport flexibility is introduced (M1/H0), it puts upward pressure on electricity costs, raising the average to 56.58 EUR/MWh. However, this increase is not uniform across building types. Residential buildings show moderate cost increases, while commercial buildings are more strongly affected. The difference in magnitude suggests that commercial entities are more sensitive to the increased competition for low-cost electricity. The impact of added load becomes even more pronounced with the integration of V2G technology (M2/H0), further driving up costs to an average of 57.64 EUR/MWh. Commercial buildings face steeper increases compared to residential buildings, indicating a stronger sensitivity to the added load and potential cannibalization effects between electric vehicles with V2G and heat pump operation. Commercial buildings, which typically benefit from lower electricity costs due to higher daytime consumption, are more heavily impacted by the competition for low-cost electricity, while residential buildings see a more moderate cost increase. Finally, when both V2G and thermal storage are utilized (M2/H1), electricity costs stabilize somewhat, with the average cost reducing to 55.77 EUR/MWh.

This use case shows a greater convergence in prices across building types. For instance, residential buildings using GSHPs (Res1 GSHP) see a cost reduction from 62.31 EUR/MWh in M2/H0 to 60.41 EUR/MWh in M2/H1, illustrating how the additional flexibility from thermal storage offsets the upward pressure from V2G. Commercial buildings, although still affected by V2G, also experience some relief from the cost increases, though to a lesser extent than residential buildings.

#### 4.5. Discussion

The discussion of the findings spans multiple perspectives, encompassing system-level impacts, sectoral and technological dimensions, and user-specific implications. On the system level, the results indicate that decentralized flexibility has a minimal effect on average wholesale electricity prices but significantly reduces price volatility by smoothing the residual load curve. This aligns with findings by Härtel and Korpås (2021) and Böttger and Härtel (2022), which emphasize flexibility's stabilizing effects on wholesale prices. Flexibility from EVs, especially those with V2G capabilities, reduces both the frequency and intensity of peak demand hours and helps smooth demand fluctuations, with negligible stabilizing effects observed for heat pumps. Although this study focuses on 2030, a year in which electricity price volatility is still moderate, the expected rise in RES penetration could amplify volatility, making decentralized flexibility increasingly valuable.

Our findings also suggest that flexibility contributes to reducing national  $\rm CO_2$  emissions by aligning demand with variable renewable generation and mitigating

market-driven RES curtailment. This effect is particularly pronounced in Germany, where fossil fuels are expected to remain a substantial part of the energy mix in 2030. However, as RES shares continue to increase, the potential for flexibility to reduce emissions may lessen, as e.g. seen in the study by Kirkerud et al. (2021) on Norway's RES-dominant energy system.

Although decentralized flexibility improves total system welfare, the welfare gains are relatively modest and vary significantly across the analyzed flexibility use cases. Under high-flexibility assumptions for both EVs and heat pumps, welfare improvements reach up to 68.7 million EUR, suggesting only a moderate system-wide impact. Modeling results further indicate that higher flexibility potential due to longer flexibility windows, such as those of flexible and especially bidirectional EV charging, play a critical role, with the resulting welfare benefits being over three times greater than those achievable with flexible heat pumps only. The observed price stickiness in electricity costs for heat production via heat pumps arises due to low or absent RES generation during cold, dark winter hours, when heat demand is high.

Nevertheless, the quantified impact of flexibility on total welfare may be overestimated, as this study assumes sufficient distribution grid capacity to support market-oriented flexibility provision. In cases where distribution grid congestion occurs, the ability to provide flexibility, and thus achieve related welfare gains, may be restricted. This constraint could vary for EVs and heat pumps depending on regional load profiles and grid infrastructure. Given the findings in Lilienkamp and Namockel (2025), our results may still approximate welfare gains accurately, particularly for a moderate penetration of RES, EVs, and heat pumps in 2030, where distribution grid constraints are less pronounced, even with herding behavior. Nonetheless, such constraints could become increasingly critical with higher penetration rates.

Moreover, by focusing exclusively on the wholesale (day-ahead) market, this analysis omits the welfare gains that decentralized flexibility might yield in balancing and intraday markets. These markets typically exhibit higher price volatility than the day-ahead market due to real-time supply-demand imbalances and the need to compensate for unpredicted RES generation changes. Addressing different markets with decentralized flexibility would introduce opportunity costs, potentially reducing the effects on the day-ahead market.

The introduction of decentralized flexibility redistributes welfare across market participants, shifting surplus from conventional producers to consumers. This shift primarily affects gas-fired power plants, which see reduced surplus due to lower frequency and intensity of peak demand hours. The observed decrease in peak load suggests that flexibility could lower the need for investments in costly backup generation. However, as this analysis relies on a dispatch model that assumes sunk investment costs, it does not capture the potential influence of decentralized flexibility on optimal investment decisions.

Furthermore, our results suggest a potential cannibalization effect among flexible assets, with decentralized flexibility significantly reducing the surplus for centralized assets like batteries. This occurs as decentralized flexibility reduces the demand for off-peak electricity, limiting centralized assets' profitability. Although our analysis highlights potential cannibalization effects, it does not address trade-offs between centralized and decentralized flexibility investments. Here, co-optimization of investment and dispatch decisions would provide a long-term equilibrium, ensuring optimal capacity configuration with profitability of all assets.

For RES generators, the impact on producer surplus is minor, consistent with findings by Bernath et al. (2021), who identified limited impacts on the market values of renewable power plants. Notably, PV producers experience increased surplus across all flexible use cases, particularly with V2G-enabled EVs, which shift demand to better align with daytime solar generation. However, potential network congestion, particularly at the distribution level, could constrain the observed increasing PV integration.

Our modeling results highlight that all user groups benefit from lower electricity costs due to decentralized flexibility, regardless of their participation in flexibility provision. However, this analysis only addresses the procurement component of the end-user electricity price, approximated by marginal electricity generation costs, and excludes taxes, levies, and network fees, which together constitute a significant portion of end-user electricity price (EWI, 2023b). This omission limits the analysis, as these additional price components may alter the economic gains of flexibility for various end-user groups.

The benefits from decentralized flexibility provision vary significantly by user group, with flexibility potential largely determining cost savings. In the road transport sector, the range of the observed average electricity costs across mobility clusters increases with increasing flexibility. Charging flexibility - especially with V2G capabilities - yields more substantial savings for EV owners with more frequent and longer parking periods. Within the building sector, we observe that introduction of additional flexibility through thermal storage leads to a convergence of electricity costs across building types. Commercial buildings, due to their load profiles with less pronounced evening peaks, benefit more from additional thermal storage. However, they are also more affected by the introduction of V2G, as the additional flexibility from EVs increases competition for low-cost electricity during off-peak hours. This analysis, however, does not account for the costs of providing flexibility, such as e.g. investments in smart meters or bidirectional charging. Some consumers may benefit from flexibility investments without bearing associated costs, while others can bear costs but realize minimal benefits. For user groups with minor cost savings, the net gains from flexibility may be negligible after factoring in these expenses. The profitability of flexibility provision is therefore highly dependent on specific consumption patterns and the flexibility windows. For certain user groups, flexibility may be unprofitable once these costs are considered. Our findings highlight the advantage of broader flexibility windows, particularly for EVs, and underline the limitations that heat restrictions and price stickiness in electricity costs for heat production impose on the flexibility potential of heat pumps.

#### 4.6. Conclusion

EVs and heat pumps can play a pivotal role in the future energy system, significantly influencing electricity price formation. The deployment of end-user flexibility not only shapes price dynamics but also brings about considerable redistributional effects within the electricity market. This paper assesses the distributional effects of decentralized flexibility by enhancing the established European energy system model DIMENSION to better represent user-specific behavior and flexibility potential in the road transport and heating sectors. Methodologically, we extended the model's resolution by incorporating diverse end-consumer groups and flexibility options, enabling a more granular analysis of welfare effects at the end-user level. This approach allows us to capture the effects of shifting electricity demand, using technologies such as EVs and heat pumps, on market outcomes not only at the system level, but also across sectors and among different user groups. By simulating multiple flexibility use cases for Germany, we quantify how welfare gains and losses are distributed between electricity producers and consumers, and how these outcomes vary depending on the flexibility potential and usage behavior of different technologies and user groups. This user- and technology-specific quantification of redistributional effects adds to the existing literature by offering a more differentiated perspective on the economic implications of end-user flexibility.

#### 4.6.1. Main results

At the system level, our results show that while decentralized flexibility has a limited impact on average wholesale price levels, it significantly reduces price volatility by smoothing demand peaks and aligning load with renewable energy generation. EVs, due to their larger flexibility windows, contribute more prominently to volatility reduction than heat pumps. This flexibility also facilitates CO<sub>2</sub> emissions reductions by decreasing RES curtailment, underscoring its potential to support a low-carbon energy system as renewable energy shares increase.

At the sectoral and technology-specific levels, decentralized flexibility enhances overall system welfare, generating gains of up to 68.7 million EUR. However, these benefits are unevenly distributed. Conventional generation technologies, particularly natural gas plants, experience reduced revenues due to lower peak prices. RES, particularly solar PV, see modest gains from better demand alignment, while battery storage faces competitive pressure from EV flexibility, leading to a cannibalization effect in the market. The transport sector, with its higher

flexibility potential, delivers greater welfare gains than the heating sector, high-lighting EVs' significant role in system cost savings. Overall, by lowering peak prices through increased flexibility, the average electricity costs for consumers decrease. However, the magnitude of this effect varies depending on the specific flexibility use case.

At the user level, while consumers as a whole benefit from lower electricity procurement costs, the extent of these benefits differs significantly across user groups and the flexibility use case. These variations are highly dependent on the consumption characteristics and flexibility time windows. In the transport sector, EV owners with greater flexibility potential, such as those who park for extended periods, experience the largest cost savings, especially with V2G capabilities. In the heating sector, commercial buildings with flatter load profiles benefit most from flexibility, while residential buildings see moderate cost changes. The competition introduced by EV flexibility impacts commercial users especially, raising off-peak prices and indicating the potential cannibalization across decentralized flexible assets.

#### 4.6.2. Future research

Based on our findings, we identify several relevant areas for further investigation. While this work focuses on the market-oriented provision of flexibility, future research should incorporate network constraints - particularly at the distribution level - to capture interactions between decentralized flexibility and grid congestion. The interplay between market-driven flexibility provision and price or volume signals from distribution system operators could create significant challenges in the future, underscoring the need for further investigation. Expanding the scope to include balancing and intraday markets would provide a more comprehensive view of flexibility's overall system benefits, as these markets play a key role in managing renewable variability and maintaining grid reliability. From the end-user perspective, the introduction of multiple markets, along with the associated opportunity costs, would add complexity but also unlocks greater opportunities for profit making. Additionally, exploring the evolution of components in end-user electricity prices - such as taxes, levies, and network charges - would clarify how these factors influence flexibility's financial viability and the savings potential for different user groups. Similarly, while our analysis sheds light on redistribution between end-user sectors and heterogeneous user groups, further research can examine how decentralized flexibility affects different social or income groups, as redistributional impacts could vary significantly across socioeconomic demographics.

# 5. Understanding the fundamentals of hydrogen price formation and its relationship with electricity prices - Insights for the future energy system

#### 5.1. Introduction

The global energy transition toward climate neutrality has positioned hydrogen  $(H_2)$  as a promising pillar in the decarbonization of multiple sectors. As an energy carrier, hydrogen demand could span across industries, potentially exhibiting relatively rigid demand patterns, and could extend into sectors like (central) heating and electricity, where demand might be more dynamic. The heating sector might experience temperature-dependent variations, leading to both seasonal and intraday fluctuations, while the electricity sector could exhibit significant volatility, driven by the use of hydrogen in power generation. Furthermore, the sourcing of hydrogen can be diverse, with imports from non-European regions, domestic production, or imports from neighboring countries, each contributing to diverse prices for hydrogen.

Much like for electricity (EL), heterogeneity and volatility in hydrogen supply and demand could lead to a dynamic price structure when hydrogen is traded in the market. The European Energy Exchange intends to development market mechanisms for hydrogen (EEX, 2025). Additionally, recent infrastructure plans propose hydrogen pipelines to connect different market regions (ENTSO-E and ENTSOG, 2024). In such a setting, the diverse supply and demand structures for hydrogen would shape market equilibrium, influencing hydrogen prices accordingly. Those effects can also be diverse because of the interdependencies with the electricity sector. Additionally, the presence of hydrogen storage, acting both as suppliers and consumers, would introduce further complexity into the pricing dynamics.

Despite the increasing focus on hydrogen within the energy transition, significant uncertainties remain around the level and volatility of future hydrogen prices. These uncertainties hinder investments in hydrogen infrastructure, particularly in storage and electrolyzers, due to unclear profitability (Odenweller and Ueckerdt, 2025). Major concerns are the unpredictability of price developments and competition with alternative technologies, such as electricity and pumped hydro storage, which offer comparable energy storage solutions. This uncertainty, coupled with a fundamental lack of understanding of how region-

specific and daily hydrogen prices emerge, limits investor confidence and reduces planning security.

This study seeks to address these challenges by investigating the fundamentals of hydrogen price formation and their interdependencies with electricity prices. The analysis includes a comparison of price structures, followed by more granular assessments depending on different market situations. Co-integration and correlation analysis asses the interdependencies between hydrogen and electricity prices. Regression analysis determines key drivers on price formation. In addition, price ratios and the statistical properties of prices in both markets are investigated. The robustness of these findings is further evaluated through sensitivity analysis across different system configurations. To compute the relevant data for the analysis, the European energy system model DIMENSION is expanded to enable high-resolution, integrated dispatch calculations for both electricity and hydrogen systems, incorporating up-to-date cost data for hydrogen imports and updated infrastructure parameters.

Different literature streams already address the effects of cross-sector integration of hydrogen. Its importance as a sector-coupling technology necessitates integrated modeling approaches that consider both electricity and hydrogen systems. Several studies have explored such integrated models, often focusing on robust investment decisions under varying scenarios. For instance, Caglayan et al. (2020) developed a robust energy system design that considers hydrogen infrastructure, quantifying the necessary storage capacities. Their focus on robustness against different weather years highlights the significance of external factors in hydrogen system planning. Similarly, Kondziella et al. (2023) used 192 scenarios to assess uncertainty regarding hydrogen storage demand, while Frischmuth et al. (2024) also examined the role of uncertainty in storage needs. In addition, Gawlick and Hamacher (2023) investigated optimal energy systems that integrate both electricity and hydrogen, and Lüth et al. (2023) analyzed the trade-offs between electricity and hydrogen infrastructure, emphasizing the sensitivity of investment decisions to hydrogen prices. The role of hydrogen in cost minimization and infrastructure planning has also been addressed by Gils et al. (2021), who identified hydrogen transport infrastructure as essential for reducing supply costs. Additionally, Durakovic et al. (2023) studied the impact of hydrogen production on electricity prices across different European regions, while Bellocchi et al. (2023) focused on hydrogen's role in decarbonization pathways for Italy's energy system, showing that while CO<sub>2</sub> emissions could be reduced by 49%, the associated annual costs would increase by 8%. Neumann et al. (2023) compared system costs across different levels of hydrogen network expansion, and Frischmuth and Härtel (2022) examined how varying hydrogen procurement strategies influence investment decisions. Last, Keutz and Kopp (2025) investigate how different Take-or-pay rates influence the need for hydrogen storage. They find that a higher amount of inflexible long-term contracts for hydrogen increase the need for hydrogen storage.

The interactions between hydrogen and electricity have been the subject of increasing attention, especially in terms of how sector coupling technologies influence electricity prices. Mathematical models, often calculated over 8760 hours to simulate a full year, have provided insights into these dynamics. For example, Liski and Vehviläinen (2023) demonstrated how marginal changes in electricity demand can alter equilibrium prices, resulting in distributional effects between producers and consumers. Ruhnau (2022) explored how electrolysers' electricity consumption increases electricity prices during peak hours and stabilizes the market value of renewable technologies. Frischmuth and Härtel (2022) analyzed how hydrogen procurement strategies affect electricity prices and price duration curves.

Research examining the influence of electricity prices and energy assets on hydrogen prices remains relatively limited. Early studies, such as Hesel et al. (2022), explored the bidirectional relationship between electricity and hydrogen, demonstrating that renewable energy sources and electrolysers are complementary technologies that enhance each other's profitability. Schönfisch (2022) investigated the development of a global hydrogen market and concluded that cross-border trade in pure hydrogen becomes economically viable in scenarios with high shares of renewable energy-based low-carbon hydrogen production. This viability is driven by the uneven global distribution of low-cost renewable energy resources, creating significant hydrogen price differentials between countries with high demand but limited renewable potential and those with abundant, cost-effective resources. Koirala et al. (2021) introduced a framework integrating electricity, hydrogen, and methane markets, with a focus on the Netherlands, highlighting hourly price interactions but leaving daily dynamics for other countries such as Germany unexplored. Finally, Frischmuth et al. (2024) conducted a high-resolution dispatch analysis of hydrogen storage but did not address the daily variability in hydrogen prices. In summary, while existing research has provided valuable insights into integrated energy systems featuring hydrogen and electricity, the more granular interactions between these two markets on a daily basis with a focus on Germany, as well as the underlying market dynamics that govern their price relationships, remain insufficiently explored. Examining the price relationship between these two markets would provide valuable knowledge to policymakers, investors, and researchers, enabling them to evaluate different decarbonization options without necessarily running energy system models.

This paper seeks to address the existing research gap by answering two key questions: How do short-term effects, such as weather and demand variability, shape hydrogen and electricity price dynamics? How do short-term price interactions change under different energy system configurations? To answer these questions, the paper presents enhancements to the existing European energy system model DIMENSION by a daily resolution of Power-to-X (PtX) fuels<sup>36</sup>. In

<sup>&</sup>lt;sup>36</sup>Power-to-X fuels, as defined in this study, refer to synthetic fuels such as diesel, gasoline, hydrogen, kerosene, natural gas, or oil. The model incorporates all production technologies for these fuels that are considered climate-neutral.

addition, enhancements cover the integration of hydrogen storage, cross-border trade capacities, and up-to-date data for oversea imports via long-term contracts (LTCs).

To address the uncertainty around the future system developments, sensitivities reflect varying levels of hydrogen demand and degrees of interconnection between countries through Net transfer capacities (NTCs) for hydrogen. Doing so, this research paper makes the following contributions to the existing literature:

- Development of an enhanced energy system model for the integrated optimization of the European electricity and hydrogen market.
- Analysis of hydrogen and electricity price structures, volatility, and interdependencies.
- Examination of short-term effects and system configurations that influence hydrogen and electricity price dynamics.

The analysis focuses on Germany and assumes a liquid market for hydrogen in 2050 with daily resolution to isolate and quantify the effects of market-oriented provision of hydrogen next to electricity. Moreover, the analysis is limited to changes in shadow prices derived from the equilibrium constraints for electricity and hydrogen, interpreted as market prices, without considering other components of prices, mark-ups or policy instruments. Thus, an important part of this study is the reflection on the model's limitations and assumptions that influence price formation, as well as a discussion of their implications for the future energy system.

The results indicate that dynamics between hydrogen and electricity are governed by short-term interactions. Electricity prices respond closely to renewable generation and demand, while hydrogen prices are less responsive to these factors. Instead, hydrogen price formation is more structurally determined, particularly by storage dynamics and cross-border trade. The strength of the relationship between the two markets is found to depend heavily on market situations: strong coupling occurs in situations with low residual load, when electrolysis is price-setting, while decoupling emerges under high residual load, when hydrogen storage discharge dominates price formation. Furthermore, driven by the consideration of LTCs and cross-border trade limitations, the electricity-to-hydrogen price ratio averages 0.56, which is lower than in prior sudies (0.7–1.2), which abstract from these characteristics. Scenario analysis shows that expansion of NTCs for hydrogen slightly weakens price coupling, with an exception in situations with high residual load where correlation of hydrogen and electricity prices increases. Demand reduction exerts only minor effects. Overall, the relationship between hydrogen and electricity prices remains consistent across configurations but sensitive to short-term system dynamics. Finally, the results suggest that relying solely on short-term price formation may not ensure cost recovery for

hydrogen storage and electrolysis. In particular, LTC prices for hydrogen reflect both capital and operational costs, whereas the modeled short-term price formation is based on shadow prices. To address this price discrepancy, capacity remuneration, cost mark-ups, or risk premiums may be needed to ensure investment viability and the development of a liquid market for hydrogen.

The paper is structured as follows: Section 5.2 describes the modeling approach and the system configurations investigated within this research. In Section 5.3, the price formation for hydrogen and the relationship with electricity prices is investigated in the reference scenario, providing a baseline understanding of the underlying interdependence and dynamics. Then, in Section 5.4, the robustness of these findings is tested by considering different system configurations. Section 5.5 addresses the broader implications of the findings regarding the future energy system, as well as their limitations. Finally, Section 5.6 summarizes and suggests directions for future research.

#### 5.2. Methodology, input data and scenario design

This study investigates the fundamentals of hydrogen price formation and its relationship with electricity prices based on shadow prices. To this end, the European energy system model DIMENSION (Emelianova and Namockel, 2025, Helgeson, 2024, Helgeson and Peter, 2020, Richter, 2011) is employed and extended to derive daily prices for hydrogen from the respective equilibrium constraint, analogous to electricity. The shadow prices reflect the cost of supplying one additional unit of the corresponding energy carrier at a given point in time. Throughout the paper, the shadow prices are interpreted as prices under the condition of complete markets, perfect information, and perfect competition. In this context, strong duality, given linearity and a convex objective function, is assumed between the electricity and hydrogen markets in the integrated energy system model. Daily values for a full year serve as the basis for the empirical analysis, with a particular focus on short-term influences, such as weather variability and demand fluctuations, that shape the dynamics of hydrogen and electricity prices. Price formation mechanisms and the interrelationship between the two markets are assessed through co-integration, and correlation and regression analyses, complemented by a comparison of statistical properties. To capture heterogeneous market conditions, the data are segmented into subsets using a k-Means clustering algorithm, enabling a more granular examination of price interactions across different market situations. Next to a reference scenario, different system configurations are introduced to evaluate the robustness of the findings.

The following sections outline the model extensions and assumptions related to PtX fuels, with a particular focus on hydrogen (Section 5.2.1), and describe the system configurations investigated in this study (Section 5.2.2).

#### 5.2.1. Modeling the equilibrium for hydrogen

The equilibrium constraint represents the central element of the model extension, as it determines the marginal generation costs for each fuel modeled. The constraint is formulated not only for hydrogen but also for other PtX-fuels such as diesel, gas, gasoline, kerosene, and oil, denoted as  $f \in F$ . This constraint applies across all countries within the model's scope,  $b, b_1 \in B$ , and considers external regions  $r \in R$  as potential suppliers. Various technologies  $a \in A$ , including electrolysis and hydrogen storage, are considered alongside different sectors  $s \in S$ , each with distinct characteristics. The equilibrium ensures that, for each day  $d \in D$ , supply equals demand across all fuels, as described in Equation (5.1). Throughout the study, the notations presented in Tables D.1 to D.3 in the Appendix are consistently used, with optimization variables distinguished from exogenous parameters by uppercase letters for the former. The formulation reflects an investment decision framework with reduced temporal granularity. In dispatch simulations, selected variables (denoted by '\*') are fixed to represent a given capital stock and long-term import decisions.

$$PIPE^{*}(b,f)/365 + \sum_{r \in R} SHIP^{*}(r,b,f)/365$$

$$+ \sum_{b_{1} \in B} TRADE(d,b_{1},b,f) + \sum_{h \in H} \sum_{a \in A} \frac{24}{H} * PROD(d,h,a,b,f)$$

$$\geq \sum_{s \in S} USE(d,b,s,f) + \sum_{a \in A} INSTOR(d,b,a,f)$$

$$+ \sum_{b_{1} \in B} TRADE(d,b,b_{1},f) \quad \forall d \in D \land b \in B \land f \in F.$$

$$(5.1)$$

On the supply side, imports are available via pipeline  $(PIPE^*)$  or ship  $(SHIP^*)$  from regions outside the model scope. Additionally, trade is possible with neighboring countries within the model scope, given that infrastructure exists between two countries. Domestic PtX production, such as electrolysis, is captured by PROD with hourly resolution. On the demand side, consumption of PtX-fuels across various sectors is represented by USE. For hydrogen, storage injection is separately represented as INSTOR. Similarly, trade is modeled on the demand side as well. In the subsequent sections, the fundamental characteristics of these supply and demand options are described in greater detail.

114

<sup>&</sup>lt;sup>37</sup>Reduced temporal granularity refers to a representative subset of days (D) and hours (H) rather than a full year with hourly resolution.

 $<sup>^{38}</sup>$ The term USE covers the exogenously defined hydrogen demand in end-use sectors such as industry, transport or buildings and also includes the endogenous fuel consumption in the energy sector.

#### PROD - Domestic production of hydrogen

Domestic hydrogen production is performed using alkaline water electrolysis, with efficiencies ranging from 72% to 77%. The operation of electrolysis is fully market-oriented, with production quantities determined by market conditions. Additionally, the variable PROD also covers the hydrogen supply by different types of hydrogen storage.

#### SHIP - Hydrogen import via ship from non-EU regions

Imports via ship are modeled as long-term contracts (LTCs). The contract volume is a fixed parameter in the dispatch simulation, determined by an investment model run. The total amount of fuel imported from a specific exporting region  $r \in R$  across all European countries is constrained by the export potential of that region, denoted as ptxPotShip in MWh<sub>th</sub>/year, as formulated in Equation (5.2). Additionally, only countries with access to the ocean are eligible to import PtX-fuels via ships. These imports are restricted by the capacity of the import terminals, ptxTerminal, as described in Equation (5.3). The associated import costs, represented by the variable  $COSTS^{SHIP}$  in Equation (5.4), are considered in the overall objective function of the energy system model.

$$\sum_{b} SHIP^{*}(r, b, f) \le ptxPotShip(r, f) \quad \forall r \in R \land f \in F$$
 (5.2)

$$\sum_{r} SHIP^{*}(r, b, f)/365 \le ptxTerminal(b, f) \quad \forall b \in B \land f \in F$$
 (5.3)

$$COSTS^{Ship} = \sum_{b \in B} \sum_{r \in R} \sum_{f \in F} SHIP^*(r, b, f) * ptxCostsShip(r, f)$$
 (5.4)

The data for PtX imports via ship are sourced from the EWI Global PtX Cost Tool 2.0, which provides the potential and costs for various PtX fuels from multiple exporting regions (Klaas et al., 2024). The cost data represent the levelized cost of hydrogen, including both variable and investment costs. This encompasses the costs of hydrogen production as well as the infrastructure required for importation, such as terminals and conversion facilities. The supply cost function for hydrogen imports is illustrated in Appendix D.2. The supply curve relies on several key assumptions. The analysis assumes that exporting countries maintain a baseload supply profile throughout the year. Accordingly, the utilization of import terminals is assumed to remain constant across the entire modeling period. From each exporting region, only the cost of the cheapest production and transportation method is considered. The utilized potential for hydrogen production is assumed to be 20% of the technical potential. Only regions with a minimum production potential of 50  $TWh_{th}$  per year are included in the analysis. North Africa and Ukraine are excluded from the supply cost function, as these import options are modeled as bilateral imports via pipelines.

For hydrogen imports, the parameter ptxTerminal is fixed at 10,000 MWh<sub>th</sub> per day for countries with access to the global hydrogen market, defined as those having a coastal border.

#### PIPE - Hydrogen import via pipeline from non-EU regions

Pipeline imports are modeled via four distinct import routes as LTCs. Two of these routes originate in North Africa, connecting Spain and Italy via pipelines to this region. The other three routes originate in Ukraine, with Hungary, Romania, and Slovakia acting as the importing countries through pipeline connections. According to Equation (5.5), the selected import volume is endogenous but must not exceed the available potential. As indicated by the equilibrium constraint, the imports are evenly distributed throughout the year, assuming sufficient pipeline capacity. The import costs are computed by multiplying the imported volume by the associated cost, as defined in Equation (5.6). Like imports via ship, pipeline imports in dispatch simulations are held constant according to the determined amount in the invest decision.

$$PIPE^*(b, f) \le ptxPotPipe(b, f) \quad \forall b \in B \land f \in F$$
 (5.5)

$$COSTS^{Pipe} = \sum_{b \in B} \sum_{f \in F} PIPE^*(b, f) * ptxCostsPipe(b, f)$$
 (5.6)

Data from TYNDP 2024 (ENTSO-E and ENTSOG, 2024) are utilized to determine the import potential for both Ukraine and North Africa. Spain and Italy have an import potential of 331 TWh<sub>th</sub> per year each. Ukraine's potential is distributed as follows: 55 TWh<sub>th</sub> annually for Hungary, 63 TWh<sub>th</sub> for Romania, and 114 TWh<sub>th</sub> for Slovakia. Cost data are derived from the Global PtX Cost Tool 2.0 (Klaas et al., 2024), with an import price of 501.57  $\bigcirc$ /MWh<sub>th</sub> from Ukraine and 202.26  $\bigcirc$ /MWh<sub>th</sub> from North Africa.

#### TRADE - Hydrogen trade with neighboring countries

Cross-border hydrogen trade follows a NTC approach, analogous to electricity markets. The total traded volume (TRADE) cannot exceed NTC limits (tradeCap), as defined in Equation (5.7).

$$TRADE(d, b_1, b, f) \le tradeCap(b_1, b, f) \quad \forall d \in D \land b, b_1 \in B \land f \in F \quad (5.7)$$

Based on the TYNDP 2024 data (ENTSO-E and ENTSOG, 2024), an initial grid setup is established in the Reference Scenario, while a sensitivity explores a higher degree of interconnection (see Section 5.2.2). The interconnections involving Great Britain, Norway, and Switzerland are defined by custom assumptions. All NTC values are detailed in Appendix D.3.

#### Hydrogen storage

In comparison to all other PtX-fuels, storage is explicitly modeled only for hydrogen. The model incorporates four distinct types of hydrogen storage: reallocation of existing pore and cavern gas storage, as well as the construction of new pore and cavern storage facilities. Hydrogen storage technologies are formally defined as  $a \in A^{H_2Stor}$ , a subset of A.

The modeling of hydrogen storage follows principles similar to those used for electricity storage, but with additional detail to capture the diverse sources of hydrogen allocation. In addition to satisfying national hydrogen demand, hydrogen from domestic production, and imports via ships, pipelines, or trade can also be directed to storage. This allocation is reflected by the following Equations (5.8) to (5.11).

$$INSTOR^{Prod}(d, h, a, b, f) \le PROD(d, h, a, b, f)$$
$$\forall h \in H \land d \in D \land a \in A \land b \in B \land f \in F$$
 (5.8)

$$INSTOR^{Pipe}(d, b, f) \le PIPE(b, f)/365$$
$$\forall d \in D \land b \in B \land f \in F$$
 (5.9)

$$INSTOR^{Ship}(d, r, b, f) \le SHIP(r, b, f)/365$$
$$\forall d \in D \land r \in R \land b \in B \land f \in F$$
 (5.10)

$$INSTOR^{Trade}(d, b_1, b, f) \le TRADE(d, b_1, b, f)$$

$$\forall d \in D \land b, b_1 \in B \land f \in F$$
(5.11)

The daily stored quantity of hydrogen (in  $MWh_{th}$ ) is computed using Equation (5.12) as the sum of contributions from all four sources.

$$\sum_{a \in A} INSTOR(d, b, a, f) = \sum_{h \in H} \sum_{a \in A} \frac{24}{H} * INSTOR^{Prod}(d, h, a, b, f)$$

$$+ INSTOR^{Pipe}(d, b, f)$$

$$+ \sum_{r \in R} INSTOR^{Ship}(d, r, b, f)$$

$$+ \sum_{b_1 \in B} INSTOR^{Trade}(d, b_1, b, f)$$

$$\forall d \in D \land b, b_1 \in B \land a \in A^{H2Stor} \land f \in F$$

$$(5.12)$$

The maximum storage withdrawal per day is constrained by the withdrawal speed in  $MWh_{th}/day$ . The speed depends on the installed storage capacity (in  $MWh_{th}$ ), multiplied with an volume factor (in h), as expressed in Equation (5.13). For all different hydrogen storage technologies, the ratio of capacity to volume is assumed to be 1:340 based on EWI (2024a). Also, based on insights

from EWI (2024a), the ratio for the injection speed is set to 1:9. This reflects the observed characteristics of hydrogen storage systems, which exhibit more constant injection during surplus periods and faster withdrawal during peak load hours in the power sector.

$$\sum_{h \in H} \frac{24}{H} * PROD(d, h, b, a, f) \leq INSTCAP^*(a, b) * vol(a)$$

$$\forall d \in D \land b \in B \land a \in A^{H_2Stor} \land f \in F$$
(5.13)

$$INSTOR(d, b, a, f) \leq INSTCAP^{*}(a, b) * vol(a) * inject(a)$$

$$\forall d \in D \land b \in B \land a \in A^{H_2Stor} \land f \in F$$
(5.14)

At the beginning of the model period, Equation (5.15) sets the initial storage level. The initial level equals half the capacity plus storage injection, adjusted for the storage efficiency ( $\eta$ ), minus hydrogen supply to the grid. The efficiency is assumed to be 93%, which is the average value for hydrogen storage given in Tsiklios et al. (2023).

$$LEVEL(d, a, b, f) = INSTCAP^*(a, b) * vol(a) * 0.5$$
  
+INSTOR(d, b, a, f) \*  $\eta(a) - \sum_{h \in H} \frac{24}{H} PROD(d, h, a, b, f)$   
$$\forall d = d1 \land a \in A^{H_2Stor} \land b \in B \land f \in F$$
 (5.15)

Throughout the model period, the storage level must remain below the maximum storage volume, as shown in Equation (5.16).

$$LEVEL(d, a, b, f) \le INSTCAP^*(a, b) * vol(a)$$

$$\forall d \in D \land a \in A^{H_2Stor} \land b \in B \land f \in F$$
(5.16)

The model ensures day-to-day continuity in storage levels through Equation (5.17).

$$LEVEL(d+1,a,b,f) = LEVEL(d,a,b,f)$$

$$+\eta(a)*INSTOR(d+1,b,a,f) + \sum_{h\in H} \frac{24}{H}*PROD(d,h,a,b,f)$$

$$\forall d\in D \land a \in A^{H_2Stor} \land b \in B \land f \in F$$

$$(5.17)$$

Finally, the annual storage balance is enforced to ensure no net gain or loss of hydrogen storage over the year, as described in Equation (5.18).

$$\sum_{d \in D} [\eta(a) * INSTOR(d, b, a, f) - \sum_{h \in H} \frac{24}{H} * PROD(d, h, a, b, f)] = 0$$

$$\forall a \in A^{H_2Stor} \land b \in B \land f \in F$$

$$(5.18)$$

#### USE - Sectoral hydrogen demand

Hydrogen demand varies across sectors such as energy, transport, buildings, and industry. In the transport, buildings, and industry sectors, hydrogen demand follows an exogenous profile: for transport and industry, the demand is flat, whereas for buildings, it is both seasonal and volatile due to heating and cooling needs. In the energy sector, hydrogen can be used in two main ways, with consumption patterns typically influenced by market conditions: for electricity generation and district heating through combined heat and power (CHP) systems. In the case of CHP, the heat supply must align with a fixed demand profile. Additionally, the production of other synthetic fuels is modeled using closed-system processes. In these processes, electricity is used to produce hydrogen, which is directly further transformed using  $\mathrm{CO}_2$ .

#### 5.2.2. Scenario design and related assumptions

With the presented model improvements, this study applies a two-step modeling approach to investigate short-term hydrogen and electricity price dynamics in a climate-neutral energy system in 2050. In the first step, a long-term investment optimization is used to generate feasible and policy-aligned energy system configurations. Alongside exogenous scenario specifications — such as minimum renewable capacities and trade infrastructure capacities — endogenous decisions, including LTCs for hydrogen, are optimized. Alternative system configurations are derived by varying key assumptions, namely the extent of cross-border hydrogen trade infrastructure, hydrogen demand, and their combination. In the second step, high-resolution dispatch simulations are carried out under the fixed system configurations from step one. This enables a detailed examination of short-term price formation, volatility, and market interactions. Shadow prices for electricity and hydrogen, derived from equilibrium constraints, serve as the basis for the subsequent analysis. Figure 5.1 illustrates the stepwise modeling approach. Discrepancies between Step I and Step II in terms of system outcomes and related shadow prices are discussed in Section 5.5.

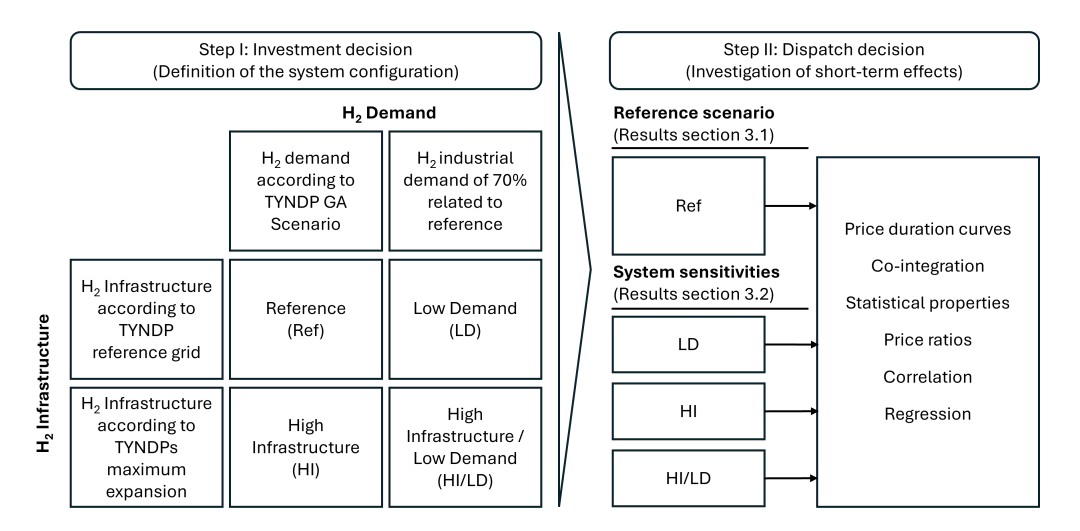


Figure 5.1.: Overall model approach covering a reference scenario and three system sensitivities

The left side of the figure illustrates the different defined system configurations with variations in terms of infrastructure and demand. The names for the different sensitivities are displayed in the cells. The right side of the figure outlines the analysis conducted in the result sections, for both the base case and the system sensitivities, based on independent dispatch decision.

All scenarios incorporate capacity trajectories and minimum renewable energy targets in line with TYNDP 2024 (ENTSO-E and ENTSOG, 2024). Fuel prices are based on the "Stated Policies" scenario from IEA (2024), while hydrogen import prices via ship follow a supply cost curve provided in Appendix D.2. The CO<sub>2</sub> price is endogenously derived via a cap-and-trade mechanism, assuming net-zero emissions by 2050. Electricity NTC values are sourced from the Global Ambition scenario of TYNDP 2024 (Appendix D.3). The sector- and fuel-specific energy demand for the reference scenario is likewise based on this scenario. Weather conditions are represented using a synthetic year with average full-load hours, following the "Trend Scenario" from the German EEG forecast (Netztransparenz, 2024).

Assumptions on hydrogen NTC values and industrial hydrogen demand vary across the four scenarios, leading to different invest decisions and thus different system configurations. In the reference scenario (Ref), NTC capacities for hydrogen reflect the reference grid of the TYNDP 2024. In the sensitivities HI and HI/LD, a more connected energy system is modeled by increasing the NTC values for hydrogen. The NTC values for the reference scenario and all sensitivities are detailed in Appendix D.3. In the sensitivities LD and HI/LD, the hydrogen demand in the industry sector is lowered by 30%, based on own assumption.

## 5.3. The relationship between electricity and hydrogen prices

The analysis of short-term effects on the structure of hydrogen and electricity prices, as well as their interrelationship, is conducted in several steps to ensure a comprehensive understanding of these dynamics. Following a description of the underlying system configuration (Section 5.3.1), the price duration curves and statistical properties for both energy carriers are first analyzed separately to identify their fundamental structures (Section 5.3.2). Then, the result of data segmentation into subsets reflecting distinct market situations is presented (Section 5.3.3). For each subset, the existence of co-integration is assessed (Section 5.3.4). Subsequently, the statistical properties of hydrogen and electricity prices are examined, by additionally considering electricity-to-hydrogen price ratios (Section 5.3.5). Finally, regression and correlation analyses are conducted within each subset to identify key drivers of price formation and to evaluate coupling and decoupling dynamics between the two markets (Section 5.3.6).

#### 5.3.1. System configuration

The system configuration, based on the investment decision in Step I, forms the basis for the dispatch modeling and the further analysis. All installed capacities for Germany, determined in this step, are detailed in Appendix D.4. In the reference scenario, 55 TWh of hydrogen storage capacity and 76.5 GW of electrolysis capacity is built in Germany. Additionally, LTCs for hydrogen imports via ship and pipeline are endogenously selected in the investment run, resulting in 190.8 TWh of oversea hydrogen imports for Germany.

Based on these installed capacities and selected LTC imports, the dispatch decision (Step II) provides the detailed energy balances and corresponding shadow prices. The resulting sector-specific electricity and hydrogen demand is provided in Appendix D.5. Appendix D.6 illustrates the daily hydrogen balance, while Appendix D.7 presents the daily storage levels across Europe.

#### 5.3.2. Price formation and price duration curves

To get an initial understanding of price formation and price structures, hydrogen and electricity prices are first analyzed separately. Figure 5.2 presents daily prices in both unsorted and sorted order, where the descending sorted order represents the price duration curve. In addition, Table 5.1 summarizes the corresponding statistical properties.

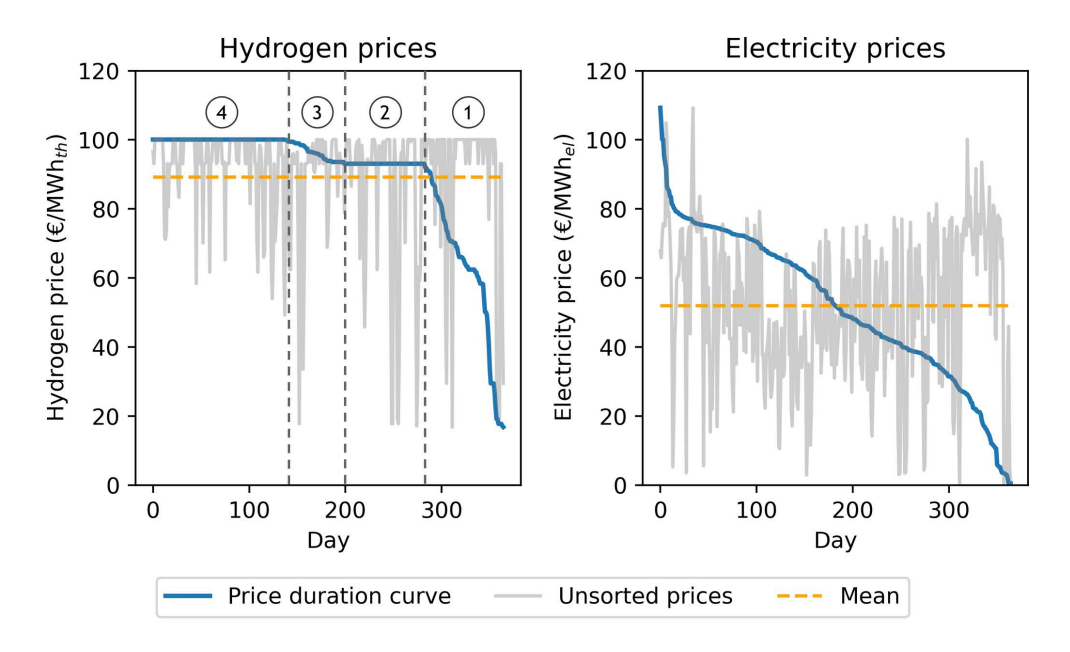


Figure 5.2.: Price data and duration curves for hydrogen and electricity

The price data are shown for Germany. Hourly electricity prices are weighted by the corresponding demand to calculate daily prices. Both electricity and hydrogen prices represent the shadow prices of their respective equilibrium constraints.

Table 5.1.: Statistical summary of hydrogen and electricity prices for the full year

Statistic	$\mathbf{H}_2$	$\mathbf{EL}$
$\mathbf{Mean}^1$	89.19	51.95
$\mathbf{Median}^1$	93.89	51.91
Std. $dev.^1$	18.27	21.90
$\mathbf{C}\mathbf{V}^2$	0.20	0.41
$Minimum^1$	16.83	0.50
$\mathbf{Maximum}^1$	100.09	109.27

 $<sup>^1</sup>$  in €/MWh;  $^2$  no unit; CV is the coefficient of variation, which normalizes the standard deviation to the mean.

Price formation in both the hydrogen and electricity market is associated with a wide range of prices, each with distinct statistical characteristics.

One key factor driving the emergence of differntiated prices both for hydrogen and electricity lies in the hourly variability of electricity prices. In line with Böttger and Härtel (2022) and Antweiler and Muesgens (2025), diverse generation technologies — such as biogas, nuclear, gas, and biomass — and various flexibility options on both the supply and demand sides result in a broad spectrum of electricity price levels. Given that the hydrogen system interacts with the electricity system on a daily basis (analogous to the current methane system), hourly electricity prices are aggregated to volume-weighted daily values. In this

process, factors such as the frequency of high and low prices throughout the day, along with the level of demand, significantly influence the resulting electricity price structure. As a result, a continuous price duration curve without distinct plateaus emerges for electricity. Prices experience high volatility with a coefficient of variation (CV) of 0.41 around a mean value of  $51.95 \, \text{€/MWh}_{el}$ . The low mean is driven by 1122 hours of close-to-zero prices, and only a few hours with peak prices of around 145  $\, \text{€/MWh}_{el}$ . Additionally, transmission constraints contribute to volatility, as evidenced by variations in mean electricity prices across countries.<sup>39</sup>

The hydrogen price duration curve, with a mean value of  $89.19 \, \text{€/MWh}_{th}$ , lies substantially above that of electricity, primarily due to electrolysis and storage inefficiencies. The quantities and high prices for hydrogen imports from non-European countries are not part of the hydrogen price duration curve, as they are modeled as LTCs with quantities selected in the investment decision stage. The structure of the price duration curve is defined by several distinct segments, shaped by the availability and operation of hydrogen storage next to the behavior of electrolysis. Hydrogen price convergence across countries indicates that the system does not face significant transmission grid limitations of cross-zonal trade. Nevertheless, cross-border trade congestion can occur on single days.

The first segment in the hydrogen price duration curve exhibits a range of prices between 16.83 and 91.91  $\mbox{\ensuremath{\ensuremath{\mathbb{C}}}}/MWh_{th}$ , reflecting periods when storage charging capacity in Germany or exporting options are insufficient to align prices. In these situations, electrolyzers are price-setting, with hydrogen prices determined by electricity prices adjusted by the efficiency of the electrolyzer. Importantly, price-setting is not necessarily driven by local electricity prices. For example, if electricity prices diverge across countries due to transmission congestion, but hydrogen trade remains unconstrained, electrolyzers in different regions may still determine local hydrogen prices based on diverging electricity price levels. The second segment is marked by a price plateau at 93.08  $\mbox{\ensuremath{\ensuremath{\mathbb{C}}}}/MWh_{th}$ , during which storage charges at partial capacity. Here, the availability of storage and trade enables temporal and regional balancing, making storage the price-setting tech-

 $<sup>^{39}\</sup>text{Average}$  electricity prices across European countries range from 9.88 €/MWh<sub>el</sub> in Denmark to 69.03 €/MWh<sub>el</sub> in Slovakia. Price differentials between single countries, such as 4.15 €/MWh<sub>el</sub> between Germany and France and 7.11 €/MWh<sub>el</sub> between Germany and Poland, indicate the presence of specific transmission congestion.

<sup>&</sup>lt;sup>40</sup>The dispatch model minimizes variable costs, excluding sunk and investment costs. In contrast, LTC quantities and prices are endogenously selected in the investment stage based on LCOH, which includes both capital and operational costs. This results in price discrepancies between the two optimization steps. Since short-term prices may not fully reflect investment costs, risk premiums and mark-ups may be necessary from investors' perspective (see Section 5.5 for further discussion on cost recovery).

<sup>&</sup>lt;sup>41</sup>Mean values for hydrogen in other countries next to Germany are in the same magnitude, with a median value of 91.10 €/MWh<sub>th</sub>. Denmark is the country with the lowest mean price of 53.79 €/MWh<sub>th</sub>. Ireland, Great Britain, Spain and Portugal instead face prices above 100 €/MWh<sub>th</sub>, mainly driven by limited trade capacities with other countries (see Appendix D.3).

nology. In the third segment, hydrogen storage in Germany is neither charging nor discharging and demand is met through domestic electrolysis or imports from neighboring countries. As in the first segment, electrolyzers determine the hydrogen price. Despite the market-oriented operation of electrolyzers with moderate annual average full load hours (3,215 h/a), domestic hydrogen production is even maintained in situations of elevated electricity prices. This results in relatively high hydrogen prices within the price duration curve. The final segment reveals a second price plateau, corresponding to periods of storage discharge. The difference between the two pronounced plateaus reflects the storage efficiency of 93%.

Overall, price formation in the hydrogen market is linked to those in the electricity market by electrolysis, with hydrogen storage occurring as the price-setting technology in certain situations. Cross-border trade results in prices linkages between both markets across countries. Additionally, hydrogen prices exhibit lower volatility than electricity prices, as reflected in both the standard deviation and CV, indicating limited technological heterogeneity and the pronounced stabilizing effect of storage and trade.

Electricity price formation, in turn, is further influenced by its bidirectional dependence on the hydrogen market. Hydrogen shadow prices affect the costs of hydrogen-based electricity generation and heat production via CHP, which, in turn, influence electricity market outcomes. This mutual dependency creates a dynamic pricing environment where the situation in both markets directly impacts price-setting in the other.

To explore these interdependencies in greater detail, the following sections systematically examine the relationship between hydrogen and electricity prices by considering different market situations.

#### 5.3.3. Data separation

The dataset of daily price pairs is segmented into four distinct subsets, each representing a specific combination of electricity and hydrogen market conditions. This classification enables a more granular analysis of price dependencies and variations in statistical properties. A k-Means clustering algorithm is applied using two key dimensions. The first dimension captures electricity market conditions, represented by electrical residual load (RL). The second dimension characterizes the hydrogen market using hydrogen residual load as a proxy. Hydrogen residual load is derived by subtracting the constant hydrogen import via ship from the exogenous demand profile across the transport, buildings, and industry sectors. The clustering algorithm systematically assigns price pairs to one of four distinct market conditions, categorized by combinations of high or low electrical residual load and high or low hydrogen residual load:

- High electrical residual load / High hydrogen residual load (El. high RL / H<sub>2</sub> high RL)
- High electrical residual load / Low hydrogen residual load (El. high RL / H<sub>2</sub> low RL)
- Low electrical residual load / High hydrogen residual load (El. low RL / H<sub>2</sub> high RL)
- Low electrical residual load / Low hydrogen residual load (El. low RL /  $H_2$  low RL)

Figure 5.3 visualizes this separation of price data. The appendix D.8 provides additional visualization of the hydrogen supply and demand mix in each subset together with the corresponding electrical residual load.

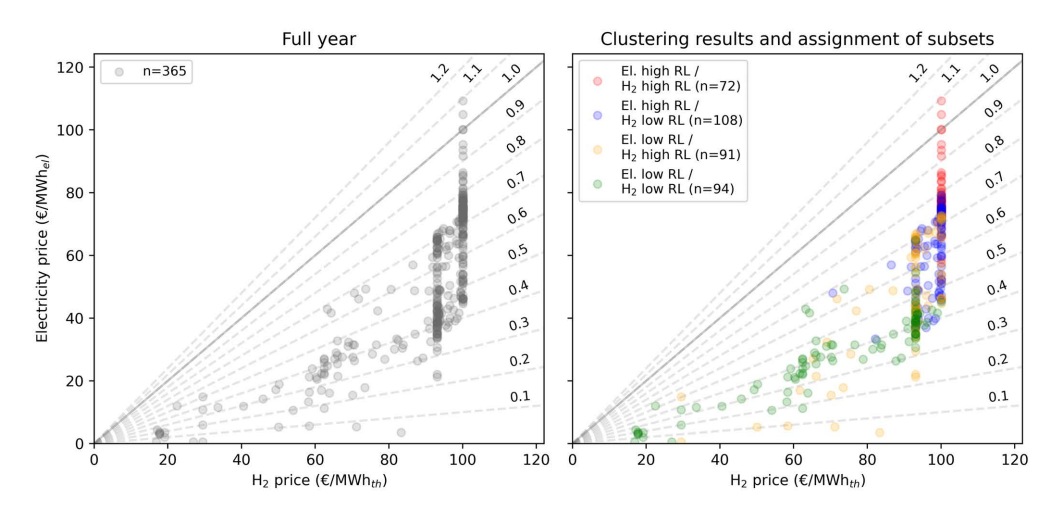


Figure 5.3.: Daily pairs of electricity and hydrogen prices split in four subsets

Gray dots represent the entire year (365 data points). Colored dots indicate data points belonging to one of the four market condition clusters. Hourly electricity prices are weighted by demand to calculate daily averages. Both electricity and hydrogen prices represent the shadow prices of their respective equilibrium constraints.

#### 5.3.4. Analysis of co-integration

The segmentation of price data into distinct market conditions raises the question of whether hydrogen and electricity prices exhibit co-integration within specific subsets. Co-integration would suggest that the two price series share a long-term equilibrium relationship despite short-term fluctuations. To assess this, an Augmented Dickey-Fuller (ADF) test is conducted on both the hydrogen and electricity price time series (see Appendix D.9 for the details). The results reject the presence of a unit root for both series, indicating that hydrogen and electricity prices are stationary. Since stationarity is a necessary condition for co-integration, this confirms that hydrogen and electricity prices do not share a long-

term equilibrium relationship. Instead, their relationship is primarily governed by short-term interactions, influenced by fluctuations in residual loads, storage dynamics, and market conditions. This result supports the use of correlation analysis and regression models to examine price dependencies, rather than cointegration models, which are typically suited for non-stationary series.

To explore these short-term dependencies in greater detail, the next section presents the statistical properties for the full dataset and for each subsets, followed by a regression analysis with the same distinction.

#### 5.3.5. Analysis of statistical properties

This section analyzes and compares the statistical properties of hydrogen and electricity prices over the full year and across the four subsets. To establish an initial understanding of the differences between subsets and the price characteristics within each, Table 5.2 presents a summary of key statistical indicators, including mean, median, standard deviation, coefficient of variation, and the minimum and maximum values.

Table 5.2.: Statistical	summary of	hydrogen	and	electricity	prices f	or each	subset
Table 9.2 Statistical	Summar v Or	HVUIOECH	anu	CICCUITCION	DITCES I	or cacii	SUDSCI

Statistic	Full	year	El. hi	El. high RL		El. high RL		El. low RL		El. low RL	
			$\mathbf{H}_2$ high $\mathbf{R}\mathbf{L}$		$\mathbf{H}_2$ lo	$\mathbf{w} \; \mathbf{RL}$	$\mathbf{H}_2$ hig	gh RL	$\mathbf{H}_2$ low $\mathbf{R}\mathbf{L}$		
	$\mathbf{H}_2$	EL	$\mathbf{H}_2$	$\mathbf{EL}$	$\mathbf{H}_2$	$\mathbf{EL}$	$\mathbf{H}_2$	$\mathbf{EL}$	$\mathbf{H}_2$	$\mathbf{EL}$	
$Mean^1$	89.19	51.95	100.07	77.32	97.13	59.64	89.71	46.68	71.23	28.77	
$Median^1$	93.89	51.91	100.09	75.51	99.46	62.44	93.08	46.16	75.14	31.20	
Std. $dev.^1$	18.27	21.90	0.14	9.22	4.30	12.22	13.62	18.05	24.69	13.58	
$\mathbf{C}\mathbf{V}^2$	0.20	0.42	0.00	0.12	0.04	0.20	0.15	0.39	0.35	0.47	
Minimum <sup>1</sup>	16.83	0.50	98.88	52.49	70.62	33.35	29.47	0.50	16.83	0.50	
Maximum <sup>1</sup>	100.09	109.27	100.09	109.27	100.09	79.30	100.09	72.73	100.09	64.75	

in €/MWh; 2 no unit; CV is the coefficient of variation, which normalizes the standard deviation to the mean.

The subset analysis reveals distinct price formation behaviors under different residual load conditions. Electrical residual load, which varies widely between negative and positive values (standard deviation: 0.39), exerts a stronger influence on price variation across subsets than hydrogen residual load, which remains strictly positive with limited variability (standard deviation: 0.06). Nonetheless, differences between high and low hydrogen residual load subsets are also pronounced. This is due to the characteristic that high residual load conditions typically correlate with situations with additional hydrogen demand in the power and heating sectors, while low residual load coincides with increased hydrogen production during periods of surplus renewable electricity feed-in. These dynamics reinforce intra-annual price differentiation.

Across subsets, high hydrogen residual load results in elevated and stable hydrogen prices, reflecting limited flexibility and the reliance on storage discharge or imports. In contrast, low hydrogen residual load is associated with greater

price dispersion and volatility, as electrolysis becomes the dominant price-setting technology. Similarly, high electrical residual load is associated with higher and more stable prices for both energy carriers, whereas low electrical residual load coincides with lower and more volatile prices, particularly pronounced for hydrogen.

Price levels and volatility are predominantly governed by the ability of the system to respond dynamically to short-term supply and demand fluctuations. Storage operation emerges as a key determinant of hydrogen price formation, with its charging and discharging behavior moderating or amplifying price movements depending on residual load conditions within the different subsets.

Looking at specific market situations in detail reveals that market conditions with high electrical residual load and high hydrogen residual load exhibit the highest mean prices for both energy carriers. Hydrogen prices in this subset are highly stable (CV=0.00), reflecting minor sensitivity to residual load fluctuations and storage discharging behavior as the dominant price-setting mechanism. While electricity prices in this subset are also on a high level, their higher, but moderate CV of 0.12 indicates greater short-term variability, influenced by demand fluctuations and renewable generation variations.

When electrical residual load is high, but hydrogen residual load is low, price variability for both carriers is also low, though prices and the underlying price formation characteristics in this subset are more heterogeneous. Storage discharging, associated with hydrogen price alignment, can be observed in 13% of the days within the subset. This subset also covers days when storage is charging (15%) or when storage is in a neutral position (72%) in Germany. Notably, despite storage is neither charging nor discharging domestically, storage behavior in neighboring countries can affect domestic price formation, provided sufficient trade capacity is available. Thus, in this cluster, all price-setting mechanisms — electrolyzers, storage charging, and storage discharging — are present, but most of the price prices reflect price-setting by electrolyzers at the upper end of the residual load duration curve. These dynamics support the finding that elevated electrical residual load drives hydrogen demand, particularly in the power sector, despite hydrogen residual load is low.

In contrast, low electrical residual load combined with high hydrogen residual load leads to decreasing price of both hydrogen and electricity. In this subset, hydrogen storage is predominantly charging or inactive, with full charging observed on approximately 26 out of 91 days. These 26 days face demand-side flexibility constraints, driven by increased renewable feed-in and corresponding domestic hydrogen production, which lowers prices. However, elevated hydrogen residual load in this subset limits further price reductions.

Finally, when both residual loads are low, price levels for both hydrogen and electricity are the lowest across subsets. Hydrogen storage is actively charging, often at full capacity, contributing to downward price movements. Electrolysis determines price-formation of hydrogen prices, with price levels linked to

those for electricity. Additionally, due to constrained storage charging capacity, this subset exhibits the highest price volatility for hydrogen (CV = 0.35) and comparably high volatility for electricity, indicating price movements driven by fluctuating residual load.

#### Electricity-to-hydrogen price ratios

Beyond the statistical properties of hydrogen and electricity prices, the distribution of daily electricity-to-hydrogen price ratios across the year and within the different subsets are examined in greater detail. The ratios serve as a valuable indicator for policymakers, investors and researchers when evaluating the energy system and different decarbonization options, or calculating the profitability of assets such as electrolyzers, without necessarily running energy system models. Table 5.3 illustrates the properties of the distribution of price ratios.

			·		*
Statistic	Full year	El. high RL	El. high RL	El. low RL	El. low RL
		$\mathbf{H}_2$ high $\mathbf{R}\mathbf{L}$	$\mathbf{H}_2$ low $\mathbf{R}\mathbf{L}$	$\mathbf{H}_2$ high $\mathbf{R}\mathbf{L}$	$\mathbf{H}_2$ low $\mathbf{R}\mathbf{L}$
Maximum	1.09	1.09	0.79	0.73	0.70
$3^{rd}$ quartile	0.72	0.79	0.71	0.65	0.43
Median	0.56	0.75	0.66	0.49	0.39
$1^{st}$ quartile	0.41	0.73	0.52	0.41	0.35
Minimum	0.02	0.52	0.39	0.02	0.02

Table 5.3.: Statistic on the distribution of daily electricity-to-hydrogen price ratios

The statistics in price ratios reflect the distribution of daily values from the perspective of the hydrogen market in daily resolution. 50% of the data are located between the first and third quartiles. Due to the aggregation from hourly electricity prices, values may differ when analyzed from the electricity market perspective using higher temporal resolution.

Over the full year, the median electricity-to-hydrogen price ratio is 0.56, reflecting inherent electrolysis conversion losses and the structural cost differential between electricity and hydrogen, especially under conditions where hydrogen storage is price-setting or cross-border trade is constrained. Daily price ratios range from 0.02 to 1.09, with a moderate interquartile range<sup>42</sup> (IQR) of 0.31, indicating that there are only a few situations across the year, where hydrogen and electricity prices either diverge or are closely aligned.

A comparison of the subset-specific results reveals that electricity market conditions significantly influence the electricity-to-hydrogen price ratio. In particular, high electrical residual load conditions tend to correspond with higher price ratios. Price ratios are highest in situations with high residual load in both markets, and lowest when hydrogen production benefits from surplus renewable feed-in while demand remains moderate.

In situations with both high electrical residual load and high hydrogen residual load ( $El.\ high\ RL\ /\ H_2\ high\ RL$ ), the electricity-to-hydrogen price ratio is high

 $<sup>^{42}</sup>$ The interquartile range reflects the difference between the third and the first quartile of the data set.

(0.75) with low variability, as the IQR is only 0.06. This pattern reinforces the observation that both prices tend to be high and stable when residual load increases for both electricity and hydrogen.

When hydrogen residual load is low but electrical residual load remains high ( $El.\ high\ RL\ /\ H_2\ low\ RL$ ) improved supply-side flexibility allows electrolyzers to more frequently set hydrogen prices, while persistently high electricity prices lead to an elevated ratio. Variability of the price ratio within this subset is comparatively low, again indicating relatively stable price relationships.

Conversely, under low electrical residual load with high hydrogen residual load, the price ratio is smaller, exhibiting the largest variability (IQR = 0.24) due to heterogeneous storage behaviors and volatile prices.

Finally, the lowest ratio of 0.39 occurs when both residual loads are low. This low ratio is partly explained by pronounced cross-border transmission congestion in electricity markets relative to hydrogen markets. As detailed in Section 5.3.2, electricity prices vary across countries, whereas hydrogen prices remain more aligned. Electrolyzers operating in regions with higher electricity prices and unconstrained hydrogen trade tend to elevate local hydrogen prices above German levels. The inverse applies when neighboring countries exhibit lower electricity prices and unrestricted hydrogen flows. Nevertheless, the observed price ratios suggest the former situation dominates in this subset.

#### 5.3.6. Analysis of coupling and decoupling dynamics

To analyze the relationship between hydrogen and electricity prices in greater detail, correlation and regression analyses are applied to the full dataset and four distinct market subsets. This enables a more granular understanding of price dependencies under varying system conditions.

Table 5.4 presents the correlation coefficients alongside the results of two regression models. These models explain electricity and hydrogen price formation as functions of renewable generation, inflexible electricity demand, and hydrogen residual load. The regression results reveal structural characteristics in price formation across the year, and distinct coupling and decoupling dynamics when analyzing the different subsets.

Table 5.4.: Regression and correlation results

	Full ye	ear	El. hig	gh RL	El. hig	gh RL	El. lo	v RL	El. lov	v RL
			$\mathbf{H}_2$ hig	gh RL	$\mathbf{H}_2$ lo	w RL	$\mathbf{H}_2$ hig	h RL	$\mathbf{H}_2$ lov	v RL
Direct interaction between electricity and hydrogen price										
Coefficient of correlation	0.77		0.08		0.45		0.70	0.70		
	Expla	natio	on of elec	tricity p	orices					
Regression model 1: $Price_{el} = \alpha + \beta *$	RES +	$\gamma * I$	$Load_{el} + \epsilon$	$\delta * Resi$	dualload	$H_2 + \epsilon$				
intercept $(\alpha)$	0.25		23.83		18.13		-52.00		7.35	
renewable generation coefficient $(\beta)$	-21.12	**	-14.95	**	-22.11	**	-25.96	**	-26.93	**
electrical load coefficient $(\gamma)$	31.23	**	15.34	**	31.96	**	38.78	**	35.79	**
hydrogen residual load coefficient $(\delta)$	0.04	**	0.04	*	0.02		0.09	*	0.04	*
$\mathbb{R}^2$	0.85		0.65		0.57		0.71		0.78	
	Expla	nati	on of hyo	drogen p	rices		•			
Regression model 2: $Price_{H_2} = \alpha + \beta$	*RES +	- γ *	$Load_{el}$ +	$\delta * Res$	idualloa	$d_{H_2} + \epsilon$				
intercept $(\alpha)$	69.86	**	99.89	**	74.79	**	70.94	*	84.85	*
renewable generation coefficient $(\beta)$	-13.29	**	-0.05		-5.59	**	-16.11	**	-46.55	**
electrical load coefficient $(\gamma)$	25.54	**	0.13		6.81	**	26.30	**	71.05	**
hydrogen residual load coefficient $(\delta)$	0.00		0.00		0.02	*	0.01		-0.01	
$\mathbb{R}^2$	0.49		0.05		0.32		0.46		0.75	

Significance levels: \*\* p-value<0.01; \* p-value<0.1.

The hydrogen residual load is calculated by subtracting the constant hydrogen import via ship from the exogenous demand profile in the end-use sectors. Electrical load equals the sum of the exogenous demand profiles in the end-use sectors.

#### Full-year relationships

The full-year regression and correlation results indicate a moderate degree of coupling between hydrogen and electricity markets. The correlation coefficient of 0.77 suggests that, on average, price movements in one market are partly reflected in the other. However, the underlying price drivers differ.

Electricity prices (Regression model 1) are primarily driven by supply and demand dynamics in the power sector. The strong negative impact of renewable generation ( $\beta=-21.12$ ) reflects the well-documented merit-order effect, where higher renewable availability reduces electricity prices. Conversely, the coefficient for electrical load ( $\gamma=31.23$ ) highlights demand-driven price fluctuations. The hydrogen residual load also contributes significantly, although the effect is small in magnitude ( $\delta=0.04$ ). The high explanatory power ( $R^2=0.85$ ) indicates that all three factors explain nearly all variation in electricity prices.

Hydrogen prices (Regression model 2) are less reflected by system dynamics, as indicated by the significance of the intercept. Additionally, the coefficient for hydrogen residual load is not statistically significant in the full-year model or in most of the subsets, again reflecting limited responsiveness. Renewable generation ( $\beta = -13.29$ ) and electrical load ( $\gamma = 25.54$ ) are significant, indicating that electricity market conditions influence hydrogen price formation through their effect on electrolysis costs. Nevertheless, the lower explanatory power ( $R^2 = 0.49$ ) suggests that hydrogen price dynamics are only partially captured by these variables, reflecting additional, uncovered structural effects.

#### Coupling and decoupling dynamics

The subset analysis reveals that the strength of price coupling between hydrogen and electricity varies substantially depending on residual load conditions. Electricity prices are highly responsive to short-term fluctuations in supply and demand, while hydrogen prices exhibit more structural characteristics driven by the interplay between storage, electrolysis, and imports/exports. Strong price coupling of hydrogen and electricity prices occurs only in flexible, electrolysis-dominated regimes with low residual loads. In contrast, high residual load conditions lead to decoupling of prices, as structural constraints outweigh linkage of prices.

Looking at the subsets in more detail reveals that in the subset with low residual load for both hydrogen and electricity ( $El.\ low\ RL\ /\ H_2\ low\ RL$ ), coupling is strongest. The coefficient of correlation reaches 0.90, the highest among all subsets. The high value confirms that price formation in this subset is largely governed by shared cost drivers, particularly renewable availability and electrical load. Regression model 1 even indicates that next to these two drivers, electricity prices are explained by hydrogen residual load, with a slightly significant coefficient. In general, strong coupling in this subset can be attributed to hydrogen production via electrolysis, which directly links its cost to electricity prices.

In subsets with asymmetric residual load conditions — either high hydrogen or high electricity residual load (El. low RL /  $H_2$  high RL and El. high RL /  $H_2$  low RL) - the strength of coupling declines to moderate levels. Correlation coefficients are 0.70 and 0.45, respectively, and the explanatory power of regression model 2 declines ( $R^2 = 0.46$  and 0.32). These lower values reflect the role of hydrogen storage and cross-border trade, which partially decouple hydrogen price formation from short-term electricity price movements. Notably, coupling remains stronger in the subset with low electrical residual load, underscoring the dominate role of electrical residual load in influencing price coupling. As coupling declines, the intercept in the hydrogen price regression becomes significant — especially in the El. high RL /  $H_2$  low RL subset — indicating a shift from market-based to fixed determinants of price formation.

When both residual loads are high ( $El.\ high\ RL\ /\ H_2\ high\ RL$ ), the relationship between hydrogen and electricity prices weakens significantly, leading to decoupling of price dynamics. The correlation coefficient drops to 0.08, and model 2 explains only 5% of the variation in hydrogen prices. While electricity prices remain sensitive to system dynamics ( $R^2=0.65$ ), hydrogen prices are increasingly governed by storage discharge. The lack of statistically significant coefficients beyond the intercept in the hydrogen model confirms the structural decoupling of price dynamics between the two markets in this subset.

# 5.4. Impact of the system configurations on the relationship between electricity and hydrogen prices

This section investigates how different energy system configurations affect price formation and the relationship between electricity and hydrogen prices. Three sensitivities are analyzed to test the robustness of the results: a scenario with expanded cross-border hydrogen trade infrastructure (HI), one with reduced industrial hydrogen demand (LD), and a combined scenario incorporating both assumptions (HI/LD).

Section 5.4.1 outlines the key structural changes in energy system configuration resulting from the altered assumptions. Section 5.4.2 examines the corresponding shifts in statistical properties, including changes in electricity-to-hydrogen price ratios. Section 5.4.3 then evaluates how the system sensitivities affect the price formation characteristics, as well as the coupling and decoupling dynamics between hydrogen and electricity prices.

#### 5.4.1. Changes in system configurations and derived price data

The expansion of hydrogen trade capacities reduces constraints in cross-border hydrogen flows. Similarly, lower hydrogen demand relaxes supply requirements. These changes result in deviating energy system configurations, determined endogenously in the investment stage, which subsequently affects the dispatch decision outcomes (see Appendix D.4 to D.7). The most pronounced effects are observed in the volume of hydrogen imports and installed storage capacities. While the HI scenario leads to a reduction in hydrogen storage capacity in Germany and across Europe, the LD scenario increases storage capacity domestically, with European capacity remaining close to the reference scenario. The combination of both changes (HI/LD) results in the lowest import volumes and storage capacities across the four scenarios.

Each sensitivity provides a new set of hydrogen and electricity price data. These form the basis of the respective price duration curves (Appendix D.10). While the four structural segments observed in the reference scenario remain present, their size and level shift slightly.

Price pairs in each sensitivity are again assigned to four clusters based on residual load characteristics, using the same k-Means algorithm as before. Figure 5.4 shows the resulting classification.

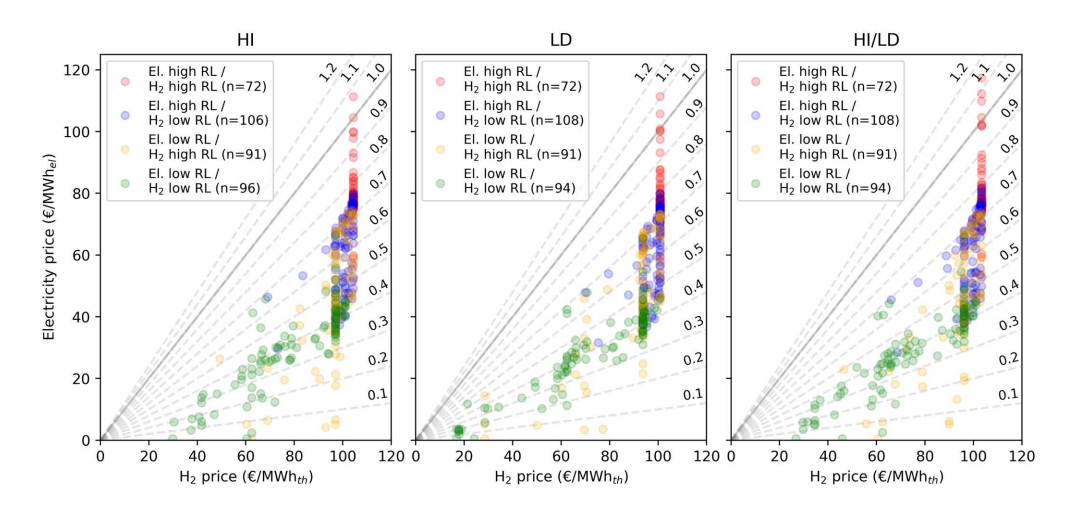


Figure 5.4.: Electricity and hydrogen price pairs split in four subsets for the three system sensitivities

Each column represents one system sensitivity. Daily prices are assigned to one of the four clusters, representing different residual loads conditions. The daily electricity prices are weighted by hourly demand. Both electricity and hydrogen prices represent the shadow prices of their respective equilibrium constraints.

While the cluster assignments provide an initial intuition, the following sections analyze statistical properties and coupling mechanisms in greater depth to evaluate the robustness of the former findings.

# 5.4.2. Analysis of changes in statistical properties and price ratios

The changes of statistical properties of hydrogen and electricity prices across the full year and the four subsets under different system configurations are summarized in Table 5.5. These properties include the mean, median, standard deviation, coefficient of variation, and the range (minimum and maximum values) for each system scenario.

Overall, the statistical properties remain robust. While changes in corssborder hydrogen trade infrastructure and demand influence price levels and volatility to some extent, the overall price patterns and segment structures remain the same. The largest deviations from the reference scenario occur in the HI scenario, reflecting increased flexibility in terms of cross-border trade. By contrast, the LD scenario induces only minor changes, as lower hydrogen demand is largely offset by reduced hydrogen imports. The combined scenario (HI/LD) mirrors the effects of the HI case but with slightly diminished intensity, suggesting that variations in cross-border trade infrastructure have a greater impact on price characteristics than demand-side adjustments.

Table 5.5.: Statistical summary of hydrogen and electricity prices for the system sensitivities

Statistic	System	Full	year	El. hi	gh RL	El. hig	gh RL	El. lo	w RL	El. lo	w RL
				$\mathbf{H}_2$ hig	gh RL	$\mathbf{H}_2$ lov	w RL	$\mathbf{H}_2$ hig	h RL	$\mathbf{H}_2$ lov	w RL
		$\mathbf{H}_2$	EL	$\mathbf{H}_2$	EL	$\mathbf{H}_2$	$\mathbf{EL}$	$\mathbf{H}_2$	$\mathbf{EL}$	$\mathbf{H}_2$	$\mathbf{EL}$
$Mean^1$	Ref	89.19	51.95	100.07	77.32	97.13	59.64	89.71	46.68	71.23	28.77
	HI	4.87	0.54	4.10	1.06	3.03	0.33	6.32	0.52	6.64	1.05
	LD	0.02	0.35	0.68	0.93	0.34	0.26	-0.05	0.48	-0.77	-0.09
	$_{ m HI/LD}$	2.63	0.85	3.12	2.42	1.68	0.67	4.23	0.75	1.81	-0.02
$Median^1$	Ref	93.89	51.91	100.09	75.51	99.46	62.44	93.08	46.16	75.14	31.20
	HI	6.00	0.07	4.24	1.64	1.52	0.35	3.95	0.62	3.60	-0.27
	LD	1.33	0.42	0.67	0.70	0.06	0.16	0.63	0.47	-4.47	-1.06
	$_{ m HI/LD}$	4.48	0.85	3.28	1.54	0.48	0.53	3.05	0.97	-2.96	-2.18
Std. dev. <sup>1</sup>	Ref	18.27	21.90	0.14	9.22	4.30	12.22	13.62	18.05	24.69	13.58
	HI	-2.80	0.20	0.33	0.06	0.87	0.61	-3.92	0.46	-4.52	-0.14
	LD	0.83	0.36	0.02	0.35	0.65	0.23	1.68	0.16	0.42	0.15
	$_{ m HI/LD}$	-1.16	0.88	0.38	1.80	1.49	0.60	-2.62	0.29	-3.03	-0.15
$\mathbf{C}\mathbf{V}^2$	Ref	0.20	0.42	0.00	0.12	0.04	0.20	0.15	0.39	0.35	0.47
	HI	-0.04	0.00	0.00	0.00	0.01	0.01	-0.05	0.00	-0.09	-0.02
	LD	0.01	0.01	0.00	0.00	0.01	0.01	0.02	0.00	0.01	0.01
	$_{ m HI/LD}$	-0.01	0.01	0.00	0.02	0.02	0.01	-0.03	0.00	-0.05	0.00
Minimum <sup>1</sup>	Ref	16.83	0.50	98.88	52.49	70.62	33.35	29.47	0.50	16.83	0.50
	HI	12.93	0.00	3.09	-0.55	-1.63	-3.71	19.80	0.00	12.93	0.00
	LD	0.00	0.00	0.52	0.54	-0.71	-1.78	-1.01	0.00	0.00	0.00
	$_{ m HI/LD}$	9.89	0.00	2.05	1.09	-4.53	-4.85	17.10	0.00	9.89	0.00
Maximum <sup>1</sup>	Ref	100.09	109.27	100.09	109.27	100.09	79.30	100.09	72.73	100.09	64.75
	HI	4.24	2.03	4.24	2.03	4.24	0.55	4.24	1.72	0.96	1.59
	LD	0.68	2.09	0.67	2.09	0.68	0.54	0.68	0.56	0.67	0.57
	$_{ m HI/LD}$	3.28	8.11	3.28	8.11	3.28	2.42	3.28	1.06	0.84	1.14

in  $\mbox{\ensuremath{\mathbb{C}}/MWh}$ .  $^2$  no unit. The values for the reference scenario are absolute numbers. The numbers for the three sensitivities are the deviations from the reference. The color scheme visualizes the deviation in percent with a dark red corresponding to deviations up to -100% and a dark green with deviations above 100% and higher.

In more detail, expanded corss-border hydrogen trade infrastructure increases mean hydrogen prices across the year and all subsets. This is primarily due to the alignment of domestic prices with previously higher-price neighboring countries, now connected through expanded trade capacity. The CV declines slightly for the full year, but diverges across subsets: volatility decreases under low electrical residual load and increases under high electrical residual load conditions. The number of days when storage discharge sets hydrogen prices declines substantially (from 78 to 45), while price-setting by electrolysis becomes more frequent, increasing price diversity. In subsets with low electrical residual load, more trade capacity mitigates storage and trade constraints, promoting price convergence. The expansion of cross-border hydrogen trade infrastructure also results in higher electricity prices throughout the year and across subsets, which correlates with the characteristics observed in the hydrogen market.

Reducing industrial hydrogen demand by 83.8 TWh<sub>th</sub> does not significantly affect mean hydrogen prices, but slightly increases volatility. As hydrogen imports decline by 90.0 TWh<sub>th</sub>, the share of baseload supply decreases, leading to

a rising relative influence of more volatile hydrogen residual load. This amplifies price volatility, since European storage capacity remains largely unchanged.

The combined scenario reflects a mixture of the two individual sensitivities. Overall, the effect of the HI outweighs the effect of the LD scenario, but effects are weaker compared to the HI sensitivity alone regarding the full year characteristics. An exception is observed in the subset El.  $low\ RL\ /\ H_2\ low\ RL$ , where median hydrogen prices slightly decline. In subsets with high electrical residual load, volatility increases more noticeably than in the HI scenario, although differences remain minor.

#### Electricity-to-hydrogen price ratio

As in the reference scenario, the electricity-to-hydrogen price ratios serve as a key indicator of the economic linkage between both markets, with its robustness of particular interest. Figure 5.5 illustrates how the distribution of daily price ratios emerges under different system configurations, driven by variations in cross-border hydrogen trade infrastructure and demand.

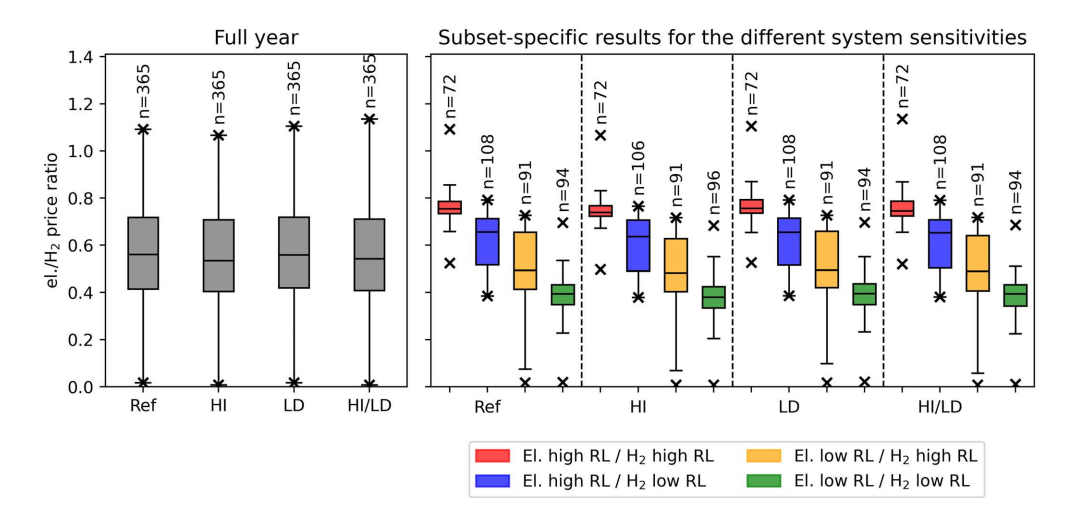


Figure 5.5.: Distribution of the daily electricity-to-hydrogen price ratio for different system sensitivities and subsets

The gray bars reflect the entire year with 365 data points. The colored bars refer to one of the four subsets. The minimum and maximum values are represented by crosses. The median is depicted by the black line, while the colored box between the lower and upper quantiles represents 50% of all values. The maximum whiskers are equal or lower to 1.5 times the Inter-Quartile Range (range of the colored box). The statistics in price ratios reflect the distribution of daily values from the perspective of the hydrogen market. Due to the aggregation from hourly electricity prices, maximum values may differ when analyzed from the electricity market perspective using higher temporal resolution.

Overall, the distribution of electricity-to-hydrogen price ratios remains stable across the different system sensitivities. This finding reinforces the conclusion

that the fundamental price relationship between hydrogen and electricity remains unaffected.

In the HI scenario, the electricity-to-hydrogen price ratio decreases slightly both on an annual average and within all subsets. This decline is primarily due to a stronger increase in hydrogen prices relative to electricity prices. As discussed in Section 5.4.2, hydrogen price alignment with previously higher-price neighboring regions drives this increase. As a consequence, enhanced cross-border trade reduces the cost advantage that domestic electrolysis had during periods of low electricity prices.

The LD and HI/LD scenarios both have a minimal impact on the electricity-to-hydrogen price ratio. The mean hydrogen and electricity prices remain roughly stable throughout the year, showing only minor deviations. Within the subsets, mean hydrogen and electricity prices move in the same direction relative to the reference scenario, resulting in a largely unchanged price ratio (see Table 5.5).

### 5.4.3. Analysis of changes in coupling and decoupling dynamics

Finally, to assess the robustness of the interdependencies between hydrogen and electricity prices, a correlation and regression analysis is conducted again across the various system sensitivities. Table 5.6 presents the correlation coefficients alongside the results of two regression models.

Changes in cross-border hydrogen trade infrastructure affect the strength of price coupling and the explanatory power of key variables. In the HI and HI/LDscenarios, price coupling weakens in most subsets compared to the reference case, as indicated by lower correlation coefficients under conditions of low or asymmetric residual load. This suggests that increased corss-border trade availability reduces the short-term responsiveness of hydrogen prices to electricity market dynamics in these situations. By contrast, in the subset with high residual load in both markets (El. high  $RL / H_2$  high RL), price decoupling weakens significantly. The coefficient of correlation increases from 0.08 in the reference scenario to 0.20 (HI) and 0.25 (HI/LD), and the explanatory power of the regression model improves ( $\mathbb{R}^2$  increases from 0.05 to 0.30 and 0.34, respectively). This shift reflects a greater role of electrolysis in setting hydrogen prices, even during periods of elevated electricity prices, as storage discharge becomes less frequent. Nevertheless, correlation in this subset remains lower than in others, indicating persistent decoupling. Electricity price formation is largely unaffected by changes in crossborder hydrogen trade infrastructure, both over the full year and within subsets. In contrast, hydrogen price formation shows some increased sensitivity to hydrogen residual load for the full-year, though this effect remains insignificant in most subsets. In the El. high  $RL / H_2$  high RL subset, explanatory power increases substantially, with renewable generation and electrical load becoming significant drivers, highlighting a partial transition to more market-aligned hydrogen price dynamics in situations with high residual load.

Table 5.6.: Regression results and correlation for the system sensitivities

	Full year	El. high RL	El. high RL	El. low RL	El. low RL
			H <sub>2</sub> low RL		$H_2$ low RL
t interact	ion between	- 0	ydrogen price	2 0	
Ref	0.77	0.08	0.45	0.70	0.90
HI	0.75	0.20	0.44	0.61	0.86
LD	0.78	0.08	0.46	0.73	0.90
HI/LD	0.77	0.25	0.48	0.67	0.88
E	xplanation	of electricity price	es		
$RES + \gamma$	$\gamma * Load_{el} +$	$\delta * Residual load$	$H_2 + \epsilon$		
Ref	0.25	23.83	18.13	-52.00	7.35
HI	-24.15 *	-1.11	3.31	-95.16 *	-34.18
LD	-2.69	22.33	16.30	-54.41	4.36
HI/LD	-17.66 *	6.18	7.48	-81.19 *	-32.26
Ref	-21.12 **	-14.95 **	-22.11 **	-25.96 **	-26.93 **
HI	-21.21 **	-14.64 **	-23.05 **	-26.72 **	-26.22 **
LD	-21.36 **	-15.64 **	-22.51 **	-26.08 **	-26.90 **
HI/LD	-21.85 **	-17.84 **	-23.31 **	-26.17 **	-25.93 **
Ref	31.23 **	15.34 **	31.96 **	38.78 **	35.79 **
HI	29.86 **	* 13.99 **	33.70 **	37.68 **	32.79 **
LD	31.92 **	* 16.49 **	33.33 **	39.13 **	36.13 **
HI/LD	32.55 **	* 20.70 **	35.35 **	37.61 **	34.29 **
Ref	0.04 *	* 0.04 *	0.02	0.09 *	0.04 *
HI	0.05 **	* 0.05 *	0.03	0.10 *	0.06 *
LD	0.04 *	* 0.04 *	0.02	0.09 *	0.04 *
HI/LD	0.05 **	* 0.04 *	0.02	0.10 **	0.06 *
Ref	0.85	0.65	0.57	0.71	0.78
HI	0.84	0.62	0.55	0.70	0.76
LD	0.85	0.67	0.58	0.70	0.77
HI/LD	0.85	0.67	0.59	0.69	0.73
E	xplanation	of hydrogen price	S		
*RES +	$\gamma * Load_{el}$	$+\delta * Residual load$	$d_{H_2} + \epsilon$		
			74.79 **	70.94 *	84.85 *
nei					
HI	47.35 **	* 103.33 **	77.56 **	73.61 *	-31.75
1		100.00	77.56 ** 72.07 **	73.61 * 69.83 *	-31.75 79.53 *
н	47.35 *	* 100.54 **	11.50	10.01	
HI LD	47.35 ** 68.81 **	* 100.54 ** 101.92 **	72.07 **	69.83 *	79.53 *
	Ref   HI   LD   HI/LD   EF   HI   LD   HI/LD   HI/LD   HI/LD   EF   HI/LD   H	$\begin{array}{c c} \text{t interaction betweer} \\ \hline \text{Ref} & 0.77 \\ \hline \text{HI} & 0.75 \\ \hline \text{LD} & 0.78 \\ \hline \text{HI/LD} & 0.77 \\ \hline \\ \hline & \text{Explanation of states} \\ \hline \text{RES} + \gamma * Load_{el} + \\ \hline \text{Ref} & 0.25 \\ \hline \text{HI} & -24.15 \\ \hline \text{LD} & -2.69 \\ \hline \text{HI/LD} & -17.66 \\ \hline \text{Ref} & -21.12 \\ \hline \text{LD} & -21.36 \\ \hline \text{HI} & -21.21 \\ \hline \text{LD} & -21.36 \\ \hline \text{HI} & -21.23 \\ \hline \text{Ref} & 31.23 \\ \hline \text{HI} & 29.86 \\ \hline \text{HI} & 29.86 \\ \hline \text{LD} & 31.92 \\ \hline \text{HI/LD} & 32.55 \\ \hline \text{Ref} & 0.04 \\ \hline \text{HI/LD} & 0.05 \\ \hline \text{Ref} & 0.85 \\ \hline \text{HI} & 0.84 \\ \hline \text{LD} & 0.85 \\ \hline \hline \text{HI/LD} & 0.85 \\ \hline \hline \\ \hline \text{Explanation} \\ \hline \\ $	$\begin{array}{c ccccccccccccccccccccccccccccccccccc$	ti interaction between electricity and hydrogen price $  Ref   0.77   0.08   0.45  $ $  HI   0.75   0.20   0.44  $ $  LD   0.78   0.08   0.45  $ $  HI/LD   0.77   0.25   0.48  $ $  Explanation of electricity prices   Explanation of hydrogen pric$	$ \begin{array}{ c c c c c } \textbf{tinteraction between electricity and hydrogen price} \\ \hline \textbf{Ref} & 0.77 & 0.08 & 0.45 & 0.70 \\ \textbf{HI} & 0.75 & 0.20 & 0.44 & 0.61 \\ \textbf{LD} & 0.78 & 0.08 & 0.46 & 0.73 \\ \textbf{HI/LD} & 0.77 & 0.25 & 0.48 & 0.67 \\ \hline \hline \textbf{Explanation of electricity prices} \\ \hline \textbf{*RES} + \gamma * Load_{el} + \delta * Residualload_{H_2} + \epsilon \\ \hline \textbf{Ref} & 0.25 & 23.83 & 18.13 & -52.00 \\ \textbf{HI} & -24.15 & -1.11 & 3.31 & -95.16 & * \\ \textbf{LD} & -2.69 & 22.33 & 16.30 & -54.41 \\ \textbf{HI/LD} & -17.66 & 6.18 & 7.48 & -81.19 & * \\ \hline \textbf{Ref} & -21.12 & ** & -14.95 & ** & -22.11 & ** & -25.96 & ** \\ \textbf{HI} & -21.21 & ** & -14.64 & ** & -23.05 & ** & -26.72 & ** \\ \textbf{LD} & -2.136 & ** & -15.64 & ** & -22.51 & ** & -26.17 & ** \\ \textbf{HI/LD} & -21.85 & ** & -17.84 & ** & -23.31 & ** & -26.17 & ** \\ \textbf{Ref} & 31.23 & ** & 15.34 & ** & 31.96 & ** & 38.78 & ** \\ \textbf{HI} & 29.86 & ** & 13.99 & ** & 33.70 & ** & 37.68 & ** \\ \textbf{LD} & 31.92 & ** & 16.49 & ** & 33.33 & ** & 39.13 & ** \\ \textbf{HI} & 29.86 & ** & 13.99 & ** & 33.70 & ** & 37.68 & ** \\ \textbf{LD} & 31.92 & ** & 16.49 & ** & 33.33 & ** & 39.13 & ** \\ \textbf{HI} & 0.05 & ** & 0.04 & * & 0.02 & 0.09 & * \\ \textbf{HI} & 0.05 & ** & 0.05 & * & 0.03 & 0.10 & * \\ \textbf{Ref} & 0.04 & ** & 0.04 & 0.02 & 0.09 & * \\ \textbf{HI} & 0.85 & 0.65 & 0.57 & 0.71 \\ \textbf{HI} & 0.84 & 0.62 & 0.55 & 0.70 \\ \textbf{LD} & 0.85 & 0.67 & 0.58 & 0.70 \\ \textbf{HI/LD} & 0.85 & 0.67 & 0.59 & 0.69 \\ \hline \textbf{Explanation of hydrogen prices} \\ * RES + \gamma * Load_{el} + \delta * Residualload_{H_2} + \epsilon \\ \hline \end{array}$

| HI/LD | 0.50 | 0.30 Significance levels: \*\* p-value<0.01; \* p-value<0.1.

electrical load coefficient  $(\gamma)$ 

 $\mathbb{R}^2$ 

hydrogen residual load coefficient  $(\delta)$ 

LD

Ref

HI

LD

Ref

НІ

LD

 $_{
m HI}$ 

LD

HI/LD

HI/LD

HI/LD

-14.01

-1190

25.54

20.02

27.02

23.17

0.00

0.02

0.00

0.02

0.49

0.48

0.50

The hydrogen residual load is calculated by subtracting the constant hydrogen import via ship from the exogenous demand profile in the transport, buildings, and industry sector. Electrical load equals the sum of the exogenous demand profiles in the end-use sectors.

-0.06

-0.41

0.13

1.23

0.15

1.45

0.00

0.00

0.00

0.00

0.05

0.30

-6.22

-7.03

6.81

9.97

9.65

11.87

0.02

0.01

0.02

0.01

0.32

0.28

0.32

-18.29

-12.24

26.30

19.02

29.99

22.04

0.01

0.01

0.01

0.02

0.46

0.38

0.47

-47.10

-37 54

71.05

46.06

71.36

52.32

-0.01

0.09

0.00

0.10

0.75

0.59

0.75

A reduction in hydrogen demand in the LD scenario has no substantial impact on price formation for either hydrogen or electricity. However, the correlation between the hydrogen and electricity prices increases slightly in most subsets, indicating that lower hydrogen demand marginally strengthens price coupling. The explanatory power of the regression models remains broadly consistent with the reference case.

Overall, the results indicate that structural changes in cross-border hydrogen trade infrastructure and demand can influence both the strength of price coupling and the explanatory power of key price drivers, while effects are structural consistent across scenarios. NTC expansion generally weakens coupling, but improves price dependencies in situations with high residual load in both the hydrogen and electricity market. Demand reduction has limited effects on price formation, but modestly enhances price alignment between markets. Across all scenarios, electricity prices continue to be shaped primarily by short-term electricity market fundamentals, while hydrogen prices remain influenced by more structural characteristics driven by the interplay between storage, electrolysis, and imports and exports.

#### 5.5. Discussion

This study analyzes shadow prices for electricity and hydrogen, providing fundamental insights into price formation mechanisms. However, to address the findings' real-world implications, it is crucial to discuss how these shadow prices and identified characteristics might translate into actual market prices and how they could align with the future energy system. In this context, the limitations of the modeling approach are explored. Additionally, the discussion examines how hydrogen import prices, storage dynamics, and cross-border trade may influence market outcomes. Finally, an outlook on challenges and opportunities in developing a functional hydrogen market is given.

Price formation depends not only on fundamental market dynamics but also on underlying model assumptions and limitations.

A key characteristic of the modeling framework is the separation of the investment and dispatch stages, which must be considered when interpreting shadow prices. In Step I, long-term investment decisions—including hydrogen import volumes via LTCs — are optimized based on full cost recovery. These LTC prices reflect LCOH, which include both capital and operational expenditures, as well as infrastructure components such as import terminals, reconversion facilities, and shipping. In contrast, Step II simulates short-term dispatch under fixed capacities and imports, optimizing only variable costs. Shadow prices in Step II are consistent with those for electricity, but exclude sunk and capital costs. The prices for hydrogen imports from non-European countries do not shape the hydrogen price duration curve. As a result, the daily shadow prices derived in Step II often fall below the marginal prices for imported hydrogen in Step I. This points to an oversizing of imports. However, Step I is not intended to provide a complete cost-optimal system, but rather to construct feasible and policy-aligned system configurations. These configurations serve as the basis for the high-resolution dispatch analysis in Step II, which is central to this paper. No iterative feedback loop exists between the two stages. Nevertheless,

the fundamental differences between investment and dispatch market outcomes have important implications for price interpretation. While investment decisions ensure full cost recovery for infrastructure such as electrolyzers, storage, and renewables, the dispatch model does not guarantee financial viability for individual assets. Relying solely on shadow prices for valuation may therefore underestimate the revenue requirements for these assets. To bridge this gap, additional price components — such as capacity payments, mark-ups, or risk premiums — may be necessary to ensure cost recovery and incentivize investment. Furthermore, risk premiums arising from market uncertainties could widen the gap between modeled shadow prices and actual market prices. As such, the price levels derived in this study should be viewed as lower bounds.

Daily hydrogen price fluctuations in the model revolve around the mean value. Hydrogen storage shifts supply over time without altering overall market conditions. Expanding hydrogen storage capacity would directly reduce price volatility by mitigating both high and low residual load situations. During low residual load periods, increased storage charging would absorb excess hydrogen, leading to higher prices in those situations. Conversely, during periods with high residual load, larger storage reserves would provide additional supply, exerting downward pressure on prices. In an extreme case of unlimited storage capacity, daily hydrogen prices would correspond to one of two price levels. One price level would reflect storage discharging and the other would emerge in charging situations. The gap between the two price levels would reflect the storage efficiency. Weather variability and renewable electricity generation profiles also appear to play a crucial role in shaping price fluctuations. More stable electricity generation, achieved through a higher share of wind power relative to PV or by integrating battery storage, could further contribute to reduced hydrogen price volatility. In such cases, storage operation would likely exhibit fewer seasonal fluctuations, leading to more balanced storage usage throughout the year, as demonstrated in INES (2025).

The results indicate that the average hydrogen-to-electricity price ratio is approximately 0.56 on an annual basis, with substantial daily variations. This finding contrasts with previous studies, such as dena (2021), Prognos et al. (2020), Fraunhofer ISI et al. (2021), and Böttger and Härtel (2022), who estimate the ratio to range between 0.7 and 1.2, with an average of 0.9. The discrepancy may be driven by a key methodological difference regarding the treatment of hydrogen imports, the consideration of hydrogen storage, and trade restrictions. In the dispatch decision of the presented model, import volumes are fixed ex ante and do not respond to market signals. As a result, system flexibility is provided solely by electrolysis and storage. By contrast, studies assuming flexible hydrogen imports allow the model to import at a fixed price whenever needed. This assumption enables imports to act as a buffer, stabilizing hydrogen prices and maintaining a tighter link between electricity and hydrogen prices. In the fixed import setting of this study, rising hydrogen prices during high residual load situations cannot be offset by additional imports. Consequently, the hydrogen

price becomes less responsive to short-term electricity price fluctuations, reducing the average electricity-to-hydrogen price ratio. Nonetheless, hydrogen price levels might decrease if LTC contracts are better aligned with seasonal demand variations rather than maintaining constant import volumes throughout the year. Additionally, reducing the share of LTC-based imports while increasing the share of flexible imports, reflected by lower Take-or-pay rates, has been shown to lower overall system costs (Keutz and Kopp, 2025), indicating lower hydrogen price levels and thus higher price ratios. Additionally, infrastructure availability influences price ratios. The clustering analysis indicates that the lowest electricityto-hydrogen price ratios occur during periods when both hydrogen and electrical residual loads are low. In these situations, electrolysis predominantly sets prices. Indicated by overall price alignment of hydrogen prices across countries, crossborder trade appears to be generally unconstrained, whereas electricity prices in Germany experience stronger downward movements compared to neighboring countries. Consequently, although hydrogen prices generally correlate with electricity prices, higher electricity prices in countries next to Germany exert upward influence on hydrogen prices. Thus, compared to the former mentioned studies, more cross-border trade congestions may occur.

Beyond short-term price formation characteristics, the high price for hydrogen LTCs in the investment decision stage may present significant challenges for the long-term demand developments across various end-use sectors. The industrial sector, in particular, could face economic pressure that incentivizes shifting to cost-competitive alternative fuels or relocating to regions with lower energy costs, potentially altering regional hydrogen demand. Recent studies support this view: Weißenburger et al. (2024) show hydrogen demand has price elasticity and declines at high prices, but still remains substantial across sectors. Similarly, Fraunhofer ISI (2023) find that while transport and some industrial sectors reduce demand at high prices, a significant share remains inelastic due to limited alternatives or relocation challenges. EWI (2024b) further notes heterogeneous willingness to pay across sectors — with transport and some industrial sectors characterized by a high willingness to pay. In this study, hydrogen demand is modeled as exogenous and price-inelastic, but literature suggests substantial demand persistence despite price pressures, supporting this assumption. Nevertheless, to account for potential long-term demand reductions in response to sustained high price levels, the LD sensitivity provides insights into the possible implications of reduced hydrogen consumption.

Finally, the analysis shows that the hydrogen equilibrium constraint faces a limited degree of heterogeneity, with storage, electrolyzers, trade and power plant consumption representing the primary flexibilities. Limited heterogeneity in flexibility may pose a challenge for the development of a functional and liquid hydrogen market. Insufficient demand responsiveness can weaken price signals and hinder efficient market interactions. Without mechanisms to en-

hance flexibility, the establishment of a hydrogen market could remain difficult. Other studies, such as Schönfisch (2022), also pronounce that regional and heterogeneous hydrogen price structures could emerge across Europe, with trade capacities as one flexibility option playing a key role in linking these markets. Thus, the construction of sufficient cross-border hydrogen trade infrastructure next to storage appears important for enabling market maturity and ensuring that hydrogen price disparities between European countries do not result in economic imbalances, where some regions face prohibitively high costs while others benefit from significantly lower hydrogen prices.

### 5.6. Conclusion

In climate-neutral energy systems, hydrogen is expected to play a pivotal role across diverse applications with distinct demand and supply patterns. However, significant uncertainty remains regarding its price level, volatility and interdependencies with electricity prices. While optimal system configurations of an integrated energy system were in scope of previous studies, the granular interplay between hydrogen and electricity prices under varying short-term market conditions has been insufficiently explored. This study fills this gap by investigating the fundamental price formation of hydrogen and the relationship between hydrogen and electricity prices across different system configurations with a focus on Germany and for a climate-neutral Europe. This was achieved by expanding the energy system model DIMENSON towards a more granular representation of PtX fuels with different supply and demand options within the equilibrium constraint. The resulting shadow prices were analyzed using co-integration tests, regression and correlation metrics, price ratio distributions, and statistical properties.

### 5.6.1. Main results

The analysis suggests that the fundamental relationship between hydrogen and electricity prices in a future, climate-neutral energy system is likely to be predominantly influenced by short-term market conditions. Electricity prices appear to respond closely to renewable generation and demand fluctuations, as shown by significant regression results. By contrast, hydrogen prices are less responsive to these factors and seem to be more structurally influenced. Factors such as storage behavior and cross-border trade can moderate hydrogen price formation. The results point to strong price coupling under low residual load conditions dominated by electrolysis-driven pricing, promoting a general linkage with the electricity market. In situations with high residual load, more pronounced decoupling may occur, with hydrogen price formation driven by storage discharge and supply limitations, highlighting the potential impact of constrained system flexibility. The electricity-to-hydrogen price ratio averages approximately 0.56,

lower than previously reported values, largely due to assumptions on inflexible hydrogen imports.

Scenario analyses indicate that variations in cross-border hydrogen trade infrastructure and demand modestly influence price formation and price coupling strength: The expansion of NTCs fo hydrogen slightly weakens price coupling independent on the underlying market situation driven by residual load, but with an exception for high residual load situations, where previously identified decoupling weakens. Reduced hydrogen demand has minimal impact. Despite these variations, the fundamental price relationship remains stable yet sensitive to short-term system dynamics.

While these findings offer insights based on shadow prices, real-world market prices are likely to diverge. Shadow prices do not ensure investment cost recovery, and do not include risk premia, or capacity mark-ups. In particular, hydrogen imports are priced based on full cost recovery via long-term contracts, leading to a structural price gap between imported and domestically produced hydrogen. As a result, short-term price signals alone may be insufficient to support investment in hydrogen storage and electrolysis, underscoring the importance of complementary mechanisms such as long-term contracts or regulatory support to ensure the development of a liquid market for hydrogen.

#### 5.6.2. Future research

Based on the findings, this work reveals several areas for further investigation. Further analysis could assess how the development of regional and international hydrogen trade networks affects price formation. This includes evaluating the interplay between domestic production, imports, and exports for other regions next to Germany. Although this study highlights short-term price dynamics, future research could also explore the long-term development of coupling between hydrogen and electricity markets by considering multiple years. Thus, changes in price dynamics within a longer period of time can be analyzed. Future research could also further investigate the competitiveness of specific assets and prove robustness across different market situations. Especially the comparison of the profitability of hydrogen storage next to electricity storage could be interesting. Furthermore, the provided understanding of market situations within this study could lay the basis to further investigate different design options for contracts for difference or hydrogen purchase agreements, similar to power purchase agreements. Last, future modeling efforts should address short- and long-term supply and demand elasticities to capture their influence on market dynamics. Other model improvements could also consider more diverse weather situations or more flexible hydrogen supply profiles via ship.

# A. Supplementary material for chapter 2

# A.1. Sets, parameters and decision variables

Table A.1.: Sets

Set	Unit	Description
$q \in Q$	-	Time
$c, c' \in G_{el}$	-	Component that generates electricity
$c, c' \in L_{el}$	-	Component that consumes electricity
$c, c' \in G_{th}$	-	Component that generates heat
$c, c' \in L_{th}$	-	Component that consumes heat
$n, m \in N$	-	Node
$n \in \alpha_c$	-	Set of nodes that belong to a component. Mapping
		nodes to components
$c \in \alpha_n$	-	Set of components that belong to a node. Mapping
		components to nodes
$k \in K$	-	Line

Table A.2.: Decision variables

Variable	Unit	Description
$P_{c,q}^{g_{el}}$	$kWh_{el}$	Electrical energy generated by each generation unit
/1		c in time interval $q$
$P_{c,q}^{g_{el},s}$	$kWh_{el}$	Electrical energy generated by each generation unit
		c in time interval $q$ and sold at the wholesale market
$P_{c,q}^{g_{el},f}$	$kWh_{el}$	Electrical energy generated by each generation unit
7.		c in time interval $q$ and feed in to the grid
$P_{c,c^{\prime},q}^{g_{el},p}$	$kWh_{el}$	Electrical energy generated by each generation unit
- / · / <b>1</b>		c in time interval $q$ and provided to a load $c'$ on-site
$P_{c,q}^{l_{el}}$	$kWh_{el}$	Electrical energy consumed by each consumption
/1		unit $c$ in time interval $q$
$P_{c,q}^{l_{el},p}$	$kWh_{el}$	Electrical energy procured from wholesale or an elec-
7.		tricity provider and consumed by each consumption
		unit $c$ in time interval $q$
$P_{c,c',q}^{l_{el}}$	$kWh_{el}$	Electrical energy procured from a generation unit $c'$
· / · / <u>1</u>		on-site and consumed by each consumption unit $c$ in
		time interval $q$
$P_{c,q}^{g_{th}}$	$kWh_{th}$	Thermal energy generated by each generation unit $c$
7.		in time interval $q$
$P_{c,c',q}^{g_{th}}$	$kWh_{th}$	Thermal energy generated by each generation unit $c$
		in time interval $q$ and provided to consumption unit
,		c'
$P_{c,q}^{l_{th}}$	$kWh_{th}$	Thermal energy consumed by each consumption unit
,		c in time interval $q$
$P_{c,c',q}^{l_{th}}$	$kWh_{th}$	Thermal energy generated by generation unit $c'$ and
, , , <u>, , , , , , , , , , , , , , , , </u>		consumed by each consumption unit $c$ in time inter-
		$\operatorname{val} q$
$SOC_{c,q}^{el}$	$kWh_{el}$	Electrical energy inside a storage unit $c$ in time in-
-		terval $q$
$SOC_{c,q}^{th}$	$kWh_{th}$	Thermal energy inside a storage unit $c$ in time inter-
		$\operatorname{val} q$

Table A.3.: Parameters

		Table A.3.: Parameters
Parameter	Unit	Description
$A_d, A_u$	_	Matrixes of flow distribution in the grid model
$C_d, C_u$	-	Matrixes of flow contribution in the grid model
$d_{c,q}$	_	grid connection of storage unit [0; 1]
$e^{-c,q}$	_	factor that curtails maximum charging power
$F_{n,m}^{in}$	$kW_{el}$	Power injected in a bus $m$ from a connected bus $n$
-n,m	ei	in the grid model
$F_{n,m}^{out}$	$kW_{el}$	Power drained from bus $n$ to a connected bus $m$ in
n,m	ro r r et	the grid model
$gdf_{k,n,q}$	_	Matrix with generation distribution factors
$g u \kappa, n, q$ $j e l$	$kW_{el}$	installed capacity of each electrical component $c$
$i_c$ $ith$	$kW_{th}$	
$i_c^{el}$ $i_c^{el}$ $i_c^{th}$ $i_c^{soc,el}$ $i_c^{soc,th}$		installed capacity of each thermal component c
$t_c^{c,c}$	$kWh_{el}$	installed capacity of each electrical storage c
$i_c^{soc,vii}$	$kWh_{th}$	installed capacity of each thermal storage c
$laf_{k,n,q}$	- C /1 II/1	Matrix with load distribution factors
$m_c^f \ m_c^l$	$\in /kWh_{el}$	feed-in tariff for each generation unit $c$
$m_c^\iota$	$\in /kWh_{el}$	subsidy for the own consumption of electricity gen-
Doct	1 777	erated by a chp unit $c$
$P_{k,q}^{aci}$	$kW_{el}$	actual active power on a grid element
$P_{k,q}^{act} \ P_{k,q}^{act,noControllab}$	$^{ble}kW_{el}$	actual active power on a grid element affected by
		buses with non controllable assets
$P_{k,q}^{act,Controllable}$	$kW_{el}$	actual active power on a grid element affected by
' <u>*</u>		buses with controllable assets
$P_{k,q}^{gap,Controllable}$	$kW_{el}$	remaining active power on a grid element before ca-
		pacity limit is reached
$P_{k,q}^{max,Controllabl}$	$e \ kW_{-1}$	maximum active power of a grid element affected by
k,q	ro r r et	buses with controllable assets
$P_n$	$kW_{el}$	Total nodal flow in the grid model
$P^g$	$kW_{el}$	Nodal generation in the grid model
$P_n^g \ P_n^l$	$kW_{el}$	Nodal load in the grid model
$n \\ n \\ w$	$\in /kWh_{el}$	wholesale price
$p_q^w$	$kWAr_{el}$	actual reactive power on a grid element
$Q_{k,q}^{act}$		
$Q_{k,q}^{act,noControllal}$	$\kappa W A r_{el}$	actual reactive power on a grid element affected by
act Controllable		buses with non controllable assets
$Q_{k,q}^{act,Controllable}$	$kWAr_{el}$	actual reactive power on a grid element affected by
		buses with controllable assets
$Q_{k,q}^{gap,Controllable}$	$kWAr_{el}$	remaining reactive power on a grid element
$r_{c,q}$	$kWh_{el}$	Electrical energy that is consumed by electric vehi-
· <del>-</del>		cles through driving
$s_q$	-	time depended availability profile
$S_q^{max} \ S_{k,q}^{max}$	VA	maximum apparent power of a grid element
$t^{n,q}$	$\in /kWh_{el}$	taxes and levies
$\eta_{c,q}^{el}$	_	component-dependent and time-dependent electrical
·c,q		efficiency
$\eta_{c,q}^{th}$	_	component-dependent and time-dependent thermal
rc,q		efficiency
$f_c$	$\in /kWh_{el}$	component-dependent fuel costs
J C	-/ei	r dependent ract conto

# A.2. Calculation of maximum active power on each line and transformer

To formulate the equations (2.27) and (2.28) for the market model, the maximum active power for each line and transformer, only affected by nodes with controllable assets, has to be known. Based on the knowledge of the values for  $P^{act}$  and  $Q^{act}$  as a result of the AC power flow, the values of  $P^{gap,Controllable}$  and  $Q^{gap,Controllable}$  have to be calculated. It is assumed that the gap can only be controlled by readjusting the operation of assets which are part of the virtual power plant. Consequently,  $Q^{gap,Controllable}$  is only affected by electric vehicles. As formulated in equation (2.17) the reactive power of loads is defined as a fixed ratio of active power. The variable  $Q^{gap,Controllable}$  can therefore be replaced by the term  $k * P^{gap,Controllable}$  where  $P^{gap,Controllable}$  is the variable and k is the constant. The maximum apparent power can now be calculated as it is shown in equation (A.1).

$$S^{max} = \sqrt{(P^{act} + P^{gap,Controllable})^2 + (Q^{act} + Q^{gap,Controllable})^2}$$
 (A.1)

To calculate the maximum value of  $P^{gap,VPP}$  the equation (A.1) had to be transformed in order to apply the formula. The result is shown in equation (A.2). To simply this equation, the parameters a, b and c are introduced which represent the constant factors.

$$0 = (1 + k^{2}) * P^{gap,Controllable^{2}}$$

$$+ (2P^{act} + 2kQ^{act}) * P^{gap,Controllable}$$

$$+ (P^{act^{2}} + Q^{act^{2}} + S^{max^{2}})$$

$$= a * P^{gap,Controllable^{2}} + b * P^{gap,Controllable} + c$$

$$(A.2)$$

Finally, the maximum additional active power  $P^{max,Controllable}$  can be calculated by applying equation (A.3). The result  $p^{gap,Controllable}$  can either be positive in case the line is not overloaded or negative, if the transmitted power has to be reduced.

$$P^{gap,Controllable} = \max\left[\frac{1}{2a} * (-b \pm \sqrt{b^2 - (4ac)})\right]$$
 (A.3)

$$P^{max,Controllable} = (P^{act,Controllable} + P^{gap,Controllable}) * \eta$$
 (A.4)

As a last step, the maximum active power that can be injected by nodes with controllable assets is calculated by adding  $p^{max,Controllable}$  and  $p^{gap,Controllable}$  as it is shown in equation (A.4). The factor  $\eta$  reflects a virtual buffer to additionally ensure that line loading does not exceed 100%. Its value is assumed to be equal 0.90.

# A.3. Properties of the low voltage grids

Table A.4.: Properties of low voltage grids 1-6 depending on the penetration rate of electric vehicles

Low voltage grid	LV1	LV2	LV3	LV4	LV5	LV6
Simbench type	rural3	rural2	rural2	rural1	rural1	rural1
Line length [m]	560	1467	1467	2352	2352	2352
Number buses	14	96	96	128	128	128
Transformer rated capacity [MVA]	0.16	0.25	0.25	0.40	0.40	0.40
Maximum load without EVs [MW]	0.10	0.23	0.23	0.40	0.40	0.40
dRate 30	0.04	0.12	0.12	0.10	0.10	0.13
Number EVs	4	21	24	28	38	48
EV penetration [%]	31	23	26	31	32	41
Number of Households (HH)	13	93	93	118	118	118
with no EV, no HP, no PV, no Storage	5	51	48	55	48	45
with EV, no HP, no PV, no Storage	0	0	0	0	1	0
with no EV, HP, no PV, no Storage	4	9	11	21	19	22
with EV, no HP, PV, no Storage	0	0	0	0	0	0
with no EV, HP, PV, no Storage	0	2	3	1	4	1
with no EV, no HP, PV, Storage	0	5	6	11	10	7
with BV, HP, no PV, Storage	1	9	12	11	15	23
with EV, no HP, PV, Storage	0	0	0	0	0	0
with no EV, HP, PV, Storage	0	5	2	2	1	4
with EV, HP, PV, Storage	3	12	11	17	20	16
dRate 50	-	12	11	11	20	10
Number EVs	7	38	44	63	57	58
EV penetration [%]	54	41	47	53	48	49
Number of Households (HH)	13	93	93	118	118	118
with no EV, no HP, no PV, no Storage	5	38	39	32	32	31
with EV, no HP, no PV, no Storage	0	13	9	23	17	14
with no EV, HP, no PV, no Storage	1	7	6	14	15	18
with EV, no HP, PV, no Storage	3	2	5	7	4	4
with no EV, HP, PV, no Storage	0	1	0	0	4	1
with no EV, no HP, PV, Storage	0	4	4	8	9	7
with EV, HP, no PV, Storage	1	10	15	12	15	23
with EV, no HP, PV, Storage	0	1	2	3	0	0
with no EV, HP, PV, Storage	0	5	1	1	1	3
with EV, HP, PV, Storage	3	12	12	18	20	17
dRate 70						
Number EVs	9	60	64	85	81	81
EV penetration [%]	69	65	69	72	69	69
Number of Households (HH)	13	93	93	118	118	118
with no EV, no HP, no PV, no Storage	3	21	24	19	19	18
with EV, no HP, no PV, no Storage	2	30	24	36	30	27
with no EV, HP, no PV, no Storage	1	5	2	10	9	12
with EV, no HP, PV, no Storage	3	4	9	11	10	10
with no EV, HP, PV, no Storage	0	1	0	0	2	1
with no EV, no HP, PV, Storage	0	2	3	4	7	3
with EV, HP, no PV, Storage	1	10	15	12	17	23
with EV, no HP, PV, Storage	0	3	3	7	3	4
with no EV, HP, PV, Storage	0	4	1	0	0	3
with EV, HP, PV, Storage	3	13	12	19	21	17

Table A.5.: Properties of low voltage grids 7-12 depending on the penetration rate of electric vehicles

	L	ow volta	ge grid		LV7	LV8	LV9	LV10	LV11	LV12
		Simbench	type		rural1	semi-	semi-	semi-	semi-	urban
		Difficience	1 type			urban2	urban2	urban2	urban1	diban
		Line leng			2352	746	746	746	1790	1078
		Number			128	43	43	43	110	58
			capacity [		0.40	0.40	0.40	0.40	0.63	0.63
	Maximun			[MW]	0.18	0.11	0.11	0.09	0.20	0.22
		dRate								
		Number			34	14	16	10	35	36
		V penetra			29	36	41	26	34	68
			seholds (H	,	118	39	39	39	104	53
with	no EV,	no HP,	no PV,	no Storage	45	16	12	17	48	15
with	EV,	no HP,	no PV,	no Storage	0	1	1	1	0	0
with	no EV,	HP,	no PV,	no Storage	20	3	3	5	11	7
with	EV,	no HP,	PV,	no Storage	0	0	0	0	0	0
with	no EV,	HP,	PV,	no Storage	3	1	2	1	3	1
with	no EV,	no HP,	PV,	Storage	14	3	5	3	6	3
with	EV,	HP,	no PV,	Storage	21	8	7	5	18	7
with	EV,	no HP,	PV,	Storage	0	0	0	0	0	0
with	no EV,	HP,	PV,	Storage	2	2	1	3	1	2
with	EV,	HP,	PV,	Storage	13	5	8	4	17	18
		dRate								
		Number			59	28	20	21	49	42
		V penetra		TTT)	50	72	51	54	47	79
			seholds (H	,	118	39	39	39	104	53
with	no EV,	no HP,	no PV,	no Storage	32	7	10	14	36	12
with	EV,	no HP,	no PV,	no Storage	13	10	3	4	12	3
with	no EV,	HP,	no PV,	no Storage	14	1	3	1	10	4
with	EV,	no HP,	PV,	no Storage	6	2	0	4	1	3
with	no EV,	HP,	PV,	no Storage	2	1	1	1	3	1
with	no EV,	no HP,	PV,	Storage	10	1	4	1	6	3
with	EV,	HP,	no PV,	Storage	22	8	8	5	18	7
with	EV,	no HP,	PV,	Storage	4	2	1 1	2	0	$\begin{bmatrix} 0 \\ 2 \end{bmatrix}$
with	no EV, EV,	HP, HP,	PV, PV,	Storage	1 14	6	8	$\begin{bmatrix} 1 \\ 6 \end{bmatrix}$	18	18
WITH	ъv,	dRate		Storage	14	U	0	U	10	10
-		Number			87	30	26	31	68	53
	E.	Number V penetra			74	77	67	79	65	100
		•	seholds (H	тн)	118	39	39	39	104	53
with	no EV,	no HP,	no PV,	no Storage	18	5	7	5	21	7
with	EV,	no HP,	no PV,	no Storage	27	12	6	13	27	8
with	no EV,	HP,	no PV,	no Storage	6	1 1	2	13	8	1
with	EV,	no HP,	PV,	no Storage	14	2	1	4	3	6
with	no EV,	HP,	PV,	no Storage	2	1	1	1	2	1
with	no EV,	no HP,	PV,	Storage	5	1	3	0	5	2
with	EV,	HP,	no PV,	Storage	22	8	8	5	19	7
with	EV,	no HP,	PV,	Storage	9	2	2	3	19	1
with	no EV,	HP.	PV,	Storage	0	1	0	1	0	0
with	EV,	HP,	PV,	Storage	15	6	9	6	18	$\frac{0}{20}$
W 1011	⊥ v ,	111,	1 V,	Diorage	10		J 3		10	20

# B. Supplementary material for chapter 3

# B.1. The full Bass model

For the computation of regional transition pathways of electric vehicles, the Bass diffusion model is used. In this section, it is explained how the formula in Equation (3.3) is derived. According to Rogers' concept of the diffusion of innovation (1962), P(t) is "the probability that an initial purchase will be made at time t given that no purchase has yet been made" (Bass, 1969).

$$P(t) = \frac{f(t)}{1 - F(t)} = p + \frac{q}{m}A(t) = p + qF(t)$$
(B.1)

The parameter p is the coefficient of innovators meaning the probability of initial purchases at the start of the innovation and q is the coefficient of imitators, signalling the pressure they feel from the increasing number and m is the total market size. f(t) is the likelihood of purchase at time t. F(t) is the cumulative diffusion level at time t, further described in Equation (B.2). A(t) expresses the cumulative number of adopters a(t) in the interval (0,t), presented in Equation (B.3) based on Bass (1969) and Van der Kam et al. (2018).

$$F(t) = \frac{A(t)}{m} = \int_0^t f(t)dt$$
 (B.2)

$$A(t) = \int_0^T a(t)dt = m \int_0^T f(t)dt = mF(t)$$
 (B.3)

The number of adopters a(t) itself can be calculated according to Equation (B.4)

$$a(t) = mf(t) = P(t)[m - A(t)] = \left[p + \frac{q \int_0^T a(t)dt}{m}\right][m - \int_0^T a(t)dt]$$
 (B.4)

Also, f(t) can be extended as:

$$f(t) = [p + qF(t)][1 - F(t)] = p + (q - p)F(t) - q[F(t)]^{2}$$
(B.5)

#### B. Supplementary material for chapter 3

To find F(t), this non-linear differential Equation (B.6) needs to be solved:

$$dt = \frac{dF}{(p + (q - p)F - qF)}$$
(B.6)

This equals to:

$$F = \frac{q - pe^{(-t+C)(p+q)}}{q(1 + e^{(-t+C)(p+q)})}$$
(B.7)

Since F(0) = 0, the integration constant may be evaluated:

$$-C = \frac{1}{p+q} ln(\frac{q}{p})$$
 (B.8)

Therefore:

$$F(t) = \frac{1 - e^{-(p+q)t}}{1 + \frac{q}{p}e^{-(p+q)t}}$$
 (B.9)

or:

$$A(t) = m \frac{1 - e^{-(p+q)t}}{1 + \frac{q}{p}e^{-(p+q)t}}$$
(B.10)

To normalize the beginning of the diffusion  $t_0$  at 0, this function can be written as:

$$A(t) = m \frac{1 - e^{-(p+q)(t-t_0)}}{1 + \frac{q}{p}e^{-(p+q)(t-t_0)}}$$
(B.11)

which is derived from Van der Kam et al. (2018).

## B.2. Function transformation to $\Delta t$

This section displays the transformation of the diffusion curve function given in Equation (3.3) to the diffusion curve function in Equation (3.6). The objective is to calculate t given all other variables and parameters stay constant. Recall Equation (3.3):

$$F(t,\hat{s},\hat{p},\hat{q}) = \hat{s} * \frac{1 - e^{-(\hat{p}+\hat{q})(t-t_0)}}{1 + \frac{\hat{q}}{\hat{p}}e^{-(\hat{p}+\hat{q})(t-t_0)}} \qquad |*(1 + \frac{\hat{q}}{\hat{p}}e^{-(\hat{p}+\hat{q})(t-t_0)})$$
(B.12)

For the sake of simplicity, F(t) will be written as F in this function transformation. The transformation steps are shown in Equations (B.13) to (B.20).

$$F(1 + \frac{\hat{q}}{\hat{p}}e^{-(\hat{p}+\hat{q})(t-t_0)}) = \hat{s} * (1 - e^{-(\hat{p}+\hat{q})(t-t_0)}) \qquad |\text{solving the brackets (B.13)}$$

$$F + F \frac{\hat{q}}{\hat{p}}e^{-(\hat{p}+\hat{q})(t-t_0)} = \hat{s} - \hat{s}e^{-(\hat{p}+\hat{q})(t-t_0)} \qquad |*\hat{p}| \text{ (B.14)}$$

$$\hat{p}$$

$$\hat{p}F + \hat{q}Fe^{-(\hat{p}+\hat{q})(t-t_0)} = \hat{s}\hat{p} - \hat{s}\hat{p}e^{-(\hat{p}+\hat{q})(t-t_0)} \qquad |-\hat{p}F + \hat{s}\hat{p}e^{-(\hat{p}+\hat{q})(t-t_0)}$$
(B.15)

$$\hat{s}\hat{p}e^{-(\hat{p}+\hat{q})(t-t_0)} + \hat{q}Fe^{-(\hat{p}+\hat{q})(t-t_0)} = \hat{s}\hat{p} - \hat{p}F$$
 (B.16)

$$(\hat{s}\hat{p} + \hat{q}F)e^{-(\hat{p}+\hat{q})(t-t_0)} = \hat{s}\hat{p} - \hat{p}F \qquad |*\frac{1}{\hat{s}\hat{p}+\hat{q}F}|$$
(B.17)

$$e^{-(\hat{p}+\hat{q})(t-t_0)} = \frac{\hat{s}\hat{p} - \hat{p}F}{\hat{s}\hat{p} + \hat{q}F}$$
 |  $ln$  (B.18)

$$-(\hat{p}+\hat{q})(t-t_0) = \ln(\frac{\hat{s}\hat{p}-\hat{p}F}{\hat{s}\hat{p}+\hat{q}F}) \qquad |*\frac{1}{-(\hat{p}+\hat{q})}|$$
(B.19)

$$t - t_0 = \frac{\ln(\frac{\hat{s}\hat{p} - \hat{p}F}{\hat{s}\hat{p} + \hat{q}F})}{-(\hat{p} + \hat{q})} + t_0 \text{ (B.20)}$$

$$t = \frac{\ln(\frac{\hat{s}\hat{p} - \hat{p}F}{\hat{s}\hat{p} + \hat{q}F})}{-(\hat{p} + \hat{q})} + t_0 \text{ (B.21)}$$

To calculate the time difference  $\Delta t$  between a given time  $t_{set}$  when a NUTS 3 region reaches a certain diffusion level  $F(t)^{nuts3}$ , and the time when the same level is reached on the national diffusion curve, the following Equation (B.22) is the result.

$$\Delta t = t - t_{set} = \frac{\ln(\frac{\hat{s}\hat{p} - \hat{p}F}{\hat{s}\hat{p} + \hat{q}F})}{-(\hat{p} + \hat{q})} + t_0 - t_{set}$$
(B.22)

# B.3. Descriptive analysis of mobility data

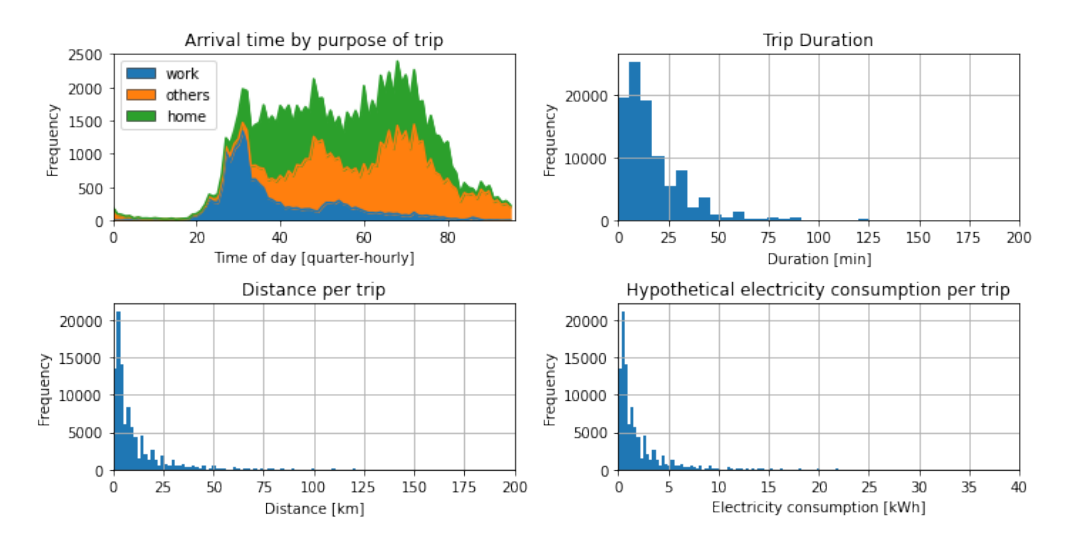


Figure B.1.: Key parameters of the used MOP dataset (KIT - Institut für Verkehrswesen, 2021)

# B.4. Distribution of daily energy consumption per EV

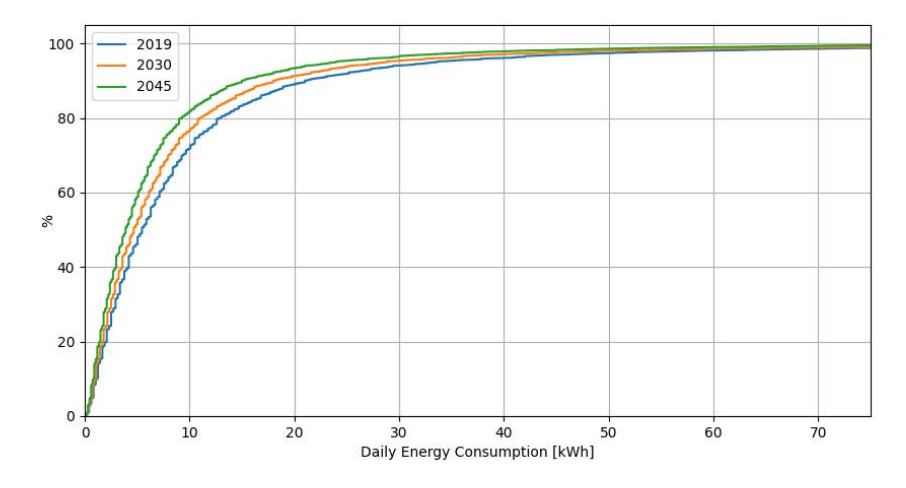


Figure B.2.: Distribution of daily energy consumption per EV based on average specific fleet consumption by year

# B.5. Weekend flexibility clusters and in-depth analysis of the flexibility clusters

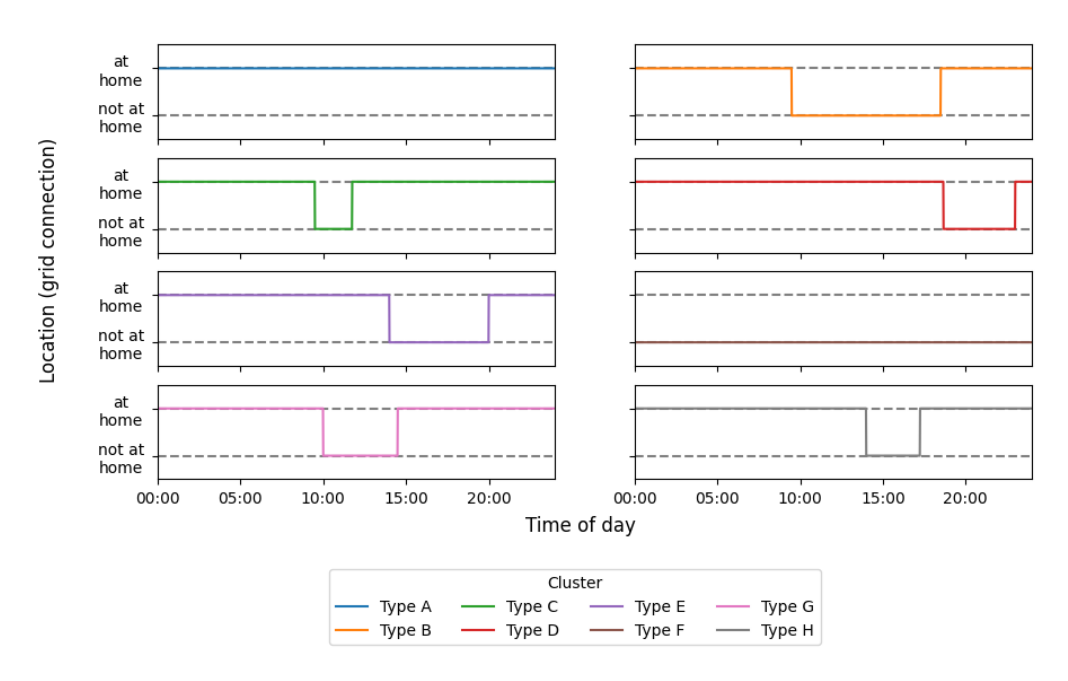


Figure B.3.: Flexibility clusters for weekends

Note: The figure shows the cluster centroids' binary grid connection time series (at home, not at home) for weekends. Cars are assumed to be connected to the grid and provide flexibility while at home. The cluster centroids determine the time window for potential flexibility provision for all profiles assigned to a respective cluster.

The clusters are evaluated based on the Pearson correlation coefficient and the Hamming similarity, a metric for binary time series. The latter indicates for most weekday and weekend clusters similarities beyond 80%, which are considered reasonably high scores. Cluster 4 for weekends shows with 79% the lowest similarity score. However, with only 6% of the observations for weekends, at the same time, it is the smallest cluster. The Pearson correlation coefficient indicates a high correlation for the majority of the clusters. Exceptions in this regard are the Clusters 5 and 7 for weekdays and the Clusters 1 and 6 for weekends. Here, the Pearson correlation coefficient is close to zero, although still positive. For the weekday cluster 7 and the weekend cluster 1, this is attributed to their large size and due to the fact that the clusters bundle the profiles with only short intervals of not being connected to the grid scattered during the day. For the weekday cluster 5 and the weekend cluster 6, the low correlation coefficient is also due to the characteristics of the clusters. Both clusters bundle the observations with hardly any grid connection at home, with the clusters' medoids not showing a grid connection at all. The small connection intervals of the different observations are scattered during the day, leading to a low correlation value. Given the

#### B. Supplementary material for chapter 3

clusters medoids and the high similarity score, these clusters appear nonetheless meaningful.

Table B.1.: Characteristics of the weekday flexibility clusters

Metric	Share of observations	Pearson correlation	Hamming similarity
Cluster 1	12%	0.69	84%
Cluster 2	12%	0.78	89%
Cluster 3	10%	0.50	87%
Cluster 4	12%	0.78	89%
Cluster 5	8%	0.14	93%
Cluster 6	8%	0.65	85%
Cluster 7	27%	0.04	86%
Cluster 8	9%	0.53	82%

Notes: The pearson coefficient is a value between -1 (no correlation) and 1 (perfect correlation). The hamming similarity is a value between 0% (no similarity) and 100% (perfect similarity). The metrics indicate the correlation and the similarity of the observations within a cluster.

Table B.2.: Characteristics of the weekend flexibility clusters

			- <i>y</i>
Metric	Share of observations	Pearson correlation	Hamming similarity
Cluster 1	31%	0.03	91%
Cluster 2	10%	0.64	81%
Cluster 3	12%	0.56	89%
Cluster 4	6%	0.50	79%
Cluster 5	8%	0.64	84%
Cluster 6	12%	0.16	89%
Cluster 7	10%	0.60	85%
Cluster 8	11%	0.61	90%

Notes: The pearson coefficient is a value between -1 (no correlation) and 1 (perfect correlation). The hamming similarity is a value between 0% (no similarity) and 100% (perfect similarity). The metrics indicate the correlation and the similarity of the observations within a cluster.

# B.6. Shares of charging scenarios

Table B.3.: Shares of charging scenarios per settlement type

settlement type	h	h,w	h,o	h,w,o	W	О	w,o	Total
rural community	22%	22%	22%	22%	4%	4%	4%	100%
smaller provincial town	22%	22%	22%	22%	4%	4%	4%	100%
larger provincial town	21%	21%	21%	21%	6%	6%	6%	100%
smaller medium town	18%	18%	18%	18%	9%	9%	9%	100%
larger medium town	20%	20%	20%	20%	7%	7%	7%	100%
smaller metropolis	16%	16%	16%	16%	13%	13%	13%	100%
larger metropolis	10%	10%	10%	10%	19%	19%	19%	100%

Notes: The row total may differ from 100% due to rounding errors. Charging locations: at home (h), at work (w), others (o)

## B.7. Distribution of demand to federal states

To distribute the national demand of each sector among the federal states, data from Länderarbeitskreis Energiebilanzen (2022) is used. The data includes the demand of all federal states separately by sector for the years 1990-2019. The demand in this model is allocated among the federal states based on the distribution of sector-specific demand in 2019. An exception is the state of Saarland, where the most recent data available is from 2016 (Table B.4). It is assumed that this distribution does not change fundamentally over time.

Table B.4.: Distribution keys of sectoral electricity demand to federal states

Sector	BW	BY	BE	ВВ	НВ	НН	HE	MV
Households	14%	16%	3%	3%	1%	3%	8%	2%
Small-scale industries, trade & services	15%	16%	5%	3%	1%	3%	9%	2%
Industry	12%	15%	1%	3%	1%	2%	5%	1%
Rail transport	11%	19%	8%	5%	1%	3%	11%	2%
Conversion sector	9%	9%	1%	10%	1%	3%	2%	1%
Sector	NI	NW	RP	SL	SN	ST	SH	TH
Sector Households	NI 9%	NW 23%		SL 1%	SN 4%	ST 2%	SH 4%	TH 2%
Households	9%	23%	5%	1%	4%	2%	4%	2%
Households Small-scale industries, trade & services	9% 9%	23% 20%	5% 4%	1% 1%	4% 4%	2% 3%	4% 3%	2% 3%

Note: The row total may differ from 100% due to rounding errors.

# B.8. Demand profiles

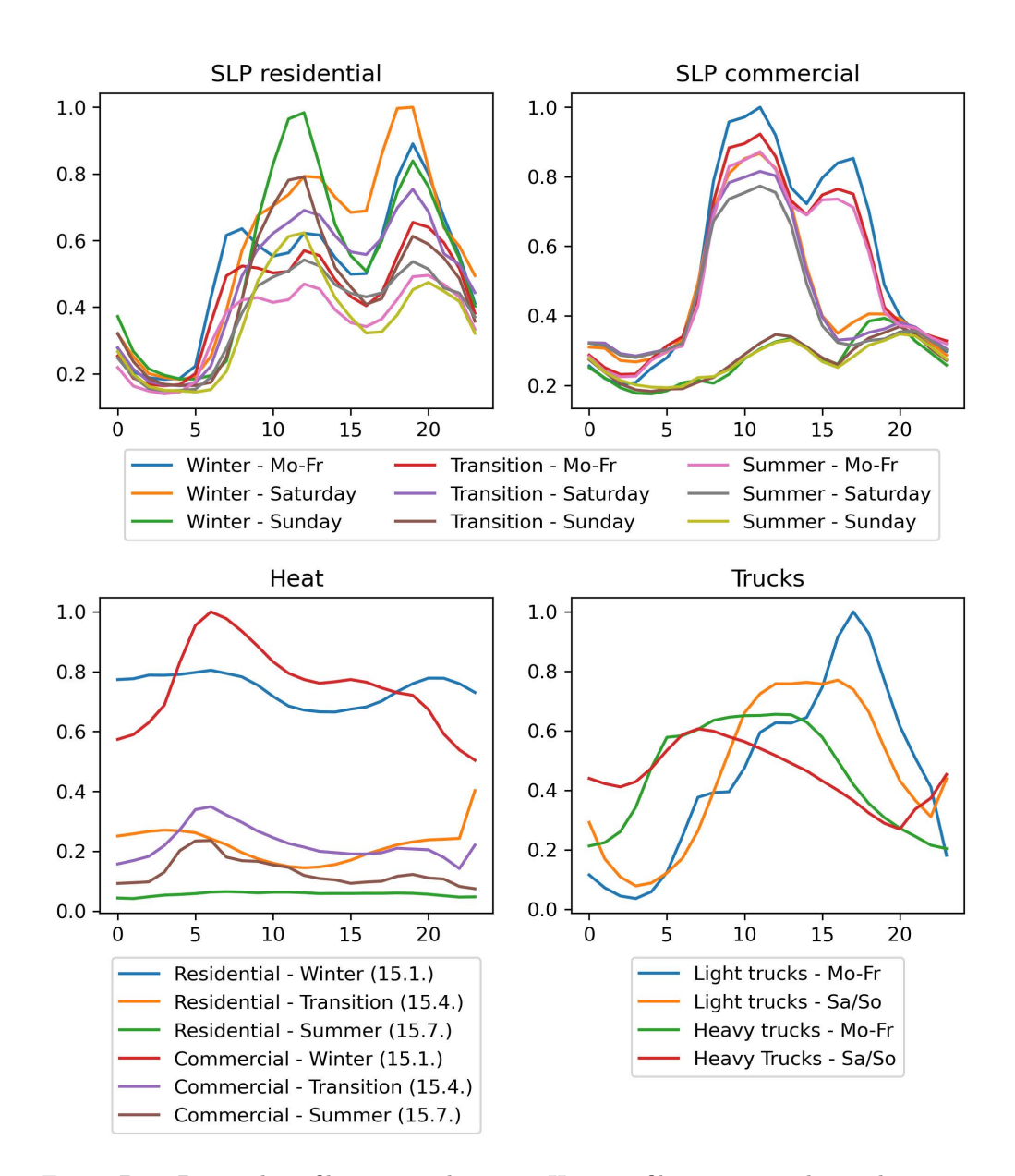


Figure B.4.: Demand profiles per application. Heat profiles are exemplary: shown are the profiles for the region DEA23 (Cologne) on 3 exemplary days of the year.

# B.9. Residual load duration curves

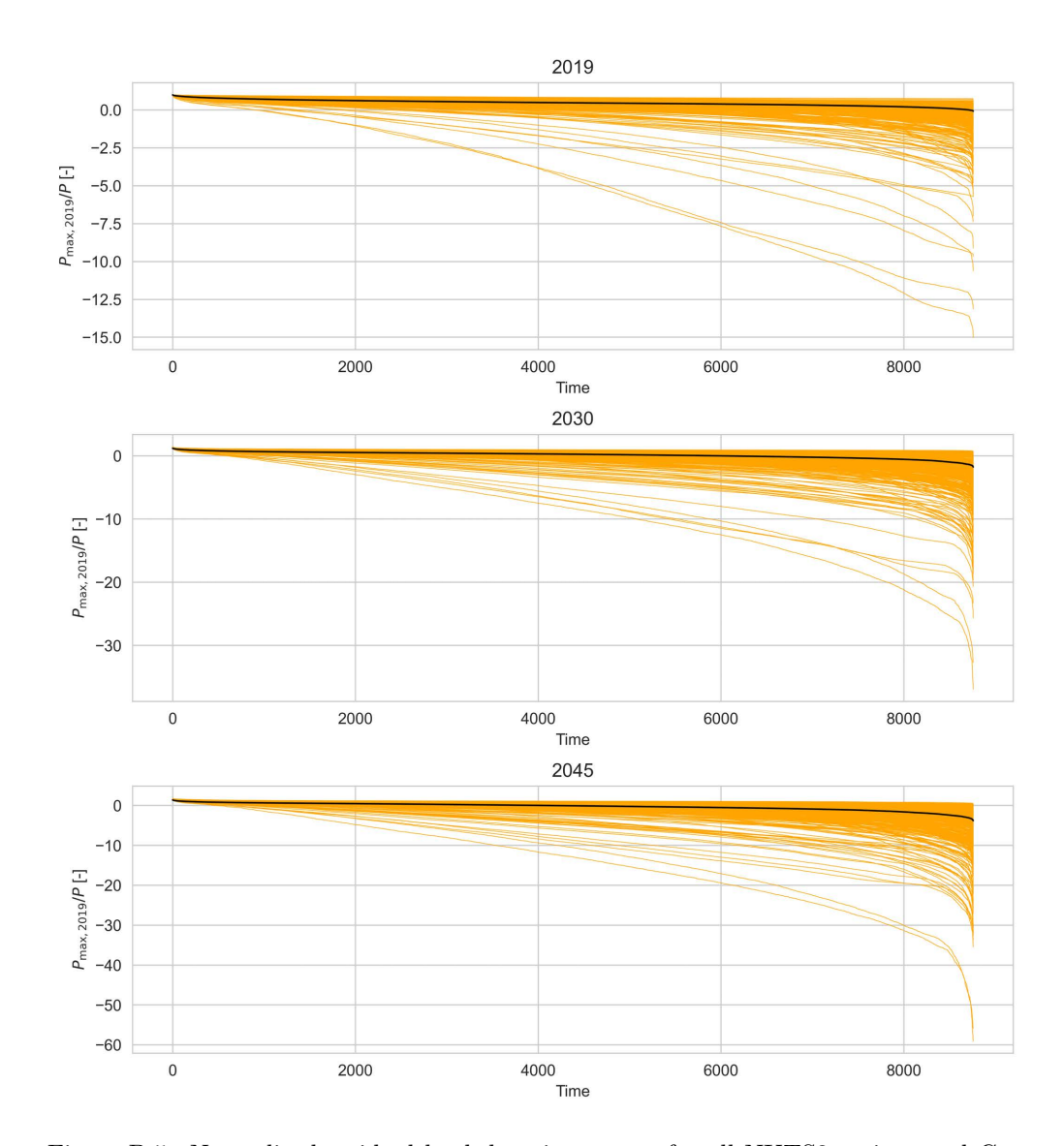


Figure B.5.: Normalized residual load duration curves for all NUTS3 regions and Germany for 2019, 2030 and 2045

Note: Each subplot visualizes the normalized residual load duration curves for each NUTS3 region (in orange) and Germany (in black) for a given year. Normalization was performed by dividing each value of the residual load curve by its maximum value in 2019.

# B.10. Cluster properties

Table B.5.: Properties of the regions within the three cluster in 2045

Property	Indicator	Cluster   Wind	Cluster PV	Cluster Load
Population density	Minimum	36	66	125
(people per $km^2$ )	Maximum	437	1585	4761
	Mean	117	264	1165
Number of EVs	Minimum	14	31	56
(cars per $km^2$ )	Maximum	167	606	1811
	Mean	55	119	471
Wind Onshore capacity	Minimum	0.22	0.00	0.00
$(MW \text{ per } km^2)$	Maximum	1.94	1.26	0.95
	Mean	0.75	0.29	0.15
total PV capacity	Minimum	0.19	0.16	0.00
$(MW \text{ per } km^2)$	Maximum	1.59	2.18	2.35
	Mean	0.62	0.69	0.34
large-scale PV capacity	Minimum	0.19	0.16	0.00
$(MW \text{ per } km^2)$	Maximum	1.59	2.18	2.34
	Mean	0.62	0.69	0.34
rooftop PV capacity	Minimum	0.13	0.15	0.23
$(MW \text{ per } km^2)$	Maximum	2.04	5.41	7.46
	Mean	0.38	0.86	2.20

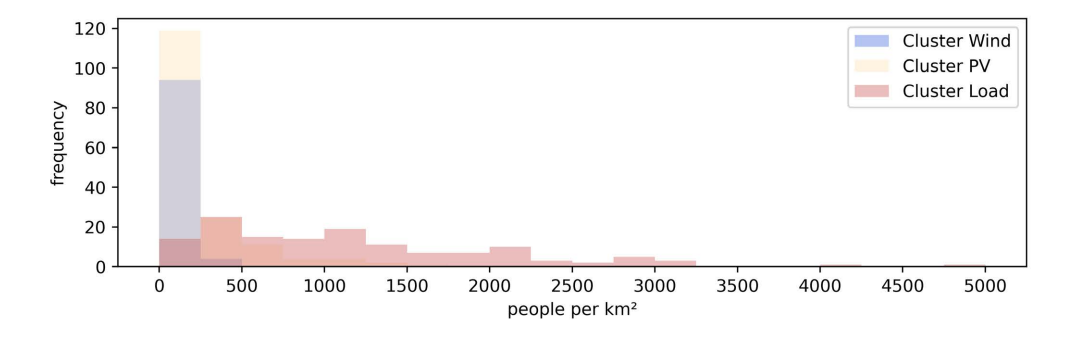


Figure B.6.: Distribution of the population density within each cluster in 2045

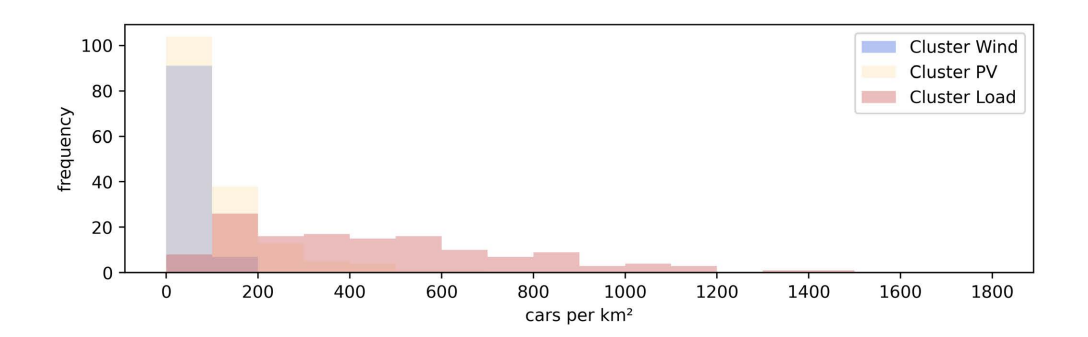


Figure B.7.: Distribution of EVs per  $km^2$  within each cluster in 2045

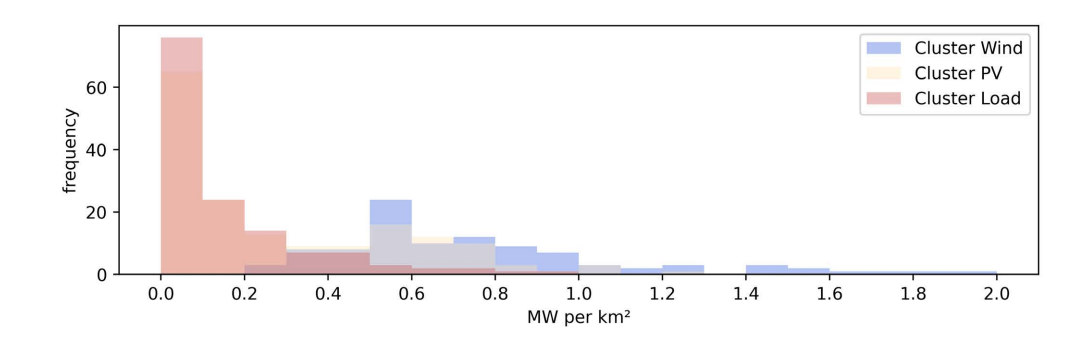


Figure B.8.: Distribution of Wind Onshore capacities per  $km^2$  within each cluster in 2045

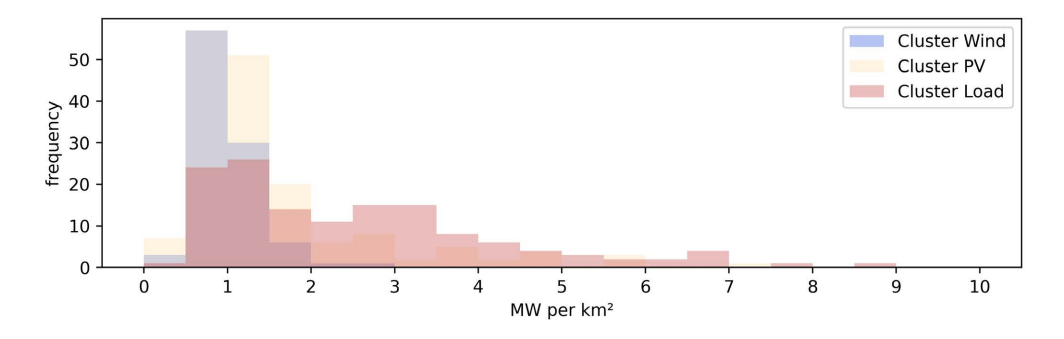


Figure B.9.: Distribution of PV capacities (large-scale PV and rooftop PV) per  $km^2$  within each cluster in 2045

#### B. Supplementary material for chapter 3

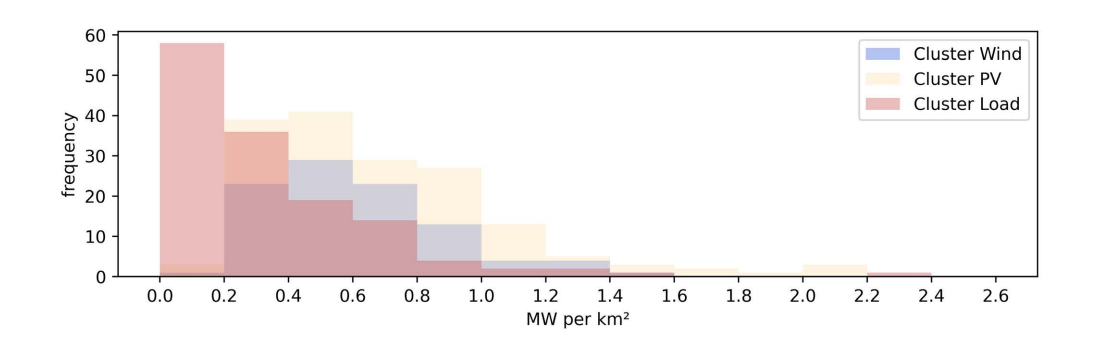


Figure B.10.: Distribution of large-scale PV capacities per  $km^2$  within each cluster in  $2045\,$ 

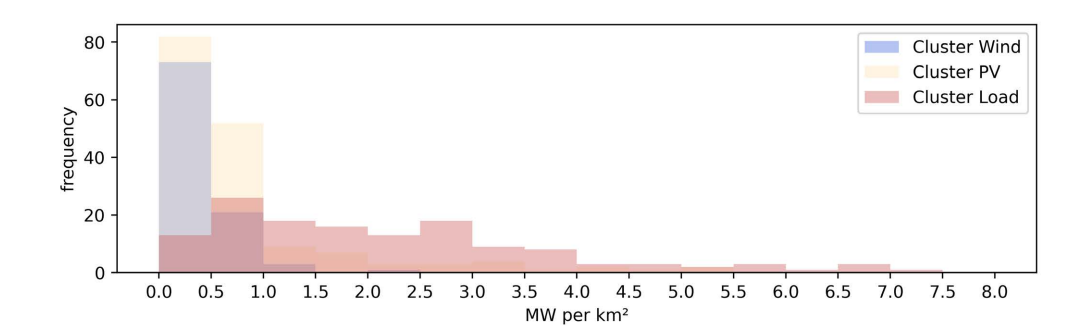


Figure B.11.: Distribution of rooftop PV capacities per  $km^2$  within each cluster in 2045

# C. Supplementary material for chapter 4

# C.1. Sets, parameters and decision variables

Table C.1.: Sets

	TT •,	D '
$\mathbf{Set}$	${f Unit}$	Description
$a \in A$	-	All technologies
$a \in A_{Cars}$	-	All electric vehicles
$a \in A_{noFlexCars}$	-	Electric vehicles that are not flexible
$a \in A_{FlexCars}$	-	Electric vehicles that are flexible
$a \in A_{v2gCars}$	-	Electric vehicles that flexible and capable of bidi-
		rectional charging
$a \in A_{Heating}$	-	All decentralized heating technologies
$a \in A_{thStorage}$	-	Thermal storage technologies
$a \in A_{HP}$	-	Heat pump technologies
$a \in B_a$	-	Mapping heating technologies to building types
$a \in U_a$	-	Mapping mobility clusters to electric vehicles
$b \in B$	-	Building types
$d \in D$	-	Days
$h \in H$	-	Hours
$u \in U$	-	Mobility clusters

Table C.2.: Decision variables

Variable	$\mathbf{Unit}$	Description
$E_{d,a}^{el,daysaldo}$	$MWh_{el}$	Net electrical energy consumed by each electric
		vehicle $a \in A_{Cars}$ on day $d \in D$
$E_{d,a}^{th,daysaldo}$	$MWh_{th}$	Net thermal energy consumed by each thermal
,		storage technology $a \in A_{thStorage}$ on day $d \in D$
$E_{d,h,a}^{th,level}$	$MWh_{th}$	Thermal energy stored in thermal storage $a \in$
ω,π,ω		$A_{thStorage}$ in hour $h \in H$ on day $d \in D$
$P_{d,h,a}^{el,in}$	$MW_{el}$	Electrical power consumed by each technology
		$a \in A$ in hour $h \in H$ on day $d \in D$
$P_{d,h,a}^{el,out}$	$MW_{el}$	Electrical power generated by each technology
a,n,a		$a \in A$ in hour $h \in H$ on day $d \in D$
$P_{d,h,a}^{th,in}$	$MW_{el}$	Thermal power consumed by each technology $a \in$
α,π,α		$A_{Heatin}$ in hour $h \in H$ on day $d \in D$
$P_{d,h,a}^{th,out}$	$MW_{el}$	Thermal power generated by each technology $a \in$
		$A_{Heating}$ in hour $h \in H$ on day $d \in D$

Table C.3.: Parameters

Parameter	Unit	able C.3.: Parameters  Description
	%	Share of heating demand for each building type
$lpha_b$	70	be $B$
Cth	MW	
$C_a^{th}$	IVI VV	Installed thermal capacity for each technology
7		$a \in A_{Heating}$
$dp_{d,h,u}$	-	Normalized demand structure for each mobility
1 th		cluster $u \in U$ , hour $h \in H$ and day $d \in D$
$dp_{d,h,b}^{th}$	-	Normalized heat demand structure for each build-
_	~	ing type $b \in B$ , hour $h \in H$ and day $d \in D$
$ds_{d,a}$	%	Relative electricity demand of each electric vehi-
		cle $A \in A_{Cars}$ on day $d \in D$
$\eta_a$	%	Time-independent efficiency of technology $a \in A$
$\eta_{d,h,a}$	%	Efficiency of technology $a \in A$ on day $d \in D$ in
		hour $h \in H$
$fc_a$	kWh/km	Fuel consumption of each electric vehicle $a \in$
		$A_{Cars}$
$flex_{d,h,u}^{neg}$	-	Normalized negative flexibility potential for each
		mobility cluster $u \in U$ in hour $h \in H$ on day
		$d \in D$
$flex_{d,h,u}^{pos}$	-	Normalized positive flexibility potential for each
, ,		mobility cluster $u \in U$ in hour $h \in H$ on day
		$d \in D$
$flex_{d,h,u}^{v2g}$	-	Normalized bidirectional flexibility potential for
ω,π, ω		each mobility cluster $u \in U$ in hour $h \in H$ on
		$day \ d \in D$
$\gamma$	%	Storage losses for thermal storage
$I_a$	km	Road transport demand of each electric vehicle
		$a \in A_{Cars}$
$I^{th}$	TWh	Total heat demand
$I_b^{th}$	TWh	Heat demand of each building type $b \in B$
$vf_a$	_	Volume factor (ratio of power and energy) for
		each thermal storage $a \in A_{thStorage}$

# C.2. DIMENSION model description

#### Sector overview

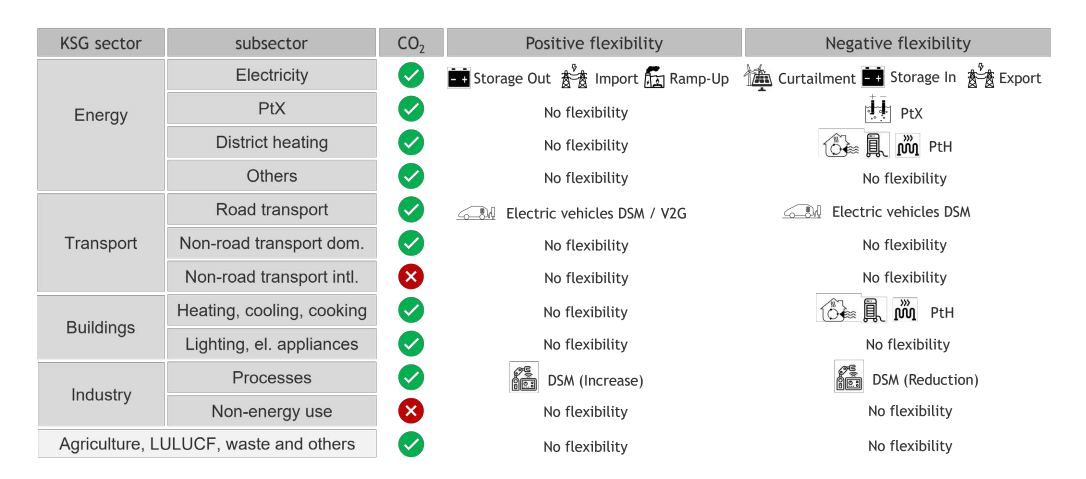


Figure C.1.: DIMENSION sector overview

Note that the column  ${\rm ^{'}CO_2^{''}}$  reflects weather  ${\rm ^{CO}_2^{''}}$ -emissions of the specific subsector are accounted for total  ${\rm ^{CO}_2}$  emissions of the corresponding sector, as defined in the Climate Protection Act (KSG).

#### Decentralized heating equations

To model decentralized heating in the buildings sector, we assume that each of the ten defined building types,  $b \in B$ , meets a fixed share of the overall heating demand. This is represented by a constant parameter  $\alpha_b$ , which assigns a specific share of the total demand to each building type. <sup>43</sup> Decentralized heating technologies,  $a \in A_{Heating}$ , are matched to the appropriate building types using the matching set  $a \in B_a$ , and, in each case, heat pumps are supplemented by an electric heating rod as backup and thermal storage, which includes both active water tanks and passive building mass storage. <sup>44</sup> Depending on its size, thermal storage can also accommodate additional water tanks, enabling more flexible operation of the heat pumps.

The equilibrium constraint, as formulated in Equation (C.1), ensures that the heating supply,  $P_{d,h,a}^{th,out}$ , from heating technologies a, matches the exogenous heat demand profile at all times. This also accounts for the endogenously optimized storage input,  $P_{d,h,a}^{th,in}$ . The heat demand profile is calculated by multiplying the

<sup>&</sup>lt;sup>43</sup>The total heating demand is distributed across various installed heating technologies, including gas, oil, biomass, and electricity, as detailed in Appendix C.3, with the electricity demand further divided among the building types equipped with heat pumps, as shown in Table 4.1.

<sup>&</sup>lt;sup>44</sup>The heat pumps are sized to satisfy 80% of the peak heat demand, with the remaining 20% handled by electric heating rods serving as auxiliary capacity.

annual heat demand of each building type,  $I_b^{th}$ , with the corresponding normalized heat demand profile  $dp_{d,h,b}^{th}$ .

$$\sum_{a \in B_a} (P_{d,h,a}^{th,out} - P_{d,h,a}^{th,in}) = I_b^{th} * dp_{d,h,b}^{th} = I^{th} * \alpha_b * dp_{d,h,b}^{th}$$

$$\forall d \in D \land h \in H \land b \in B$$
(C.1)

The electricity input required for heat generation via heat pumps,  $P_{d,h,a}^{el,in}$ , is calculated by factoring in the temperature-dependent COP, represented as  $\eta_{d,h,a}$ . Each heat pump technology is linked to its own time series for the COP, as shown in Equation (C.2).

$$P_{d,h,a}^{el,in} = \frac{P_{d,h,a}^{th,out}}{\eta_{d,h,a}} \qquad \forall d \in D \land h \in H \land a \in A_{HP}$$
 (C.2)

The thermal storage level is determined by summing the previous hour's storage level (adjusted for storage losses,  $\gamma = 0.03\%$ ) with the net thermal storage feed-in, which is multiplied by the efficiency  $\eta_{d,h,a}$  of 84%, based on Sarbu and Sebarchievici (2018), as shown in Equation (C.3). The storage levels between the last hour of one day and the first hour of the next are connected as per Equation (C.4). The storage capacity is limited by the installed capacity,  $C_a^{th}$ , adjusted by the volume factor,  $vf_a$ , as formulated in Equation (C.5). The daily balance of thermal storage is calculated by summing the endogenous storage feed-in and feed-out.

$$E_{d,h+1,a}^{th,level} = E_{d,h,a}^{th,level} * (1 - \gamma) + P_{d,h+1,a}^{th,in} * \eta_{d,h,a} - P_{d,h+1,a}^{th,out}$$

$$\forall d \in D \land h \in H \land a \in A_{thStorage}$$
(C.3)

$$E_{d+1,h,a}^{th,level} = E_{d,h,a}^{th,level} * (1 - \gamma) + P_{d+1,h,a}^{th,in} * \eta_{d,h,a} - P_{d+1,h,a}^{th,out}$$

$$\forall d \in D \land h = H \land a \in A_{thStorage}$$
(C.4)

$$E_{d,h,a}^{th,level} \le C_a^{th} * vf_a \qquad \forall d \in D \land h \in H \land a \in A_{thStorage}$$
 (C.5)

To reflect the flexibility provided by both passive and active thermal storage, the volume factor  $vf_a$  incorporates two components: the thermal inertia of the building mass and the installed water tank capacity. While active thermal storage is represented by explicit storage capacity (e.g., water tanks), the passive component captures the ability of the building mass to temporarily buffer heat due to its thermal inertia.

This passive storage potential is estimated through a simplified approach that quantifies how long a building can passively maintain indoor temperatures within

comfort limits - without active heating - based on its specific transmission heat loss. This approach is used as the model considers aggregated building mass per building type rather than simulating individual buildings. We estimate the thermal storage capacity as the amount of heat that can be stored in the building mass when its temperature changes by a defined amount. The stored energy is calculated as  $Q = c \cdot m \cdot \Delta T$ , where c is the specific heat capacity of the material, m is the mass of the relevant structural components (e.g., walls, floors), and  $\Delta T$  is the allowable indoor temperature deviation (Sarbu and Sebarchievici, 2018). For typical materials and room configurations, we assume a storage capacity of  $60 \text{ Wh/m}^2\text{K}$ , which results in  $120 \text{ Wh/m}^2$  for an acceptable temperature change of the comfort zone by 2 K as suggested by Le Dréau and Heiselberg (2016). To estimate the passive storage duration, we divide this by the building's specific transmission heat loss (KfW, 2024). This yields the number of hours the stored energy can offset the transmission losses.

To evaluate the effects of varying degrees of flexibility, the volume factor for thermal storage is adjusted across different use cases as described in Section 4.3.2.

#### Road transport equations

In the following, we present the key equations for the road transport module. Depending on the use case (see Section 4.3), an EV, denoted by a, is classified as either passive ( $a \in A_{noFlexCars}$ ), flexible ( $a \in A_{FlexCars}$ ), or capable of bidirectional charging ( $a \in A_{v2gCars}$ ). Furthermore, EVs are distributed across ten different mobility clusters u, corresponding to the set  $U_a$ .

The fundamental constraint, expressed in Equation (C.6), necessitates that the power consumption by EVs,  $P_{d,h,a}^{el,in}$ , for each day d and hour h, equals the product of exogenous road transport demand  $I_a$  (in km), fuel consumption  $fc_a$  (in kWh/km), and the exogenous, normalized demand profile  $dp_{d,h,u}$  for each mobility cluster.

$$P_{d,h,a}^{el,in} = I_a * fc_a * \sum_{u \in U_a} dp_{d,h,u} \qquad \forall d \in D \land h \in H \land a \in A_{noFlexCars}$$
 (C.6)

To account for a system-oriented flexible charging, we formulate Equations (C.7) to (C.10). These constraints ensure that while an EV can be charged flexibly, the total daily amount of charging must remain constant, assuming users are unlikely to alter their driving habits across multiple days. The first two equations establish the balance of EV's battery storage. First, the daily storage balance is computed as the difference between the energy inflow and

<sup>&</sup>lt;sup>45</sup>The method is a simplification suited for system-level modeling, as it does not account for spatial heat distribution, dynamic heat transfer, or interactions with building control strategies. More detailed modeling approaches - such as those described in Bloess et al. (2018) - can capture these effects more accurately.

outflow, with the outflow - associated with Vehicle-to-Grid (V2G) - adjusted by the round-trip efficiency  $\eta_a$  of the battery. Second, the balance must equal the product of the exogenous road transport demand, fuel consumption, and the exogenously determined daily demand share,  $ds_{d,a}$  (in %), ensuring that EV's storage is balanced within a day.

$$E_{d,a}^{el,daysaldo} = \sum_{h} (P_{d,h,a}^{el,in} - P_{d,h,a}^{el,out} * \eta_a)$$

$$\forall d \in D \land a \in (A_{FlexCars} \lor A_{v2qCars})$$
(C.7)

$$E_{d,a}^{el,daysaldo} = I_a * fc_a * ds_{d,a}$$

$$\forall d \in D \land a \in (A_{FlexCars} \lor A_{v2gCars})$$
(C.8)

Flexible charging is constrained within positive and negative flexibility limits, computed for each mobility cluster. Although flexible cars generally follow the demand profile  $dp_{d,h,u}$ , they are allowed to deviate within the upper and lower bounds  $flex_{d,h,u}^{neg}$  and  $flex_{d,h,u}^{pos}$ , respectively.

$$P_{d,h,a}^{el,in} \ge I_a * fc_a * \sum_{u \in U_a} (dp_{d,h,u} - flex_{d,h,u}^{pos})$$

$$\forall d \in D \land h \in H \land a \in (A_{FlexCars} \lor A_{v2gCars})$$
(C.9)

$$P_{d,h,a}^{el,in} \leq I_a * fc_a * \sum_{u \in U_a} (dp_{d,h,u} + flex_{d,h,u}^{neg})$$

$$\forall d \in D \land h \in H \land a \in (A_{FlexCars} \lor A_{v2aCars})$$
(C.10)

For use cases involving bidirectional charging, bidirectional charging is only allowed for cars assigned to the corresponding set  $A_{v2gCars}$ . The V2G potential  $flex_{d,h,u}^{v2g}$  in Equation (C.12) is defined for each mobility cluster as the sum of the positive and negative flexibility potential.

$$P_{d,h,a}^{el,out} = 0 \qquad \forall d \in D \land h \in H \land a \in (A_{FlexCars} \lor A_{v2gCars}) \quad \text{(C.11)}$$

$$P_{d,h,a}^{el,out} \leq I_a * fc_a * \sum_{u \in U_a} flex_{d,h,u}^{v2g} \qquad \forall d \in D \land h \in H \land a \in A_{v2gCars} \quad \text{(C.12)}$$

Additional constraints link the road transport sector to the energy system, accounting for factors such as  $CO_2$  emissions, total energy consumption or variable costs, following Helgeson and Peter (2020).

### C.3. Data

### Key input data

Table C.4.: Overview of key input data sources

Country	Parameter	Input data	Source
EU28 <sup>a</sup>	Demand and	Sector- and fuel-specific energy	(ENTSO-E and
	capacity	demand, nuclear capacity tra-	ENTSOG, 2024)
		jectories, minimum RES targets,	
		cross-border net transfer capaci-	
		ties (NTCs)	
	Time series	RES profiles (wind, solar) for the	(ENTSO-E,
		weather year 2015	2022b)
Germany	Demand	Sector- and fuel-specific energy	(dena, 2021)
		demand	
	Capacity	Coal phase-out	(BMJ, 2022)
	Capacity	District heating supply share	(dena, 2021)
	Capacity	Heat pump capacity goal for	(BMWK, 2022b)
		2030	
	Capacity	Targeted number of EVs for 2030	(BMWK, 2022a)

 $<sup>^{\</sup>mathrm{a}}$  The modeled region includes EU28 excluding Cyprus and Malta and including Great Britain and Norway.

### Heating shares for individual heating

Table C.5.: Heating shares for decentralized heating in Germany in 2030

Gas	Oil	Biomass	Hydrogen	Electricity
53%	18%	7%	0%	22%

Note that each value reflects the share of heat that is covered by a certain fuel type. The assumptions follow dena (2021).

### Commodity and CO<sub>2</sub> prices

Table C.6.: Commodity prices and EU Carbon Permits in 2030

Oil	Coal	Lignite	Gas	$\mathbf{CO}_2$
[EUR/MWh]	[EUR/MWh]	[EUR/MWh]	$[\mathrm{EUR}/\mathrm{MWh}]$	$[\mathrm{EUR/t}]$
46.8	8.6	5.5	21.5	88

Note that prices for oil, coal and gas are based on the "Stated Policies" scenario in IEA (2023c), while the lignite price follows ENTSO-E and ENTSOG (2024). The assumed price of emission allowances refers to the ICIS Modeling group, with its results visualized in Pahle et al. (2022).

### Installed capacities

Table C.7.: Installed capacities in Germany per generation group and corresponding efficiencies

Technology group	Capacity in GW	Efficiency in %
Waste CHP	1.3	17
Lignite	8.7	-
- Lignite no CHP	8.0	32-35
- Lignite CHP	0.7	37-41
Coal	8.0	-
- Coal no CHP	6.0	37-46
- Coal CHP	2.0	39-45
Gas	40.2	=
- Gas OCGT	5.6	28-40
- Gas CCGT	5.0	40-60
- Gas CHP	19.6	42-56
- H2-ready OCGT	6.7	40
- H2-ready CHP	3.3	56
Wind Offshore	30.0	100
Wind Onshore	115.0	100
Photovoltaic	215.0	100
Biomass	8.0	=
- Biomass no CHP	3.5	39
- Biomass CHP	4.5	31-49
Hydropower	5.3	100
DSM (Industry)	1.8	100
Battery	13.1	90
PHS	9.9	76
Electrolysis	10.0	68

The capacities of lignite and coal are determined based on the coal phase-out trajectory outlined in BMJ (2022). Targets for Wind Onshore, Wind Offshore, and PV capacities align with the objectives defined in the Easter Package (Bundesrat, 2022). Initial capacities for gas-fired power plants are sourced from the list of power stations as of April 15th, 2024, as published by the BNetzA (BNetzA, 2024). Subsequently, an additional 10 GW of H2-ready power plants are assumed by 2030, as per the guidelines outlined in The Federal Government (2024). We assume that one third of these capacities is built as CHP.

### Electricity demand

Table C.8.: Electricity demand in TWh

KSG sector	subsector	2030
Energy	PtX*	19.8
	District heating*	12.8
	Others	4.6
Transport	Road transport*	51.6
	Non-road transport (domestic)	19.6
Buildings	Heating, cooling, cooking*	54.2
	Lightning, el. appliances	202.7
Industry	Processes	263.1
Total net demand	-	629.3

Note that endogenously determined electricity demand is labeled with \*. The respective demand is depicted based on the reference use case (M0/H0).

### Heating shares for central heating (district heat)

Table C.9.: Heating shares for central heating (district heat)

Technology/Fuel	2030
Biosolid	6.9%
Biogas	1.6%
Waste	13.9%
Industrial heat	6.8%
Solar thermal	1.6%
Geothermal heat	2.4%
Hydrogen	1.0%
Gas	49.7%
Heat pump	4.2%
Coal	8.3%
Lignite	3.5%
Total	100.0%

Note that each value reflects the share of heat that is covered by a certain fuel type. The assumptions follow dena (2021) but are slightly adjusted to account for current developments.

### C.4. Additional results

### Welfare redistribution

	_						>1
	Waste CHP	-0.00	-0.02	-0.00	-0.00	-0.02	
	Biomass	-0.00	-0.02	-0.00	-0.01	-0.02	
	Biomass CHP	-0.00	-0.01	-0.00	-0.00	-0.01	
	Coal CHP	-0.00	-0.00	-0.00	-0.00	-0.00	- 12
	Gas OCGT	-0.00	-0.00	-0.00	-0.00	-0.00	
	H2-ready OCGT	-0.00	-0.00	-0.00	-0.00	-0.00	
	Lignite	-0.00	-0.00	-0.00	-0.00	-0.00	- 11
	DSM Ind. reduce	-0.00	-0.00	0.00	-0.00	-0.00	
Ser	Coal	-0.00	-0.00	-0.00	-0.00	-0.00	
Producer	Gas CHP	-0.02	-0.12	-0.01	-0.03	-0.12	- 11
ē	H2-ready CHP	-0.01	-0.04	-0.00	-0.01	-0.04	
ц	Gas CCGT	-0.01	-0.05	-0.00	-0.01	-0.05	
	Hydro	-0.00	-0.02	-0.00	-0.00	-0.02	- 10
	Battery discharge	-0.04	-0.16	-0.00	-0.05	-0.16	1
	PHS discharge	-0.03	-0.14	-0.01	-0.04	-0.15	
	Wind Offshore	-0.02	-0.07	-0.00	-0.02	-0.07	
	Power Import	-0.11	-0.60	-0.02	-0.14	-0.63	- 10
	PV	0.04	0.34	0.01	0.05	0.36	
	Wind Onshore	-0.04	-0.07	-0.00	-0.03	-0.06	
	DSM Ind. increase	0.00	0.00	-0.00	-0.00	0.00	- 95
	Electrolysis	-0.01	-0.03	0.00	-0.01	-0.03	
	HP (central)	-0.00	-0.00	-0.00	-0.00	-0.00	
_	Battery charge	0.02	0.06	0.00	0.02	0.06	- 90
Consumer	PHS charge	0.01	0.03	0.00	0.01	0.03	
sur	Non Roadtransport	0.00	0.02	0.00	0.00	0.02	
on	Power Export	-0.01	-0.07	-0.00	-0.01	-0.08	- 85
O	Road Transport	0.16	0.66	0.00	0.16	0.66	
	Buildings Heating	0.01	0.02	0.04	0.04	0.05	
	Buildings Appliances	0.05	0.12	0.01	0.06	0.12	- 80
	Industry	0.05	0.21	0.01	0.06	0.21	00
_	All Producer	-0.26	-0.97	-0.04	-0.30	-0.99	
	All Consumer	0.30	1.01	0.06	0.35	1.04	_ <
		M1/H0 (Transport)	M2/H0 (Transport)	M0/H1 (Heating)	M1/H1 (Interaction)	M2/H1 (Interaction)	

Figure C.2.: Changes in total producer and consumer surplus under different use cases, measured in billion  ${\rm EUR}$ 

Note: The columns represent the absolute changes in the total producer and consumer surplus across different technology and end-user groups for the defined flexibility use cases, compared to the reference use case (M0/H0). The estimated deviations in relative terms are visualized via heatmap.

<90%

M2/H1

#### >110% -8.00 Res1 ASHP 195.51 -0.16 1.04 -8.27 -5.61 108% 4.36 -8.81 Res2 ASHP 356.59 0.09 -8.14 -3.05 106% -0.81 Res3 ASHP 74.02 0.08 1.22 -0.63 0.55 104% Com1 ASHP 60.09 0.30 1.76 -4.76 -4.27 -2.17 - 102% Com2 ASHP 143.95 0.97 6.67 -6.17 -4.86 1.12 - 100% Res1 GSHP 40.09 -0.05 0.14 -1.42 -1.39 -1.01 98% Res2 GSHP 71.61 -0.04 0.61 -1.48 -1.40 -0.63 96% Res3 GSHP 15.17 0.00 0.18 -0.14 -0.12 0.07 94% Com1 GSHP 12.39 0.04 0.29 -0.89 -0.81 -0.44 92%

1.15

M2/H0

(Transport)

### Changes in total electricity costs

Com2 GSHP

M0/H0

M1/H0

(Transport)

Figure C.3.: Changes in total electricity costs across building types under different flexibility use cases, in million EUR

-1.17

M0/H1

(Heating)

M1/H1

(Interaction)

Note: The first column represents the total electricity costs for heat pump operation. The subsequent columns represent the absolute changes in total electricity costs across different building types for the defined flexibility use cases, compared to the reference use case (M0/H0). The estimated deviations in relative terms are visualized via heatmap.



Figure C.4.: Changes in total electricity costs for different mobility clusters under different flexibility use cases, in million EUR

Note: The first column represents the total electricity costs for EV charging. The subsequent columns represent the absolute changes in total electricity costs across different mobility clusters for the defined flexibility use cases, compared to the reference use case (M0/H0). The deviations in relative terms are visualized via heatmap.

### Flexibility decisions in the decentralized heating sector

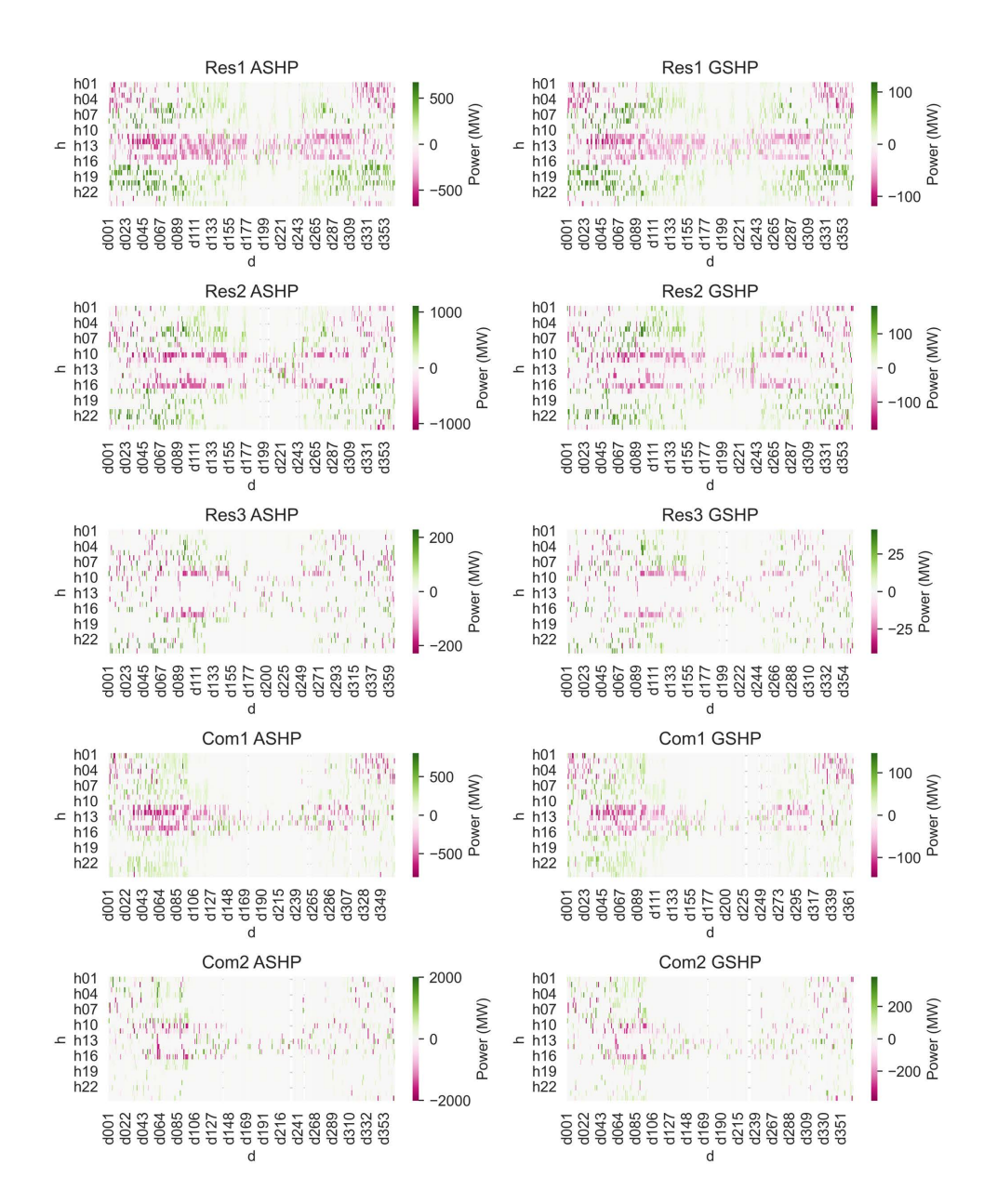


Figure C.5.: Flexibility decisions across different building types for the use case  $\rm M0/H1$  compared to  $\rm M0/H0$ 

### Flexibility decisions in the road transport sector

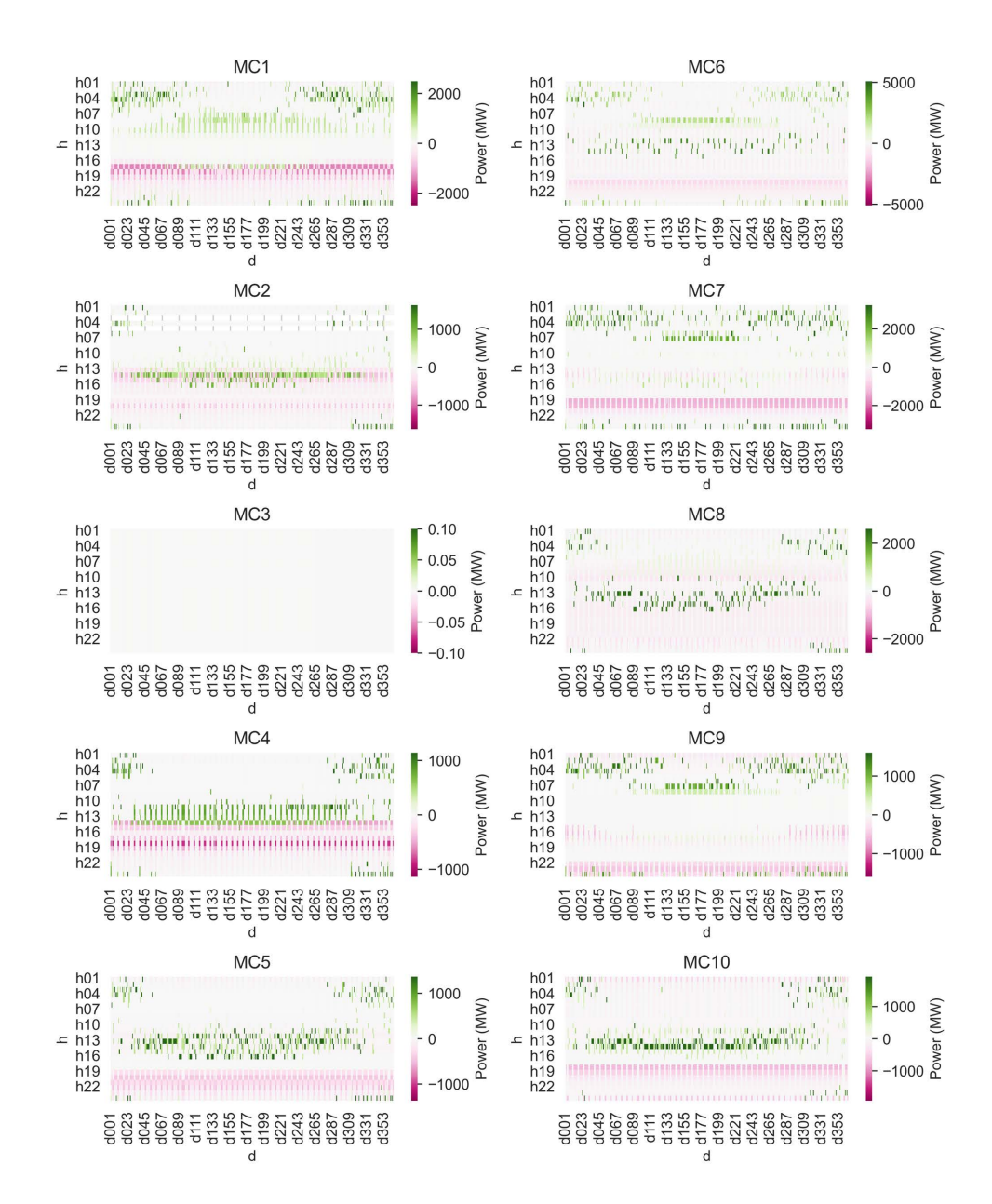


Figure C.6.: Flexibility decisions across different mobility clusters for the use case M1/H0 compared to M0/H0

### C. Supplementary material for chapter 4

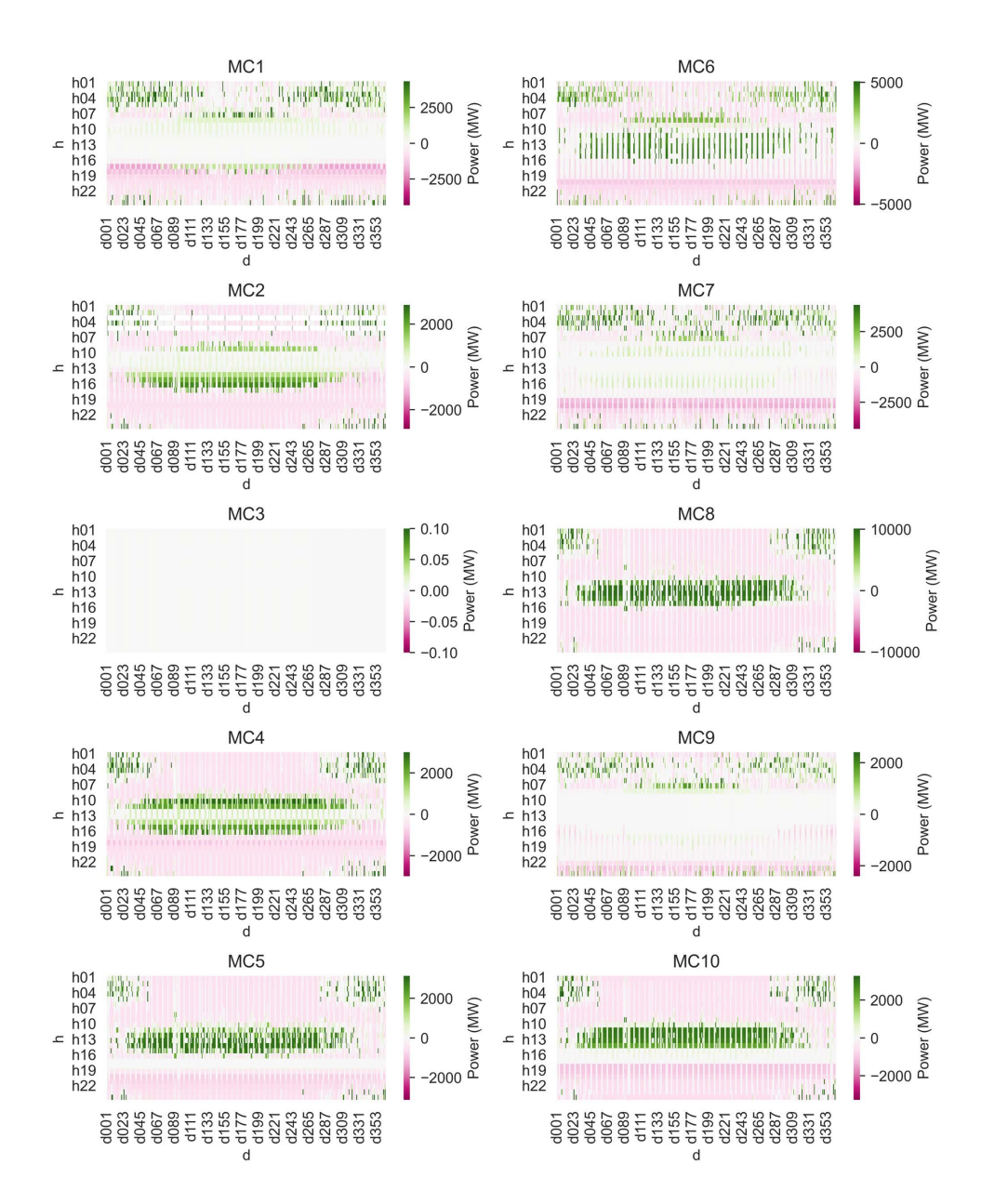


Figure C.7.: Flexibility decisions in the road transport sector for the use case  $\rm M2/H0$  compared to  $\rm M0/H0$ 

### Residual load duration curve

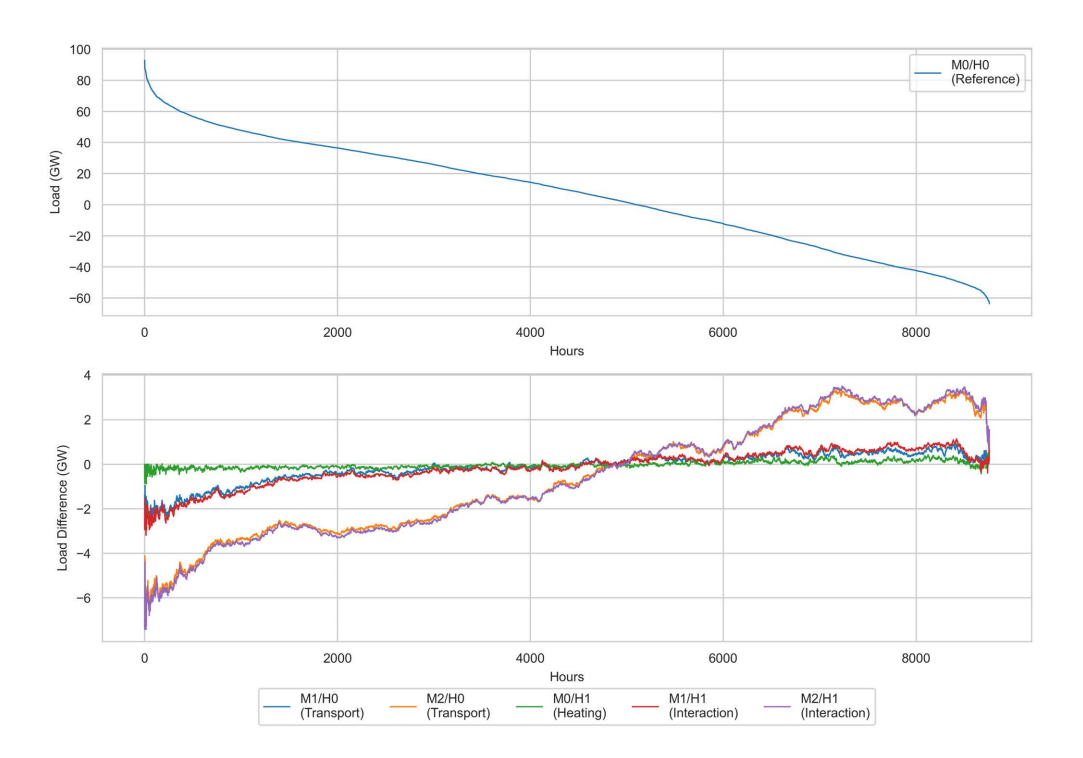


Figure C.8.: Residual load duration curve in the reference use case M0/H0 (above) and its deviations in flexibility use cases (below)

Note that we define the residual load by subtracting the renewable electricity generation from the inflexible as well as flexible demand within the heating and transport sectors. We calculate the deviations by subtracting the load duration curve values of the reference use case (M0/H0) from those of the other use cases.

# D. Supplementary material for chapter 5

# D.1. Sets, parameters and decision variables

Table D.1.: Sets

Set	$\mathbf{Unit}$	Description		
$a \in A$	=	All technologies		
$a \in A^{H_2Stor}$	-	Hydrogen storage		
$b, b_1 \in B$	-	Country		
$d \in D$	-	Day		
$f \in F$	-	Fuel		
$h \in H$	-	Hour		
$r \in R$	-	Hydrogen exporting region outside		
		Europe		
$s \in S$	-	Sector		

Table D.2.: Parameters

Parameter	Unit	Description
	Cint	Round-trip efficiency of storage tech-
$\eta(a)$	-	- •
		a.
instcap(a,b)	MW	Installed capacity of technology $a$ in country $b$ .
inject(a)	-	Quotient of injection speed to with-
, ,		drawal speed for storage technology $a$ .
ptxPotPipe(b, f)	$MWh_{th}$	Import potential of fuel $f$ via pipeline
$F \longrightarrow F \longrightarrow (V, J)$	/ / * * * * * * * * * * * * * * * *	to country $b$ .
ptxPotShip(r, f)	$MWh_{th}$	Import potential of fuel f from export-
$p(x_1   o(Snip(i,j))$	IVI VV Itth	
1/1 ()	7.4117.1	ing region $r$ .
ptxTerminal(b, f)	$MWh_{th}$	Terminal capacity for handling fuel $f$
		in country $b$ .
ptxCostsPipe(b,f)	$\mathrm{EUR}/\mathrm{MWh}_{th}$	Variable cost of importing fuel $f$ via
		pipeline to country $b$ .
ptxCostsShip(r, f)	$\mathrm{EUR}/\mathrm{MWh}_{th}$	Variable cost of importing fuel $f$ via
1 ( ) ( )	,	ship from region $r$ .
$tradeCap(b_1, b, f)$	$MWh_{th}/\mathrm{day}$	Net transfer capacity (NTC) for trade
$v_i = u_i $	111 // //// (101)	of fuel $f$ between countries $b_1$ and $b$ .
vol(a)	h	Volume factor (storage capacity per
001(a)	11	,
		unit of installed power) for storage
		technology $a$ .

Table D.3.: Decision variables

Variable	Unit	Description
$COSTS^{Pipe}$		
	EUR	Annual costs for fuel imports via pipeline from outside the EU.
$COSTS^{Ship}$	EUR	Annual costs for fuel imports via ship from outside the EU.
USE(b,d,s,f)	$MWh_{th}$	Fuel $f$ consumption in sector $s$ of country $b$ on day $d$ .
INSTOR(d,b,a,f)	$MWh_{th}$	Fuel $f$ stored in facility $a$ in country $b$ on day $d$ .
$INSTOR^{Pipe}(d,b,f)$	$MWh_{th}$	Pipeline-imported fuel $f$ stored in country $b$ on day $d$ .
$INSTOR^{Prod}(d, h, a, b, f)$	$MWh_{th}$	Domestically produced fuel $f$ via technology $a$ stored in country $b$ on day $d$ and hour $h$ .
$INSTOR^{Ship}(d,r,b,f)$	$MWh_{th}$	Ship-imported fuel $f$ from region $r$ stored in country $b$ on day $d$ .
$INSTOR^{Trade}(d, b_1, b, f)$	$MWh_{th}$	Imported fuel $f$ from neighboring country $b_1$ stored in country $b$ on day $d$ .
LEVEL(d, a, b, f)	$MWh_{th}$	Storage level of fuel $f$ using technology $a$ in country $b$ on day $d$ .
PIPE(b,f)	$MWh_{th}$	Pipeline imports of fuel $f$ into country $b$ .
SHIP(r,b,f)	$MWh_{th}$	Ship imports of fuel $f$ from region $r$ to country $b$ .
$TRADE(d, b_1, b, f)$	$MWh_{th}$	Export of fuel $f$ from country $b_1$ to country $b$ on day $d$ .
$TRADE(d, b, b_1, f)$	$MWh_{th}$	Export of fuel $f$ from country $b$ to country $b_1$ on day $d$ .
PROD(d, h, a, b, f)	$MWh_{th}$	Domestic production of fuel $f$ in country $b$ on day $d$ , hour $h$ , using technology $a$ .

# D.2. $H_2$ supply curve

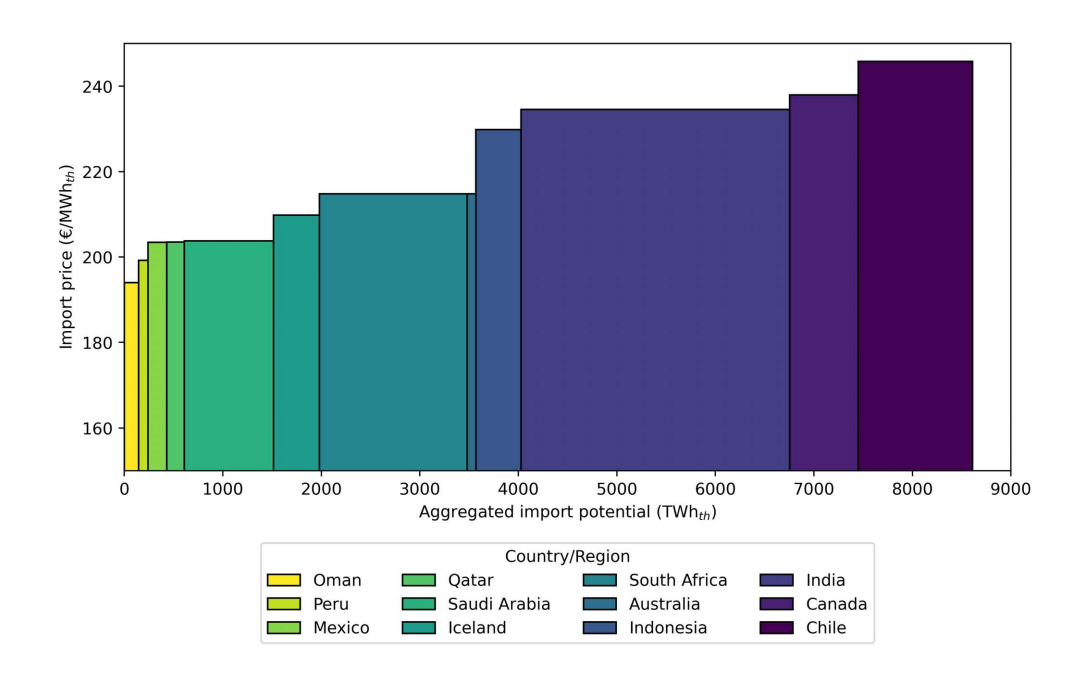


Figure D.1.: Supply curve for  $H_2$  imports via ship

The hydrogen import price reflects the price for a long-term contract with baseload supply throughout the year. The price also reflects the levelized costs of hydrogen (LCOH) of the exporting region, covering both operational and capital expenditures.

# D.3. Trade capacities

Table D.4.: Trade capacities for hydrogen and electricity

		$Hydrogen [MW_{th}]$				Electricit	$y [MW_{el}]$
Countries		Scenarios	Scenarios $Ref$ and $LD$   Scenarios $HI$ and $HI/LD$		All scenarios		
a	b	from a	from b	from a	from b	from a	from b
		to b	to a	to b	to a	to b	to a
AT	CH	0	0	0	0	1,200	1,200
AT	$\mathbf{CZ}$	0	0	0	0	900	900
AT	$\mathbf{DE}$	6,250	6,250	6,250	6,250	7,500	7,500
AT	$\mathbf{H}\mathbf{U}$	6,250	0	6,250	0	800	800
AT	IT	5,250	7,000	9,125	7,000	1,375	1,995
AT	$\mathbf{SI}$	0	0	1,375	667	1,450	1,450
$\mathbf{BE}$	$\mathbf{DE}$	3,790	3,790	4,998	4,998	1,000	1,000
$\mathbf{BE}$	$\mathbf{FR}$	4,500	4,500	8,333	8,333	5,800	7,300
$\mathbf{BE}$	GB	0	0	8,333	8,333	2,400*	2,400*
$\mathbf{BE}$	$\mathbf{L}\mathbf{U}$	580	580	1,413	1,413	1,100	1,000
$\mathbf{BE}$	$\mathbf{NL}$	2,000	2,000	10,000	10,000	4,400	4,400
$\mathbf{BE}$	NO	0	8,333	8,333	8,333	0	0
$\mathbf{BG}$	$\mathbf{G}\mathbf{R}$	3,330	3,150	3,665	3,671	2,200	1,900
BG	$\mathbf{RO}$	740	740	5,811	5,811	2,550*	2,550*
$\mathbf{CH}$	$\mathbf{DE}$	0	0	10,000	10,000	4,500*	5,000

Continued on next page

	Hydrogen $[MW_{th}]$					Electricit	$y [MW_{el}]$
Cour	ntries	Scenarios Ref and LD   Scenarios HI and HI/LD			enarios		
a	b	from a	from b	from a	from b	from a	from b
	~	to b	to a	to b	to a	to b	to a
CH	FR	0	0	4,167	4,167	3,200	5,500
CH	IT	5,630	3,670	5,630	3,670	5,800*	3,110*
CZ	DE	6,000	6,000	13,300	13,300	3,000*	3,000*
CZ	$_{ m PL}$	0,000	0,000	1,250	1,250	1,600	1,000
CZ	SK	0	6,000	6,500	6,500	2,300	2,160*
DE	DK1	2,100	2,100	10,000	10,000	3,500	3,500
DE	DK1	0	0	0	0	600	600
DE	FR	8,000	8,500	10,125	10,125	4,800	4,800
DE	GB	0,000	0,900	0	0	2,800	2,800
DE	LU	0	0	0	0	3,700*	3,700*
DE	NL	500	15,630	23,300	23,296	6,000	6,000
DE	NO	17,250	,	17,250	,	1,444*	1,444*
DE	PL	4,170	17,250 $8,330$	9,467	17,250 $9,461$	3,000*	3,000
DE	SE	0	8,550 0	9,467	9,461	1,500*	3,000 1,491
DE DK1	DK2	0	0	0	0	600	600
DK1 DK1	GB	0	0	0	0	1,400	1,400
DK1 DK1	NL	0	0	0	0	700	700
DK1	NO	0	0	0	0	1,632	1,632
DK1	SE	0	0	0	0	1,032 $1,415$	1,032 $1,415$
DK1 DK2	$_{ m PL}$	0	0	0	0	1,415 500	1,415 500*
DK2 DK2	SE	0	0	0	0		
EE	FI	4,170	8,330	8,337	8,330	2,200	1,800
EE	LV	· ·		· '	*	1,176	1,176
ES	$\mathbf{FR}$	8,330 9,000	4,170 $9,000$	8,330 9,000	5,285 $9,000$	1,444* 8,000	1,259* 8,000
ES	PT	3,380	3,380	3,380	3,380	6,200	5,500
FI	NO	0	0	0	0	150*	5,500 150*
FI	SE	27,750	27,750	37,917	37,917	4,500	4,500
FR	GB	0	0	0	0	6,800*	6,800*
FR	IE	0	0	0	0	700	700
FR	IT	0	0	0	0	4,485	2,160
FR	LU	0	0	0	0	380*	2,100
GB	IE	0	0	1,189	1,189	1,750	1,750
GB	NL	0	0	0	0	2,800*	2,800*
GB	NO	0	0	0	0	1,444*	1,444*
GR	IT	0	0	0	0	1,500*	1,500*
HR	HU	0	0	5,350	5,350	1,700*	1,700*
HR	SI	0	0	667	1,375	3,200	3,200
HU	RO	3,200	3,200	6,400	6,400	3,027	2,300*
HU	SI	0	0	817	817		
HU	SK	4,170				1,700	1,700
IT	SK SI	4,170	$_{0}^{4,170}$	8,337 817	8,337 817	1,900* 1,080	3,360* 1,153
LT	LV	4,170	8,330	7,903	8,330	1,080 1,300*	1,153 1,300*
LT	$\frac{\mathbf{L}\mathbf{v}}{\mathbf{PL}}$	· ·			*	· · · · · · · · · · · · · · · · · · ·	*
ı		8,330	4,170	8,330	7,150	700	700
LT NL	SE NO	0	0	0	0	1,300	1,300
NO NO	SE	0	0	0	0	723*	723*
_		_	-		-	3,695	3,995
PL	SE	0	0	0	0	600	600
PL	$\mathbf{S}\mathbf{K}$	0	0	0	0	894*	1,110

Hydrogen capacities in Scenario A are based on the reference grid from ENTSO-E and ENTSOG (2024). Scenario B assumes full utilization of all investment candidates. Electricity NTC values are derived from the ENTSO-E and ENTSOG (2024) "Global Ambition" scenario for the weather year 2009. Adjustments marked with \* indicate that if the value was smaller than the corresponding value from the ERAA 2024 (ENTSO-E, 2024) for 2035, the higher value was used.

### D.4. Installed capacities

Table D.5.: Installed electrical capacities in Germany per generation group in  $GW_{el}$  and corresponding efficiencies for the different system configuration scenarios

Technology group	Efficiency	Ref	HI	LD	HI/LD
Gas	-	-	-	-	-
- Gas OCGT	28-40	$\operatorname{Inf}$	$\operatorname{Inf}$	$\operatorname{Inf}$	$\operatorname{Inf}$
- Gas CCGT	40-60	16.5	15.9	14.6	11.4
- Gas CHP	42-56	2.7	2.9	2.7	2.9
- H <sub>2</sub> OCGT	40	$\operatorname{Inf}$	$\operatorname{Inf}$	$\operatorname{Inf}$	$\operatorname{Inf}$
- $H_2$ CCGT	60	12.7	15.0	13.5	10.8
- H <sub>2</sub> CHP	56	10.7	10.7	10.7	10.7
Wind Offshore	100	70.0	70.0	70.0	70.0
Wind Onshore	100	160.0	160.0	160.0	160.0
Photovoltaic	100	400.0	400.0	400.0	400.0
Biomass	-	-	-	-	-
- Biomass no CHP	39	0.0	0.0	0.0	0.0
- Biomass CHP	31-49	8.0	8.0	8.0	8.0
Hydropower	100	5.3	5.3	5.3	5.3
DSM (Industry)	100	5.4	5.4	5.4	5.4
Battery	90	36.0	36.0	36.0	36.0
PHS	76	8.5	8.5	8.5	8.5
Electrolysis	72-77	76.5	74.4	76.5	76.5

Targets for Wind Onshore, Wind Offshore, and PV capacities align with the objectives defined in the Easter Package (Bundesrat, 2022). For battery storage, a ratio between power and capacity of 1:2 is assumed based on ENTSO-E and ENTSOG (2024). OCGT power plants for  $\rm H_2$  and Gas have sufficient capacities to keep the model feasible.

Table D.6.: Installed hydrogen storage capacities in Germany in  $TWh_{th}$  and corresponding efficiencies for the different system configuration scenarios

Technology group	Efficiency	$\mathbf{Ref}$	HI	${f LD}$	${ m HI/LD}$
Cavern conversion	93	29.7	29.7	29.7	24.8
Cavern new	93	11.6	5.9	27.0	6.6
Pore conversion	93	0.0	0.0	0.0	0.0
Pore new	93	0.0	0.0	0.0	0.0

For hydrogen, the country-specific storage capacities align with the local potentials derived from Caglayan et al. (2021).

# D.5. Electricity and hydrogen demand

Table D.7.: Electricity and hydrogen demand in TWh for different sectors and system configuration scenarios

	R	ef	H	ΙΙ	L	D	HI	$^{\prime}\mathrm{LD}$
Sector	$\mathbf{H}_2$	El.	$\mathbf{H}_2$	El.	$\mathbf{H}_2$	El.	$\mathbf{H}_2$	El.
Energy								
Electricity*	67.8	43.3	67.8	42.7	67.8	43.7	67.9	43.3
PtX*	38.7	331.0	33.3	331.1	54.7	330.0	32.6	331.5
District heating*	0.0	26.1	0.0	26.1	0.0	26.1	0.0	26.1
Others	0.0	31.1	0.0	31.1	0.0	31.1	0.0	31.1
Transport								
Road transport	90.0	104.2	90.0	104.2	90.0	104.2	90.0	104.2
Non-road transport (dom.)	4.4	17.0	4.4	17.0	4.4	17.0	4.4	17.0
Non-road transport (inter.)	4.4	0.0	4.4	0.0	4.4	0.0	4.4	0.0
Buildings								
Heating, cooling, cooking	78.6	109.9	78.6	109.9	78.6	109.9	78.6	109.9
Lightning, el. appliances	0.0	176.7	0.0	176.7	0.0	176.7	0.0	176.7
Industry								
Processes	279.2	256.0	279.2	256.0	195.4	256.0	195.4	256.0
Non-energy	127.6	0.0	127.6	0.0	127.6	0.0	127.6	0.0
Agriculture	18.9	5.5	18.9	5.5	18.9	5.5	18.9	5.5
Total	710	1133	704	1133	641	1133	620	1134

Note that endogenously determined demand is labeled with \*.

# D.6. Hydrogen balances

Table D.8.:  $H_2$  origin and export balance in  $TWh_{th}$ 

	Ref	HI	LD	$_{ m HI/LD}$
Supply				
Domestic production and storage supply	281.9	274.6	296.0	276.6
Import from EU	408.0	781.9	426.1	814.8
Import via ship*	241.3	87.6	151.3	69.7
Demand				
Export to EU	221.6	439.9	231.5	541.2
Storage loading	38.7	33.3	54.7	32.6
Sectoral demand	670.9	670.9	587.2	587.3

<sup>\*</sup> The import via ship is determined with the invest decision and fixed in the dispatch run.

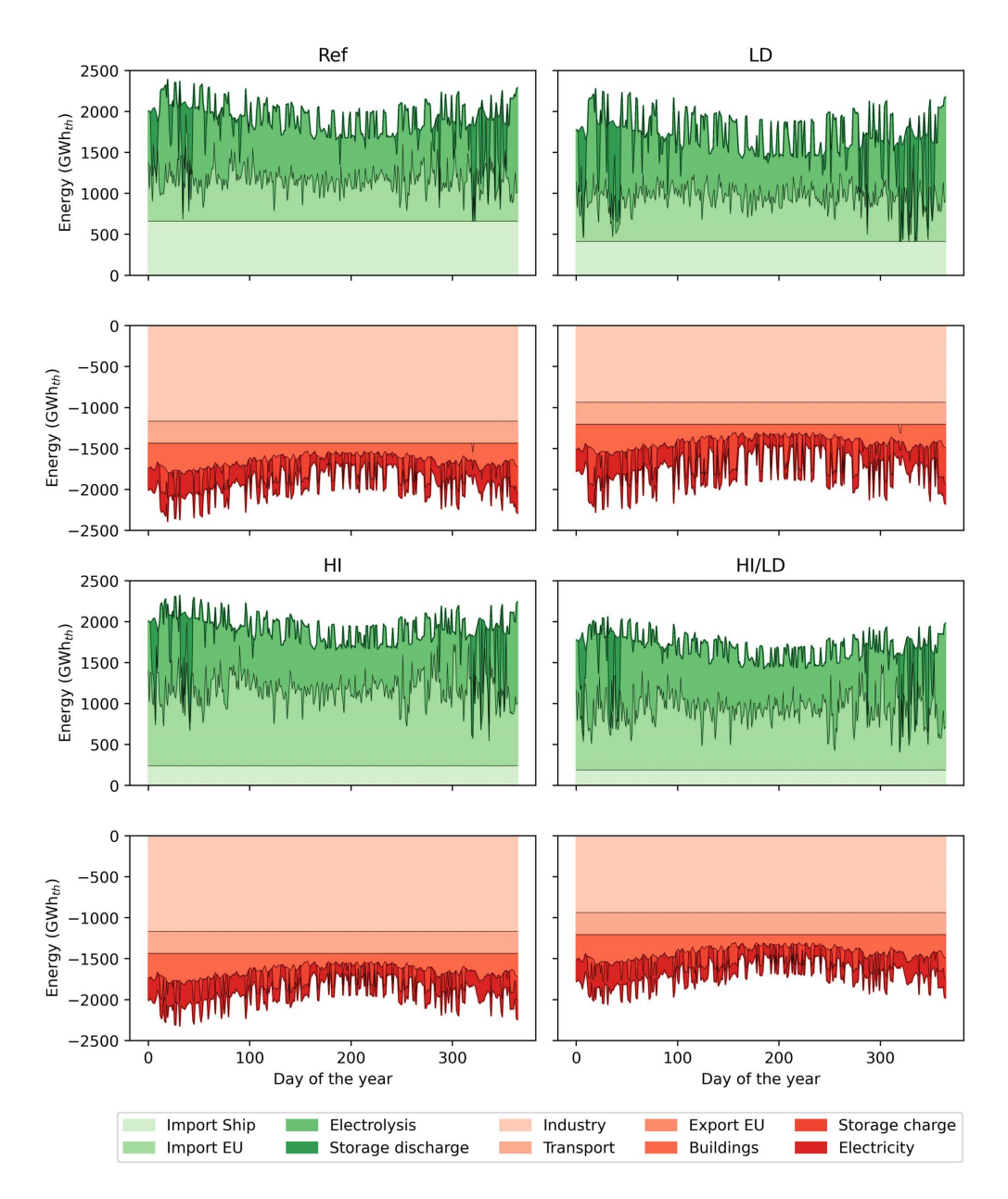


Figure D.2.: Daily  $\mathrm{H}_2$  balance for the different system sensitivities

# D.7. Storage level

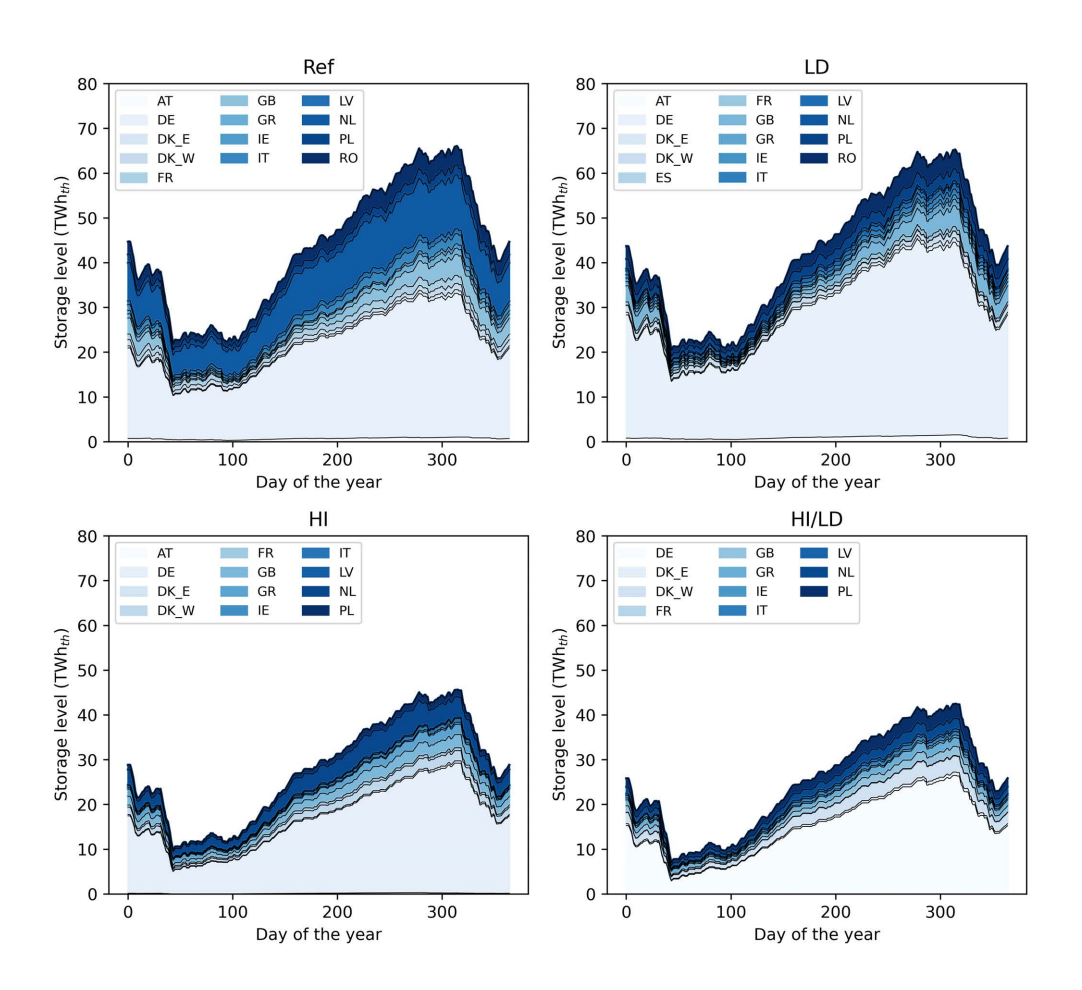


Figure D.3.:  $H_2$  storage level in Europe in each sensitivity

## D.8. H<sub>2</sub> balance and residual load in each subset for the reference scenario

The full dataset includes price data for hydrogen and electricity, along with the corresponding demand and supply values across different technologies, sectors, and assets. It is divided into four subsets, each capturing distinct market conditions characterized by variations in electrical and hydrogen residual load. These subsets are visualized in Figure D.4.

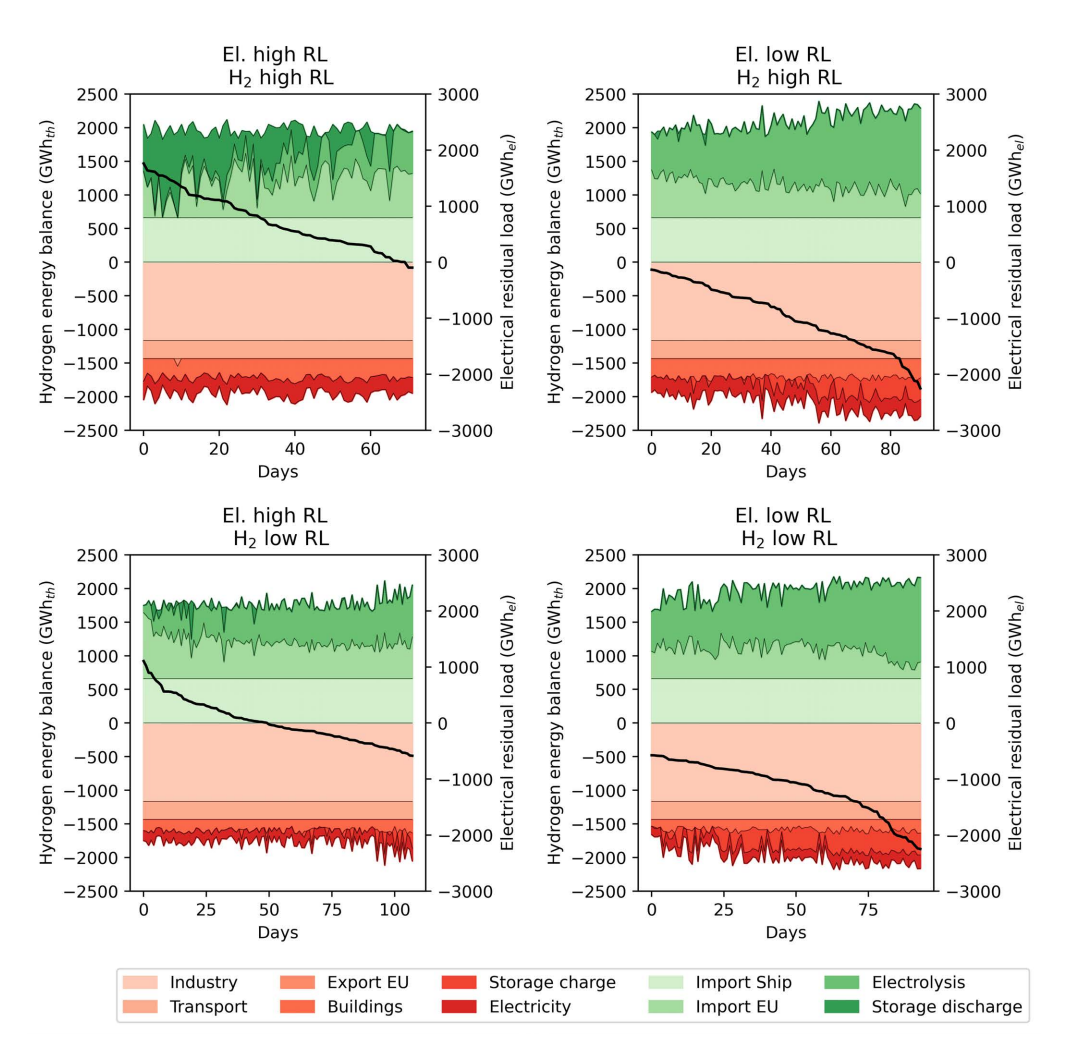


Figure D.4.: Daily  $H_2$  balance in each subset with the corresponding residual load in sorted order

The electrical residual load is represented on the secondary y-axis and is displayed in descending order. The  $H_2$  supply and demand mix is visualized for the corresponding days, aligned with the sorted order of the residual load values.

### D.9. Check for co-integration

The separation of price data according to different market situations raises the question of whether hydrogen and electricity prices may be co-integrated within individual subsets. For co-integration analysis to be applicable, it is first necessary to confirm that the price series are non-stationary. The stationarity of electricity and hydrogen price time series was assessed using the ADF test. Table D.9 presents the results, which demonstrate that none of the subsets exhibit non-stationarity in both series. This conclusion is supported by p-values well below the 0.05 significance threshold, indicating that the series are stationary. A stationary time series is characterized by statistical properties, such as mean and variance, that remain constant over time, implying the absence of long-term trends or unit roots. In technical terms, stationary series are integrated of order zero (I(0)). Co-integration analysis is typically used for non-stationary time series (I(1)) that share a linear relationship, resulting in residuals that are stationary. Since all series in each subset are stationary, co-integration analysis cannot be applied. The stationary nature of these time series implies that their dynamics can be effectively analyzed using conventional statistical methods, such as regression analysis and correlation metrics, without accounting for long-term equilibrium relationships. Furthermore, the absence of non-stationarity suggests that the relationship between hydrogen and electricity prices is predominantly shaped by short-term interactions rather than shared long-term trends. This provides a foundation for focusing on dynamic interactions within specific market conditions, enabling a more nuanced understanding of their dependencies.

Table D.9.: Results of the ADF-test for stationarity

Scenario		El. hi	$_{ m gh}$ $_{ m RL}$	El. hi	gh RL	El. lo	$\sim RL$	El. lo	m w~RL
		$\mathbf{H}_2$ high $\mathbf{R}\mathbf{L}$		$H_2$ low RL		$\mathbf{H}_2$ high RL		$\mathbf{H}_2$ low RL	
		$H_2$	$\operatorname{EL}$	$H_2$	EL	$H_2$	$\operatorname{EL}$	$H_2$	EL
Ref	ADF statistic	-6.819	-6.846	-7.996	-6.315	-6.300	-8.298	-9.267	-9.230
	p-value	0.000	0.002	0.000	0.000	0.000	0.000	0.000	0.000
	stationary	Yes	Yes	Yes	Yes	Yes	Yes	Yes	Yes
HI	ADF statistic	-4.907	-6.908	-8.453	-5.260	-7.816	-8.460	-7.841	-8.996
	p-value	0.000	0.004	0.000	0.000	0.001	0.000	0.000	0.000
	stationary	Yes	Yes	Yes	Yes	Yes	Yes	Yes	Yes
LD	ADF statistic	-6.819	-6.892	-8.355	-6.234	-8.016	-8.293	-9.181	-5.237
	p-value	0.000	0.002	0.000	0.000	0.000	0.000	0.000	0.000
	stationary	Yes	Yes	Yes	Yes	Yes	Yes	Yes	Yes
HI/LD	ADF statistic	-6.819	-6.892	-8.355	-6.234	-8.016	-8.293	-9.181	-5.237
	p-value	0.000	0.002	0.000	0.000	0.000	0.000	0.000	0.000
	stationary	Yes	Yes	Yes	Yes	Yes	Yes	Yes	Yes

The significance level for stationarity is p-value>0.05.

# D.10. Hydrogen and electricity price duration curves

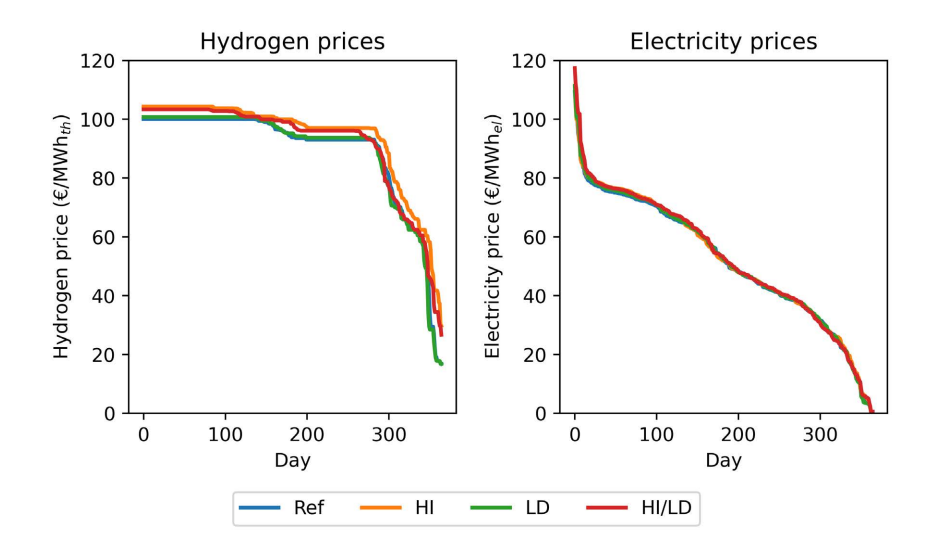


Figure D.5.: Price duration curves for hydrogen and electricity

The price data are shown for Germany. Hourly electricity prices are weighted by the corresponding demand to calculate daily prices. Both electricity and hydrogen prices represent the shadow prices of their respective equilibrium constraints.

# **Bibliography**

- Agora and FfE (2023). Agora Energiewende und Forschungsstelle für Energiewirtschaft e. V. Haushaltsnahe Flexibilitäten nutzen. Wie Elektrofahrzeuge, Wärmepumpen und Co. die Stromkosten für alle senken können. https://www.agora-energiewende.de/fileadmin/Projekte/2023/2023-14\_DE\_Flex\_heben/A-EW\_315\_Flex\_heben\_WEB.pdf.
- Agora Verkehrswende, Agora Energiewende, and Regulatory Assistance Project (RAP) (2019). Verteilnetzausbau für die Energiewende Elektromobilität im Fokus. https://static.agora-energiewende.de/fileadmin/Projekte/20 18/Netzausbau\_Elektromobilitaet/AgoraRAP2019\_VerteilnetzausbauElektromobilitaet.pdf.
- Amann, G., Bermúdez, V., Kovacs, E. B., Gallego, S., Giannelos, S., Iliceto, A., et al. (2022). E-Mobility Deployment and Impact on Grids: Impact of EV and Charging Infrastructure on European T&D Grids Innovation Needs. https://smart-networks-energy-transition.ec.europa.eu/system/files/2022-12/ETIP%20SNET%20E-Mobility%20White%20Paper\_pdf.pdf.
- Antweiler, W. and Muesgens, F. (2025). The new merit order: The viability of energy-only electricity markets with only intermittent renewable energy sources and grid-scale storage. *Energy Economics*, 145:108439.
- Arnold, F., Lilienkamp, A., and Namockel, N. (2024). Diffusion of electric vehicles and their flexibility potential for smoothing residual demand A spatiotemporal analysis for Germany. *Energy*, 308:132619.
- Ayyadi, S. and Maaroufi, M. (2018). Diffusion models for predicting electric vehicles market in morocco. In 2018 International Conference and Exposition on Electrical And Power Engineering (EPE), pages 0046–0051.
- Bass, F. M. (1969). A New Product Growth for Model Consumer Durables. Management Science, 15:215–227.
- BBSR (2022). Laufende Raumbeobachtung Raumabgrenzungen: Siedlungsstrukturelle Gebietstypen. https://www.bbsr.bund.de/BBSR/DE/forsc hung/raumbeobachtung/Raumabgrenzungen/deutschland/kreisgebietsre formen/SiedlungsstrukturelleGebietstypen\_alt/gebietstypen.html.
- Becker, T. A., Sidhu, I., and Tenderich, B. (2009). Electric vehicles in the US a new model with forecasts to 2030. Center for Entrepreneuship and technology, University of California, Berkeley, 2009.1.v.2.0.

- Bellocchi, S., Colbertaldo, P., Manno, M., and Nastasi, B. (2023). Assessing the effectiveness of hydrogen pathways: A techno-economic optimisation within an integrated energy system. *Energy*, 263:126017.
- Berger, R. (1981). Comparison of the Gompertz and Logistic Equations to Describe Plant Disease Progress. *Phytopathology*, 71(7):716-719. https://www.apsnet.org/publications/phytopathology/backissues/Documents/1981Articles/Phyto71n07\_716.PDF
- Bernath, C., Deac, G., and Sensfuß, F. (2021). Impact of sector coupling on the market value of renewable energies a model-based scenario analysis. *Applied Energy*, 281:115985.
- Birk, S., Fleer, J., Holtz, G., Jeddi, S., Lilienkamp, A., Namockel, N., Schönfisch, M., and Wagner, D. J. (2021). Geschäftsmodelle für Regionale Virtuelle Kraftwerke. https://www.ewi.uni-koeln.de/cms/wp-content/uploads/2022/04/210420\_VISE\_Endbericht\_v1.0.pdf.
- Birk Jones, C., Vining, W., Lave, M., Haines, T., Neuman, C., Bennett, J., and Scoffield, D. R. (2022). Impact of Electric Vehicle customer response to Time-of-Use rates on distribution power grids. *Energy Reports*, 8:8225–8235.
- Blaschke, M. J. (2022). Dynamic pricing of electricity: Enabling demand response in domestic households. *Energy Policy*, 164:112878.
- Bloess, A., Schill, W.-P., and Zerrahn, A. (2018). Power-to-heat for renewable energy integration: A review of technologies, modeling approaches, and flexibility potentials. *Applied Energy*, 212:1611–1626.
- BMJ (2022). Bundesministerium für Justiz Gesetz zur Reduzierung und zur Beendigung der Kohleverstromung (Kohleverstromungsbeendigungsgesetz KVBG). https://www.gesetze-im-internet.de/kvbg/BJNR181810020.html.
- BMWK (2022a). Eckpunktepapier zur Diskussion der Beschleunigung des Wärmepumpenhochlaufs Vorhaben und Maßnahmen zum 2. Wärmepumpen-Gipfel. https://www.bmwk.de/Redaktion/DE/Downloads/Energie/2-waermepumpen-gipfel-eckpunktepapier.pdf?\_\_blob=publicationFile&v=6.
- BMWK (2022b). Regulatory environment and incentives for using electric vehicles and developing a charging infrastructure. https://www.bmwk.de/Redaktion/EN/Artikel/Industry/regulatory-environment-and-incentives-for-using-electric-vehicles.html.
- BNetzA (2020). Bundesnetzagentur für Elektrizität, Gas, Telekommunikation, Post und Eisenbahnen Genehmigung des Szenariorahmens 2021-2035. https://www.netzentwicklungsplan.de/sites/default/files/paragraphs-files/Szenariorahmen\_2035\_Genehmigung\_1.pdf.

- BNetzA (2022). Markstammdatenregister. https://www.marktstammdatenregister.de/MaStR.
- BNetzA (2023). Bundesnetzagentur. Festlegungsverfahren zur Integration von steuerbaren Verbrauchseinrichtungen und steuerbaren Netzanschlüssen nach § 14a Energiewirtschaftsgesetz. https://www.bundesnetzagentur.de/DE/Beschlusskammern/BK06/BK6\_83\_Zug\_Mess/841\_SteuVE/BK6\_SteuVE\_node.html.
- BNetzA (2024). Kraftwerksliste der Bundesnetzagentur (Stand: 15. April 2024). https://www.bundesnetzagentur.de/DE/Fachthemen/ElektrizitaetundGas/Versorgungssicherheit/Erzeugungskapazitaeten/Kraftwerksliste/start.html.
- Borenstein, S. and Holland, S. P. (2005). On the efficiency of competitive electricity markets with time-invariant retail prices. *RAND Journal of Economics*, 36(3):469–493.
- Brown, T. and Reichenberg, L. (2021). Decreasing market value of variable renewables can be avoided by policy action. *Energy Economics*, 100:105354.
- Bundesrat (2022). Gesetz zu Sofortmaßnahmen für einen beschleunigten Ausbau der erneuerbaren Energien und weiteren Maßnahmen im Stromsektor. https://www.clearingstelle-eeg-kwkg.de/sites/default/files/2022-07/03 15-22.pdf.
- BWP (2023). Branchenstudie 2023: Marktentwicklung Prognose Handlungsempfehlungen. https://www.waermepumpe.de/fileadmin/user\_upload/waermepumpe/05\_Presse/01\_Pressemitteilungen/BWP\_Branchenstudie\_2023\_DRUCK.pdf.
- Böttger, D. and Härtel, P. (2022). On wholesale electricity prices and market values in a carbon-neutral energy system. *Energy Economics*, 106:105709.
- Caglayan, D. G., Heinrichs, H. U., Robinius, M., and Stolten, D. (2021). Robust design of a future 100% renewable european energy supply system with hydrogen infrastructure. *International Journal of Hydrogen Energy*, 46(57):29376–29390.
- Caglayan, D. G., Weber, N., Heinrichs, H. U., Linßen, J., Robinius, M., Kukla, P. A., and Stolten, D. (2020). Technical potential of salt caverns for hydrogen storage in Europe. *International Journal of Hydrogen Energy*, 45(11):6793–6805.
- CEER, Council of European Energy Regulators (2020). CEER Paper on DSO Procedures of Procurement of Flexibility. https://www.ceer.eu/documents/104400/-/-/f65ef568-dd7b-4f8c-d182-b04fc1656e58.

- Copernicus Climate Change Service (2020). Climate and energy indicators for Europe from 1979 to present derived from reanalysis. Copernicus Climate Change Service (C3S) Climate Data Store (CDS). 10.24381/cds.4bd77450.
- Council of European Union and European Parliament (2019). Directive (EU) 2019/944 of the European Parliament and of the Council. http:https://eur-lex.europa.eu/legal-content/EN/TXT/PDF/?uri=CELEX:32019L09 44&from=EN.
- Daneshzand, F., Coker, P. J., Potter, B., and Smith, S. T. (2023). EV smart charging: How tariff selection influences grid stress and carbon reduction. *Applied Energy*, 348:121482.
- dena (2018). dena-Leitstudie integrierte Energiewende: Impulse für die Gestaltung des Energiesystems bis 2050. Deutsche Energie-Agentur GmbH (dena), ewi Energy Research & Scenarios gGmbH: Berlin/Köln, Germany. https://www.dena.de/fileadmin/dena/Dokumente/Pdf/9262\_dena-Leitstudie\_Integrierte\_Energiewende\_Ergebnisbericht.pdf.
- dena (2021). dena-Leitstudie Aufbruch Klimaneutralität. Klimaneutralität 2045 Transformation der Verbrauchssektoren und des Energiesystems. https://www.ewi.uni-koeln.de/cms/wp-content/uploads/2022/03/211005\_EWI-G utachterbericht\_dena-Leitstudie-Aufbruch-Klimaneutralitaet.pdf.
- dena (2022). Vergleich der "Big 5"-Klimaneutralitätsszenarien. https://www.dena.de/newsroom/publikationsdetailansicht/pub/vergleich-der-big-5-klimaneutralitaetsszenarien/.
- dena and Prognos (2020). Privates Ladeinfrastrukturpotenzial in Deutschland. https://www.dena.de/fileadmin/dena/Publikationen/PDFs/2020/dena-STUDIE\_Privates\_Ladeinfrastrukturpotenzial\_in\_Deutschland.pdf.
- Deutscher Bundestag (2021). Erstes Gesetz zur Änderung des Bundes-Klimaschutzgesetzes, Bundesgesetzblatt Jahrgang 2021 Teil I Nr. 59, ausgegeben zu Bonn am 30. August 2021. https://www.bgbl.de/xaver/bgbl/start.xav?startbk=Bundesanzeiger\_BGBl&start=//\*%5B@attr\_id=%27bgbl121s3905.pdf%27%5D#\_\_bgbl\_\_%2F%2F\*%5B%40attr\_id%3D%27bgbl 121s3905.pdf%27%5D\_\_1675782713390.
- Durakovic, G., Del Granado, P. C., and Tomasgard, A. (2023). Powering Europe with North Sea offshore wind: The impact of hydrogen investments on grid infrastructure and power prices. *Energy*, 263:125654.
- Dynge, M. F., Crespo del Granado, P., Hashemipour, N., and Korpås, M. (2021). Impact of local electricity markets and peer-to-peer trading on low-voltage grid operations. *Applied Energy*, 301:117404.
- Ebner, M., Fiedler, C., Jetter, F., and Schmid, T. (2019). Regionalized Potential Assessment of Variable Renewable Energy Sources in Europe. In 2019 16th International Conference on the European Energy Market (EEM), pages 1–5.

- EEX (2025). A hydrogen market for decarbonising the economy. https://www.eex.com/en/markets/hydrogen.
- Emelianova, P. and Namockel, N. (2025). Welfare redistribution through flexibility Who pays? *Energy Policy*, 205:114684.
- Englberger, S., Abo Gamra, K., Tepe, B., Schreiber, M., Jossen, A., and Hesse, H. (2021). Electric vehicle multi-use: Optimizing multiple value streams using mobile storage systems in a vehicle-to-grid context. *Applied Energy*, 304:117862.
- ENTSO-E (2022a). Actual Generation per Production Type. https://transparency.entsoe.eu/generation/r2/actualGenerationPerProductionType/show.
- ENTSO-E (2022b). European Resource Adequacy Assessment (ERAA) 2022. https://www.entsoe.eu/outlooks/eraa/2023/eraa-downloads/.
- ENTSO-E (2022c). National estimates scenario ERAA 2021 Hourly demand time-series, Demand Forecasting Methodology. https://eepublicdownloads.azureedge.net/clean-documents/sdc-documents/ERAA/Demand%20Forecasting%20Methodology%20and%20Insights%20(ERAA%202021).pdf.
- ENTSO-E (2024). European Resource Adequacy Assessment (ERAA) 2024. https://www.entsoe.eu/outlooks/eraa/2024/eraa-downloads/.
- ENTSO-E and ENTSOG (2024). TYNDP 2024. https://2024.entsos-tyndp-scenarios.eu/.
- European Commission (2010). Interpretative Note On Directive 2009/72/EC Concerning Common Rules For The Internal Market In Electricity And Directive 2009/73/EC Concerning Common Rules For The Internal Market In Natural Gas. Commission Staff Working Paper. https://energy.ec.europa.eu/system/files/2014-10/2010\_01\_21\_the\_unbundling\_regime\_0.pdf.
- EWI (2023a). Auswirkungen des Gebäudeenergiegesetzes auf Wohngebäude Mögliche Entwicklungen und kritische Erfolgsfaktoren bei der Umsetzung. ht tps://www.ewi.uni-koeln.de/cms/wp-content/uploads/2023/06/23061 3\_EWI\_Analyse\_Gebaeudeenergiegesetzentwurf.pdf.
- EWI (2023b). EWI Policy Brief Strompreisbestandteile, Strompreispaket und Verteilungseffekte. https://www.ewi.uni-koeln.de/cms/wp-content/uploads/2023/11/Policy\_Brief\_Strompreise\_v1.pdf.
- EWI (2023c). Update: Auswirkungen des Gebäudeenergiegesetzes auf Wohngebäude Aktualisierung auf Grundlage des Bundestagsbeschlusses vom 08.09.2023. https://www.ewi.uni-koeln.de/cms/wp-content/uploads/2 023/09/Update\_Auswirkungen\_GEG\_EWI\_September\_2023-1.pdf.

- EWI (2024a). Hydrogen storage in Germany and Europe: Model-based analysis up to 2050. Institute of Energy Economics at the University of Cologne. https://www.ewi.uni-koeln.de/cms/wp-content/uploads/2024/08/20240823\_Selected-results-Hydrogen-storage-in-Germany-and-Europe-Model-based-analysis-up-to-2050.pdf.
- EWI (2024b). The financing gap in the hydrogen market ramp-up: Analysis of demand and price scenarios. https://www.ewi.uni-koeln.de/cms/wp-content/uploads/2024/10/241004\_Financing\_Gap\_Endbericht.pdf.
- Felling, T. and Fortenbacher, P. (2022). Extended social welfare decomposition for multi-energy systems. In 2022 18th International Conference on the European Energy Market (EEM), pages 1–7.
- Flataker, A., Malmin, O. K., Hjelkrem, O. A., Rana, R., Korpås, M., and Torsæter, B. N. (2022). Impact of home- and destination charging on the geographical and temporal distribution of electric vehicle charging load. In 2022 18th International Conference on the European Energy Market (EEM), pages 1–6.
- Fraunhofer ISI (2023). Price-Elastic Demand for Hydrogen in Germany Methodology and Results. https://publica-rest.fraunhofer.de/server/api/core/bitstreams/4a8b916d-2af1-46bb-b790-55148cfe0a5e/content.
- Fraunhofer ISI, Consentec GmbH, ifeu, and TU Berlin (2021). Langfristszenarien für die Transformation des Energiesystems in Deutschland 3. Technical report. Federal Ministry of Economic Affairs and Climate Action. https://www.isi.fraunhofer.de/content/dam/isi/dokumente/cce/2021/LFS\_Kurzberic ht.pdf.
- Frings, C. and Helgeson, B. (2022). Developing a Model for Consumer Management of Decentralized Options. *EWI Working Papers*, 22/05.
- Frischmuth, F., Berghoff, M., Braun, M., and Härtel, P. (2024). Quantifying seasonal hydrogen storage demands under cost and market uptake uncertainties in energy system transformation pathways. *Applied Energy*, 375:123991.
- Frischmuth, F. and Härtel, P. (2022). Hydrogen sourcing strategies and cross-sectoral flexibility trade-offs in net-neutral energy scenarios for europe. *Energy*, 238:121598.
- Gawlick, J. and Hamacher, T. (2023). Impact of coupling the electricity and hydrogen sector in a zero-emission European energy system in 2050. *Energy Policy*, 180:113646.
- German Federal Government (2022). Transformation to a climate-neutral industry. https://www.bundesregierung.de/breg-en/search/battery-cell-plant-vw-salzgitter-2060434.

- German Government (2022). Nachhaltige Mobilität Nicht weniger fortbewegen, sondern anders. https://www.bundesregierung.de/breg-de/themen/klimaschutz/nachhaltige-mobilitaet-2044132#:~:text=Nachhaltige%20Mobilit%C3%A4t%20Nicht%20weniger%20fortbewegen,um%20%C3%BCber%2040%20Prozent%20sinken.
- German TSOs (2022). Szenariorahmen zum Netzentwicklungsplan Strom 2037 mit Ausblick 2045, Version 2023, Entwurf der Übertragungsnetzbetreiber. ht tps://www.netzentwicklungsplan.de/sites/default/files/paragraphs-files/Szenariorahmenentwurf\_NEP2037\_2023.pdf.
- Gillingham, K., Newell, R. G., and Palmer, K. (2009). Energy efficiency economics and policy. *Annu. Rev. Resour. Econ.*, 1(1):597–620.
- Gils, H. C., Gardian, H., and Schmugge, J. (2021). Interaction of hydrogen infrastructures with other sector coupling options towards a zero-emission energy system in Germany. *Renewable Energy*, 180:140–156.
- Gompertz, B. (1825). XXIV. On the nature of the function expressive of the law of human mortality, and on a new mode of determining the value of life contingencies. In a letter to Francis Baily, Esq. FRS &c. *Philosophical transactions of the Royal Society of London*, (115):513–583.
- Goutte, S. and Vassilopoulos, P. (2019). The value of flexibility in power markets. *Energy Policy*, 125:347–357.
- Gunkel, P. A., Bergaentzlé, C., Græsted Jensen, I., and Scheller, F. (2020). From passive to active: Flexibility from electric vehicles in the context of transmission system development. *Applied Energy*, 277:115526.
- Heilmann, C. and Wozabal, D. (2021). How much smart charging is smart? *Applied Energy*, 291:116813.
- Heitkoetter, W., Medjroubi, W., Vogt, T., and Agert, C. (2020). Regionalised heat demand and power-to-heat capacities in Germany An open dataset for assessing renewable energy integration. *Applied energy*, 259:114161.
- Helgeson, B. (2024). Europe, the Green Island? Developing an integrated energy system model to assess an energy-independent, CO2-neutral Europe. *EWI Working Papers*, 24/02.
- Helgeson, B. and Peter, J. (2020). The role of electricity in decarbonizing European road transport Development and assessment of an integrated multisectoral model. *Applied Energy*, 262.
- HErZ, Hans-Ertel Centre for Weather Research (University of Bonn Germany) and DWD, Deutscher Wetterdienst (2022). COSMO-REA6. https://reanalysis.meteo.uni-bonn.de/?Download\_Data\_\_\_COSMO-REA6.

- Hesel, P., Braun, S., Zimmermann, F., and Fichtner, W. (2022). Integrated modelling of European electricity and hydrogen markets. *Applied Energy*, 328:120162.
- Hirth, L. (2013). The market value of variable renewables: The effect of solar wind power variability on their relative price. *Energy Economics*, 38:218–236.
- Hirth, L., Ueckerdt, F., and Edenhofer, O. (2016). Integration costs revisited an economic framework for wind and solar in electricity systems. *Renewable Energy*, 74:925–939.
- Holm, A., Winiewska, B., and Oschatz, B. (2021). Klimaneutralität 2045-Transformation des Gebäudesektors - Gebäudespezifische Modellierung und Begleitung des Studienprozesses. Gutachten im Rahmen der dena-Leitstudie Aufbruch Klimaneutralität. https://www.dena.de/dena-leitstudie-auf bruch-klimaneutralitaet/gutachten/.
- Huld, T., Gottschalg, R., Beyer, H. G., and Topič, M. (2010). Mapping the performance of PV modules, effects of module type and data averaging. Solar Energy, 84(2):324–338.
- Härtel, P. and Korpås, M. (2021). Demystifying market clearing and price setting effects in low-carbon energy systems. *Energy Economics*, 93:105051.
- IEA (2022a). Global EV Outlook 2022 Securing supplies for an electric future. International Energy Agency, France. https://iea.blob.core.windows.net/assets/ad8fb04c-4f75-42fc-973a-6e54c8a4449a/GlobalElectricVehicleOutlook2022.pdf.
- IEA (2022b). Grid Integration of Electric Vehicles A manual for policy makers. International Energy Agency, France. https://iea.blob.core.windows.net/assets/21fe1dcb-c7ca-4e32-91d4-928715c9d14b/GridIntegrationofElectricVehicles.pdf.
- IEA (2023a). Electricity Grids and Secure Energy Transitions, IEA, Paris, License: CC BY 4.0. https://www.iea.org/reports/electricity-grids-and-secure-energy-transitions.
- IEA (2023b). Global EV Outlook 2023. International Energy Agency, France. https://iea.blob.core.windows.net/assets/dacf14d2-eabc-498a-826 3-9f97fd5dc327/GEV02023.pdf.
- IEA (2023c). World Energy Outlook 2023. International Energy Agency, France. https://iea.blob.core.windows.net/assets/42b23c45-78bc-4482-b0f9-eb826ae2da3d/WorldEnergyOutlook2023.pdf.
- IEA (2024). World Energy Outlook 2024. International Energy Agency, France. https://iea.blob.core.windows.net/assets/140a0470-5b90-4922-a0e 9-838b3ac6918c/WorldEnergyOutlook2024.pdf.

- INES (2025). MAHS Market Assessment for Hydrogen Storage. https://energien-speichern.de/wp-content/uploads/2025/01/INES-Praesentation\_MAHS-Ergebnisse.pdf.
- infas, DLR, IVT, and infas 360 (2018). Mobilität in Deutschland (im Auftrag des BMVI). www.mobilitaet-in-deutschland.de.
- Jenn, A. and Highleyman, J. (2022). Distribution grid impacts of electric vehicles: A California case study. *iScience*, 25(1):103686.
- Keutz, J. and Kopp, J. H. (2025). Assessing the impact of take-or-pay rates in long-term contracts for hydrogen imports on a decarbonized european energy system under weather variability. *Applied Energy*, 389:125784.
- KfW (2024). The efficiency house levels for existing properties and listed buildings. https://www.kfw.de/inlandsfoerderung/Privatpersonen/Besteh ende-Immobilie/Energieeffizient-sanieren/Das-Effizienzhaus/.
- Kirkerud, J., Nagel, N. O., and Bolkesjø, T. (2021). The role of demand response in the future renewable northern European energy system. *Energy*, 235:121336.
- KIT Institut für Verkehrswesen (2021). Deutsches Mobilitätspanel (MOP) Wissenschaftliche Begleitung und Auswertungen Bericht 2020/2021: Alltagsmobilität und Fahrleistung. https://mobilitaetspanel.ifv.kit.edu/downloads/Bericht\_MOP\_20\_21.pdf.
- Kiviluoma, J. and Meibom, P. (2010). Influence of wind power, plug-in electric vehicles, and heat storages on power system investments. *Energy*, 35(3):1244–1255.
- Klaas, A.-K., Moritz, M., Wohlleben, D., and Sprenger, T. (2024). EWI Global PtX Cost Tool 2.0. https://www.ewi.uni-koeln.de/en/publications/ewi-global-ptx-cost-tool/.
- Kockel, C., Nolting, L., Priesmann, J., and Praktiknjo, A. (2022). Does renewable electricity supply match with energy demand? A spatio-temporal analysis for the German case. *Applied Energy*, 308:118226.
- Koirala, B., Hers, S., Morales-España, G., Özdemir, , Sijm, J., and Weeda, M. (2021). Integrated electricity, hydrogen and methane system modelling framework: Application to the Dutch Infrastructure Outlook 2050. Applied Energy, 289:116713.
- Kondziella, H., Specht, K., Lerch, P., Scheller, F., and Bruckner, T. (2023). The techno-economic potential of large-scale hydrogen storage in Germany for a climate-neutral energy system. *Renewable and Sustainable Energy Reviews*, 182:113430.
- Kraftfahrt-Bundesamt (2023). Bestand. https://www.kba.de/DE/Statistik/Fahrzeuge/Bestand/bestand\_node.html.

- Kraftfahrt-Bundesamt (2024a). Bestand nach Gemeinden (FZ 3). https://www.kba.de/DE/Statistik/Produktkatalog/produkte/Fahrzeuge/fz3\_b\_uebersicht.html?nn=3514348.
- Kraftfahrt-Bundesamt (2024b). Bestand nach Zulassungsbezirken (FZ 1). https://www.kba.de/DE/Statistik/Produktkatalog/produkte/Fahrzeuge/fz1\_b\_uebersicht.html?nn=3514348.
- Kröger, D., Peper, J., and Rehtanz, C. (2023). Electricity market modeling considering a high penetration of flexible heating systems and electric vehicles. *Applied Energy*, 331:120406.
- Kumar, R. R., Guha, P., and Chakraborty, A. (2022). Comparative assessment and selection of electric vehicle diffusion models: A global outlook. *Energy*, 238:121932.
- Kühnbach, M., Bekk, A., and Weidlich, A. (2021). Prepared for regional self-supply? On the regional fit of electricity demand and supply in Germany. Energy Strategy Reviews, 34:100609.
- Kłos, M., Wawrzyniak, K., and Jakubek, M. (2015). Decomposition of power flow used for optimizing zonal configurations of energy market. In 2015 12th International Conference on the European Energy Market (EEM), pages 1–5.
- Laffont, J.-J. and Tirole, J. (1993). A theory of incentives in procurement and regulation. MIT press.
- Le Dréau, J. and Heiselberg, P. (2016). Energy flexibility of residential buildings using short term heat storage in the thermal mass. *Energy*, 111:991–1002.
- Lilienkamp, A. and Namockel, N. (2025). Integrating EVs into distribution grids
   Examining the effects of various DSO intervention strategies on optimized charging. Applied Energy, 378:124775.
- Liski, M. and Vehviläinen, I. (2023). Redistribution through technology: Equilibrium impacts of mandated efficiency in three electricity markets. https://ceepr.mit.edu/wp-content/uploads/2023/04/MIT-CEEPR-WP-2023-10.pdf.
- Länderarbeitskreis Energiebilanzen (2022). Vollständige Energiebilanz. https://www.lak-energiebilanzen.de/eingabe-dynamisch/?a=e900.
- Lüth, A., Seifert, P. E., Egging-Bratseth, R., and Weibezahn, J. (2023). How to connect energy islands: Trade-offs between hydrogen and electricity infrastructure. *Applied Energy*, 341:121045.
- Martinez-Anido, C. B., Brinkman, G., and Hodge, B.-M. (2016). The impact of wind power on electricity prices. *Renewable energy*, 94:474–487.
- Meiers, J. and Frey, G. (2024). A Case Study of the Use of Smart EV Charging for Peak Shaving in Local Area Grids. *Energies*, 17(1).

- Meinecke, S., Sarajlić, D., Drauz, S. R., Klettke, A., Lauven, L.-P., Rehtanz, C., Moser, A., and Braun, M. (2020). SimBench A Benchmark Dataset of Electric Power Systems to Compare Innovative Solutions Based on Power Flow Analysis. *Energies*, 13(12).
- Muessel, J., Ruhnau, O., and Madlener, R. (2022). Modeling Volatility and Flexibility of Electric Vehicles' Energy Consumption. FCN Working Paper, 17.
- Muraleedharakurup, G., McGordon, A., Poxon, J., and Jennings, P. (2010). Building a better business case: the use of non-linear growth models for predicting the market for hybrid vehicles in the uk. *Ecological Vehicles and Renewable Energies. Monaco*.
- Nacmanson, D. W. J., Zhu, J., and Ochoa, P. L. (2021). Milestone 6: Network modelling and ev impact assessment. Report UoM-ENA-C4NET-EV\_Integration\_M6\_v03, Department of Electrical and Electronic Engineering at the University of Melbourne.
- Nagel, N. O., Kirkerud, J. G., and Bolkesjø, T. F. (2022). The economic competitiveness of flexibility options: A model study of the European energy transition. *Journal of Cleaner Production*, 350:131534.
- Namockel, N. (2025). Understanding the fundamentals of hydrogen price formation and its relationship with electricity prices Insights for the future energy system. *EWI Working Papers*, 25/06.
- Netztransparenz (2024). Mittelfristprognose zur deutschlandweiten Stromerzeugung aus EEG-geförderten Kraftwerken für die Kalenderjahre 2025 bis 2029. https://www.netztransparenz.de/de-de/Erneuerbare-Energien-und-Umlagen/EEG/EEG-Finanzierung/Mittelfristprognosen/Mittelfristprognose-2025-2029.
- Neumann, F., Zeyen, E., Victoria, M., and Brown, T. (2023). The potential role of a hydrogen network in Europe. *Joule*, 7(8):1793–1817.
- Newville, M., Stensitzki, T., Allen, D. B., Rawlik, M., Ingargiola, A., and Nelson, A. (2016). Lmfit: Non-Linear Least-Square Minimization and Curve-Fitting for Python. Astrophysics Source Code Library, record ascl:1606.014.
- Odenweller, A. and Ueckerdt, F. (2025). The green hydrogen ambition and implementation gap. *Nature Energy*.
- Pahle, M., Sitarz, J., Osorio, S., and Görlach, B. (2022). The EU-ETS price through 2030 and beyond: A closer look at drivers, models and assumptions. https://ariadneprojekt.de/media/2023/01/Ariadne-Documentation\_ETSWorkshopBruessel\_December2022.pdf.

- Palensky, P. and Dietrich, D. (2011). Demand side management: Demand response, intelligent energy systems, and smart loads. *IEEE Transactions on Industrial Informatics*, 7(3):381–388.
- Pavlidou, A. (2010). Diffusion of the diffusion curve: A research on the SS-curvescurves in relation to technological clusters. *Utrecht University, Faculuty of Geoscience, Utrecht*.
- Pflugradt, N., Stenzel, P., Kotzur, L., and Stolten, D. (2022). LoadProfileGenerator: An Agent-Based Behavior Simulation for Generating Residential Load Profiles. *Journal of Open Source Software*, 7(71):3574.
- Powell, S., Cezar, G. V., Min, L., Azevedo, I. M. L., and Rajagopal, R. (2022). Charging infrastructure access and operation to reduce the grid impacts of deep electric vehicle adoption. *Nature Energy*, 7(10):932–945.
- Prognos, Fraunhofer ISI, GWS, and IINAS (2021). Energiewirtschaftliche Projektionen und Folgeabschätzungen 2030/2050-Gesamtdokumentation der Szenarien. https://www.isi.fraunhofer.de/content/dam/isi/dokument e/ccx/2021/energiewirtschaftliche-projektionen-und-folgeabschaet zungen-2030-2050.pdf.
- Prognos, Öko-Institut, and Wuppertal-Institut (2020). Klimaneutrales Deutschland Studie im Auftrag von Agora Energiewende, Agora Verkehrswende und Stiftung Klimaneutralität. Technical report. https://www.agora-energiewende.de/fileadmin/Projekte/2020/2020\_10\_KNDE/A-EW\_195\_KNDE\_WEB.pdf.
- Radecke, J., Hefele, J., and Hirth, L. (2019). Markets for Local Flexibility in Distribution Networks A Review of European Proposals for Market-based Congestion Management in Smart Grids. ZBW Leibniz Information Centre for Economics, Kiel, Hamburg.
- Rebenaque, O., Schmitt, C., Schumann, K., Dronne, T., and Roques, F. (2023). Success of local flexibility market implementation: A review of current projects. *Utilities Policy*, 80:101491.
- Reibsch, R., Gemassmer, J., and Katerbau, T. (2024). Low voltage grid resilience: Evaluating electric vehicle charging strategies in the context of the grid development plan germany. *eTransportation*, 20:100323.
- Repenning, J., Harthan, R., Blanck, R., Böttcher, H., Braungardt, S., Bürger, V., et al. (2023). Klimaschutzinstrumente-Szenario 2030 (KIS-2030) zur Erreichung der Klimaschutzziele 2030. *Umweltbundesamt (Climate Change, 30)*.
- Resch, M., Bühler, J., Schachler, B., and Sumper, A. (2021). Techno-Economic Assessment of Flexibility Options Versus Grid Expansion in Distribution Grids. *IEEE Transactions on Power Systems*, 36(5):3830–3839.

- Richter, J. (2011). DIMENSION A dispatch and investment model for European electricity markets. *EWI Working Papers*, 11/03.
- Rinaldi, A., Soini, M. C., Streicher, K., Patel, M. K., and Parra, D. (2021). Decarbonising heat with optimal PV and storage investments: A detailed sector coupling modelling framework with flexible heat pump operation. Applied Energy, 282:116110.
- Ruhnau, O. (2022). How flexible electricity demand stabilizes wind and solar market values: The case of hydrogen electrolyzers. *Applied Energy*, 307:118194.
- Ruhnau, O. and Muessel, J. (2022). When2Heat Heating Profiles. Open Power System Data (2022-02-22). https://data.open-power-system-data.org/when2heat/.
- Sarbu, I. and Sebarchievici, C. (2018). A comprehensive review of thermal energy storage. Sustainability, 10(1):191.
- Schill, W.-P. and Gerbaulet, C. (2015). Power system impacts of electric vehicles in Germany: Charging with coal or renewables? *Applied Energy*, 156:185–196.
- Schittekatte, T., Mallapragada, D., Joskow, P. L., and Schmalensee, R. (2022). Electricity retail rate design in a decarbonizing economy: An analysis of time-of-use and critical peak pricing. *CEEPR Working Paper Series*, 2022-015.
- Schittekatte, T., Mallapragada, D., Joskow, P. L., and Schmalensee, R. (2023). Reforming retail electricity rates to facilitate economy-wide decarbonization. *Joule*.
- Schnaars, D. P., Kienscherf, P. A., Gruber, K., Çam, D. E., and Schroer, K. (2022). EWI EV Preparedness Index. https://www.ewi.uni-koeln.de/en/publikationen/ev-preparedness/.
- Schneider, M., Barrios, H., and Schnettler, A. (2018). Evaluation of unscheduled power flows in the European transmission system. In 2018 IEEE International Energy Conference (ENERGYCON), pages 1–6.
- Schönfisch, M. (2022). Charting the development of a global market for low-carbon hydrogen. EWI Working Papers, 22/03.
- Song, X. (2013). Forecast of Electric Vehicles in China Based on Bass Model. https://api.semanticscholar.org/CorpusID:112646378.
- Spiliotis, K., Ramos Gutierrez, A. I., and Belmans, R. (2016). Demand flexibility versus physical network expansions in distribution grids. *Applied Energy*, 182:613–624.
- Stute, J. and Klobasa, M. (2024). How do dynamic electricity tariffs and different grid charge designs interact? Implications for residential consumers and grid reinforcement requirements. *Energy Policy*, 189:114062.

- SWM (2022). Lastprofil Wärmepumpe. https://www.swm-infrastruktur.d e/strom/netzzugang/bedingungen/waermepumpe.
- The Federal Government (2024). Power Station Strategy to develop hydrogen power stations. https://www.bundesregierung.de/breg-en/news/power-station-strategy-2257994.
- Tsiklios, C., Schneider, S., Hermesmann, M., and Müller, T. E. (2023). Efficiency and optimal load capacity of E-Fuel-Based energy storage systems. *Advances in Applied Energy*, 10:100140.
- United Nations (2023). Net Zero Coalition. https://www.un.org/en/climatechange/net-zero-coalition.
- Valogianni, K., Ketter, W., Collins, J., and Zhdanov, D. (2020). Sustainable Electric Vehicle Charging using Adaptive Pricing. Production and Operations Management, 29(6):1550–1572.
- Van der Kam, M., Meelen, A., van Sark, W., and Alkemade, F. (2018). Diffusion of solar photovoltaic systems and electric vehicles among Dutch consumers: Implications for the energy transition. *Energy Research & Social Science*, 46:68–85.
- VDEW (1999). Repräsentative VDEW-Lastprofile. https://www.bdew.de/energie/standardlastprofile-strom/.
- Virtuelles Institut (2022). Abschlussbericht Kompetenzzentrum Virtuelles Institut Strom zu Gas und Wärme. Technical Report Band I Systemmodellierung zur Identifikation von innovativen PtX-Anwendungen.
- von Bonin, M., Dörre, E., Al-Khzouz, H., Braun, M., and Zhou, X. (2022). Impact of Dynamic Electricity Tariff and Home PV System Incentives on Electric Vehicle Charging Behavior: Study on Potential Grid Implications and Economic Effects for Households. *Energies*, 15(3).
- VWG (2022a). Arbeitnehmerentgelt, Bruttolöhne und -gehälter in den kreisfreien Städten und Landkreisen der Bundesrepublik Deutschland 2000 bis 2020, Reihe 2, Kreisergebnisse Band 2, Berechnungsstand: November 2021.
- VWG (2022b). Bruttoinlandsprodukt, Bruttowertschöpfung in den kreisfreien Städten und Landkreisen der Bundesrepublik Deutschland 1992 und 1994 bis 2020, Reihe 2, Kreisergebnisse Band 1, Berechnungsstand: November 2021.
- Weißenburger, B., Wietschel, M., Lux, B., and Rehfeldt, M. (2024). The long term price elastic demand of hydrogen A multi-model analysis for Germany. Energy Strategy Reviews, 54:101432.
- Won, J.-R., Yoon, Y.-B., and Lee, K.-J. (2009). Prediction of electricity demand due to phevs(plug-in hybrid electric vehicles) distribution in korea by using diffusion model. In 2009 Transmission & Distribution Conference & Exposition: Asia and Pacific, pages 1–4.

Zhu, Y., Tokimatsu, K., and Matsumoto, M. (2017). Study on the Diffusion of NGVs in Japan and Other Nations Using the Bass Model, chapter VI-7, pages 765–778. Springer Singapore, Singapore.

# Curriculum Vitae

### CURRICULUM VITAE

# Nils Namockel

### PERSONAL DATA

Date of Birth	23rd April 1994
Place of Birth	Нассор

Place of Birth Hagen Nationality German

### RESEARCH INTERESTS

Flexibility, Electric Vehicles, Energy System Modeling, Hydrogen

### EDUCATION

since 11/2019	Institute of Energy Economics (EWI) and Department of Economics, University of Cologne Doctoral Candidate in Economics
04/2017 - 09/2019	RWTH Aachen University Master of Science in Business Administration and Engineering: Electrical Energy Technology
02/2017 - 07/2017	Tongji University, Shanghai Study abroad
10/2013 - 10/2016	<b>RWTH Aachen</b> Bachelor of Science in Business Administration and Engineering: Electrical Energy Technology
06/2013	Gymnasium Hohenlimburg, Hagen Maturity/Abitur

### WORKING EXPERIENCE

since $06/2025$	Institute of Energy Economics at the University of Cologne (EWI) Project Lead
11/2019 - 05/2025	Institute of Energy Economics at the University of Cologne (EWI) Research Associate
10/2018 - 09/2019	Siemens AG, Munich Working Student & Master Thesis Student
09/2017 - 10/2018	Institute for High Voltage Technologies, RWTH Aachen University Student Assistant
11/2016 - 02/2017	P3 group, Aachen Internship
04/2016 - 07/2016	RWE International SE, Dortmund Internship

### LANGUAGES

German	Mother tongue
English	Proficient

### **Articles in Peer-Reviewed Journals:**

- Emelianova, P., Namockel, N. (2025). Welfare redistribution through flexibility Who pays?. Energy Policy 205: 114684, doi:10.1016/j.enpol.2025.114684.
- Lilienkamp, A., Namockel, N. (2025). Integrating EVs into distribution grids Examining the effects of various DSO intervention strategies on optimized charging. *Applied Energy* 378, Part A, 124775, doi:10.1016/j.apenergy.2024.124775.
- Arnold, F., Lilienkamp, A., Namockel, N. (2024). Diffusion of Electric Vehicles and Their Flexibility Potential for Smoothing Residual Demand a Spatio-Temporal Analysis for Germany. *Energy* 308, 132619, doi:10.1016/j.energy.2024.132619.
- Huber, M., Namockel, N., Rezgui, R., Küppers, M., Heger, H.J. (2021). Electrification seeds
   A flexible approach for decentralized electricity supply in developing countries. Energy for Sustainable Development 62, 176-185, doi:10.1016/j.esd.2021.04.001.

### Working Papers:

- Lilienkamp, A., Namockel, N., Ruhnau, O. (2025). Flexibility in electricity wholesale markets and distribution grids: An integrated model and its application to electric vehicles in Germany. *EWI Working Paper* No. 25/08.
- Namockel, N. (2025). Understanding the fundamentals of hydrogen price formation and its relationship with electricity prices – Insights for the future energy system. EWI Working Paper No. 25/06.
- Vey, M., Namockel, N., Ruhnau, O. (2025). Green charged decision-making: How two-part remuneration, contract flexibility, and environmental nudging drive vehicle-to-grid participation. *EWI Working Paper* No. 25/01.
- Emelianova, P., Namockel, N. (2024). Welfare redistribution through flexibility Who pays?.
   EWI Working Paper No. 24/09.
- Lilienkamp, A., Namockel, N. (2024). Integrating EVs into distribution grids Examining the effects of various DSO intervention strategies on optimized charging. *EWI Working Paper* No. 24/01.
- Arnold, F., Lilienkamp, A., Namockel, N. (2023). Diffusion of electric vehicles and their flexibility potential for smoothing residual demand A spatio-temporal analysis for Germany. EWI Working Paper No. 23/04.

#### Further Publications:

- N. Namockel, J. Junkermann, P. Schnaars (2025). GreenVEgaS: Gesamtsystemanalyse der Sektorenkopplung. Research project funded by Bundesministerium für Wirtschaft und Klimaschutz (BMWK).
- P. A. Kienscherf, L. Just, F. Arnold, N. Namockel, M. Moritz, T. Leibfritz (2025). Bewertung von Wärmepumpen und Hybridheizungen anhand von THG-Emissionen, Heiz- und Infrastrukturkosten. Study on behalf of Förderinitiative Wärmewende der Gesellschaft zur Förderung des Energiewirtschaftlichen Instituts an der Universität zu Köln e.V.
- A. Lilienkamp, N. Namockel, D. Schulze, J. Volk (2024). Smart Data: Mehrwertgenerierung durch Energiedaten – Trends & Transformationsprozesse – Definitorische Grundlagen. VISE Policy Brief No. 13.
- F. Arnold, H. Diers, M. Lange, A. Lilienkamp, N. Namockel, C. Schmidt, P. Schnaars, E. Schrader (2024). Mittelfristprognose zur deutschlandweiten Stromerzeugung aus EEGgeförderten Kraftwerken für die Kalenderjahre 2025 bis 2029. Report on behalf of 50Hertz Transmission GmbH, Amprion GmbH, TenneT TSO GmbH and TransnetBW GmbH.
- A. Lilienkamp, N. Namockel (2024). Datengetriebene Geschäftsmodelle in der Energiewirtschaft
   – Cluster-Analyse von Status Quo und Potenzialen. et Energiewirtschaftliche Tagesfragen, Vol.
   74 (9), pp. 13-16.
- P. Kienscherf, N. Namockel, M. Lange (2023). Strompreisbestandteile, Strompreispaket und Verteilungseffekte. EWI Policy Brief on behalf of Gesellschaft zur Förderung des Energiewirtschaftlichen Instituts an der Universität zu Köln e.V.
- J. Wagner, P. Schnaars, N. Namockel, H. Diers, J. Keutz (2022). Gasverstromung im Winter 2022/2023. Study on behalf of Gesellschaft zur Förderung des Energiewirtschaftlichen Instituts an der Universität zu Köln e.V.

- J. Bocklet, N. Namockel, P. Willers, K. Gruber (2022). Das Sofortprogramm für den Gebäudesektor. EWI Policy Brief on behalf of Förderinitiative Wärmewende der Gesellschaft zur Förderung des Energiewirtschaftlichen Instituts an der Universität zu Köln e.V.
- J. Wagner, N. Namockel, A. Lilienkamp (2022). Dezentrale Koordination Auswirkungen unterschiedlicher Ladekonzepte für Elektrofahrzeuge auf Markt und Netz. Study on behalf of Gesellschaft zur Förderung des Energiewirtschaftlichen Instituts an der Universität zu Köln e.V.
- S. Birk, J. Fleer, G. Holtz, S. Jeddi, A. Lilienkamp, N. Namockel, M. Schönfisch, J. Wagner (2022). Geschäftsmodelle für Regionale Virtuelle Kraftwerke Abschlussbericht des Virtuellen Instituts Smart Energy (VISE), Teilprojekt "Regionale Virtuelle Kraftwerke. Study on behalf of Virtuelles Institut Smart Energy (VISE).
- M. Gierkink, J. Wagner, F. Arnold, B. Czock, N. Namockel, P. Theile (2021). Auswirkungen des Koalitionsvertrags auf den Stromsektor 2030. *EWI analysis*.
- F. Arnold, E. Künle, N. Namockel, P. Theile (2021). Stromversorgungssicherheit Facetten und Herausforderungen. Weltenergierat, Energie für Deutschland 2021, Fakten, Perspektiven und Positionen im globalen Kontext. Study on behalf of Gesellschaft zur Förderung des Energiewirtschaftlichen Instituts an der Universität zu Köln e.V.
- J. Wagner, N. Namockel, K. Gruber (2021). Ökonomische Bewertung des Nutzens lokaler Koordinationsmechanismen in der Stromversorgung. Study on behalf of Siemens AG und der Allgäuer Überlandwerk GmbH.
- E. Künle, J. Zinke, A. Lilienkamp, N. Namockel (2020). Auswirkungen von Kälteperioden auf die Spitzenlast im nordwesteuropäischen Stromsystem in 2030, et Energiewirtschaftliche Tagesfragen, Vol. 70 (12), pp. 52-54.
- M. Gierkink, D. Lencz, M. Wiedmann, N. Namockel (2020). Auswirkungen des Kohleausstiegsgesetzes auf die Braunkohleverstromung im Rheinischen Revier. Study on behalf of RWE Power AG.
- P. Abiven, M. Blondel, M. Taoufiki, E. Künle, A. Lilienkamp, N. Namockel, J. Zinke (2020). Peak Power Demand in North-West Europe. *Study on behalf of ENGIE*.
- M. Knittel, N. Namockel, M. Schneider, R. Puffer (2019). Reactive power loop flows in transmission grids. 2019 IEEE Milan PowerTech. doi:10.1109/PTC.2019.8810444.

### PRESENTATIONS AND TALKS

- Wholesale electricity market modeling with distribution grid constraints. 10th International Conference on Smart Energy Systems. September 2024. Aalborg, Denmark.
- Welfare redistribution through flexibility Who pays?. 18th International Conference on Energy Economics and Technology "Exploring Energy Demand Dynamics". April 2024. Dresden, Germany.
- Welfare redistribution through flexibility Who pays?. 32th YEEES Workshop. October 2023. Nurnberg, Germany.
- Integrating EVs Smart Charging and Its Impact on Distribution Grids. 29th YEEES Workshop. May 2022. Ghent, Belgium.